Data-Driven Modeling of the Heroin and Fentanyl Epidemic and the Harvesting of Trees in West Africa

A Dissertation Presented for the

Doctor of Philosophy

Degree

The University of Tennessee, Knoxville

Tricia Marie Phillips

May 2020

© by Tricia Marie Phillips, 2020
All Rights Reserved.

To my beautiful grandmother, Meme.

Acknowledgments

I would first like to thank my incredible advisors, Suzanne Lenhart and Christopher Strickland, for their guidance during my graduate school career. To Dr. Lenhart, thank you for always starting with simple cases and slowly building up to enhance my understanding, providing me with many different opportunities to grow, and for always making time to talk about math and life. To Dr. Strickland, thank you for taking me on as your first doctoral student, guiding me while I learned how to code, and encouraging me when I doubted myself. I would also like to thank our collaborator, Orou Gaoue, for sharing his knowledge on tree populations in Benin, providing insight on important ideas in ecology, and serving as a member on my committee. Finally, I would like to thank Judy Day for her willingness to be on my committee and for her support in reaching my goals.

To Mom, Dad, Tyler, and Meme, thank you for supporting me emotionally for this very long academic journey, although you all know it will be a lifelong one. I feel very fortunate to have as supportive of a family as I do. To Cara, thank you for sticking by my side through our first year and keeping my spirits high everyday; you know I would not have made it without you. To Cameron, thank you for always encouraging me with running and reminding me to take care of my mental health. To Jesse, I cannot thank you enough for helping me get to this point; your steadfast patience with all of my questions will never be forgotten. Thank you for always believing in me. To Hannah, thank you for all of our (very long) discussions, both about school and life, that kept me going and meant so much to me. Your support is like no other and you never let me give up. I am forever indebted to you all.

Abstract

The opioid epidemic has had a strong presence in the United States in recent years. Drug overdose deaths involving opioids have skyrocketed and the lacing of heroin with fentanyl has played a significant role in this. In order to investigate the dynamics behind the opioid epidemic and predict its trajectory, we formulate a system of ordinary differential equations that incorporate the movement of individuals among classes of opioid use. We estimate parameter values by fitting to Tennessee data since the time the epidemic was established in the state. The trajectory of the epidemic suggests the number of addicts and overdose deaths will increase over the next few years and is driven by the size of the heroin/fentanyl addicted class. We measure the sensitivity of the size of the opioid addicted classes to each of the parameters at the beginning of 2023. From these results, with the hopes of mitigating the increasing trajectory of the epidemic in the near future, management scenarios for decreasing the number of addicted individuals and overdose deaths from 2020-2023 are explored. The most effective include increasing accessibility to treatment programs, monitoring individuals who have stably recovered, and increasing the use of opioid overdose-reversal drugs.

Khaya senegalensis is a tree species in Benin, West Africa that is harvested both lethally and non-lethally for its non-timber forest products by the local people for cultural and economic reasons. Both adult and juvenile trees are harvested which affects various vital rates for the tree population. To investigate the effect of size-dependent harvesting strategies on tree population dynamics, we develop a size-structured, seasonal system of difference equations with time-varying harvest for this tree species. Using data from a specific population of the species, the Soassararou population, we estimate harvesting rates and rates affected by harvest for our harvesting model applied to the Soassararou and Nipuni populations. Eigenvalue analysis is then carried out to compare population dynamics.

Table of Contents

1 Introduction **1**

2 Modeling the Heroin and Fentanyl Epidemic **3**

2.1 Background . . . 3

2.1.1 Application to Tennessee . . . 7

2.1.2 Previous Work . . . 12

2.2 Model Formulation . . . 17

2.3 Model Analysis . . . 27

2.3.1 Addiction-Free Equilibrium and Basic Reproduction Number . . . 27

2.3.2 Properties of Solutions . . . 32

2.4 Numerical Results . . . 36

2.4.1 Parameter Calculations . . . 46

2.4.2 Parameter Estimation . . . 47

2.4.3 Comparison of Models with AIC . . . 78

2.4.4 Trajectory of the Epidemic . . . 88

2.4.5 Sensitivity Analysis . . . 94

2.5 Management Strategies from 2020-2023 . . . 104

2.5.1 Accessibility to Treatment: Management Strategy . . . 108

2.5.2 Case-holding in Stably Recovered Class: Management Strategy . . . 110

2.5.3 Heroin/Fentanyl Availability Scenarios . . . 112

2.5.4 Prescription Rate Management Strategy . . . 114

2.5.5 Prescription Completion: Management Strategy . . . 114

2.5.6 Overdose-Reversal Drug Management Strategy . . . 116

2.6 Conclusions and Discussion . . . 117

3 Harvesting of Non-Timber Forest Products **120**

3.1 Background . . . 120

3.2 Model Formulation . . . 124

3.3 Matrix Compression . . . 132

3.3.1 Compressing Matrices for Specific Populations . . . 138

3.4 Explicit Harvesting Models for Each Population . . . 151

3.5 Estimation of Soassararou Adult Reproduction Function Dependent on Non-lethal Harvesting . . . 153

3.6 Estimation of Soassararou and Nipuni Harvesting Rates with Constant Harvesting Intensity . . . 159

3.7 Conclusions and Discussion . . . 168

Bibliography **171**

Appendices **187**

A Index Values and Confidence Intervals for Sobol Sensitivity Analyses . . . 188

Vita **196**

List of Tables

2.1 Estimates for the number of individuals in each category listed for years 2013-2018. *Italicized* values are numbers estimated by extrapolating from a different year, whereas **bolded** values are numbers that we estimated by information within the same year. All other numbers are actual reported data. Numbers in blue are data used directly in parameter estimation in sections 2.4.1 and 2.4.2. Sources: [1]National Survey on Drug Use and Health [98, 101, 102], [2]Controlled Substance Monitoring Database Program [85], [3]Prescription Drug Overdose Program Report/Tennessee's Annual Overdose Report [84, 86]. 37

2.2 The following table gives estimates for the number of individuals prescribed opioids each quarter in the years 2013-2018. **Bolded** values are numbers that we estimated by information within the same year. All other numbers are actual reported data. Numbers in blue are data used directly in parameter estimation. Source: [3] Prescription Drug Overdose Program Report/Tennessee's Annual Overdose Report [84, 86]. 45

2.3 Parameter values calculated from data and assumed. 47

2.4 Parameters values assumed prior to parameter estimation process. 60

2.5 Parameter bounds for parameter estimation. 61

2.6 This table displays the values of the parameters that were estimated with our model from Case 1, in which the prescribing rate, α, is a linear function of time and the prescription opioid overdose death rate, μ_A, is constant. With the estimated values for $\tilde{m}, \tilde{b}$, and $\tilde{c}$, the time-dependent parameter α starts at 0.292 in 2013 and decreases to 0.192 by 2019. 67

2.7 This table displays the values of the parameters that were estimated with our model from Case 2, in which both the prescribing rate, α, and the prescription opioid overdose death rate, μ_A, are linear functions of time. With the estimated values for $\tilde{m}, \tilde{b}$, and $\tilde{c}$, the time-dependent parameter α starts at 0.291 in 2013 and decreases to 0.192 by 2019 and with the estimated values of $\tilde{d}$ and $\tilde{e}$, the time-dependent parameter, μ_A, starts at 0.00883 in 2013 and increases to 0.0147 by 2019. 71

2.8 This table displays the values of the parameters that were estimated with our model from Case 3, in which the prescribing rate, α, is a piecewise linear function of time and the prescription opioid overdose death rate, μ_A, is constant. With the estimated values for $\tilde{m}, \tilde{b}$, and $\tilde{c}$, the time-dependent parameter α starts at 0.275 in 2013 and decreases to 0.178 by 2019. 75

2.9 This table displays the values of the parameters that were estimated with our model from Case 4, in which the prescribing rate, α, is a piecewise linear function of time and the prescription opioid overdose death rate, μ_A, is a linear function of time. With the estimated values for $\tilde{m}, \tilde{b}$, and $\tilde{c}$, the time-dependent parameter α starts at 0.270 in 2013 and decreases to 0.178 by 2019 and the time-dependent parameter, μ_A, starts at 0.00883 in 2013 and increases to 0.0147 by 2019 from estimated inputs $\tilde{d}$ and $\tilde{e}$. 79

2.10 Range of values for each parameter used for sensitivity analysis in the α piecewise linear, μ_A linear case, which are $\pm 50\%$ of the baseline values found in Table 2.4 (excluding the value of μ_A) and Table 2.9. The exception to the $\pm 50\%$ range is explained above for $\tilde{m}$, $\tilde{b}$, and $\tilde{c}$. 98

2.11 Results from LHS/PRCC sensitivity analysis of the size of the prescription opioid addicted (A) class at the beginning of 2019 for the α piecewise linear, μ_A linear case run from 2013-2019 with 800 samples. 100

2.12 Results of LHS/PRCC sensitivity analysis of the size of the heroin/fentanyl addicted (H) class at the beginning of 2019 for the α piecewise linear, μ_A linear case run from 2013-2019 with 800 samples. 101

2.13 Range of values for each parameter used for management scenario sensitivity analysis in the α piecewise linear, μ_A linear case, which are $\pm 50\%$ of the baseline values found in Table 2.4 (except μ_A) and Table 2.9 with the exception of $\tilde{g}$ and $\tilde{h}$, which are chosen specifically due to their effect on time-dependent parameters α and μ_A. 107

2.14 Results from LHS/PRCC sensitivity analysis of the size of the prescription opioid addicted class at the beginning of 2023 for the α piecewise linear, μ_A linear case run from 2020-2023 with 700 samples. 108

2.15 Results of LHS/PRCC sensitivity analysis of the size of the heroin/fentanyl addicted class at the beginning of 2023 for the alpha piecewise linear case run from 2020-2023 with 700 samples. 109

2.16 Effect on size of A and H classes at the beginning of 2023 from increasing ζ and ν at the beginning of 2020 and the effect on the total number of overdoses in the time period from 2020-2023. The baseline values for the parameters are listed in the first row. 111

2.17 Effect on size of A and H classes at the beginning of 2023 from decreasing σ at the beginning of 2020 and the effect on the total number of overdoses in the time period 2020-2023. The baseline value for σ is listed in the first row. 112

2.18 Effect on size of A and H classes at the beginning of 2023 from decreasing $\theta_1, \theta_2, \theta_3$ at the beginning of 2020 and the effect on the total number of overdoses over the time period 2020-2023. The baseline values for the parameters are listed in the first row. 113

2.19 Effect on size of A and H classes at the beginning of 2023 from decreasing θ_3 only at the beginning of 2020 and the effect on the total number of overdoses over the time period 2020-2023. The baseline values for θ_3 is listed in the first row. 114

2.20 Effect on size of A and H classes at the beginning of 2023 from decreasing α at the beginning of 2020 to reach 25% or 50% of its baseline value in 2023. The baseline value for g is listed in the first row. 115

2.21 Effect on size of A and H classes at the beginning of 2023 from decreasing ε at the beginning of 2020 and the effect on the total number of overdoses in the time period 2020-2023. The baseline value for ε is listed in the first row. 116

2.22 Effect on the total number of overdose deaths from 2020-2023 from decreasing μ_H and μ_A at the beginning of 2020 to reach 25% or 50% of their baseline values in 2023. The baseline values for the overdose rates are listed in the first row. 117

3.1 Events that occur each month for *K. Senegelensis* in Benin. 123

3.2 Rates for the Nipuni population. 139

3.3 Nipuni compressed values with prop1 representing the proportion of adult 1's out of all adults in the stable-stage distribution and prop2 representing the proportion of the adults 2's out of all adults in the stable stage distribution. 140

3.4 Rates for the Barabon population. 141

3.5 Barabon compressed values with prop1 representing the proportion of adult 1's out of all adults in the stable stage distribution and prop2 representing the proportion of adult 2's out of all adults in the stable stage distribution. . 142

3.6 Rates for the Soassararou population. 144

3.7 Soassararou population compressed values where m_2 represents the sum of probabilities of staying in the AD1 class and m_3 represents the sum of probabilities of staying in the AD2 class. 147

3.8 Rates for the Nigoussourou population. 149

3.9 Nigoussourou population compressed values where m_2 represents the sum of probabilities of staying in the AD1 class and m_3 represents the sum of probabilities of staying in the AD2 class. 150

3.10 Rates for Nipuni harvesting model using rate information from Tables 3.2 and 3.3. 152

3.11 Rates for Barabon harvesting model using rate information from Tables 3.4 and 3.5. 154

3.12 Rates for Soassararou harvesting model using rate information from Tables 3.6 and 3.7. 154
3.13 Soassararou 2005-2007 observed data used in parameter estimation process. . 162
3.14 Bounds for Soassararou harvesting model rates in parameter estimation process. 162
3.15 Rates for Soassararou harvesting model with **bold** rates determined from parameter estimation process. 164
3.16 Bounds for Nipuni harvesting model rate in parameter estimation process. . 166
3.17 Rates for Nipuni harvesting model with the **bold** rate determined from parameter estimation process. 168
3.18 Values of the dominant eigenvalue, λ_1, and the damping ratio, $\frac{\lambda_1}{|\lambda_2|}$ for the harvested Soassararou and Nipuni populations. 168
19 Sensitivity of the susceptible class at the beginning of 2019 to each of the parameters with corresponding confidence intervals listed. 188
20 Sensitivity of the prescription opioid user class at the beginning of 2019 to each of the parameters with corresponding confidence intervals listed. 189
21 Sensitivity of the prescription opioid addicted class at the beginning of 2019 to each of the parameters with corresponding confidence intervals listed. . . . 190
22 Sensitivity of the heroin/fentanyl addicted class at the beginning of 2019 to each of the parameters with corresponding confidence intervals listed. 191
23 Sensitivity of the stably recovered class at the beginning of 2019 to each of the parameters with corresponding confidence intervals listed. 192
24 Sensitivity of the susceptible class at the beginning of 2023 to each of the parameters with corresponding confidence intervals listed. 193
25 Sensitivity of the prescription opioid user class at the beginning of 2023 to each of the parameters with corresponding confidence intervals listed. 194
26 Sensitivity of the prescription opioid addicted class at the beginning of 2023 to each of the parameters with corresponding confidence intervals listed. . . . 194
27 Sensitivity of the heroin/fentanyl addicted class at the beginning of 2023 to each of the parameters with corresponding confidence intervals listed. 195

28 Sensitivity of the stably recovered class at the beginning of 2023 to each of the parameters with corresponding confidence intervals listed. 195

List of Figures

2.1 Schematic diagram for our model which displays potential transitions in and out of compartments of individuals. 20

2.2 Model simulation fit to data for the α linear, μ_A constant model. This figure includes the fit to yearly prescription opioid user data, quarterly prescription opioid data, yearly prescription opioid addict data, yearly prescription opioid addict overdose death data, yearly heroin/fentanyl addict data, and yearly heroin/fentanyl overdose death data. 68

2.3 Numerical simulation for each of the population classes with parameters from Table 2.6 for the α linear, μ_A constant case. 69

2.4 Model simulation fit to data for the α linear, μ_A linear model. This figure includes the fit to yearly prescription opioid user data, quarterly prescription opioid data, yearly prescription opioid addict data, yearly prescription opioid addict overdose death data, yearly heroin/fentanyl addict data, and yearly heroin/fentanyl overdose death data. 72

2.5 Numerical simulation for each of the population classes with parameters from Table 2.7 for the α linear, μ_A linear case. 73

2.6 Model simulation fit to data for the α piecewise linear, μ_A constant model. This figure includes the fit to yearly prescription opioid user data, quarterly prescription opioid data, yearly prescription opioid addict data, yearly prescription opioid addict overdose death data, yearly heroin/fentanyl addict data, and yearly heroin/fentanyl overdose death data. 76

2.7 Numerical simulation for each of the population classes with parameters from Table 2.8 for the α piecewise linear, μ_A constant case. 77

2.8 Model simulation fit to data for the α piecewise linear, μ_A linear model. This figure includes the fit to yearly prescription opioid user data, quarterly prescription opioid data, yearly prescription opioid addict data, yearly prescription opioid addict overdose death data, yearly heroin/fentanyl addict data, and yearly heroin/fentanyl overdose death data. 80
2.9 Numerical simulation for each of the population classes with parameters from Table 2.9 for the α piecewise linear, μ_A linear case. 81
2.10 Numerical simulations for the addicted classes with parameters from Table 2.9 for the α piecewise linear, μ_A linear case with trajectories predicted for 2019-2022. The plot on the left shows the simulations of the prescription opioid addict class and the heroin/fentanyl addict class separately and the plot on the right shows the simulation for the proportion of total addicts. 89
2.11 Numerical simulations for overdose deaths with parameters from Table 2.9 for the α piecewise linear, μ_A linear case with trajectories predicted for 2019-2022. The plot on the left shows the simulations for the prescription opioid addict overdose deaths and the heroin/fentanyl addict overdose deaths separately and the figure on the right shows the total proportion of overdose deaths. . . 89
2.12 Numerical simulations for the susceptible, prescribed user, and stably recovered classes with parameters from Table 2.9 for the α piecewise linear, μ_A linear case with trajectories predicted for 2019-2022. 90
2.13 Numerical simulations for the addicted classes by putting a weight of 2 on the heroin data and letting α be piecewise linear and μ_A be linear. Trajectories are predicted for 2019-2022. The plot on the left shows the simulations of the prescription opioid addict class and the heroin/fentanyl addict class separately and the plot on the right shows the simulation for the proportion of total addicts. 92
2.14 Numerical simulations for the addicted classes by putting a weight of 5 on the heroin data (with α piecewise linear and μ_A linear). Trajectories are predicted for 2019-2022. The plot on the left shows the simulations of the prescription opioid addict class and the heroin/fentanyl addict class separately and the plot on the right shows the simulation for the proportion of total addicts. . . 92

2.15 Numerical simulations for the addicted classes by putting a weight of 20 on the heroin data (with α piecewise linear and μ_A linear). Trajectories are predicted for 2019-2022. The plot on the left shows the simulations of the prescription opioid addict class and the heroin/fentanyl addict class separately and the plot on the right shows the simulation for the proportion of total addicts. . . 93

2.16 Numerical simulations for the addicted classes by putting a weight of 2 on the heroin data *and* the heroin overdose data (with α piecewise linear and μ_A linear). Trajectories are predicted for 2019-2022. The plot on the left shows the simulations of the prescription opioid addict class and the heroin/fentanyl addict class separately and the plot on the right shows the simulation for the proportion of total addicts. 93

2.17 Monotonicity plots of A and H with respect to 22 parameters for the α piecewise linear, μ_A linear case. Each plot is formed by sampling one parameter across its range and holding all other parameters at their baseline values. 99

2.18 Sobol sensitivity results for the size each of the classes at the beginning of 2019 for the α piecewise linear, μ_A linear case run from 2013-2019 with 4,600,000 samples. 104

2.19 Monotonicity plots of A and H with respect to 15 parameters for the α piecewise linear, μ_A linear case. Each plot is formed by sampling one parameter across its range and holding all other parameters at their baseline values. 110

2.20 Sobol sensitivity results for the size of each of the classes at the beginning of 2023 for the α piecewise linear, μ_A linear case run from 2020-2023 with 3,800,000 samples. 111

2.21 This plot shows three different cases of the piecewise linear function for the prescribing rate, α, in which α either maintains its baseline value in 2023 (black), reaches a 25% reduction in the baseline value in 2023 (green), or reaches a 50% reduction in the baseline value in 2023 (red). For management strategy analysis from 2020-2023, these cases are used to determine the effect that decreasing α has on the size of the A and H classes in 2023 and the total overdose deaths from 2020-2023. Results are shown in Table 2.20. 115

2.22 This plot shows three different cases of the function for the prescription opioid overdose death rate, μ_A, in which μ_A either maintains its baseline value in 2023 (black), reaches a 25% reduction in the baseline value in 2023 (green), or reaches a 50% reduction in the baseline value in 2023 (red). For management strategy analysis from 2020-2023, these cases are used to determine the combined effect that decreasing μ_A and μ_H have on the total overdose deaths from 2020-2023. Results are shown in Table 2.22. 117

3.1 This provides a summary of the order of events in each season for *K. Senegelensis* in Benin where in year k, the dry season goes from $2k$ to $2k+1$ and the we season goes from $2k+1$ to $2k+2$. 129

3.2 The reproduction function, $\phi_A(h_N)$, for the Soassararou population representing the average number of seedlings produced from an adult individual as a function of average proportion of foliage pruned per adult individual. When all of the foliage is removed at a harvesting level of 1, the seedling production is very close to 0 as would be expected. 160

3.3 Comparison of Soassararou harvested model simulations to Soassararou observed data during fitting process for Soassararou rates. 165

3.4 Comparison of Nipuni harvested model simulations to Soassararou observed data during fitting process for Nipuni harvesting rate. 167

Chapter 1

Introduction

Models strongly connected to data can be valuable in demonstrating dynamics in biological scenarios and in suggesting management strategies. In this dissertation, two data-driven models are developed and explore management strategies for the corresponding populations. The first model is continuous in time with a system of ordinary differential equations, representing the heroin epidemic, and the second model is discrete in time with matrices and size structure for the harvesting of forests. Parameter estimation tools are used with data in both models. Sensitivity analysis using Sobol indices [57, 90] and Latin Hypercube Sampling with Partial Rank Correlation Coefficients [72] measure the impact of parameters on outcomes.

In the model formulated to better understand the opioid epidemic, which highlights the role heroin and fentanyl plays, we view addiction as a disease and utilize a susceptible-infected-recovered (SIR) type model consisting of five population subgroups based on opioid use. This is written as a system of ordinary differential equations and is analyzed to determine the existence of a unique solution, non-negativity of solutions from non-negative initial conditions, and the basic reproduction number. We apply our model specifically to the state of Tennessee due to alarming prescribing rates and overdose deaths and utilize data from 2013-2018 [22, 98, 101, 102, 84, 86, 85]. Much of the data we use has to be interpreted and properly transformed in the context of model assumptions in order to fit to model variables and parameters. We incorporate time-dependent parameters based on information from the data and use Ordinary Least Squares to estimate parameters. Four

different models with time-dependent parameters are compared to data and the best model choice is determined by analyzing the results from Akaike Information Criterion. From the best choice model, we predict a daunting trajectory of the epidemic until 2022 where the total number of addicts and overdose deaths increases from here on out. By performing both Partial Rank Correlation Coefficient and Sobol sensitivity analyses, we are able to measure the sensitivity of the size of the opioid addicted classes at the beginning of 2019 to each of the parameters. Sensitivity analyses are run again from 2020-2023 to determine the effects parameters had on the addicted classes at the beginning of 2023, as well. Various management scenarios are examined in detail to determine the exact effect changing a certain parameter (or multiple simultaneously) would have on the number of addicted individuals and overdose deaths over these next 3 years. With practicality in mind, only the parameters that are controllable are explored. The results from the basic reproduction number, simulated solutions and trajectories, and management scenarios all intersect and support one another.

For the work on harvesting, we have a seasonal model expressed as a system of difference equations based on various sizes of the tree species and certain order of events that occur in each season. In previous work, a 5-stage population projection matrix model was developed in which there were two adult classes [44]. It is difficult to differentiate between these two adult classes while harvesting which motivated us to have only one adult class in our model [45]. Therefore, in order to use some baseline vital rates from [44] in our model, we compress the population projection matrices to 4 classes. We again utilize ordinary least squares for estimating the remaining vital rates and harvesting levels in various populations of *K. Senegelensis*, which is informed by data from direct observations in the field. We also use generalized linear modeling to find the form of the reproduction function for the Soassararou population, again using observed data. Finally, we compare eigenvalues of specific populations based on their estimated rates.

This work aims to explore practical measures for topics in two different areas umbrellaed under mathematical biology: public health and ecology. Through mathematical modeling driven by real-world data, similar tools are used to shed light on the heartbreaking reality that is the opioid epidemic and the use of environmental resources that individuals depend on for their livelihood.

Chapter 2

Modeling the Heroin and Fentanyl Epidemic

2.1 Background

The misuse of opioids, including prescription pain relievers, heroin, and synthetic opioids (such as fentanyl) is rampant in today's society [32]. The opioid crisis was declared a public health emergency in October 2017 by the United States Department of Health and Human Services [115]. Opioids have become increasingly involved in drug overdose deaths and in 2016, they were involved in 66% of drug overdose deaths [20, 116]. This was a 21% increase from 2015 and between 2014 and 2015, there was an 11% increase in the number of overdose deaths involving opioids. There were more drug overdose deaths involving opioids in 2016 (rate of 13.1 people per 100,000 at the national level) than motor vehicle deaths (rate of 12 people per 100,000) [26]. It was estimated that the total economic cost of prescription opioid dependence, abuse, and overdoses in 2013 alone was $78.5 billion [40]. Due to the health risks of the addicted individuals, public health concerns, the number of overdose deaths, and the economic burden, this is a critical issue.

A large portion of opioids consist of prescription pain relievers which are either natural (e.g. morphine and codeine), semi-synthetic (e.g. oxycodone, hydrocodone, oxymorphone), or synthetic (e.g. fentanyl, tramadol) [106]. From 1991 to 2011, there was a near tripling of prescriptions that pharmacies distributed [82]. This was in part due to a number of new

opioids that were approved by the FDA for use, such as OxyContin, Actiq, Fentora, and Onsolis (fentanyl), in addition to other unapproved opioid products for pain management [119]. Moreover, in 1995 the American Pain Society stated that pain was being under-treated in doctor offices and hospitals, and consequently, created guidelines for the improvement for pain assessment for acute and cancer cases. This included the recording of pain levels such as on a vital signs sheet [3]. In 2000, the Joint Commission required physicians to accept and respect the self-reporting of pain by patients. Therefore, by the early 2000s, drug manufacturers funded publications and physicians to support opioid use for pain control [71].

A national survey estimated there were 11.5 million individuals of 12 years of age or older in the United States that experienced pain reliever misuse in 2016 [100]. In this survey, misuse was defined as taking the prescription at a higher dose, more frequently or longer than prescribed, taking someone else's medication, or any other way not directed by a doctor [18]. Misuse of prescription pain relievers occurs for a variety of reasons and the same survey asked individuals who reported prescription pain reliever misuse to give the reason and the source for their most recent misuse [100]. The most prominent responses were to relieve physical pain, to feel good or get high, and to relax or relieve tension. The largest source was from friends/relatives or from a healthcare provider, followed by given a prescription or stolen from a health care provider. Options for treatment of opioid addiction involve medications such as buprenorphine, methadone, and naltrexone, in combination with counseling and behavioral therapies [96]. Women who take prescription opioids during pregnancy put their babies at risk for neonatal abstinence syndrome in which the drug is passed along to the baby, resulting in dependency and thus, withdrawal symptoms upon birth [21].

The misuse of prescription pain relievers has led some individuals to initiate heroin use. According to the National Survey of Drug Use and Health (NSDUH) survey information from 2002-2011, nearly 80% of heroin users reported non-medical prescription pain reliever use prior to their heroin use [78]. Here, non-medical prescription use is defined as taking prescriptions that were not prescribed to the user directly or used only for the resulting feelings. In fact, those who had prior non-medical prescription pain reliever use were 19 times more likely to initiate heroin use than those without prior use. This could in part

be due to the higher availability of heroin in recent years at a lower cost than alternative opioids [82]. Moreover, approximately 3.6 percent of non-medical prescription pain reliever users began using heroin within 5 years of their first opioid; although a small percentage, this is a significant number of individuals given the magnitude of opioid addiction [78]. In 2010, an abuse-deterrent formulation of the commonly abused prescription opioid OxyContin was released that made abuse through injection and inhalation more challenging [29, 30]. Although done with the intent of reducing opioid abuse, the study showed that many individuals switched to other drugs instead; 70% of these individuals transitioned to heroin use. One study of young adults ages 18-25 concluded that among many factors including race, education status, martial status, and other drug use, the use of non-prescribed opioid pain relievers in the past year was the biggest indicator of an individual using heroin in the past month, past year, or in their lifetime [63].

Comparing NSDUH data from 2002-2004 and 2008-2010, the average yearly rates of past year heroin use increased among non-medical opioid users, but heroin use stayed static for those who reported no non-medical use of opioids [64]. The highest rate of heroin use was among individuals with past year non-medical use of opioids ranging between 100 and 365 days of use. In the 1960's, heroin users were composed mainly of younger, nonwhite men in urban areas with their initial opioid being heroin, but in recent decades, this trend has shifted to older, white, rural and suburban men and women with their initial opioid being a prescription [31]. There is no shortage of opioids with the availability of legal prescription medication, which has made a significant proportion of society susceptible to misuse and addiction to opioids, including heroin.

Heroin is a highly-addictive illicit drug classified as an opioid and comes in the form of a white or brown powder or as a black substance resembling roofing tar [79, 80]. The drug is injected, sniffed, snorted or smoked and quickly enters the brain to bind to opioid receptors. It provides the user with feelings of euphoria, in addition to physical effects such as heavy feelings in the arms and legs, dry mouth, and sometimes nausea and vomiting. There are short and long term negative effects on the body for using the drug, and consequently, it is currently considered a schedule I drug, meaning that there is no approved medical use of heroin and there is a high likelihood for abuse [112, 79]. Addicted individuals have withdrawal

symptoms such as restlessness, diarrhea, vomiting, and cold flashes, along with cravings for the drug which makes stopping use of the drug very difficult [79]. Treatment options are the same as for prescription opioids [96, 79]. Heroin users build up a tolerance to the drug with repeated use and can overdose, in which their heart rate and breathing are slowed to a dangerous level without medical assistance [80, 79]. Due to built-up tolerance, the risk of overdose is high when individuals stop their use of the drug for a period of time (i.e. while in recovery or hospitalized) and return to use [32]. This is because they may return to the previous amount they were taking before, without knowing what their body can currently tolerate.

The effects of heroin, however, extend further than just the specific individual using the drug. Due to the sharing of needles and other equipment involved in the injection of heroin, the human immunodeficiency virus and the hepatitis C virus are more easily contracted as transmittance occurs through bodily fluids [80]. In addition, risky sexual behavior is heightened under the influence, so addicts have an increased risk of transmitting and contracting these viruses. Pregnant women who use heroin also put their babies at risk of neonatal abstinence syndrome, similar to prescription opioids [21].

Fentanyl is a synthetic opioid that is made both pharmaceutically, mainly for the treatment of advanced cancer pain (comes in the form of oral lozenges, tablets, sprays or patches), and illicitly (comes in the form of powder or counterfeit tablets) [23, 117]. It is 50 times stronger than heroin and up to 100 times stronger than morphine, and has similar effects to these drugs such as relaxation, euphoria, pain relief, and nausea [118]. The drug is often found mixed into heroin to increase the effects of heroin, and the user may or may not be aware of this mixing. In 2013, there were 942 fentanyl submissions to the Drug Enforcement Administration (DEA) nationwide, and in 2014 there were 3,344; in this same time frame, there was a drastic spike in the number of synthetic opioid overdoses, including fentanyl, which leads to the belief that the fentanyl-involved overdose deaths increased due to illicitly-manufactured fentanyl rather than that prescribed, as mentioned before [20, 117, 14]. Other reports hypothesize this, as well [84, 50].

A national survey estimated that out of the U.S. population of individuals of 12 years of age or older, 948,000 were heroin users in 2016, although this number may include under-reporting [100]. There were an estimated 13,219 overdose deaths involving heroin in 2016, a more than six-fold increase from the year 2002, despite there being roughly half as many heroin users in 2002 [99]. There was a drastic increase in the number of opioid overdose deaths involving heroin around 2010 and steadily increased to 2016 [20]. In recent years, there has been a trend of lacing heroin with fentanyl and therefore, users are unaware of the purity of the heroin they obtain [19, 32, 122]. There was a sharp increase in the number of opioid overdose deaths involving synthetic opioids, which includes fentanyl, around 2013, although death certificate data does not distinguish between prescription and illicitly manufactured fentanyl [20]. In addition, there was a drastic increase in fentanyl reports nationwide from 2014-2017 and reports suggest that the increase in overdoses involving fentanyl in this time period can mostly be attributed to illicitly manufactured fentanyl [116, 84, 50, 117, 14].

Heroin was first formulated in a hospital in 1874, but production on a commercial level did not begin until 1898, when the Bayer Company in Germany marketed and sold the new drug [109]. Prescription heroin was deemed helpful for treating bronchitis, asthma and tuberculosis, but near the turn of the century, the dangers of the drug were starting to be revealed, such as its potential for addiction. In 1920, the American Medical Association stated that heroin should not be manufactured, sold, or prescribed in the United States, and in combination with the amount of crime resulting from heroin use, a law was passed in 1924 prohibiting crude opium imports with the intention of heroin production. With the start of World War II, traffickers diluted the drug more and more, due to tighter border controls and fewer supplies entering the country. After that, heroin usage continued at varying levels and the price and purity levels have fluctuated throughout the years.

2.1.1 Application to Tennessee

The U.S. opioid prescription rate per capita from 2006-2017 was at its peak in 2012 with a rate of 81.3 prescriptions per 100 individuals [24]. Tennessee has been consistently above this number for that entire time period with the following rates for years 2006-2017: 124.8, 128.8, 132.9, 138.4, 140.0, 138.5, 136.1, 127.1, 121.3, 114.9, 107.5, and 94.4, respectively [22].

From its peak in Quarter 3 of 2014, the number of opioid prescribed individuals in the state decreased by 28% by Quarter 4 of 2018 [84]. There was a 300% increase from 2013 to 2016 of overdose deaths involving heroin in Tennessee, and in the same time period, there was a more than 450% increase in deaths involving fentanyl, mostly from illicitly manufactured fentanyl. From 2013-2017, there was over an 800% increase in overdose deaths involving fentanyl for Tennessee and a public health advisory was issued for the state in April 2017 regarding the potency and danger of the drug [86, 105]. Out of all drug overdose deaths in 2016, 18% involved fentanyl, up from 4.5% in 2013. Overall, opioid overdose deaths increased from 11.0 to 18.1 per 100,00 individuals from 2012 to 2016. In 2016, 80% of opioid overdose deaths involved multiple drugs, up from 63% in 2012. Due to these alarming statistics within the state of Tennessee, we apply our model specifically to this state, as we believe facing this problem on a smaller scale with less heterogeneity than at the national level is more informative.

Several policies have been implemented as a part of the effort to decrease prescription opioid availability and risk for addiction. The Controlled Substance Monitoring Database (CSMD) was established in 2002, which required health care professionals to submit data regarding the dispensing of controlled substances [35]. In 2012, the Tennessee Prescription Safety Act was passed that required prescribers of controlled substances to check the CSMD prior to prescribing at the beginning of a new treatment plan for certain substances, as well as inputting information about all prescriptions (strength, days of supply) into the database within 7 days of dispensing it [104]. If there is suspicion of diverting the opioids or any other illegal activity, then the CSMD must be checked, as well [35]. In 2013, policies regarding tamper-resistant prescription paper, as well as prescribing limitations to a 30-day supply and urine drug testing every 30 days for Schedule II drugs (high potential for abuse and dependence, such as oxycodone and fentanyl) were implemented. In 2014, regulations focused on chronic non-cancer pain [104]. These regulations required that prior to opioid prescribing, efforts should be made for trying alternative treatments and not automatically assuming an opioid patient should continue use because they were previously prescribed. At the initial stage of prescriptions, a limit of 4 doses a day was set, non-pain medical specialists should not prescribe methadone, and buprenorphine should not be prescribed

orally/sublingually for a chronic pain condition. For pain that is ongoing, opioid therapy should be implemented by only one prescriber and pharmacy, and the smallest effective dose should be used. Information on the policy from 2016 is discussed in Section 2.4.2, as we implement it directly in our analysis. In 2018, one part of the Governor's "TN Together" initiative limited initial prescriptions to a 3-day supply for up to 180 morphine milligram equivalents [107]. A new policy was passed in April 2019 that will be discussed in Section 2.5.4 as it is pertinent to our work with potential management strategies. Although these policies seemed to eventually have an effect on the supply of prescription opioids, they have not made a positive impact on overdose deaths which is an important goal in our work [84, 86, 85].

Meeting with various individuals in the community and attending community lectures enabled a broader understanding of the opioid crisis from various perspectives, particularly in the state of Tennessee. Sharon Davis' lecture on the "Science of Addiction" emphasized that addiction is a chronic brain disease and affects learning, judgement, decision making, stress, memory, and behavior [34]. Just like any other disease, it is preventable, treatable, changes individuals biologically (including a decreased brain metabolism) and if gone untreated, can last a lifetime. There is a lot of stigma for individuals with substance use disorder from the societal, institutional (hospitals, schools), and individual level that she argued should not exist, as it does not with other diseases. She emphasized a major problem with individuals leaving treatment and overdosing, since their tolerance decreased and they went back to the last dosage they were using prior to going into treatment [32]. Moreover, Hepatitic C has become a secondary epidemic due to those who are intraveneous drug users [80].

Davis pointed out that there are three factors for addiction: genetics, environmental, and accessibility. One study investigated how childhood experiences that include abuse, mental illness/substance abuse/criminal activity of a household member, or violence against the mother, are related to an increase in various health risk factors for the leading causes of death for adults [39]. One of these health risks is drug abuse and children exposed to 4 or more of the 7 childhood dysfunction categories had a 4- to 12- fold increase in this health risk (i.e. the higher the adverse childhood experience score, the higher the risk for addiction). James Choo, owner and director of Pain Consultants of East Tennessee spoke at the Science

Forum at the University of Tennessee, stating that the opioid crisis is a hallmark of deeper societal problems that are ignored [28]. He believes as a society we need to change the language that we use surrounding this issue: it started as a prescription drug epidemic, then it was the opioid crisis, then polysubstance abuse crisis, but now it is a trauma crisis. We need to get away from the stigma about pain and addiction and realize how closely linked to childhood trauma it is, as was discussed by Davis. He discussed how there has been an increase in the number of suicides linked with pain clinic closures, and rules and regulations that instill fear in opioid users. Some individuals are viewing Naloxone as a safety net and pushing their high up further than normal, an unintended consequence.

The Summit for Opioid Addiction and Response focused a lot on stigma, and how society needs to reduce that stigma since addiction is a chronic, relapsing brain disease and it is not a moral failing or a mind over matter situation [113]. Individuals are facing judgement and feeling limited when it comes to trying to get back into the workforce, schools, and the community. The conference called for a reduction in stigma so that individuals can be re-integrated healthfully in the community. Stigma, shame, and lack of knowledge of treatment/ability to find treatment are all barriers in individuals getting recovered. Since the supply of the drugs cannot be controlled, the demand is the current focus. However, a call was made for trauma to be addressed to understand why individuals are getting addicted in the first place (social causes) and therefore, prevention should be the focus of efforts, although it can be hard to measure. In other words, instead of chasing the drug, we should chase what is driving addiction. Another focus should be on harm reduction in which potential consequences (such as NAS, Hepatitis C, overdoses) are reduced and individuals are stabilized/helped with how to live with their chronic disease the best way possible. It's a matter of re-defining success of having a stable job and home, for example, instead of being completely drug-free. The curriculum in medical classes need to incorporate addiction, as doctors do not have the proper training despite the magnitude of the health problem.

Community recovery support groups are available, some of which are associated with churches, and most are based on a 12-step treatment program similar to the one used in Alcoholics Anonymous. Wil Cantrell, a pastor who oversees a recovery support group at his church, provided insight on the recovery end [128]. The groups are led by those who struggled

with substance use disorder themselves and are recovered. Individuals are encouraged to complete the program (usually several months) with the primary goal of getting clean, but then continue to come for a lifetime since the overall goal is to have a change in thinking and lifestyle. Cantrell discussed how addiction is a disease and has ripple effects to families and friends. In his experience, if addicts try to replace one drug with another, almost always they go back to their primary drug of choice; therefore, one of the goals of their group is to focus on lowering the *demand* of opioids and drugs in general, rather than the supply. He shared that a common way of thinking that addicts have is "drugs are not my problem, they are the solution." He discussed how the majority of the brain is subconscious and it takes several years of healthy ways of thinking to take over the subconscious. Attending a Narcotics Anonymous support group also helped provide insight on the struggles of those addicted [67]. Oftentimes individuals are using multiple drugs, and recovery meetings welcome all drug addicted individuals. Alcohol is a common "replacement" for their drug of choice but individuals often do not realize how that is also addictive and not a solution. Drugs are a response to trauma when individuals are not able to handle pain or life circumstances, but drugs subsequently create more trauma, as well.

The Metro Drug Coalition held an East Tennessee Opioid Conference that had several speakers [76]. One in five individuals have an increased risk of long-term opioid addiction with a 10-day prescription. The main drivers of drug use are: price, availability, public attitude, and perception of risk. When people are in recovery, they have time on their hands because they are used to spending that time getting drugs and using them, so it is a crucial time to focus on. The stages of change were discussed: anticontemplation in which individuals do not think they have a problem, pre-contemplation, contemplation, preparation, action, maintenance and relapse. Speakers also discussed how the success of recovery does not necessarily need to be measured by drug-free urine tests but rather whether individuals have a job, a home, a car, etc. A conference on Data, Modeling, and Policy Making to Address the Opioid Epidemic was held that discussed the need for data to be improved as there are many limitations. We need a better understanding of the exact paths that individuals take through the process of addiction, recovery, hospitalizations, overdoses, etc. to get a better handle on this problem [108].

Thanks to Sharon Davis, Laurie Meschke, Clea McNeely, and Matthew Harris of the University of Tennessee, Knoxville; Kelly Cooper of the University of Tennessee, Knoxville and Knox County Public Health Department; Wil Cantrell of Concord United Methodist Church; James Choo of Pain Consultants of East Tennessee; and the Knoxville Narcotics Anonymous Group for useful discussions, comments, and lectures on this topic. We would also like to acknowledge Nicholas Battista at The College of New Jersey and Leigh Pearcy at the University of Tennessee, Knoxville for their contributions to this topic. One of our goals is to gain a better understanding of the epidemic through mathematical modeling, and we next present some background on related previous models.

2.1.2 Previous Work

There have been several models focusing on heroin addiction. Most of them were motivated by the White and Comiskey system of ordinary differential equations (ODEs) with three compartments representing susceptibles of age 15-64, drug users not in treatment, and drug users in treatment [127]. In this model, individuals in treatment for drug use could relapse to drug use, complete treatment and be immune to drug use for the remainder of the modeling time period, or die from that class. Their model took the approach of modeling drug use similar to the way diseases are modeled. Therefore, the basic reproduction number, $\mathscr{R}_0$, was calculated and deemed most sensitive to the rate of individuals in the susceptible class becoming drug users; therefore, prevention was deemed more important than treatment for reducing drug use.

The White and Comiskey model was modified later on in several different ways, one of which considered a non-constant population [124]. Liu and Zhang [69] incorporated a relapse distribution in which there was a non-constant time to relapse. They formulated a delay-differential equation, and also removed the assumption that the population was constant. Their conclusions about the sensitivity of $\mathscr{R}_0$ to certain parameters were in line with those from White and Comiskey. Using the same three compartments, another model was formulated with the idea of the relapse rate relying on the length of time the individual had been undergoing treatment [37]. This coupled ordinary differential equation-partial differential equation (ODE-PDE) model assumed that susceptibles could only become

addicted via interaction with heroin users not undergoing treatment. Prevention was deemed more important than treatment, yet again. Fang, Li, Martcheva, and Caialso [38] also modeled heroin addiction allowing susceptibility of becoming a drug user to depend on age, resulting in a coupled ODE-PDE model. A non-autonomous version of the White and Comiskey model included a distributed time delay for becoming a drug user along with both the parameters and the total high-risk population size being time-dependent [92]. From this, an autonomous model was developed incorporating the distributed time delay, which was converted into a discrete model [1].

A three compartment model consisting of susceptibles, users not in treatment, and those in treatment, assumed that those not in treatment could not recover and return to being susceptible, and that it took two contacts with a drug user to become addicted, resulting in a nonlinear incidence rate [70]. A deviation from the three compartmental model was done that included a fourth compartment which consisted of individuals who successfully recovered from their heroin use, whether through deciding to stop use by themselves or via treatment measures [125]. The treatment of heroin users was limited by the availability of treatment facilities and resources and therefore, a saturated function for treatment was incorporated. Sensitivity analysis suggested that the contact rate with heroin users, the relapsing rate of individuals in treatment, and the saturation of heroin users in the community were most important to decrease heroin users not in treatment.

Another ODE system with non-medical prescription opioid users, individuals with prescription opioid use disorder, and illicit opioid users predicted the trajectory of the opioid crisis from 2016-2025, particularly regarding opioid overdose deaths [27]. This work compared 4 different scenarios of decreasing the incidence rate of non-medical prescription opioid use each year to see the effects on the total number of overdoses. With a decrease of 11.3% in the incidence rate for non-medical prescription opioid use (i.e. more prevention), the authors projected a 5.3% decrease in the number of opioid overdose deaths, which seems low given the time frame and substantial decrease in the number of individuals misusing. Therefore, the authors make a call to policymakers that prevention alone is not enough and that treatment, harm reduction, and decreasing exposure to illicit opioids are vital.

Investigating the effects of policies on opioid overdose deaths, an ODE system with 12 compartments was formed consisting of various levels of pain and degrees of prescription opioid and heroin use/abuse, as well as treatment status [87]. The work analyzed 11 different policies, ranging from preventive measures taken to reduce addiction to those aimed at reducing the number of addicted cases already there, and compared the results to the outcomes without these measures. The policy with the greatest impact on reducing opioid overdose deaths over a 5 year period (2016-2020) and a 10-year period (2016-2025) was increasing naloxone availability and the policy impacting overdose deaths in a negative way was drug rescheduling (here, this meant more restrictive scheduling of the opioid and more restrictions on being able to obtain a refill so that 10% fewer individuals were able to obtain their refill).

Others have taken a completely different approach, specifically using agent-based modeling. Agar [2] developed an agent-based model, consisting of a world with 2,500 patches and 100 agents each assigned an experimentation value which defined how likely that individual was to experiment with heroin (depending on their interest in trying something new, their attitude toward illicit drug use, and their desire to follow societal rules). The model was able to track the number of heroin experimenting individuals over time with one patch selected at random to contain heroin in the beginning, the agent moving randomly, and the ability for individuals to obtain heroin. Individuals could obtain heroin from their original patch, from others who have experimented, or from another patch where the transferring of heroin between agents occurred. An agent-based model consisting of the interactions of customers, street and private dealers, brokers, homeless individuals, and police was formulated based on ethnographic data in order to reproduce the observed behavior of a heroin market in Denver, CO in the 90's and study its operation [58]. The model identified that increasing the number of street brokers increases both the amount of drugs sold and the role that private dealers play in the market. Another question answered was the influence that police "busts" had on the market: street seller deals decrease in the short-term but private deals increase, as brokers switch getting drugs from the street dealer to a private dealer. In the long-term, when street dealers are no longer incarcerated and return to dealing, they are unable to get back to their pre-"bust" transaction levels as the demand has now

shifted to other sellers. Therefore, the "busts" are not very effective, by simply incarcerating street dealers, and brokers should be targeted to be removed from the market instead. In [55], this model was reduced with the goal of maintaining the results of the statistical model, but focusing on simplifying customer interactions with the other agents. The authors took out explicit interactions and replaced them with probabilities of 5 different outcomes happening from distributions and regressions, which in turn allows a decreased amount of necessary information for future study of heroin market dynamics.

A statistical regression model was formulated which found that an increase of 10% in the per capita prescription opioid rate at the county level was related to a 0.56 percentage point decrease in the labor force participation rate (working or looking for work) and a 0.1 percentage point increase in the unemployment rate (looking for work) [54]. The idea here is that individuals seem to be leaving the labor force entirely due to prescription opioids, rather than being unemployed and searching.

We are not aware of any fentanyl addiction models in particular, although two statistical models were formulated to investigate spikes in overdose mortalities throughout the country beginning in 2014 [129]. The work suggested that the increased supply of illicit fentanyl in certain geographic locations was a factor in the increased overdose mortality and that exposure to the drug explains variation in the overdose increases across the country. We will formulate a model that connects the use of fentanyl and heroin within the opioid epidemic.

The motivation for our heroin/fentanyl model comes from a prescription opioid system of ODEs by Battista, Pearcy, and Strickland [6], consisting of four classes of the national population: susceptibles, prescribed users, addicts, and individiuals in treatment. Model parameters were estimated from literature and simulations were run with these parameters/parameter ranges to compare simulated opioid overdose deaths to actual opioid overdose deaths, providing evidence this model is realistic. The existence of an addiction-free equilibrium required that prescribed users cannot become addicted to their own prescriptions and that there are no secondary addictions that come from the accessibility to excess prescription drugs, which is unrealistic. However, in this hypothetical situation, $\mathscr{R}_0 < 1$, which strongly suggests that the epidemic could not be sustained without primary and secondary addiction through prescriptions. Sobol sensitivity analysis was performed to

investigate the sensitivity of the population classes at 10 years to each of the parameters individually and to higher-order interactions among the parameters. The addicted class at this time was most sensitive to the prescription completion rate and treatment entrance rate; high values for these rates were deemed essential in reducing the addicted population fraction when considering a range of values for several other parameters, as well. Among this set of other parameters that were varied, the rate that prescribed users move to addiction and the prescription rate are important to focus on for reducing addiction, the latter of which is easier to control than the former. Investigating four parameters that are somewhat feasible for control efforts, results showed that given our current prescription rate, in 10 years the addicted population can be decreased given certain rates of completing prescriptions, entering treatment, and completing treatment. Overall, attention should be given primarily to prescription completion and treatment entrance rates, then prescription rates, and finally, treatment completion rates.

The increase in the use of heroin and fentanyl and the rise in overdose deaths in recent years provides motivation to formulate a separate model with the goal of understanding the more complicated dynamics that arise among opioid addiction with the addition of these drugs to prescription opioid use. As exemplified previously, heroin and fentanyl play a significant role in the process of opioid addiction, recovery, and overdose deaths and so its inclusion provides a more accurate overall picture of the epidemic. It is crucial to take a more detailed look at the increasing problem of overdose deaths involving opioids [20]. In 2016, synthetic opioids, which includes fentanyl, became the number one drug involved in overdose deaths in the country and thus are vital to include [65]. Previous models have not incorporated the connection between prescription opioid addiction with heroin and fentanyl addiction explicitly. Even though there are many factors that play a role in population size, susceptibility to drug use, relapse time, and other parts of the drug-using process, we consider individuals in each of the classes to be homogeneous, for simplicity of a starting model. Moreover, although there have been theoretical models on heroin formulated in the past, we offer a data-driven model due to the extensiveness of addiction and overdoses in society today. In addition, data is now available that explicitly shows drastic increases in

overdoses involving opioids in recent years and an overall increase in heroin use and illicit fentanyl presence. We utilize data from recent years to best inform our mathematical model.

To address this prevalent problem in today's society, we model the prescription opioid/heroin/fentanyl epidemic in order to understand the dynamics behind the epidemic and predict the trajectory of it. This model analyzes the epidemic since it has been established, which we believe is around 2012/2013; after this point, the number of prescriptions on the national level have dropped each year, resulting in fewer pills lying around, but leading to the use of other drugs such as heroin and fentanyl due to their lower cost and availability [20, 25, 82]. Given the sustained epidemic, we investigate possible management actions. This contrasts the prescription opioid-only model in [6] in which the focus was on the dynamics of the epidemic as it was ramping up. We identify important parameters relating to the reduction of prescription opioid/heroin/fentanyl addiction and overdoses. We have formulated a system of ordinary differential equations consisting of classes of individuals taking prescription opioids, addicted to prescription opioids, addicted to heroin and/or fentanyl, and stably recovered from addiction to any opioid, and analyzed it. Our overall goal is to explore how different management strategies may alter the epidemic trajectory; specifically, we investigate management strategies for decreasing prescription opioid, heroin, and fentanyl addiction, and overdose deaths, while still treating pain with prescriptions.

2.2 Model Formulation

To the extent of our knowledge, there have been no mathematical models incorporating both prescription opioid addiction and heroin/fentanyl addiction. Although terminology is not always clearly defined in the literature, such as opioid misuse, abuse, dependency, addiction and use disorder, we aim to focus on addiction only, where addiction to opioids is defined as having a pattern of continued non-medical use that is already, or could be, harmful [123]. We take opioid use disorder to fall in this categorization of addiction, due to the definition presented in [97] which includes sustained use even though there is interference with life

obligations. Our model consists of five population groups, represented as proportions of the entire population:

1. Susceptibles S: Individuals who are not taking prescribed opioids, nor using heroin or fentanyl.

2. Prescription opioid users P: Individuals who are prescribed opioids by a health care provider and take the opioids at a level that is not considered addicted. We note that individuals in this class could be misusing prescription opioids, but not at the level of addiction.

3. Prescription opioid addicts A: Individuals addicted to prescription opioids, but not using heroin or fentanyl, or are actively in treatment for prescription opioid addiction. For individuals who go to treatment for opioid addiction, they remain in this class for at least 4 weeks *after* being discharged from treatment; if they relapse within 4 weeks after treatment, they are still considered addicted and remain in this class for longer.

4. Heroin/fentanyl addicts H: This class is composed of individuals who are addicted to heroin or fentanyl, or are actively in treatment for heroin/fentanyl addiction. For individuals who go to treatment for heroin/fentanyl addiction, they remain in this class for at least 4 weeks *after* being discharged from treatment; if they relapse within 4 weeks after treatment, they are still considered addicted and remain in this class for longer. (We note that individuals in this class could be using other drugs or are addicted to opioids in addition to heroin or fentanyl, but they are addicted to at least one of these drugs).

5. Stably recovered individuals R: This class consists of individuals who completed treatment for prescription opioid or heroin/fentanyl addiction and did not relapse within 4 weeks *after* treatment, and therefore are considered in a "stable" recovery state.

Due to the highly addictive nature of heroin, we assume no casual use of the drug in our H class [79]. If an individual uses heroin at a level that it would be easy to stop using, they are better classified as a susceptible individual rather than a heroin addict, based on our definition of addiction. Similarly, we assume that individuals who are not prescribed fentanyl under the supervision of a health provider or use fentanyl outside of short-term,

carefully monitored settings are assumed to be addicted. We include illicit fentanyl users in the class of heroin users due to the potency of the drug, as those who transition to the H class are seeking a better high with both of these drugs (and a lower cost). In addition, a portion of those who overdose from the very powerful drug fentanyl are individuals who are using heroin that is laced with it; therefore, the use of fentanyl is oftentimes intertwined with the use of heroin [117]. There is much variability in the purity of heroin due to the lacing of the drug with fentanyl, and 1 in 5 overdose deaths have multiple drugs present so it is difficult to know the actual cause of death [20]. We believe it is difficult to separate the use of heroin and fentanyl until better data is available, so putting them in the same class is the most natural choice for a starting model. We take into account these complexities as best as possible with the information in literature.

Equation 2.1 displays our system of ODEs:

$$\begin{aligned}
\frac{\mathrm{d}S}{\mathrm{d}t} &= -\alpha S - \beta_A SA - \beta_P SP - \theta_1 SH + \varepsilon P + \mu(S+P+A+H+R) + \mu_A A + \mu_H H - \mu S \\
\frac{\mathrm{d}P}{\mathrm{d}t} &= \alpha S - \varepsilon P - \gamma P - \theta_2 PH - \mu P \\
\frac{\mathrm{d}A}{\mathrm{d}t} &= \gamma P + \sigma R\frac{A}{A+H+\omega} + \beta_A SA + \beta_P SP - \zeta A - \theta_3 AH - (\mu+\mu_A)A \\
\frac{\mathrm{d}H}{\mathrm{d}t} &= \theta_1 SH + \theta_2 PH + \theta_3 AH + \sigma R\frac{H}{A+H+\omega} - \nu H - (\mu+\mu_H)H \\
\frac{\mathrm{d}R}{\mathrm{d}t} &= \zeta A + \nu H - \sigma R\frac{A}{A+H+\omega} - \sigma R\frac{H}{A+H+\omega} - \mu R
\end{aligned} \tag{2.1}$$

with

$$S + P + A + H + R = 1.$$

We denote the initial conditions $S(0) = S_0$, $P(0) = P_0$, $A(0) = A_0$, $H(0) = H_0$, and $R(0) = R_0$, which are non-negative since they are proportions. Note that the sum of the five ODEs gives the derivative of the total population to be 0. We assume that these five compartments sum to one, so that the population is of constant size, i.e. the total death rate is equal to the incoming rate for the susceptible class since we believe overdose deaths will not significantly alter our population size. We impose this since we are working with a short time frame and believe the population will not change very much over this time period.

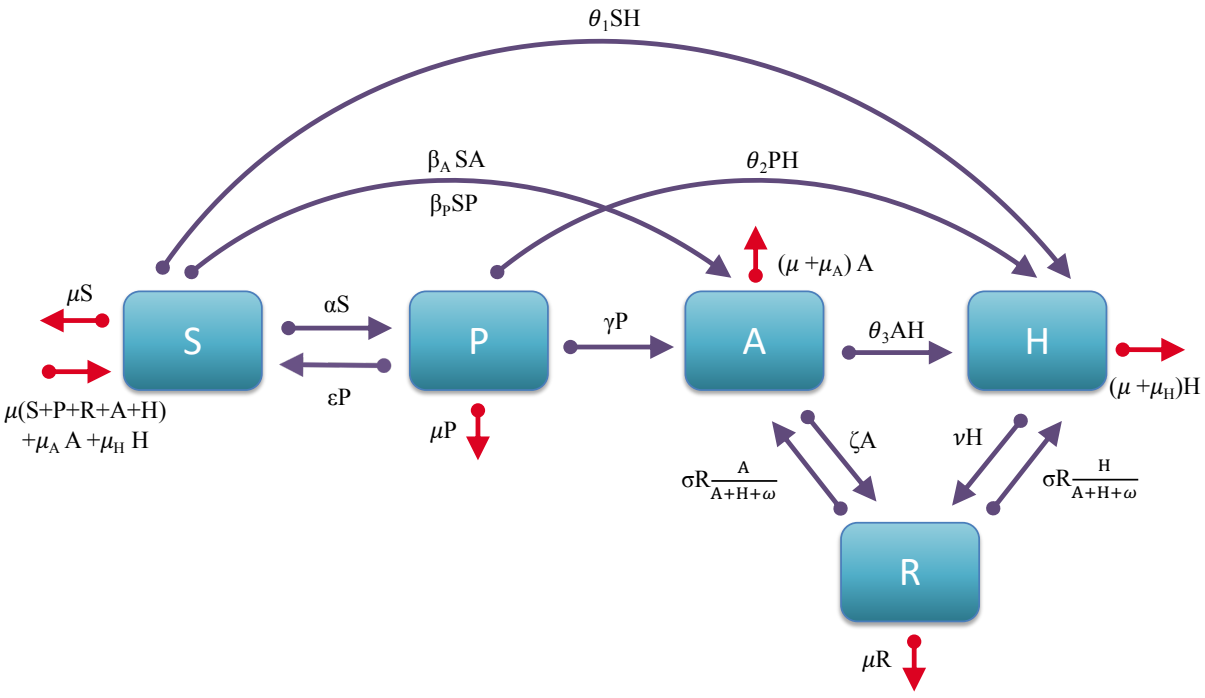


Figure 2.1: Schematic diagram for our model which displays potential transitions in and out of compartments of individuals.

Since the birth and death rate of the susceptible class, μS, is the same, the first equation in (2.1) simplifies to:

$$\frac{\mathrm{d}S}{\mathrm{d}t} = -\alpha S - \beta_A SA - \beta_P SP - \theta_1 SH + \varepsilon P + \mu(P+R) + (\mu+\mu_A)A + (\mu+\mu_H)H. \tag{2.2}$$

This compartmental model is represented by the flow diagram shown in Figure 2.1 with each arrow representing either the deterministic transition rate between one class to another or birth/death.

The parameters involved in this model are described below:

- αS: rate at which susceptible individuals are prescribed opioids (1/year)
- $\beta_A SA$: rate at which susceptible individuals become addicted to opioids by black market drugs or interaction with other prescription opioid addicts (1/year)

- $\beta_P SP$: rate at which susceptible individuals obtain extra prescription opioids by interaction with prescribed users and become addicted (1/year)

- $\theta_1 SH$: rate at which susceptible individuals become addicted to heroin or fentanyl by black market availability or interaction with other heroin or fentanyl addicts (1/year)

- εP: rate at which individuals return to the susceptible class after being prescribed opioids and not developing an addiction (1/year)

- $\mu S, \mu P, \mu A, \mu H, \mu R$: natural death rates (1/year)

- $\mu_A A$: overdose death rate for prescription opioids addicts (1/year)

- $\mu_H H$: overdose death rate for heroin or fentanyl addicts (1/year)

- γP: rate at which prescribed opioid users become addicted to prescription opioids (1/year)

- $\theta_2 PH$: rate at which prescribed opioid users become addicted to heroin or fentanyl by black market availability or interaction with other heroin or fentanyl addicts (1/year)

- $\sigma R \frac{A}{A+H+\omega}$: rate at which individuals transition from the recovered class into the prescription opioid addicted class. This is proportional to the approximate proportion of individuals in the recovered class that came from A that are relapsing back to that class. Even though we do not know where individuals came from originally, we make the assumption that individuals go back to their primary drug of choice (the reason they entered treatment), so they relapse back approximately proportional to where they came from. We include a perturbation term ω in the denominator in the case that A and H are both 0, such as in the addiction-free case. (1/year)

- ζA: rate at which addicted prescription opioid users stably recover (1/year)

- $\theta_3 AH$: rate at which the prescription opioid addicted population becomes addicted to heroin or fentanyl by black market availability or interaction with other heroin or fentanyl addicts (1/year)

- $\sigma R\frac{H}{A+H+\omega}$: rate at which individuals transition from the recovered class into the heroin/fentanyl addicted class. This is proportional to the approximate proportion of individuals in the recovered class that came from H that are relapsing back to that class. Even though we do not know where individuals came from originally, we make the assumption that individuals go back to their primary drug of choice (the reason they entered treatment), so they relapse back approximately proportional to where they came from. We include a perturbation term ω in the denominator in the case that A and H are both 0, such as in the addiction-free case. (1/year)

- νH: rate at which heroin or fentanyl addicts stably recover (1/year)

We note that one way individuals get addicted is via the black market, and although we do not have drug sellers directly involved in the model nor do they have to be addicts themselves, we do have interaction terms for addiction. This comes from the idea that the more addicted individuals there are, the more drug sellers there need to be and the general availability of the drugs is greater, so addicted individuals serve as a proxy for sellers. Thus, the more addicted individuals there are, there greater the exposure there is to the drug via the black market leading to addiction and the interaction terms $\beta_A AS$, $\theta_1 SH$, $\theta_2 PH$, and $\theta_3 AH$ represent the fact that the number of sellers and the amount of available drugs increase with A and H.

Although treatment for addiction is an enormous problem in and of itself since there is limited success (i.e. low recovery rates, discussed in detail later), we are acknowledging treatments as a part of recovery in our model, but do not go into specifics for this first model. We are classifying overdoses to mean death by opioid overdose (i.e. not from secondary factors or long term effects of using the drug). Although overdose death data includes both accidental and non-accidental deaths (i.e. suicide, assault), we assume here that if an individual died from an overdose-related death, they were addicted [85]. We also note the fact that Naloxone, an overdose-reversing medication, has saved individuals from overdoses, but we are focused on actual deaths [80].

In [126], 10% of the prescription opioid addicts they followed up with post-treatment in their study had used heroin at least five times in the previous year, which demonstrates

the importance of keeping the transitions between these two classes as possibilities. The definition of our recovered class allows the transition of individuals who recovered from one drug to initiate use of the other. It also distinguishes between the two very different groups of recovered individuals: those with a high chance of relapse (e.g. recently finished treatment) stay in A or H for at least four weeks post-treatment in our model and those with a much lower chance of relapse (e.g. successfully finished treatment in the past and has remained free of addiction for a significant amount of time) comprise our R class. This differs from the model presented in [6] in which both groups of individuals are in the R class and have equal probability of entering and leaving the class. Our definition of the recovered class creates a compartment to place individuals who have been addicted in the past and have finished treatment but are not considered actively addicted anymore. We believe these individuals should be specially considered and not viewed as the same as susceptible individuals, individuals in treatment, and those recently out of treatment. We emphasize here that we do not consider the stably recovered class to contain addicts.

The recovered class and relapse from that class are two of the key features that distinguishes our model from that of [6]. In the prescription opioid-only model [6], as the focus was on the dynamics of the epidemic as it was ramping up, relapse did not depend on the number that were addicted during the beginning of the epidemic. In contrast, since the time the epidemic has been established, there are high numbers of opioid and heroin/fentanyl addicts and therefore, the proportion in each category affects where people relapse to.

We choose to use 4 weeks after treatment with no relapse as the mark of when addicts are "successfully recovered" and can move to R. We chose this time frame due to several studies exhibiting a high level of relapse within a few weeks of discharge from treatment, which suggests individuals are not stably recovered. One study following up with opiate dependent individuals (of which 88% of the study population were heroin users) showed that 59% of the individuals discharged from treatment relapsed within 1 week and 71% within 4 weeks [94]. Moreover, 80% of individuals who relapsed after treatment did so within 4 weeks and 92% of individuals who relapsed after discharge had gone back to treatment prior to their follow-up interview (which was between 18-42 months). These statistics convey the unstable nature of an addicts' recovery, particularly within a few weeks of post-treatment

(since that's when a majority of them relapsed). In another opiate dependent group study evaluating their relapse risk, 27% had relapsed on the discharge day of their most recent treatment program, 41% had relapsed within 1 week and 65% within 4 weeks [5]. One study on prescription opioid addicts suggested that 91% of them who completed a two-phase treatment program relapsed back into addiction within 8 weeks post-treatment [126]. On the lower side, in another study an estimated 32% of the 68 opiate addicts interviewed returned to addiction within 4 weeks and 65% lapsed, which we note has potential to lead to dependence in time; at the 6 month follow-up, 50% of the 60 individuals interviewed were dependent [9]. An earlier study following up with opiate users post-treatment for 6 months showed that 32% had lapsed within 1 week post-discharge when interviewed; 71% had lapsed by the 6th week; and 44% had returned to the daily use of opiates (considered addicted) at the 2 month mark [51]. Furthermore, that study stated that several individuals who completed the withdrawal portion of the program lapsed while in the second, in-patient part of treatment (although not necessarily equating to a full relapse back into addiction). Later analysis of this study regarding relapse factors stated that 25% of those who lapsed mentioned withdrawal symptoms as playing a role in their lapses [8].

These statistics suggest that opiate-abstinence can be difficult to achieve in this initial time period post-treatment: "...the period immediately after leaving a residential treatment is of massively high risk: the great majority of lapses occurred with the first few weeks after discharge...after the first four weeks, there were few additional lapses...first few weeks after discharge as a *critical period* in the process of recovery" [51]. This suggests four weeks can be viewed as an important marker in recovery, and that individuals who bounce back to addiction/frequently relapse in this time frame should remain in their respective addicted class. Other studies suggest significant lapse and relapse rates within weeks and months for heroin addicts and opiate addicts, as well [62, 52].

Therefore, since 71% of heroin addicts relapse within 4 weeks post-treatment and an estimated 91% of prescription opioid addicts in recovery relapse back to addiction within 8 weeks post-treatment (the majority most likely within four weeks based on these other studies), we keep these individuals in the addiction class for up to 4 weeks post-treatment

since they have not stably "recovered," i.e. at a point where they are significantly less likely to fall back into addiction [94, 126].

In [51], 63% of initial lapses occurred around other opioid users, 48% in another addicts' home, and 31% in ones own home. This may lead one to believe that interactions with other addicts would play a large role with an initial lapse/relapse; however, following this study, the authors explored the circumstances that led to the lapses of these study subjects and results suggested differently [8]. The top factors that led to these initial lapses were cognitive factors (planned to use), mood states (angry, sad, lonely, etc.), and external influences (situations unrelated to drug use that led to use). This took into consideration the number of people who mentioned the factors, the total number of times the factors were mentioned, the number of individuals who deemed the factor most important, and finally, the number of individuals that indicated the factor was the initiator of a sequence of other factors, as lapsing often is a result of multiple factors occurring simultaneously. These were also the factors that were primarily contributed to the continued use of opiates. The source-driven factors, specifically social pressure (offered drugs), drug availability (in another users' home or in the area), drug-related clues (objects used for drug-taking/observing others under the influence), and interpersonal influences (seeing or thinking about certain people) had relatively little importance compared to the others mentioned above. Thus we argue individuals return to their primary drug of choice compared to what is simply available; although we are interested specifically in a return to addiction, this is within the broader category of lapses.

The work in [56] on heroin users enabled the study subjects to choose categories they deemed as most important in their relapse according to a phrase attached to the category. This was then compared to the results of independent judges selecting the categories based on individuals' responses. The highest mean ratings for the categories that the subjects chose were for the giving into temptations/urges in the presence of substance cues and direct social pressure, whereas the judges deemed negative emotional states and indirect social pressure as the most frequent reasons. However, given that subjects were provided a phrase that correlated with a certain category, one could argue that if an individual did not agree with the exact phrase, they may have chosen an alternative option that they related to more (e.g. "I felt bored" represented the entire category of "negative emotional states other than

frustration and/or anger"). Moreover, the previous study [8] applies both to opioid addicts and heroin addicts, rather than just heroin addicts. Therefore, even though we do not know where individuals in R came from originally, in our model we assume that individuals go back to their primary drug of choice (the reason they entered treatment), so they relapse back proportional to where they came from. This proportion is an approximation because it's based on the current class proportions and not the proportions when they went to R. We may explore different forms of relapse terms from R in the future to incorporate different reasons for relapse.

We do not include an interaction term between prescribed users and prescription opioid addicted individuals moving into the A class due to the assumption that their own prescription is the primary source of their addiction, and that an illicit source or interaction with addicts would be secondary. We do not have a pathway from R to P; although individuals have the potential of obtaining a legal prescription from a doctor since doctors are not necessarily informed that their patient was in recovery in the past and are "case-history blind," we believe it is not realistic that an individual who has recovered from an addiction would be able to successfully take prescription opioids in a non-addictive manner [33]. Therefore, we assume that if an individual from R began using prescription opioids, they would move to the addicted class in a very short amount of time. Although there may be exceptions to this, we make this simplifying assumption for a first model. We do not have a pathway from P to R because we make the assumption that if an individual were "misusing" prescription opioids in the P class, they would only enter treatment if it were harmful to or interfering with their life in some way, and in that case, the individual would be considered addicted and would be in the A class. Therefore, they would first transition to the addicted class, and then to a stably recovered state.

We do not have a pathway from R to S since individuals who have been to treatment and recovered are much more likely to fall into addiction than a susceptible individual, and therefore, must be viewed differently than a susceptible individual who has not been to recovery (i.e. cannot be homogeneously mixed in S). This differs from the model in [6] that allows individuals who finish treatment and are considered recovered to go back to the susceptible class. We think of individuals in our recovered class as in a permanent

state of recovery for the rest of their lives, although they are not undergoing active treatment/recovery. Along these same lines, there is no pathway from A or H to S because we are under the assumption that an addicted individual either remains addicted or goes to recovery to help their addiction and will never be characterized as a susceptible individual again. We recognize that there may be additional pathways among the classes, but the ones we have chosen to include in this first model are a result of balancing simplicity and robustness.

2.3 Model Analysis

2.3.1 Addiction-Free Equilibrium and Basic Reproduction Number

To find the addiction-free equilibrium, we set our ordinary differential equations in (2.1) equal to zero and require that $A = H = 0$ since these two compartments consist of individuals who are addicted to some type of opioid. We obtain the system as shown with Equations (2.3)-(2.6):

$$0 = -\alpha S^* - \beta_P S^* P^* + \varepsilon P^* + \mu(P^* + R^*) \tag{2.3}$$

$$0 = \alpha S^* - \varepsilon P^* - \gamma P^* - \mu P^* \tag{2.4}$$

$$0 = \gamma P^* + \beta_P S^* P^* \tag{2.5}$$

$$0 = \mu R^*, \tag{2.6}$$

with the additional condition

$$1 = S^* + P^* + A^* + H^* + R^*. \tag{2.7}$$

Equation (2.6) forces either $\mu = 0$ or $R^* = 0$; however, $\mu > 0$ since this is the natural death rate, so we require $R^* = 0$. If $P^* \neq 0$, this forces $\gamma + \beta_P S^* = 0$ from (2.5), and since all of our parameters and variables are non-negative, then it must be $\gamma = 0$ and $\beta_P = 0$. We note that $\gamma = 0$ means that individuals who are prescribed opioids cannot become addicted to

opioids, and $\beta_P = 0$ means that only black market opioids are available for susceptibles to become addicted to opioids and there are no excess prescription drugs available. Under the assumption that $\gamma = 0 = \beta_P$ to ensure the existence of our addiction-free equilibrium, we calculate the addiction-free equilibrium and the result is shown in (2.8).

If $P^* = 0$, then Equation (2.4) forces either $S^* = 0$ or $\alpha = 0$. If $S^* = 0$, then the solution $S^* = P^* = A^* = H^* = R^* = 0$ contradicts condition (2.7). If $\alpha = 0$, then we use condition (2.7) to solve for the addiction-free equilibrium of (1,0,0,0,0); this solution is included in the addiction-free equilibrium (2.8) when $\alpha = 0$, as well.

$$\begin{aligned} S^* &= \frac{\varepsilon + \mu}{\alpha + \varepsilon + \mu} \\ P^* &= \frac{\alpha}{\alpha + \varepsilon + \mu} \\ A^* &= 0 \\ H^* &= 0 \\ R^* &= 0 \end{aligned} \tag{2.8}$$

The basic reproduction number, denoted $\mathscr{R}_0$, is a term used in epidemiological models that gives the expected number of secondary disease cases that result from the introduction of a disease to a susceptible population [121]. The value of $\mathscr{R}_0$ represents how successful the spread of the disease is expected to be; if $\mathscr{R}_0 < 1$, then the disease is expected to die out and the disease-free equilibrium will be locally stable; conversely, if $\mathscr{R}_0 > 1$, then the disease is expected to spread since secondary infections from an infected individual occur and the disease-free equilibrium will be unstable.

This idea may be applied to the context of our model since for the addiction-free equilibrium to occur, γ and β_P must both be equal to 0, which means individuals can become addicted only with interactions with prescription opioid addicted individuals or heroin users so this takes the form of an infectious disease. Thus, in this case in which the prescription part is essentially taken out of the model so that it is a black-market-only driven model, $\mathscr{R}_0$ can be calculated. At the addiction-free equilibrium, the population is completely susceptible, as needed for $\mathscr{R}_0$ to be an accurate measurement of addiction potential. The disease compartments are those that contain infected individuals, or in our case, addicts

[121]. Our model incorporates two addiction compartments, A and H, since these both consist of prescription opioid or heroin/fentanyl addicted individuals. We will utilize the Next Generation Matrix Method in order to calculate $\mathscr{R}_0$ [120, 121].

For the purposes of calculating $\mathscr{R}_0$, we will assume $\gamma = 0$ and $\beta_P = 0$ in order to ensure the existence of the addiction-free equilibrium. This results in the following system:

$$\frac{\mathrm{d}S}{\mathrm{d}t} = -\alpha S - \beta_A SA - \theta_1 SH + \varepsilon P + \mu(P+R) + (\mu+\mu_A)A + (\mu+\mu_H)H \tag{2.9}$$

$$\frac{\mathrm{d}P}{\mathrm{d}t} = \alpha S - \varepsilon P - \theta_2 PH - \mu P \tag{2.10}$$

$$\frac{\mathrm{d}A}{\mathrm{d}t} = \sigma R\frac{A}{A+H+\omega} + \beta_A SA - \zeta A - \theta_3 AH - (\mu+\mu_A)A \tag{2.11}$$

$$\frac{\mathrm{d}H}{\mathrm{d}t} = \theta_1 SH + \theta_2 PH + \theta_3 AH + \sigma R\frac{H}{A+H+\omega} - \nu H - (\mu+\mu_H)H \tag{2.12}$$

$$\frac{\mathrm{d}R}{\mathrm{d}t} = \zeta A + \nu H - \sigma R\frac{A}{A+H+\omega} - \sigma R\frac{H}{A+H+\omega} - \mu R. \tag{2.13}$$

In general, the differential equations of the n disease compartments, x_i', may be written as:

$$x_i' = \mathscr{F}_i(x,y) - \mathscr{V}_i(x,y), \quad i = 1, ..., n$$

where x is a vector with the disease compartments as components, y a vector with the non-disease compartments as components, $\mathscr{F}_i$ represents the rate that secondary infections contribute to disease compartment i and $\mathscr{V}_i$ represents the rate of transitions, i.e. rate at which the disease compartment i is decreased by means of death, recovery and progression of the disease for $i = 1, 2$ [121].

Thus, for our two addicted compartments, we may write:

$$\frac{dA}{dt} = \mathscr{F}_1(x,y) - \mathscr{V}_1(x,y)$$

$$\frac{dH}{dt} = \mathscr{F}_2(x,y) - \mathscr{V}_2(x,y)$$

where $x = [A \quad H]^T$ and $y = [S \quad P \quad R]^T$. Therefore, under the assumption that A and H are the addicted compartments and abiding by the parameter restrictions stated above, the assumptions [121] of the Next Generation Method are satisfied for matrices $\mathscr{F}$ and $\mathscr{V}$ formulated here:

$$\mathscr{F} = \begin{pmatrix} \sigma R\frac{A}{A+H+\omega} + \beta_A SA \\ \theta_1 SH + \theta_2 PH + \sigma R\frac{H}{A+H+\omega} \end{pmatrix}$$
$$\mathscr{V} = \begin{pmatrix} \zeta A + \theta_3 AH + (\mu+\mu_A)A \\ -\theta_3 AH + \nu H + (\mu+\mu_H)H \end{pmatrix}.$$

These assumptions include the following:

- $\mathscr{F}_i(0,y) = 0$ and $\mathscr{V}_i(0,y) = 0$, $\forall y \geq 0$, $i = 1,2$, which ensures that new addictions arise only from interacting with those currently addicted, and there is no immigration into the addicted compartments; these guarantee that the population free of addiction remains that way.

- $\mathscr{F}_i(x,y) \geq 0$, $\forall x,y \geq 0$, $i = 1,2$ since these represent new addictions.

- $\mathscr{V}_i(x,y) \leq 0$ whenever $x_i = 0$, $i = 1,2$ since there must be inflow only when the respective compartment is empty.

- $\sum_{i=1}^{2} \mathscr{V}_i(x,y) \geq 0$, $\forall x,y \geq 0$ since this represents the total outflow from all addicted compartments.

- The addiction-free system, $\frac{\mathrm{d}S}{\mathrm{d}t}\Big|_{A,H=0}$, $\frac{\mathrm{d}P}{\mathrm{d}t}\Big|_{A,H=0}$, and $\frac{\mathrm{d}R}{\mathrm{d}t}\Big|_{A,H=0}$ has a unique equilibrium, $(\frac{\varepsilon+\mu}{\alpha+\varepsilon+\mu}, \frac{\alpha}{\alpha+\varepsilon+\mu}, 0)$ that is asymptotically stable.

Taking $F = \frac{\partial \mathscr{F}_i}{\partial x_j}(0,y_0)$ and $V = \frac{\partial \mathscr{V}_i}{\partial x_j}(0,y_0)$, $i,j = 1,2$, where $(0,\ y_0) = (\frac{\varepsilon+\mu}{\alpha+\varepsilon+\mu}, \frac{\alpha}{\alpha+\varepsilon+\mu}, 0, 0, 0)$ is the addiction-free equilibrium, we calculated the following [121]:

$$F = \begin{pmatrix} \beta_A\frac{\varepsilon+\mu}{\alpha+\varepsilon+\mu} & 0 \\ 0 & \theta_1\frac{\varepsilon+\mu}{\alpha+\varepsilon+\mu} + \theta_2\frac{\alpha}{\alpha+\varepsilon+\mu} \end{pmatrix}$$
$$V = \begin{pmatrix} \zeta+\mu+\mu_A & 0 \\ 0 & \nu+\mu+\mu_H \end{pmatrix}.$$

The eigenvalues of FV^{-1} are calculated to be:

$$\sigma(FV^{-1}) = \{\frac{\beta_A(\varepsilon+\mu)}{(\alpha+\varepsilon+\mu)(\zeta+\mu+\mu_A)}, \frac{\theta_1(\varepsilon+\mu)+\theta_2\alpha}{(\alpha+\varepsilon+\mu)(\nu+\mu+\mu_H)}\}.$$

$\mathscr{R}_0$ may then be determined as the spectral radius of FV^{-1}, in which the (i, j) entry is the expected number of secondary addictions in compartment i produced by individuals initially in compartment j. From the first eigenvalue, we have that $\frac{\beta_A(\varepsilon+\mu)}{(\alpha+\varepsilon+\mu)} = \beta_A S^*$ represents the rate of addiction of susceptible individuals if an individual addicted to prescription opioids were to be introduced into the population and $\frac{1}{(\zeta+\mu+\mu_A)}$ is the expected duration of the addiction period and therefore relates to the A class. On the other hand, the second eigenvalue $\frac{\theta_1(\varepsilon+\mu)+\theta_2\alpha}{(\alpha+\varepsilon+\mu)} = \theta_1 S^* + \theta_2 P^*$ is the rate of addiction of susceptible individuals and prescribed users from the introduction of a heroin/fentanyl addicted individual into the population with an expected duration of the addiction period to be $\frac{1}{(\nu+\mu+\mu_H)}$ which relates to the H class. Thus, the dynamics for illicit-based addiction can be thought of as split between two pathways, with one eigenvalue relating to prescription opioid addiction and the second relating to heroin/fentanyl addiction.

To compute the value of the basic reproduction number for our model, we utilize estimated parameter values shown in Table 2.9 (discussed in Section 2.4). We specifically use the values of α and μ_A in 2013, thus assuming all of our parameters are constant with respect to time for the purposes of this calculation. This results in eigenvalues of 0.00371 and 4.118, and therefore,

$$\mathscr{R}_0 = 4.118 \text{ for } 2013.$$

Since this value is greater than 1, this suggests that the epidemic would be able to sustain itself under the assumptions of $\gamma = 0$ and $\beta_P = 0$. This means that the black market/interaction with other addicts is enough by itself to sustain the epidemic, and that the addiction of prescription opioids users to their own prescriptions or availability to susceptibles of excess pills lying around does not play a huge role in this. The fact that the second eigenvalue is less than 1 suggests that the expected number of secondary addictions coming from interactions with prescription opioid addicts/black market alone would not be sufficient to keep the epidemic going and instead it would die out. This aligns with results from [6] with the form of $\mathscr{R}_0$ and the result that an illicit prescription-based epidemic would die out with the estimated parameter values. However, now with heroin and fentanyl, the epidemic is

expected to be self-sustaining with the estimated parameters and is supported by numerical analysis results later on in Section 2.4.4.

2.3.2 Properties of Solutions

We will now show that starting with non-negative initial conditions, solutions for the system of equations found in (2.1) are guaranteed to be non-negative for all time. This relies on Theorem 2.1 which is an adaptation of Theorem 2.1 in [93].

Theorem 2.1 ([93]: adapted version of Theorem 2.1, Chapter 5)**.** *Assume that when* $\vec{\phi} \in \mathbb{R}^n$ *satisfies* $\vec{\phi} \geq 0$ *with* $\phi_i(0) = 0$ *for some* i*, then* $f_i(\phi) \geq 0$*. Then, if* $\vec{\phi} \in \mathbb{R}^n$ *satisfies* $\vec{\phi} \geq 0$*, the solution of* $\dfrac{d\vec{y}}{dt} = \vec{f}(t, \vec{y})$*,* $\vec{y}(t_0) = \vec{\phi}$ *where* $f : D \to \mathbb{R}^n$ *continuous,* $D \subset \mathbb{R}^n$ *open and* $\vec{\phi} \in \mathbb{R}^n$*, satisfies* $\vec{y}(t) \geq 0$ *for all* $t \geq t_0$*.*

Theorem 2.2. *Given a vector of initial conditions* $\vec{\phi} = (S_0, P_0, A_0, H_0, R_0) \geq 0$*, if a solution* $\vec{Y}(t)$ *exists to our system of equations found in (2.1), then this solution is non-negative.*

Proof. Consider the vector of initial conditions in $\mathbb{R}^5$, $\vec{\phi} = (S_0, P_0, A_0, H_0, R_0)$. Since each vector component represents a proportion of a population, we know $\vec{\phi} \geq 0$. Assuming $\phi_i(0) = 0$ for some i, we want to show $f_i(\vec{\phi}) \geq 0$.

1) Assume $\vec{\phi} = (0, P_0, A_0, H_0, R_0) \geq 0$ and $\phi_1(0) = 0$. Then,

$$f_1(\phi) = \varepsilon P_0 + \mu(P_0 + R_0) + (\mu + \mu_A)A_0 + (\mu + \mu_H)H_0 \geq 0,$$

since all parameters and variables are non-negative.

2) Assume $\vec{\phi} = (S_0, 0, A_0, H_0, R_0) \geq 0$ and $\phi_2(0) = 0$. Then,

$$f_2(\phi) = \alpha S_0 \geq 0,$$

since α and S_0 are non-negative.

3) Assume $\vec{\phi} = (S_0, P_0, 0, H_0, R_0) \geq 0$ and $\phi_3(0) = 0$. Then,

$$f_3(\phi) = \gamma P_0 + \beta_P S_0 P_0 \geq 0,$$

since all parameters and variables are non-negative.

4) Assume $\vec{\phi} = (S_0, P_0, A_0, 0, R_0) \geq 0$ and $\phi_4(0) = 0$. Then,

$$f_4(\phi) = 0 \geq 0.$$

5) Assume $\vec{\phi} = (S_0, P_0, A_0, H_0, 0) \geq 0$ and $\phi_5(0) = 0$. Finally,

$$f_5(\phi) = \zeta A_0 + \nu H_0 \geq 0,$$

since all parameters and variables are non-negative.

Thus, whenever $\vec{\phi} \geq 0$ and $\phi_i(0) = 0$ for some i, we see $f_i(\phi) \geq 0$. Therefore, since $\vec{\phi} \geq 0$, then by Theorem 2.1, the solution $\vec{Y}(t) = (S(t), P(t), A(t), H(t), R(t)) \geq 0$ for all $t \geq 0$, as desired. □

Next, we show solutions to our system of ODEs are uniformly bounded in Theorem 2.3.

Theorem 2.3. *Solutions to system of equations 2.1 are uniformly bounded.*

Proof. We see

$$\frac{dS}{dt} + \frac{dP}{dt} + \frac{dA}{dt} + \frac{dH}{dt} + \frac{dR}{dt} = 0.$$

Since $S(0) + P(0) + A(0) + H(0) + R(0) = 1$, then $S(t) + P(t) + A(t) + H(t) + R(t) = 1$.

□

Finally, we prove the existence of a unique solution of our system using Theorems 2.4 and 2.5, which are adaptions from [60], as well as Theorem 2.6.

Theorem 2.4 ([60]: adapted version of Theorem I-1-4, Chapter 1)**.** *Consider the general initial value problem*

$$\frac{d\vec{y}}{dt} = \vec{f}(t, \vec{y}),\ \vec{y}(t_0) = \vec{\phi}.$$

Assume $\vec{f}$ is real-valued and continuous where $t \in \mathbb{R}$ and $\vec{y} \in \mathbb{R}^n$. Let $\mathscr{R}$ be defined as the rectangular region such that:

$$\mathscr{R} = \mathscr{R}((t_0, \vec{\phi}), a, b)) = \{(t, \vec{y}) : |t - t_0| \leq a, \left|\vec{y} - \vec{\phi}\right| \leq b\},$$

for a, $b > 0$. Assume $\vec{f}$ is Lipschitz on rectangle $\mathscr{R}$ (i.e. there exists a positive constant M such that

$$\left|\vec{f}(t, \vec{y_1}) - \vec{f}(t, \vec{y_2})\right| \leq M|\vec{y_1} - \vec{y_2}|$$

for $(t, \vec{y_1})$ *and* $(t, \vec{y_2})$ *on* $\mathscr{R}$*). Then a unique solution exists for all* t *within a given distance of* t_0*.*

Theorem 2.5 ([60]: adapted version of Lemma I-1-6, Chapter 1)**.** *If* $\dfrac{\partial \vec{f}(t, \vec{y})}{\partial \vec{y_i}}$ $(i = 1, ..., n)$ *exist, are continuous, and are bounded for* $t \in I$ *for some interval* I *and* $\vec{y}$ *in a region* D*, then if* D *is a convex open set,* $\vec{f}$ *is Lipschitz for* $t \in I$ *and* $\vec{y_1}$*,* $\vec{y_2} \in D$*.*

Note that these results hold for finite intervals of time but extend to all positive time when the solution is uniformly bounded.

Theorem 2.6. *For the initial value problem given in (2.1) with a given set of initial conditions, there exists a unique solution* $\vec{Y}(t) = (S(t), P(t), A(t), H(t), R(t))$*.*

Proof. Denote the right hand side of the i^{th} differential equation by f_i. We need to show $\vec{f}$ is Lipschitz by showing each f_i is Lipschitz for each input. To do so, it is sufficient to show the partial derivatives of f_i with respect to the i^{th} state variable is continuous and bounded as long as $\vec{Y_1}$, $\vec{Y_2} \in D$ where D is a convex open set by Theorem 2.5. For our system, $\vec{Y_1}$ and $\vec{Y_2}$ stay in $[0, 1]^5$. Therefore, we set $D = (0, 1.1)^5$ which is open and convex. Then, we see for f_1,

$$\frac{\partial f_1}{\partial S} = -\alpha - \beta_A A - \beta_P P - \theta_1 H \tag{2.14}$$

$$\frac{\partial f_1}{\partial P} = -\beta_P S + \varepsilon + \mu \tag{2.15}$$

$$\frac{\partial f_1}{\partial A} = -\beta_A S + \mu + \mu_A \tag{2.16}$$

$$\frac{\partial f_1}{\partial H} = -\theta_1 S + \mu + \mu_H \tag{2.17}$$

$$\frac{\partial f_1}{\partial R} = \mu \tag{2.18}$$

which are all bounded because by Theorem 2.3, the state variables are bounded, and multiplying by constant parameter values and adding/subtracting state variables, the result will remain bounded. Parameters are also bounded (real numbers). In addition, the result remains continuous.

Similarly, for f_2,

$$\frac{\partial f_2}{\partial S} = \alpha \tag{2.19}$$
$$\frac{\partial f_2}{\partial P} = -\varepsilon - \gamma - \theta_2 H - \mu \tag{2.20}$$
$$\frac{\partial f_2}{\partial A} = 0 \tag{2.21}$$
$$\frac{\partial f_2}{\partial H} = -\theta_2 P \tag{2.22}$$
$$\frac{\partial f_2}{\partial R} = 0, \tag{2.23}$$

the partial derivatives are all bounded and continuous.

Similarly, for f_3,

$$\frac{\partial f_3}{\partial S} = \beta_A A + \beta_P P \tag{2.24}$$
$$\frac{\partial f_3}{\partial P} = \gamma + \beta P S \tag{2.25}$$
$$\frac{\partial f_3}{\partial A} = \sigma R \frac{(A+H+\omega) - A}{(A+H+\omega)^2} + \beta_A S - \zeta - \theta_3 H - \mu - \mu_A \tag{2.26}$$
$$\frac{\partial f_3}{\partial H} = \sigma R \frac{(A+H+\omega) - A}{(A+H+\omega)^2} - \theta_3 A \tag{2.27}$$
$$\frac{\partial f_3}{\partial R} = \sigma \frac{A}{A+H+\omega}, \tag{2.28}$$

the resulting equations are bounded and continuous. The results are similar for the remaining equations f_i, $i = 4, 5$, since all state variables are bounded and continuous, and parameter values are bounded. Since all partial derivatives of the right hand sides exist and are bounded, then the right hand sides f_i are all Lipschitz. By Theorem 2.4, there exists a unique solution within our region D. □

Although we are unable to solve for an endemic equilibrium analytically, we are not concerned with this output because we apply our model over a short time period with time-dependent parameters to answer questions. Thus, we disregard what happens in the long-term.

2.4 Numerical Results

We apply our model to the Tennessee population specifically in order to analyze the opioid epidemic on a smaller scale than the national level. Although there is still heterogeneity across Tennessee, it is lower than the amount one would find on a national scale. Table 2.1 consists of estimates of the number of individuals in Tennessee in various categories for the years 2013-2018 found either in literature or that we estimated; explanations of each of the categories follows.

The first row of Table 2.1 provides the **total population estimates (residents) in Tennessee** each year as of July 1 of the corresponding year [111]. However, since the remainder of the data we use is specific to individuals 12 and older, we estimate the number in this age group. Since there was no information available for years 2013-2017, we rely on estimates in 2010 and 2018. In 2010, an estimated 15.5% of the population was under the age of 12 [110]. In 2018, there were an estimated 1,073,214 individuals in Tennessee aged 12 and under [36]. To figure out those who are exactly 12 years old, we take 1/8th of the individuals that are in the age group 5-12 (an estimated 665,401 total individuals), which is approximately 83,175 individuals. Thus, an estimated (1073214-83175=) 990,039 individuals are *under* the age of 12 in Tennessee in 2018. Given the total population estimate for 2018 is 6,770,010 from row 1, this means that approximately 14.6% of the population is under the age of 12. Thus, based on these two estimates, we make an assumption that 15% of the population is under the age of 12. Since we do not see a reason for this percentage to be significantly different from year to year, we assume that this percentage is constant throughout the time period we are looking at. Then, we are able to consider the **Tennessee population estimates for individuals 12 and older** in order to align with the rest of the data that is in this age range by taking off 15% of the total population estimates for each year; this is shown in the second row of Table 2.1.

Heroin users and Heroin addicts

The 2014/2015 average number of individuals 12 and older with "Past Year Heroin Use" (**heroin/fentanyl addicts**) was 14,000, the 2015/2016 average number was 14,000, and

Table 2.1: Estimates for the number of individuals in each category listed for years 2013-2018. *Italicized* values are numbers estimated by extrapolating from a different year, whereas **bolded** values are numbers that we estimated by information within the same year. All other numbers are actual reported data. Numbers in blue are data used directly in parameter estimation in sections 2.4.1 and 2.4.2. Sources: [1]National Survey on Drug Use and Health [98, 101, 102], [2]Controlled Substance Monitoring Database Program [85], [3]Prescription Drug Overdose Program Report/Tennessee's Annual Overdose Report [84, 86].

Tennessee Yearly Data	2013	2014	2015	2016	2017	2018
Total population	6,493,432	6,540,826	6,590,808	6,645,011	6,708,794	6,770,010
Population 12 and older	*5,519,417*	*5,559,702*	*5,602,187*	*5,648,259*	*5,702,475*	**5,754,509**
Heroin users	-	14,000[1]	14,000[1]	19,000[1]	-	-
Heroin addicts	-	**7,560**	**7,560**	**10,260**	-	-
Prescription opioid addicts (includes heroin addicts)	-	-	48,000[1]	42,000[1]	-	-
Prescription opioid addicts (excludes heroin addicts)	*43,418*	*42,928*	**42,816**	**37,464**	*34,805*	*31,244*
Prescribed opioid users (includes Rx addicts)	1,845,144[2]	1,824,342[2]	1,819,581[2]	1,761,363[2]	1,636,374[2]	1,468,934[2]
Prescribed opioid users (excludes Rx addicts)	*1,825,910*	*1,805,325*	**1,800,614**	**1,744,766**	*1,620,955*	*1,455,093*
Prescription opioid overdose deaths	642[3]	660[3]	690[3]	698[3]	566[3]	-
Prescription opioid addict overdose deaths	**351**	**360**	**377**	**381**	**309**	-
Heroin/fentanyl overdose deaths	112[3]	201[3]	344[3]	488[3]	702[3]	-

the 2016/2017 average number was 19,000 as shown in row 3 of Table 2.1 with the values placed in the lower of the 2 years [98, 101, 102]. The data collected in these surveys from 2014-2017 is from civilians who live in non-institutional residences (such as homes, shelters, dormitories, military bases) and does not include those who are homeless and not in a shelter, in institutions such as jails or hospitals, or active military personnel [17]. The survey is a three-step interview process and therefore consists of self-reporting of use. The survey aims to increase accuracy of self-reporting by ensuring confidentiality and utilizing an audio computer-assisted self-interviewing program to privately answer sensitive questions with headphones, ask questions the same way each time, and eliminate data entry time or errors. Thus, we recognize these estimates may be on the low side due to under-reporting of illicit drug use and the exclusion of a portion of the population that has higher than average rates of drug use. Errors come from the selection of samples, as well as non-sampling errors such as non-responses, coding errors, or reporting errors.

These numbers include those who may have used heroin just once in the past year (i.e. tried it but did not become a habit of any sort); however, it is estimated that 54% of heroin users are dependent on the drug, which gives the resulting **bold** estimates in row 4 of Table

2.1 [83]. In addition, the number of heroin users does not include fentanyl users explicitly, but we are under the assumption that those who use fentanyl are a subset of those who use heroin, and therefore, would mostly be included in these numbers. We admit the values may be slightly too low, for the cases of individuals who use fentanyl and not heroin, but data has not been found for fentanyl addicts only, and fentanyl is very often found mixed with heroin, as mentioned before. Therefore, we are working under the assumption that it would be a negligible population that is addicted to fentanyl without using heroin. Again, for these estimates, we choose the lower of the two years to place the data points; for example, 10,260 is placed in the year 2016. The values **bolded** in Table 2.1 are numbers that were based on the data of individuals from the same year, and did not rely on any extrapolated data from a different year.

Prescribed opioid users (includes Rx addicts)

The **total number of residents receiving prescription opioids for pain (i.e. prescribed)** is given in row 7 of Table 2.1, which comes from Tennessee's Controlled Substances Monitoring Database (CSMD) [85]. Although this number does not explicitly state it is for individuals 12 and older, we assume it is since it comes from the Tennessee Department of Health; if it does include individuals under 12, we assume that number is negligible. We note here that although individuals are receiving opioids for pain, individuals could be not taking them at all or selling/sharing them so this data does not account for patient behavior after filling their prescriptions.

Prescription opioid addicts (includes heroin addicts)

The 2015/2016 average number of individuals 12 and older with "Pain Reliever Use Disorder" (**prescription opioid addicts**) is 48,000 and the 2016/2017 average number was 42,000 [101, 102]. The data collection process and errors described above for heroin use are the same as here [17]. For these estimates, we choose the lower of the two years to place the data points; for example, for the 2015/2016 average, 48,000 is placed in the year 2015. We note that their definition of pain reliever use disorder includes those who meet the American Psychiatric Association (APA) criteria for dependence or abuse. Individuals must fit 3 of

the following 7 criteria to be considered dependent or abusing:

1. Significant amount of time spent in a month obtaining, using, or recovering from the substance effects effects of the substance
2. Used more often than meant to or was not able to set limits on use
3. Needed to increase use of substance to match previous effects of the drug or noticed less of an effect of the drug
4. Not able to decrease use or stop altogether despite desire to
5. Continued use despite emotional, mental, physical, or nerve problems due to the drug
6. The drug use limited or eliminated participation in important life activities
7. Certain number of withdrawal symptoms

In the APA criteria, opioid dependence is classified as having "signs and symptoms that reflect compulsive, prolonged self-administration of opioid substances that are used for no legitimate medical purpose or...are used in doses that are greatly in excess of the amount needed for pain relief...regular patterns of compulsive drug use that daily activities are typically planned around obtaining and administering opioids." This definition of dependence falls under our definition of opioid addiction. Opioid abuse, on the other hand, they consider to be less severe than dependence, and would not lead to the development of withdrawal symptoms. This latter definition does not fall under our characterization of addiction, but we make a note of this to say that this estimate for those with a pain reliever use disorder may be overestimated for what we are concerned with, but is an acceptable approximation [4]. In addition, we assume very few, if any, individuals are addicted to opioids outside of prescription opioids, but even if they are, we assume they are taking prescription opioids in some capacity, so we take pain reliever use disorder to include those with other non-prescription opioid addiction. We also remind the reader that these numbers include both individuals who are personally prescribed opioids or who may obtain them illicitly. Finally, we note that those who are addicted to opioids are considered strictly in the A class, as individuals in R are not considered addicted in our model.

Prescription opioid addicts (excludes heroin addicts)

In 2010, on the national level it was estimated that 14% of individuals who abused or were dependent on pain medications also *used* heroin [83]. It was right around this year that the number of overdose deaths involving heroin increased and continued to increase until 2016 [85, 20]. Although it is likely many of these deaths were due to the lacing of heroin with fentanyl, it seems safe to assume that the increase in overdose deaths would equate to a larger number of heroin addicts in each of those years overall (as supported by data from 2015 to 2016 in Table 2.1) and that a portion of these individuals were prescription opioid addicts that transitioned to heroin. Therefore, we assume a higher percentage of prescription opioid addicts *used* heroin in 2015 and 2016 compared to 2010 and use 20% as our estimate. (Although this may not be exact or accurate for these years, a higher percentage is a reasonable starting point to be able to work with the data we do have). However, only 54% of heroin users are *addicts*, which means that 10.8% of prescription opioid addicts are also heroin addicts (.54*.2=.108) [83]. We subtract these heroin addicts from the prescription opioid addict category each year; this results in the non-heroin addicted prescription opioid addicts for years 2015 and 2016. From 2013 to 2018, the number of prescribed opioid users was decreasing, likely due to more awareness of the problem as suggested in [66] which resulted in a decreasing prescribing rate [84]; thus, we expect the number of addicts to also be decreasing in that time period, especially due to the movement of individuals to heroin use. For 2015, we see there were 42,816 (non-heroin addicted) prescription opioid addicts compared to 1,819,581 prescribed opioid users, which is an approximate ratio of 1:42.5; thus, we use the exact ratio of addicts to prescribed opioids users for 2013 and 2014, as well, to estimate the number of opioid addicts (these values are in *italics* in Table 1 since they are extrapolated from a different year). Although the numbers are most likely higher than this, this is an estimate. We apply a similar idea for the years 2017 and 2018, utilizing data from 2016 that there are 37,464 (non-heroin addicted) prescription opioid addicts out of 1,761,363 prescription users, which is an approximate ratio of 1:47 (also *italicized* in Table 1), but we use the exact ratio to calculate.

Prescribed opioid users (excludes Rx addicts)

The total number of prescribed opioid users each year, however, includes individuals addicted to their prescriptions. In a 2015 study done among adults with prescription opioid use disorder, 44.3% of them had obtained prescription opioids for their most recent episode of misuse from 1 or more physicians [53]. We make the assumptions that individuals who are addicted to heroin are not using *prescribed* opioids, since they are more expensive and less accessible; although this study consisted of individuals with prescription opioid use disorder, regardless of their heroin addiction status, we will extrapolate this percentage to those who are non-heroin addicted [82]. We recognize this percentage may be on the low side (i.e. if heroin addicts were taken out of the study, this percentage may be higher since those non-heroin addicted would possibly obtain more from a physician source), but we take this as our best estimate. Therefore, we assume that 44.3 out of 100 non-heroin addicted prescription opioid addicts are personally prescribed opioids and subtract 44.3% of the number of non-heroin prescription opioid addicts in each year from the prescribed opioid class in the corresponding year to obtain the number of non-addicted prescribed opioid users for 2013-2017.

Heroin/fentanyl overdose deaths

In 2013 there were 63 overdoses containing heroin and 53 overdoses containing fentanyl overdoses, in 2014 there were 147 and 69, in 2015 there were 205 and 169, in 2016 there were 260 and 294, and in 2017 there were 311 and 500, respectively [84, 86]. The report acknowledges that the number of fentanyl overdoses is most likely underreported, since there were no death codes during this time frame specifying fentanyl as a contributing cause of death; instead, methods were derived to scan for fentanyl in the text for the cause of death on the death certificates. Tennessee Death Statistical Files contain codes for the cause of death based on the death text fields on death certificates, and therefore, the "contributing substances" in deaths reported here are determined by the codes or literal text in the multiple cause of death fields in the statistical files. To count as a heroin overdose, the death must meet all drug overdose criteria and contain the code for acute poisoning by heroin as a contributing cause of death, and for a fentanyl overdose, must contain text "FENTAN" in the written cause of death on the death certificate.

We assume all fentanyl overdoses come from the heroin/fentanyl addicted class (rather than split between the A and H classes) since reports suggest that most fentanyl overdoses come from illicitly manufactured fentanyl rather than prescription, as discussed before [116, 84, 50, 117, 14]. However, in order to avoid double counting deaths in a multiple cause of death scenario, we make the assumption that fentanyl would be the cause of death over heroin or prescription opioids due to the potency of the drug (and since the criteria above does not state "as a contributing cause of death," we assume this means it is the cause of death if it is involved). Therefore, to eliminate double counting from the H class, we use information that in 2016, 25.4% of heroin overdose deaths had fentanyl as a contributing substance, and thus, 260-0.254(260)=194 heroin overdose deaths did not contain fentanyl. Similarly, for 2015, 14.6% contained fentanyl, leaving 205-0.146(205)=175 heroin overdose deaths without fentanyl. There is no data on the overlap of heroin and fentanyl deaths in 2013 or 2014, but using information from the opioid overdose graph in [20] separated by type of opioid, the sharpest increase in synthetic opioid overdose deaths occurred from 2015-2016, with less of an increase every year prior. Therefore, since there were about 10% more heroin deaths that contained fentanyl from 2015 to 2016 (jumped from 14.6% to 25.4%), we will make the assumption that there was less of an increase from 2014 to 2015, and will assume 10% of heroin overdose deaths contained fentanyl (i.e. a 4.6% increase). This gives 147-.1(147)=132 heroin deaths. Similarly, we will assume 7% of heroin overdose deaths contained fentanyl in 2013 (an even smaller increase from 2013 to 2014). This results in an estimate of 59 heroin overdose deaths. In order to estimate the number of heroin overdoses in 2017, the slope of the graph seems about the same in [20] from 2016-2017 as the year prior. Therefore, we will estimate that about 35% of heroin overdoses involved fentanyl, leaving 311-.35(311)=202 heroin overdoses.

We add together these estimates of heroin overdoses and fentanyl overdoses stated above for Tennessee to obtain the **total number of overdose deaths of TN residents with heroin or fentanyl as a contributing cause of death** each year shown in row 11 of Table 2.1. Although these numbers do not explicitly state they are for individuals 12 and older, we assume they are since they comes from the Tennessee Department of Health; if they do include individuals under 12, we assume that number is negligible. Age-specific graphs start

at age 15 on the Data Dashboard and in the report, so it is unclear if the numbers reported include 12-14 [84, 85]. Although we assume there is a negligible number of overdoses in this young age range, we make a note that our overdose numbers could be low due to the lack of death code for fentanyl.

Prescription opioid overdose deaths and Prescription opioid addict overdose deaths

We use data to determine the number of prescription opioid overdose deaths which include natural, semi-synthetic, and synthetic opioids [84]. We note that due to unclear definitions of prescription opioids on the report and not mutually exclusive categories of contributing substances of opioid overdose deaths, the most accurate method to determine the number of prescription opioid overdose deaths is to take the total number of opioid overdose deaths of each year and subtract off the heroin and fentanyl overdoses (again, we are assuming that if an overdose contains more than one drug, then heroin or fentanyl were the cause of death rather than prescription opioids, so this leaves overdose deaths by prescription opioids only). In 2013, this gives 754-112=642; in 2014, 861-201=660; in 2015, 1,034-344=690; in 2016, 1,186-488=698; and in 2017, 1,268-702=566 prescription opioid overdose deaths.

Tennessee Death Statistical Files contain codes for the cause of death based on the death text fields on death certificates, and therefore, the "contributing substances" in deaths reported here are determined by the codes in the multiple cause of death fields in the statistical files. To count as an overdose in this category, the death must meet all drug overdose criteria and contain one of three codes: acute poisoning by natural or semi-synthetic opioids, acute poisoning by methadone, or acute poisoning by synthetic opioids other than methadone.

Therefore, the **total number of overdose deaths of TN residents with prescription opioids as a contributing cause of death** for 2013-2017 are shown in row 9 of Table 2.1. However, it is estimated that only 54.6% of these individuals were actually at an increased risk for an opioid-related overdose death; we assume that if an individual met the criteria for at least one high-risk factor (≥ 4 prescribers, ≥ 4 pharmacies, or > 100 MME's), that they were considered addicted to prescription opioids [7]. Estimates for individuals who were addicted and overdosed are shown in row 10 of Table 2.1. Although these numbers

do not explicitly state they are for individuals 12 and older, we assume they are since they come from the Tennessee Department of Health; if they do include individuals under 12, we assume that number is negligible. Age-specific graphs start at age 15 on the Data Dashboard and in the report, so it is unclear if the numbers reported include 12-14 [84, 85]. Although we assume there is a negligible number of overdoses in this young age range, we make a note that our overdose numbers may be high if too few heroin/fentanyl deaths were subtracted from the total.

Prescribed opioid users quarterly

The Tennessee Department of Health also has estimates for the **number of patients (residents) receiving opioids for pain each quarter from 2013-2018**, as shown in Table 2.2 [84, 86]. In both reports, a graph is given without specific numbers, so we utilized the online tool WebPlotDigitizer to give best estimates to the values plotted [88]. However, these numbers again include those who are opioid addicted. To be able to calculate an estimate for the number of non-addicted prescribed opioid users, we need an estimate of the number of opioid addicts in each quarter. We calculate the ratio of prescribed opioid users each quarter compared to the entire year, and use this same ratio to calculate the number of prescription opioid addicts per quarter. (Although this may not be exact, it is a reasonable starting point to be able to work with the data we do have). For instance, in 2013 Quarter 1, there were 856,000 prescribed opioid users (includes addicts), which is approximately 46% of the 1,845,144 prescribed opioid users (includes addicts) over the entire year. Therefore, we assume a similar ratio for (non-heroin addicted) opioid addicts, which gives an estimate of 20,142 prescription opioid addicts in 2013 Quarter 1. However, we care about approximately how many of these are using opioids that they are personally prescribed, which following similar calculations as before, is $.443 \cdot 20142 = 8,923$ individuals; this number must be subtracted from 856,000 resulting in the estimated number of non-addicted prescribed opioid users in 2013 Quarter 1. We do this calculation for all quarters from 2013-2018. We note here that although individuals are receiving opioids for pain, individuals could be not taking them at all or selling/sharing them so this data does not account for patient behavior after filling their prescriptions.

Table 2.2: The following table gives estimates for the number of individuals prescribed opioids each quarter in the years 2013-2018. **Bolded** values are numbers that we estimated by information within the same year. All other numbers are actual reported data. Numbers in blue are data used directly in parameter estimation. Source: [3] Prescription Drug Overdose Program Report/Tennessee's Annual Overdose Report [84, 86].

Quarter	Prescribed opioid users (includes Rx addicts)	Prescribed opioid users (excludes Rx addicts)
2013 Quarter 1	856,000[3]	**847,077**
2013 Quarter 2	870,000[3]	**860,931**
2013 Quarter 3	874,000[3]	**864,889**
2013 Quarter 4	856,000[3]	**847,077**
2014 Quarter 1	842,000[3]	**833,223**
2014 Quarter 2	860,000[3]	**851,035**
2014 Quarter 3	871,000[3]	**861,921**
2014 Quarter 4	850,000[3]	**841,140**
2015 Quarter 1	836,000[3]	**827,285**
2015 Quarter 2	861,000[3]	**852,025**
2015 Quarter 3	865,000[3]	**855,983**
2015 Quarter 4	854,000[3]	**845,098**
2016 Quarter 1	840,000[3]	**832,085**
2016 Quarter 2	829,000[3]	**821,189**
2016 Quarter 3	801,000[3]	**793,453**
2016 Quarter 4	783,000[3]	**775,622**
2017 Quarter 1	783,000[3]	**775,622**
2017 Quarter 2	772,000[3]	**764,726**
2017 Quarter 3	747,000[3]	**739,961**
2017 Quarter 4	713,000[3]	**706,282**
2018 Quarter 1	695,000[3]	**688,451**
2018 Quarter 2	690,000[3]	**683,498**
2018 Quarter 3	648,000[3]	**641,894**
2018 Quarter 4	631,000[3]	**625,054**

We acknowledge that many data points are only estimates since there is a nesting of the classes, but believe they are a good starting point for our purposes here.

2.4.1 Parameter Calculations

The age-adjusted death rate (μ) and overdose death rates (μ_A and μ_H) are calculated from available mortality information.

The **age-adjusted death rate** for Tennessee in 2016 was calculated to be 728.8 out of 100,000 individuals, or approximately 41,165 people out of a total population 12 and older of 5,648,259 [68]. Subtracting off the number of people who died from a prescription opioid or heroin/fentanyl overdose in 2016 from the A or H class results in 40,296 people who died that year. This implies that (5,648,259-40,296)/5,648,259 ≈ 0.993 is the proportion of the population that remains by the beginning of 2017. If we consider T_0 to be the total population in 2016, we can find the continuous-time rate at which individuals die naturally from the equation $0.993T_0{=}T_0e^{-\mu t}$, which results in the natural death rate $\boldsymbol{\mu \approx 0.00710}$.We calculate the **prescription opioid addict overdose death rate** in the year 2015, since we have a reasonable estimate for the number of (non-heroin) prescription opioid addicted individuals in that year and is toward the middle of our time frame. To find the continuous-time rate at which individuals are dying from the addicted class, we consider the equation $kA_0 = A_0e^{-\mu_A t}$, where A_0 is the number of individuals addicted to prescription opioids in 2015 and k is the proportion of these individuals in the addicted class at the start of 2016 (when $t = 1$). In 2015, there were 690 individuals out of the entire Tennessee population 12 and older that overdosed on prescription opioids [84]. However, it is estimated that only 54.6% of these individuals were actually at an increased risk for an opioid-related overdose death; we assume that if an individual met the criteria for at least one high-risk factor, that they were considered addicted to prescription opioids [7]. Therefore, we assume 54.6% of the 690 individuals that overdosed were addicted, which gives 377 individuals. With a total of 42,816 prescription opioid addicts (non-heroin addicted) in 2015, this means that (42,816-377)/42,816 ≈ 0.991 is the proportion of addicted individuals that remain by the beginning of the next year. This implies $0.991A_0 = A_0e^{-\mu_A(1)}$, and solving results in $\boldsymbol{\mu_A \approx 0.00884}$. We note that since we want a rate of overdose deaths out of the addicted class, we use

Table 2.3: Parameter values calculated from data and assumed.

Parameter (rate)	Value Assumed	Units
μ	0.00710	$\frac{1}{\text{year}}$
μ_A	0.00884	$\frac{1}{\text{year}}$
μ_H	0.0466	$\frac{1}{\text{year}}$
ω	10^{-10}	dimensionless

the number of non-heroin addicted prescription opioid addicts, although the overdose death data we estimated above is out of all prescription opioids addicts, whether they are addicted to heroin or not. However, since we do not know the number of overdoses specifically for non-heroin addicted prescription opioid addicts, we use this simplification that all of the prescription opioid overdose deaths we estimated above are from this group.

Similarly, we may calculate the **heroin/fentanyl addict overdose death rate**. There were 7,560 heroin/fentanyl addicts in 2015 and 344 total heroin or fentanyl related overdoses. We make the simplifying assumption that if an individual died of a heroin or fentanyl overdose they were addicted to either of the drugs. This means that (7,560-344)/7,560 ≈ 0.954 is the proportion of heroin users that remain at $t = 1$, which implies $0.954H_0 = H_0 e^{-\mu_H(1)}$, which results in $\boldsymbol{\mu_H \approx 0.0466}$, the continuous-time rate at which individuals are dying from the heroin class.

We make a note that individuals that do not have an opioid use disorder and die because of an opioid overdose are counted in the "natural mortality rate." Results from all three death rates are shown in Table 2.3.

2.4.2 Parameter Estimation

In order to estimate the remaining parameters for our model, we utilize the ordinary least squares method. We formulate an objective function to minimize, which consists of the squared differences between data and model simulations, and is weighted by the size of the data squared. The data utilized (shown in blue in Table 2.1) are the proportion of non-addicted prescription users (years 2013-2017), prescription opioid addicts (years 2013-2017), heroin/fentanyl addicts (years 2014-2016) out of the entire population in a given year, as well

as the heroin/fentanyl overdoses (2013-2017) and prescription opioid overdoses (2013-2016, excluding the 2017 data point as it is an outlier compared to the rest of the years and therefore not representative of the major trend). These represent the proportion of individuals in P at some point during each of the years 2013-2017, the proportion of individuals in A at some point during each of the years 2014-2015, the proportion of individuals in H at some point during each of the years 2014-2016, and individuals dying out of the H and A class, respectively. From Table 2.2, we have the proportion of the population that is in P each quarter of the years 2013-2018. This results in a total of 48 data points.

We simulate the proportions in each of these classes throughout the year in the following way. In order to count the proportion of individuals in P, A, or H at some point throughout a certain year, we need to count those who are in each of the classes *at all* during the year, even if they leave or come back at some point. We note that although the data we use is about the total proportion of people who are in the class at some point throughout the year (i.e. unique individuals), in our model, we neglect higher order terms (i.e. people who go in and out of the P class multiple times), since we can't keep track of individuals.

To get the output from the model of the proportion of non-addicted prescription opioid users in each year, we take the proportion of non-addicted prescription opioid users at the beginning of each of the years and add on the proportion of individuals that enter the P class at any point during the year. This latter part comes from integrating over those who enter the P class: $\int_0^t X'(t)dt = \int_0^t \alpha S(t)dt$ which is equal to $X(t) - X(0)$; here, we take $X(0) = 0$. For every year except 2013, a subtraction must be done since integrating gives the proportion from time 0 to time t, but we only want the proportion from time $t-1$ to time t (i.e. the new cases in a given year) to compare to data. Thus, the calculation is as follows for each year, with the last equation in each line what was calculated in the code. We note that our time step is years, but is partitioned into quarters of a year, so each entry represents the beginning of a quarter in some year. For example, y(9,2) represents the 9^{th} quarter since the beginning of 2013 (which is the first quarter of 2015) and 2 represents the second differential equation, which represents the P class.

2013: $P_0 + \int_0^1 \alpha S dt = y(1,2) + y(5,6) - y(1,6)$

2014: $y(5,2) + \int_1^2 \alpha S dt = y(5,2) + \int_0^2 \alpha S dt - \int_0^1 \alpha S dt = y(5,2) + y(9,6) - y(5,6)$

2015: $y(9,2) + \int_2^3 \alpha S dt = y(9,2) + \int_0^3 \alpha S dt - \int_0^2 \alpha S dt = y(9,2) + y(13,6) - y(9,6)$

2016: $y(13,2) + \int_3^4 \alpha S dt = y(13,2) + \int_0^4 \alpha S dt - \int_0^3 \alpha S dt = y(13,2) + y(17,6) - y(13,6)$

2017: $y(17,2) + \int_4^5 \alpha S dt = y(17,2) + \int_0^5 \alpha S dt - \int_0^4 \alpha S dt = y(17,2) + y(21,6) - y(17,6)$

2018: $y(21,2) + \int_5^6 \alpha S dt = y(21,2) + \int_0^6 \alpha S dt - \int_0^5 \alpha S dt = y(21,2) + y(25,6) - y(21,6)$

We denote

$$\text{Data1} = \begin{bmatrix} 1825910/5519417 \\ 1805325/5559702 \\ 1800614/5602187 \\ 1744766/5648259 \\ 1620955/5702475 \\ 1455093/5754509 \end{bmatrix}$$

as the vector of values that represents the total proportion of the population that is in the P class at some point during the years 2013-2017 and

$$\text{Estim1} = \begin{bmatrix} y(1,2) + y(5,6) - y(1,6) \\ y(5,2) + y(9,6) - y(5,6) \\ y(9,2) + y(13,6) - y(9,6) \\ y(13,2) + y(17,6) - y(13,6) \\ y(17,2) + y(21,6) - y(17,6) \\ y(21,2) + y(25,6) - y(21,6) \end{bmatrix}$$

represents the total proportion that the model simulates as being in the P class at some point during the years 2013-2017, as described above. The vector Diff1=Estim1-Data1 represents the difference in these values each of the years. In order to find the relative error we calculate

$$\sqrt{\sum_{i=1}^{6} \text{Diff1(i)}^2} / \sqrt{\sum_{i=1}^{6} \text{Data1(i)}^2}.$$

To get the output from the model of the proportion of (non-heroin addicted) prescription opioid addicts in each of the years 2013-2018, we take the initial proportion of prescription opioid addicts in each of these years and add the proportion of individuals that enter the A class at any point during the year. This latter part comes from integrating over those who enter the A class: $\int_0^t L'(t)dt = \int_0^t (\gamma P + \sigma R \frac{A}{A+H+\omega} + \beta_A SA + \beta_P SP)dt$ which is equal to $L(t) - L(0)$; here, we take $L(0) = 0$. Similar to above with the subtraction of integrals to calculate for a specific year, we have:

2013: $A_0 + \int_0^1 (\gamma P + \sigma R \frac{A}{A+H+\omega} + \beta_A SA + \beta_P SP)dt = y(1,3) + y(5,7) - y(1,7)$

2014: $y(5,3) + \int_1^2 (\gamma P + \sigma R \frac{A}{A+H+\omega} + \beta_A SA + \beta_P SP)dt = y(5,3) + y(9,7) - y(5,7)$

2015: $y(9,3) + \int_2^3 (\gamma P + \sigma R \frac{A}{A+H+\omega} + \beta_A SA + \beta_P SP)dt = y(9,3) + y(13,7) - y(9,7)$

2016: $y(13,3) + \int_3^4 (\gamma P + \sigma R \frac{A}{A+H+\omega} + \beta_A SA + \beta_P SP)dt = y(13,3) + y(17,7) - y(13,7)$

2017: $y(17,3) + \int_4^5 (\gamma P + \sigma R \frac{A}{A+H+\omega} + \beta_A SA + \beta_P SP)dt = y(17,3) + y(21,7) - y(17,7)$

2018: $y(21,3) + \int_5^6 (\gamma P + \sigma R \frac{A}{A+H+\omega} + \beta_A SA + \beta_P SP)dt = y(21,3) + y(25,7) - y(21,7)$

Similar to above,

$$\text{Data2} = \begin{bmatrix} 43418/5519417 \\ 42928/5559702 \\ 42816/5602187 \\ 37464/5648259 \\ 34805/5702475 \\ 31244/5754509 \end{bmatrix}$$

and

$$\text{Estim2} = \begin{bmatrix} y(1,3)+y(5,7)-y(1,7) \\ y(5,3)+y(9,7)-y(5,7) \\ y(9,3)+y(13,7)-y(9,7) \\ y(13,3)+y(17,7)-y(13,7) \\ y(17,3)+y(21,7)-y(17,7) \\ y(21,3)+y(25,7)-y(21,7) \end{bmatrix}$$

represent the actual and simulated total proportion of individuals in A at some point during the years 2013-2018. Again, we have Diff2=Estim2-Data2 being the vector of differences in these values each of the years and the relative error is calculated by

$$\sqrt{\sum_{i=1}^{6} \text{Diff2(i)}^2} / \sqrt{\sum_{i=1}^{6} \text{Data2(i)}^2}.$$

To obtain the output from the model of the proportion of heroin/fentanyl addicts for each year 2014-2016, we take the initial proportion of heroin/fentanyl addicts in each of these years and add the proportion of individuals that enter the H class at any point during the year. This latter part comes from integrating over those who enter the H class: $\int_0^t M'(t)dt = \int_0^t (\theta_1 SH + \theta_2 PH + \theta_3 AH + \sigma R \frac{H}{A+H+\omega})dt$ which is equal to $M(t) - M(0)$; here, we take $M(0) = 0$. Similar to above with the subtraction of integrals to calculate for a specific year, we have:

2014: $y(5,4) + \int_1^2 (\theta_1 SH + \theta_2 PH + \theta_3 AH + \sigma R \frac{H}{A+H+\omega})dt = y(5,4) + y(9,8) - y(5,8)$

2015: $y(9,4) + \int_2^3 (\theta_1 SH + \theta_2 PH + \theta_3 AH + \sigma R \frac{H}{A+H+\omega})dt = y(9,4) + y(13,8) - y(9,8)$

2016: $y(13,4) + \int_3^4 (\theta_1 SH + \theta_2 PH + \theta_3 AH + \sigma R \frac{H}{A+H+\omega})dt = y(13,4) + y(17,8) - y(13,8)$.

Here,

$$\text{Data3} = \begin{bmatrix} 7560/5559702 \\ 7560/5602187 \\ 10260/5648259 \end{bmatrix}$$

and

$$\text{Estim3} = \begin{bmatrix} y(5,4) + y(9,8) - y(5,8) \\ y(9,4) + y(13,8) - y(9,8) \\ y(13,4) + y(17,8) - y(13,8) \end{bmatrix}$$

represent the actual and simulated total proportion of individuals in H at some point during the years 2014-2016, with Diff3=Estim3-Data3 being the vector representing the difference in these values each year. The relative error is calculated as

$$\sqrt{\sum_{i=1}^{3} \text{Diff3(i)}^2} / \sqrt{\sum_{i=1}^{3} \text{Data3(i)}^2}.$$

Next, to obtain the output from the model of the proportion of prescription opioid users each quarter from 2013-2018, we take the initial proportion of prescription opioid users in each quarter and add the proportion of individuals that enter the P class at any point during the quarter. Since we do not know the exact population in each quarter for Tennessee (only have yearly estimates), we keep the yearly population as constant for each quarter, so this is an approximation. This latter part comes from integrating over those who enter the P class: $\int_0^t X'(t)dt = \int_0^t \alpha S(t)dt$ which is equal to $X(t) - X(0)$; as before, we take $X(0) = 0$. Similar to above, we will use subtraction of integrals to calculate for a specific quarter:

2013 Quarter 1: $P_0 + \int_0^{0.25} \alpha S dt = y(1,2) + y(2,6) - y(1,6)$

2013 Quarter 2: $y(2,2) + \int_{0.25}^{0.5} \alpha S dt = y(2,2) + \int_0^{.5} \alpha S dt - \int_0^{0.25} = y(2,2) + y(3,6) - y(2,6)$

2013 Quarter 3: $y(3,2) + \int_{0.5}^{0.75} \alpha S dt = y(3,2) + \int_0^{.75} \alpha S dt - \int_0^{0.5} \alpha S dt = y(3,2) + y(4,6) - y(3,6)$

2013 Quarter 4: $y(4,2) + \int_{0.75}^{1} \alpha S dt = y(4,2) + \int_0^{1} \alpha S dt - \int_0^{0.75} \alpha S dt = y(4,2) + y(5,6) - y(4,6)$

$\vdots$

2018 Quarter 4: $y(24,2) + \int_{5.75}^{6} \alpha S dt = y(24,2) + \int_0^{6} \alpha S dt - \int_0^{5.75} \alpha S dt = y(24,2) + y(25,6) - y(24,6)$.

The data used to compare to the model are shown here:

$$\text{Data4} = \begin{bmatrix} 847077/5519417 \\ 860931/5519417 \\ 864889/5519417 \\ 847077/5519417 \\ 833223/5559702 \\ 851035/5559702 \\ 861921/5559702 \\ 841140/5559702 \\ 827285/5602187 \\ 852025/5602187 \\ 855983/5602187 \\ 845098/5602187 \\ 832085/5648259 \\ 821189/5648259 \\ 793453/5648259 \\ 775622/5648259 \\ 775622/5702475 \\ 764726/5702475 \\ 739961/5702475 \\ 706282/5702475 \\ 688451/5754509 \\ 683498/5754509 \\ 641894/5754509 \\ 625054/5754509 \end{bmatrix}$$

and

$$\text{Estim4} = \begin{bmatrix} y(1,2) + y(2,6) - y(1,6) \\ y(2,2) + y(3,6) - y(2,6) \\ y(3,2) + y(4,6) - y(3,6) \\ y(4,2) + y(5,6) - y(4,6) \\ \vdots \\ y(23,2) + y(24,6) - y(23,6) \\ y(24,2) + y(25,6) - y(24,6) \end{bmatrix}$$

represents simulated total proportion of individuals in P at some point during a given quarter in the years 2013-2018, with Diff4=Estim4-Data4 being the vector representing the difference in these values each quarter. The relative error is calculated as

$$\sqrt{\sum_{i=1}^{24} \text{Diff4(i)}^2} / \sqrt{\sum_{i=1}^{24} \text{Data4(i)}^2}.$$

Including both sets of data from Data1 and Data4 is useful in our model. Entries in Data1 represent the number of unique individuals that are prescribed opioids in a certain year. However, someone could continue taking opioids and be counted in the next year, as well, meaning these values represent non-unique individuals across years. Similarly, entries in Data4 represent the number of unique prescribed individuals in a certain quarter, but since an individual can be prescribed in more than one quarter, they are non-unique individuals across quarters. Thus, the values of four quarters in Data4 that represent a certain year *do not* add to the total number of prescribed unique individuals in that year since individuals could be counted multiple times in the quarters. We use both yearly and quarterly data since that is more information for our system and provides a cap on the total number of unique individuals in a certain year.

To obtain the output from the model of the proportion of prescription opioid addicts that overdose each year from 2013-2016, we integrate over those who die via an overdose out of the prescription opioid addicted class using $\int_0^t J'(t) = \int_0^t \mu_A A(t)$. Note that we omit the

2017 data point as it does not fit the general trend of increasing overdose deaths as time goes on and therefore, we believe this outlier affects the fitting of the model to the data in a way that does not represent the general trend. A subtraction must be performed since integrating gives the proportion from time 0 to time t, but we only want the proportion from time $t-1$ to time t (i.e. the new overdoses in a given year) and given that our mesh is quarters of a year, we have the following calculations for each year:
2013: $\int_0^1 \mu_A A = y(5,9) - y(1,9)$
2014: $\int_1^2 \mu_A A = y(9,9) - y(5,9)$
2015: $\int_2^3 \mu_A A = y(13,9) - y(9,9)$
2016: $\int_3^4 \mu_A A = y(17,9) - y(13,9)$.

Specifically,

$$\text{Data5} = \begin{bmatrix} 348/5519417 \\ 381/5559702 \\ 463/5602187 \\ 551/5648259 \end{bmatrix}$$

and

$$\text{Estim5} = \begin{bmatrix} y(5,9) - y(1,9) \\ y(9,9) - y(5,9) \\ y(13,9) - y(9,9) \\ y(17,9) - y(13,9) \end{bmatrix}$$

represent the actual and simulated total proportion of individuals that overdose from the prescription opioid addicted class at some point during the years 2013-2016, with Diff5=Estim5-Data5 being the vector representing the difference in these values each year.

The relative error is calculated as

$$\sqrt{\sum_{i=1}^{4} \text{Diff5(i)}^2} / \sqrt{\sum_{i=1}^{4} \text{Data5(i)}^2}.$$

Finally, to obtain the output from the model of the proportion of heroin/fentanyl addicts that overdose each year 2013-2017, we integrate over those who die via an overdose out of the heroin/fentanyl addicted class using $\int_0^t K'(t) = \int_0^t \mu_H H(t)$. A subtraction must be performed since integrating gives the proportion from time 0 to time t, but we only want the proportion from time $t-1$ to time t (i.e. the new overdoses in a given year) and given that our mesh is in quarters, we have the following for each year:

2013: $\int_0^1 \mu_H H = y(5,10) - y(1,10)$

2014: $\int_1^2 \mu_H H = y(9,10) - y(5,10)$

2015: $\int_2^3 \mu_H H = y(13,10) - y(9,10)$

2016: $\int_3^4 \mu_H H = y(17,10) - y(13,10)$

2017: $\int_4^5 \mu_H H = y(21,10) - y(17,10)$.

In this case,

$$\text{Data6} = \begin{bmatrix} 116/5519417 \\ 216/5559702 \\ 374/5602187 \\ 554/5648259 \\ 811/5702475 \end{bmatrix}$$

and

$$\text{Estim6} = \begin{bmatrix} y(5,10) - y(1,10) \\ y(9,10) - y(5,10) \\ y(13,10) - y(9,10) \\ y(17,10) - y(13,10) \\ y(21,10) - y(17,10) \end{bmatrix}$$

represent the actual and simulated total proportion of individuals that overdose from the heroin/fentnayl addicted class at some point during the years 2013-2017, with Diff6=Estim6-Data6 being the vector representing the difference in these values each year. The relative error is calculated as

$$\sqrt{\sum_{i=1}^{5} \text{Diff6(i)}^2} / \sqrt{\sum_{i=1}^{5} \text{Data6(i)}^2}.$$

Since we wish to minimize the difference between the data in all six of these data sets and the corresponding values that our model simulates, we add together their relative norms and set this as our objective function value to minimize. Thus our

$$\text{objective function} =$$

$$\sum_{j=1}^{2} \frac{\sqrt{\sum_{i=1}^{6} \text{Diffj(i)}^2}}{\sqrt{\sum_{i=1}^{6} \text{Dataj(i)}^2}} + \frac{\sqrt{\sum_{i=1}^{3} \text{Diff3(i)}^2}}{\sqrt{\sum_{i=1}^{3} \text{Data3(i)}^2}} + \frac{\sqrt{\sum_{i=1}^{24} \text{Diff4(i)}^2}}{\sqrt{\sum_{i=1}^{24} \text{Data4(i)}^2}} + \frac{\sqrt{\sum_{i=1}^{4} \text{Diff5(i)}^2}}{\sqrt{\sum_{i=1}^{4} \text{Data5(i)}^2}} + \frac{\sqrt{\sum_{i=1}^{5} \text{Diff6(i)}^2}}{\sqrt{\sum_{i=1}^{5} \text{Data6(i)}^2}}$$

Note that we take the relative error in each of these due to the differences in magnitude of the data.

In order to minimize our objective function, we use the MultiStart algorithm and fmincon local solver from the Global Optimization Toolbox in MATLAB [74]. Multiple points are used in order to find multiple local minima of the given problem, and ultimately the global minimum. First, MultiStart checks the problem inputs by running fmincon once to make sure they are valid. Then, given the user-supplied starting point and a desired n starting points total, MultiStart generates n-1 starting points, choosing starting points based on a

uniform distribution (i.e. equal probability for each point to be chosen) within the bounds provided.

Next, MultiStart runs fmincon with these starting points and runs until the maximum time allotted by the user for each iteration; if it exceeds that many seconds, then it exits the iteration without giving a solution. The fmincon solver is a local solver that finds the minimum of a constrained, nonlinear, multivariable function [73]. In our case, our objective function relies on solutions from our ODEs, in which we give realistic bounds on our parameters. (Note: to solve our ODEs, we use the MATLAB ode15s (stiff ODE) solver due to a sharp corner in the solution of P that results with using ode45). The default optimization algorithm of fmincon is the interior point algorithm which sets components of starting points to be strictly between the bounds if they initially are not. The fmincon local solver is a gradient-based method with a two-step process for iterations, and the set of initial values that lead to the same solution is known as the basin of attraction. The local solver finds the local minimum in the basin of attraction of each starting point, and therefore, MultiStart searches through multiple basins of attraction for the optimum [75].

MultiStart runs all start points and stops when either it runs out of start points or its total run time exceeds the maximum time allotted [74]. First order optimality measures how close a point x is to optimal, and it is necessary to be 0 at a minimum, but the solver requires it to be less than an optimality tolerance with a default of $1e^{-6}$. The solver returns the solution, the value of the objective function at the solution, and an exitflag in which a positive value of the latter means that a local minimum has been found.

Solutions are considered identical by the solver if they are within a default $1e^{-6}$ relative distance from one another and their objective function values are also within a default $1e^{-6}$ relative difference from one another. Once MultiStart has stopped, it sorts the local solutions based on the value of the objective function from lowest to highest. It then loops over all of the local solutions j starting with the best solution to find all solutions k such that:

$$|\text{Fval(k)-Fval(j)}| \leq \text{FunctionTolerance} \cdot \max(1, |\text{Fval(j)}|)$$

$$|\text{x(k)-x(j)}| \leq \text{XTolerance} \cdot \max(1,|\text{x(j)}|).$$

This looping allows solutions to be recognized as the same (i.e. within $1e^{-6}$ of each other) and repeat solutions to be thrown out (i.e. same local min from different starting points). Then entries based on this information are stored in the GlobalOptimSolution object vector containing information on where the local minimum is, the corresponding value of the objective function, and the starting points that led to the minimum. Once complete, a summary is given that provides information on the number of fmincon runs that converged, did not converge, or had errors. Although GlobalSearch has a similar method to finding global minima and is most efficient, it rejects many starting points unless they have a good chance of resulting in a global minimum, whereas MultiStart searches more thoroughly for a global minimum by using all generated starting points.

Since the global minimum is of interest, we use 2000 starting points, as this is a local solver (this value was chosen so that upon consecutive runs, an objective function value of 0.3273 was reached in the case with the best fit: Case 4 described later.) We run our model from the beginning of 2013 to the beginning of 2019 (6 years), keeping a short time frame so that dynamics are relatively the same in the time period with the time step in years.

Parameter Bounds

Although we have an estimate for the total number of prescription opioid users and opioid addicts in 2013, we do not know these numbers at the start of 2013; similarly, we do not know this information for the other state variables. Therefore, we estimate the initial conditions using this process, as well. Parameter values that we assume prior to parameter estimation are given in Table 2.4. Upper and lower bounds for parameters to be estimated are given in Table 2.5, as well as reasoning behind the choices for the bounds, with some parameter bounds requiring calculation described in detail below. The use of inputs $\tilde{m}$, $\tilde{b}$, $\tilde{c}$, $\tilde{d}$, and $\tilde{e}$ will be described later in this section.

Parameters β_P and β_A:

We were not able to find values in the literature specific to Tennessee regarding an illicit-induced addiction rate; however, we use information from the national level, as we do not have any evidence that this national average rate is significantly different in Tennessee. We

Table 2.4: Parameters values assumed prior to parameter estimation process.

Parameter	Value
μ	0.00710
μ_A	0.00884
μ_H	0.0466
ω	10^{-10}

do this to get an idea of the values of bounds to put on parameters β_P and β_A for our parameter estimation. In 2015, there were an estimated 2.1 million individuals 12 and older that initiated pain reliever misuse recently [61]. Using this source, we take pain relievers to be equivalent to prescription opioids. To calculate approximately how many of these would end up having a use disorder in 2015, this same study states that 12.5 million people misused prescription opioids in the past year total, and that there were 2.0 million with a prescription opioid disorder. Using these numbers, we make an estimate that the proportion of those with a use disorder out of those who misuse is

$$\frac{\text{2 million people with pain reliever use disorder in 2015}}{\text{12.5 million people who misused pain relievers in 2015}} = 0.16.$$

We extrapolate this to estimate that 16% of the 2.1 million recent initiates of misuse are those who should be counted in the use disorder category (although we do not know the timeline of developing the use disorder and it may not happen within the year, it gives a rough idea). This results in an estimate of 336,000 individuals that were recent initiates of pain reliever misuse that we will consider having a use disorder within the year 2015. In the same year, a study was done regarding the source of the most recent episode of misuse of prescription opioids among adults reporting an prescription opioid use disorder in the past year [53]. (Note: this study was for individuals age 18 and older whereas the study done in [61] was for those 12 and older; we will assume for simplicity that the information for those 18 and older will be similar to those between 12 and 18, as well.) Here, 52.8% of the prescription opioids were from a non-physician source, which included being given to/bought from a friend/relative, or bought from a drug dealer/stranger. For simplicity, let IPUD indicate individuals with a prescription use disorder. Thus,

Table 2.5: Parameter bounds for parameter estimation.

Input	Range	Reasoning behind choice of range
$\tilde{b}$	[0.1, 0.5]	Expected order of magnitude for α is 10^{-1} based on value in [6], assume y-intercept of the linear form of α will be similar.
$\tilde{m}$	[-0.1, -0.001]	Based on order of magnitude of $\tilde{b}$, assume slope of α will have a smaller order of magnitude and will be negative due to a decrease in prescribing behavior on average.
$\tilde{c}$	[-0.1, -0.001]	Assume will be more negative than $\tilde{m}$ due to steeper slope, but will keep same range as $\tilde{m}$ due to uncertainty of how much more negative.
β_A	[0.00001, 0.01]	Based on preliminary calculations (see below).
β_P	[0.00001, 0.01]	Based on preliminary calculations (see below).
ε	[1, 5]	Estimate from [6]; assume high rate because the majority of individuals finish their prescriptions (some finishing more than 1 in a year) and do so quickly. Each year from 2013-2017, approximately 50% of patients prescribed opioids for pain had active prescriptions for a week or less and about 70% had them for 30 days or less [84, 86]. We assume one higher order of magnitude than α based on the expected difference in the orders of magnitude of S and P.
γ	[0.005, 0.1]	Estimate based on value in [6]; we consider this parameter important to estimate because of the sensitivity of the prescription opioid-only model to this parameter.
θ_1	[0.05, 0.3]	Based on preliminary calculations (see below).
θ_2	[0.1, 0.4]	Based on preliminary calculations (see below).
θ_3	[10, 20]	Based on preliminary calculations (see below).
ζ	[0.0001, 0.2]	Based on preliminary calculations (see below).
ν	[0.0001, 0.2]	Based on preliminary calculations (see below).
σ	[0.1, 2]	Based on preliminary calculations (see below).
$\tilde{e}$	[0.001, 0.1]	The calculated estimate of μ_A was 0.00884, so assume the y-intercept of the linear form of μ_A will be a similar magnitude.
$\tilde{d}$	[0.0001, 0.008]	Based on order of magnitude of $\tilde{e}$ and estimated value of μ_A, assume slope of μ_A will have a smaller order of magnitude and will be positive due to an increase in prescription opioid overdoses.
P_0	[0.001, 0.35]	Assume small but no greater than 35% of the population since during 2013, the estimated total proportion of prescribed users out of the entire population is $\frac{1,825,910}{5,519,417} \approx 0.33$.
A_0	[0.0001, 0.01]	Assume small but no greater than 1% of the population since during 2013, the estimated total proportion of prescription opioid addicts out of the entire population is $\frac{43,418}{5,519,417} \approx 0.0079$.
H_0	[0.00001, 0.002]	Assume small but no greater than 0.2% of the population since during 2014 (no 2013 data available), the estimated total proportion of heroin/fentanyl addicts out of the entire population is $\frac{7,560}{5,559,702} \approx 0.0014$ so we assume a similar number in 2013.
R_0	[0.00001, 0.1]	Assume small but no greater than 10% of the population.

$$\frac{336,000 \text{ IPUD}}{320 \text{ million people}} \cdot \frac{0.528 \text{ opioid source for IPUD is illicit}}{\text{opioid sources} \cdot \text{year}}$$
$$= 0.000554 \frac{\text{IPUD obtain opioids illicitly}}{\text{opioid sources} \cdot \text{year}}.$$

From [53], we see that

$$\frac{0.138 \text{ opioids obtained from drug dealers/strangers by IPUD}}{0.528 \text{ opioids obtained illicitly by IPUD}} = 0.26$$

is the proportion of IPUD obtaining opioids by the black market or interaction with other addicts and

$$\frac{0.218 + 0.141 + 0.031 \text{ opioids given/bought from a friend/relative or other for IPUD}}{0.528 \text{ opioids obtained illicitly by IPUD}} = 0.74$$

is the proportion of IPUD obtaining opioids from extra prescriptions that are available. This means that 74% of illicit opioids come from a friend/relative/other source, whereas 26% of illicit opioids are from the black market for opioid addicts. In our model, we consider two cases in which individuals become addicted (friend/relative versus black market) and we make the assumption that these percentages also apply to the two routes that one would become an addict in the first place via illicit opioids.

Thus,

$$\frac{0.26 \text{ opioids from drug dealers/strangers}}{\text{opioids obtained illicitly}} \cdot \frac{0.000554 \text{ opioids obtained illicitly}}{\text{opioid sources} \cdot \text{year}}$$
$$= \frac{0.000141 \text{ opioids from drug dealers/strangers}}{\text{opioid sources} \cdot \text{year}}$$

is the rate that individuals illicitly obtain their prescription opioids from the black market/other addict interaction and become addicted

$$\implies \beta_A = \frac{0.000141}{\text{year}}.$$

Similarly,

$$\frac{0.74 \text{ opioids from friend/relative or other}}{\text{opioids obtained illicitly}} \cdot \frac{0.000554 \text{ opioids obtained illicitly}}{\text{opioid sources} \cdot \text{year}}$$

$$= \frac{0.000403 \text{ opioids from friend/relative or other}}{\text{opioid sources} \cdot \text{year}}$$

is the rate that individuals illicitly obtain their prescription opioids from extra pills that are available and become addicted

$$\implies \beta_P = \frac{0.000403}{\text{year}}.$$

Parameters θ_1, θ_2, and θ_3:

We consider a national study of individuals 12 and older to determine bounds on these three rates. For a national study consisting of 609,000 participants, of those that reported dependence/abuse of pain relievers in the past 12 months, 4.83% of them initiated heroin use (this is an average for the years 2009-2011). For simplicity, we assume these individuals fall into the definition of our A class. We assume that 54% of those actually became dependent on heroin, which is 2.6082% of these individuals ([83]).

In 2014, $\frac{7,560}{5,559,702} \approx 0.00136$ is the proportion of the population (unique individuals) that was in H at some point, and we assume this is similar in 2013 (or perhaps maybe a bit lower). Some individuals may transition to H multiple times and be counted again, so for the purpose of finding bounds, we will assume that any proportion from 0.0014 to 0.002 of the population (not necessarily unique individuals) is in H at least once during the year 2013. We denote this value H(2013). We make this simplifying assumption to be able to get rough estimates of ranges of potential values for these parameters.

Letting A(2013) represent the total proportion of the population that is in the A class at some point during 2013, we have that $0.026082A(2013) = \theta_3 A(2013)H(2013)$ is the proportion of the entire population that transitions from A to H in 2013. If $H(2013) = 0.002$ on the higher end of the range, then $\theta_3 = 13.04$ and if $H(2013) = 0.0014$ on the lower end of the range, then $\theta_3 = 18.63$. Therefore, we allow θ_3 to range between 10 and 20.

We do not have information on the proportion of the susceptible population that has prior non-medical pain reliever misuse, but for purposes of finding bounds on θ_1, we will make the

simplifying assumption that individuals in S have no prior non-medical pain reliever misuse. Muhuri et. al [78] estimates that 0.02% of individuals with no prior non-medical pain reliever misuse transition to heroin use in the past year on average for the years 2009-2011. Although this percentage may be low (i.e. there may be individuals in S that do have prior non-medical pain reliever misuse), we are taking this estimate to mean individuals move to the heroin class (i.e. no casual use). Therefore, the two assumptions may balance each other out, and again are for bound purposes only. Here, we calculate $0.0002\text{S}(2013)=\theta_1\text{S}(2013)\text{H}(2013)$. Setting H(2013)=0.002, as above, results in $\theta_1 = 0.1$ and setting H(2013)=0.0014 results in 0.1428. We take the bounds of θ_1 to be a bit wider, $[0.05, 0.2]$, to include situations as described in the assumptions above. The same study suggested that on average in 2009-2011, 0.34% of prior non-medical pain reliever misusers with no dependence/abuse in the past year transitioned to heroin use. For simplicity and the sake of finding bounds, we will assume individuals that fit this characterization are all in P. To find information on what percentage of individuals in P misuse, we looked at a synthesis of studies done in Vowles et al. [123], in which results from 38 studies on opioid misuse and addiction in patients with chronic pain were compared. From the high-quality studies only, it was estimated that 23.6%-24.9% of patients misused their prescriptions (which includes being addicted) and addiction rates ranged from 8.8% to 10.7%. Taking addicted users out of the misusers category since we are interested in individuals in P, we will make the assumption that 15% of those in P misuse their prescriptions. This could be current misuse or past misuse but for simplicity, we assume 15% of P individuals are currently misusing. Thus, $0.0034(.15)\text{P}(2013)=\theta_2\text{P}(2013)\text{H}(2013)$ leads to $\theta_2 = 0.255$ when H(2013)=0.002 and $\theta_2 = 0.364$ when H(2013)=0.0014. We set the bounds a bit wider to be $[0.1, 0.4]$ to make room for assumptions we have made (i.e. if 0.34% or 15% assumptions are too large for the P class).

Parameters ζ and ν:

An estimated 1 in 10 addicts go to treatment, and an estimated 70% of addicts that go to treatment relapse within 4 weeks after discharge [114, 94, 5]. In [94], 91% relapsed at some point after discharge. Thus, to get an idea on the order of magnitude of ν, the rate of being stably recovered from the heroin/fentanyl addicted class, we will use these

estimates. We would first like to calculate a reasonable lower bound on the percent of heroin/fentanyl addicts that remain in H one year after starting in H. If 1 in 10 addicts go to treatment, that means at least 90% stay in the H class for the entire year. Out of the 10% that go to treatment, 70% relapse within 4 weeks which means these individuals stay in H and the other 30% move to R. If we assume none of those who went to R come back within the year, then 0.9+0.1(0.7)=0.97 is the proportion of H that remains in H from the beginning of the year. Thus, looking at H'$= -\nu H$, solving gives H$= H_0 e^{-\nu t}$ and we assume $0.97H_0 = H_0 e^{-\nu(1)} \implies \nu \approx 0.0305$, giving us an idea of the order of magnitude of this parameter.

Since 70% relapsed within 4 weeks and we know 91% relapsed at some point after discharge, this means 21% relapsed after they transitioned to the stably recovered state. We also know that of those that relapsed in the study in [94], 92% went back to treatment sometime before 18-42 months after discharge. Therefore, in order to get a reasonable upper bound on the size of the H class for those who remain after one year, we assume the extreme case that everyone that went to R comes back to the H class. Thus, 30% of the 10% treated went to R from not relapsing within a month after discharge and we will assume that all 21% of those who relapsed back from the R class did so within the year meaning 0.1(0.3)(0.21)=0.0063 goes back to H. This gives a total proportion of 0.9763 left in H from what it began with, which gives $\nu \approx 0.024$. The same results come from looking at A'$= -\zeta A$ because we use the same estimates, so we have a general idea for the bounds for these parameters.

Parameter σ:

Of the opioid addicts who went to treatment and relapsed, 92% went back to treatment within 18-42 months in a study done in [94]. It is unknown how many of these individuals transitioned to R at all (i.e. stayed sober for more than 4 weeks post-discharge). We were not able to find the overall success rate of lifetime recovery (i.e. people accumulating in R and staying there) and therefore, we assume anywhere between 20-80% of those in R at the beginning of the year are in R by the end. Considering $\omega = 0$ for simplicity in this case, adding together the two relapse rates results in $\frac{\sigma R(A+H)}{A+H} = \sigma R$ and thus, we focus on

R'$= -\sigma R$. Letting 80% remain in R by the end of the year results in $0.8R_0 = R_0 e^{-\sigma(1)} \implies \sigma = 0.22$ and letting 20% remain, we have $0.2R_0 = R_0 e^{-\sigma(1)} \implies \sigma = 1.6$, giving an idea of orders of magnitude.

Upon holding all parameters constant from 2013-2019 in the parameter estimation process, many of the lower or upper bounds on the parameters (that we believe are realistic in Table 2.5) are achieved for the parameter values which is not informative. Thus, the global minimum is not found within the bounds and we instead explore four cases of the model with time-dependent parameters and compare our model fits to the data. In each case described hereafter, we recognize the estimated parameter values vary based on time and different locations within Tennessee, but are sufficient for analyzing the model at the state population level.

Case 1: Linear Function of Time for Prescribing Rate (α) and Constant Prescription Overdose Death Rate (μ_A)

The data seems to suggest an overall decrease in prescribing behavior in the time frame of our model, from 2013 to the beginning of 2019, and therefore, we make the prescribing rate α a time-dependent parameter. We first make the parameter a linear function of time of the form

$$\alpha = \tilde{m} \cdot t + \tilde{b}.$$

We estimate 17 inputs total (parameters and initial conditions combined, where $\tilde{m}$ and $\tilde{b}$ are both estimated for α) using the bounds found in Table 2.5 and assuming the values found in Table 2.4, where μ_A is assumed constant for this case. Out of 2000 runs, 1862 converged and Table 2.6 displays the resulting values of the inputs that were estimated with this process. The objective function value was equal to 0.4983.

Figure 2.2 shows the fits of our model to the data. The parameters from Table 2.6 result in the solution curves shown in Figure 2.3 of each of the classes from the beginning of 2013 through the beginning of 2019.

Table 2.6: This table displays the values of the parameters that were estimated with our model from Case 1, in which the prescribing rate, α, is a linear function of time and the prescription opioid overdose death rate, μ_A, is constant. With the estimated values for $\tilde{m}, \tilde{b}$, and $\tilde{c}$, the time-dependent parameter α starts at 0.292 in 2013 and decreases to 0.192 by 2019.

Input	Estimated Value	Units
$\tilde{m}$	-0.0167	$\frac{1}{\text{year}}$
$\tilde{b}$	0.292	$\frac{1}{\text{year}}$
β_A	0.0000220	$\frac{1}{\text{year}}$
β_P	0.0000108	$\frac{1}{\text{year}}$
θ_1	0.272	$\frac{1}{\text{year}}$
ε	2.559	$\frac{1}{\text{year}}$
γ	0.00500	$\frac{1}{\text{year}}$
θ_2	0.362	$\frac{1}{\text{year}}$
σ	0.100	$\frac{1}{\text{year}}$
ζ	0.0975	$\frac{1}{\text{year}}$
θ_3	19.992	$\frac{1}{\text{year}}$
ν	0.000116	$\frac{1}{\text{year}}$
P_0	0.0816	dimensionless
A_0	0.00762	dimensionless
H_0	0.000468	dimensionless
R_0	0.0000114	dimensionless
S_0	0.9103006	dimensionless

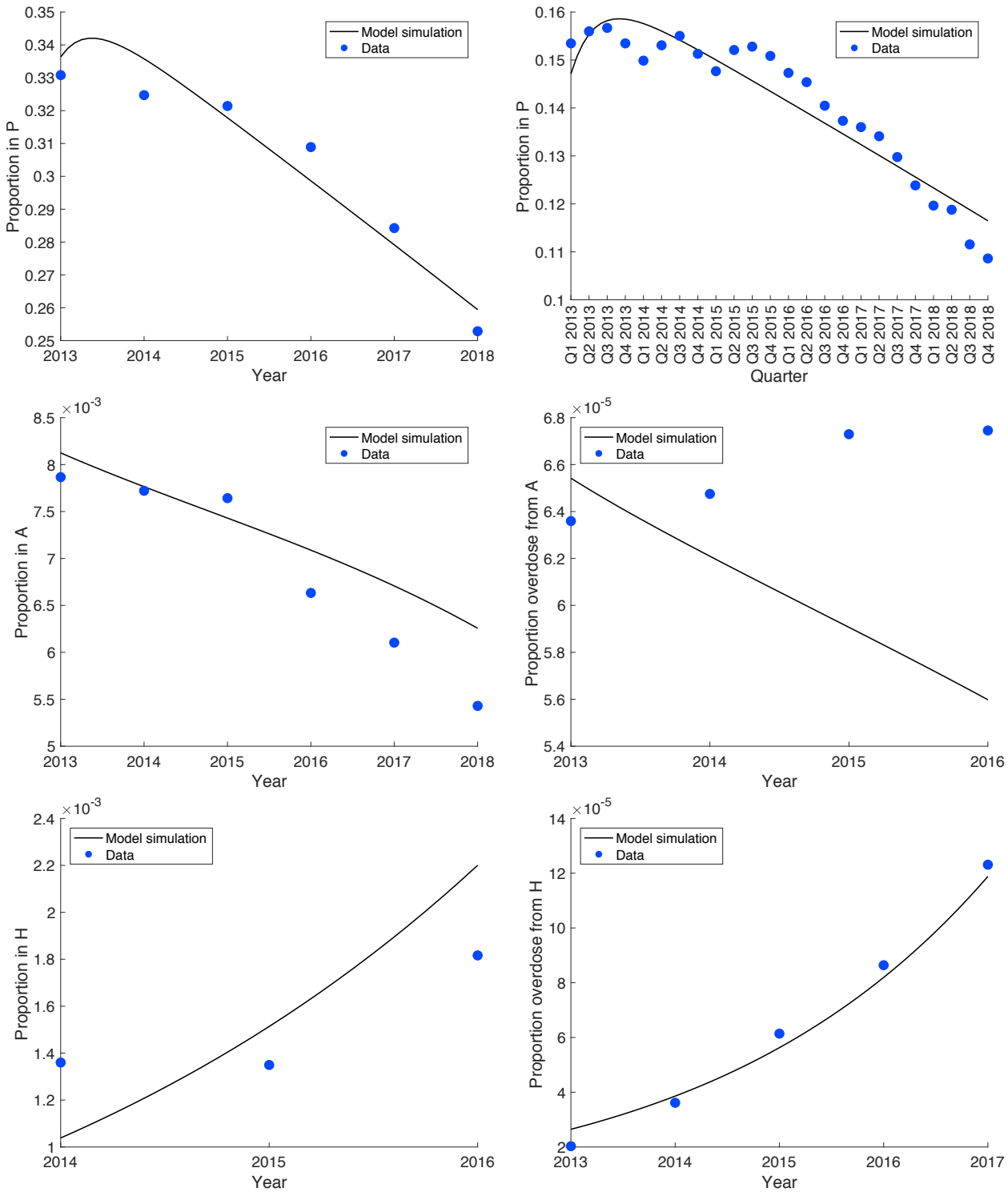


Figure 2.2: Model simulation fit to data for the α linear, μ_A constant model. This figure includes the fit to yearly prescription opioid user data, quarterly prescription opioid data, yearly prescription opioid addict data, yearly prescription opioid addict overdose death data, yearly heroin/fentanyl addict data, and yearly heroin/fentanyl overdose death data.

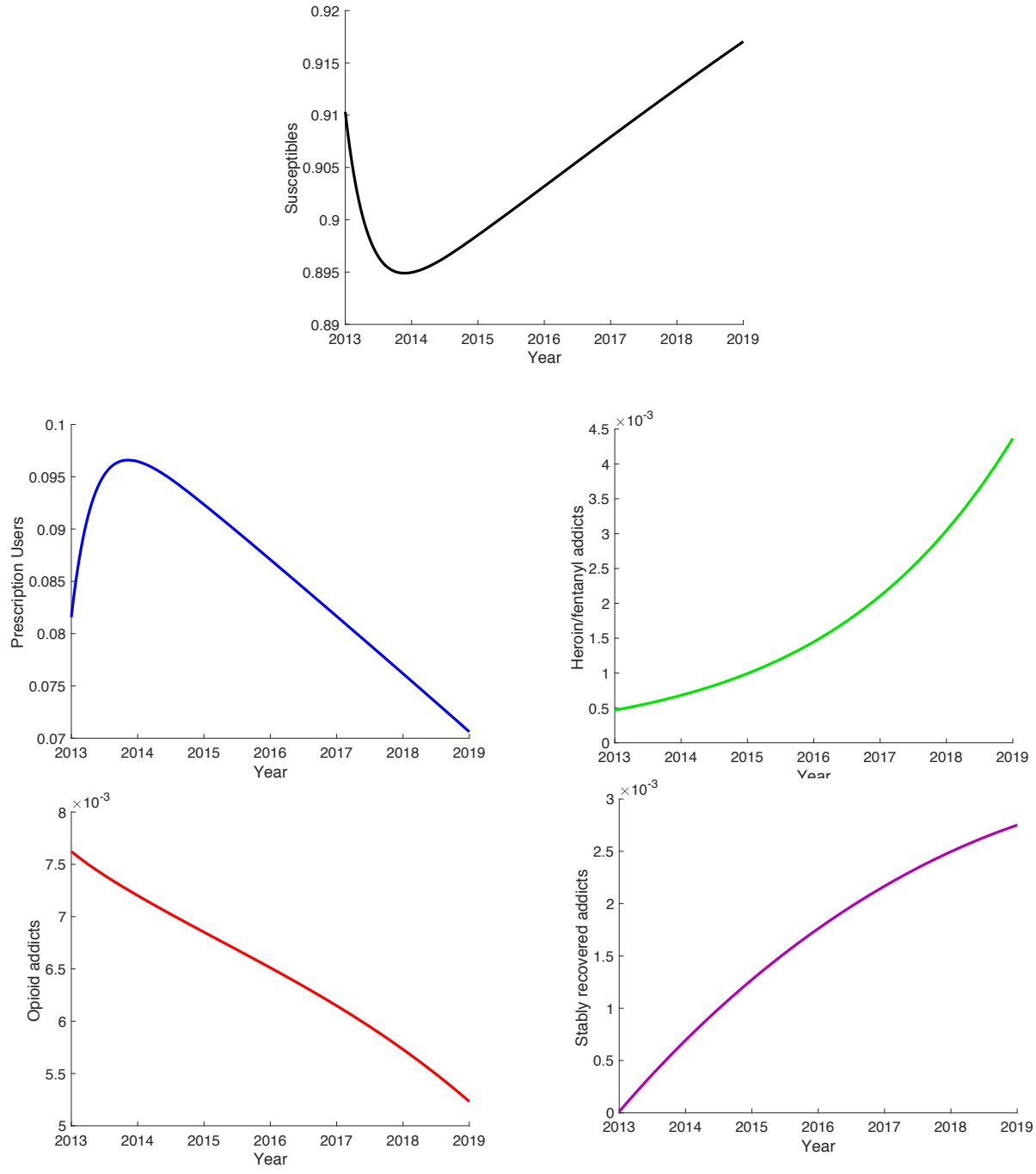


Figure 2.3: Numerical simulation for each of the population classes with parameters from Table 2.6 for the α linear, μ_A constant case.

Case 2: Linear Function of Time for both the Prescribing Rate (α) and Prescription Overdose Death Rate (μ_A)

Although the number of prescription opioid addicts decreased on average from 2015 to the beginning of 2017, the number of prescription opioid overdose deaths increased and consequently, we consider the case where the prescription overdose death rate (μ_A) is a linear time-dependent parameter, as well. We set

$$\mu_A = \tilde{d} \cdot t + \tilde{e}$$

and again have the form of

$$\alpha = \tilde{m} \cdot t + \tilde{b}.$$

Since we were not able to calculate what μ_A was for 2013 with extreme accuracy (since we only have the extrapolated number of prescription opioid addicts for 2013), we wish to estimate both $\tilde{d}$ and $\tilde{e}$, rather than setting the y-intercept and only finding the slope. The values of the assumed parameters μ, μ_H, and ω are given in Table 2.4 (note: we do not use the calculated μ_A from that table) and bounds on the parameters are given in Table 2.5. With 1831 runs converging out of 2000, the results for the 19 inputs that were estimated with this process are shown in Table 2.7. The objective function value is equal to 0.3609.

Figure 2.4 show the fits of our model simulations to data. The parameters from Table 2.7 result in the solution curves found in Figure 2.5 of each class from the beginning of 2013 through the beginning of 2019.

Case 3: Piecewise Linear Function of Time Prescribing Rate (α) and Constant Prescription Overdose Death Rate (μ_A)

In order to better capture the dynamics observed in the quarterly prescription opioid user data in which there is an evident change in prescribing behavior at the end of 2015/beginning of 2016, we make alpha piecewise linear. We choose the switching point to be Quarter 2 of 2016, as the "Tennessee Prescription Safety Act of 2016" was made effective on April 27, 2016. This policy reauthorized the Prescription Act of 2012 which required *prescribers* to check the CSMD prior to prescribing certain substances at the start of a new episode of treatment,

Table 2.7: This table displays the values of the parameters that were estimated with our model from Case 2, in which both the prescribing rate, α, and the prescription opioid overdose death rate, μ_A, are linear functions of time. With the estimated values for $\tilde{m}, \tilde{b}$, and $\tilde{c}$, the time-dependent parameter α starts at 0.291 in 2013 and decreases to 0.192 by 2019 and with the estimated values of $\tilde{d}$ and $\tilde{e}$, the time-dependent parameter, μ_A, starts at 0.00883 in 2013 and increases to 0.0147 by 2019.

Input	Estimated Value	Units
$\tilde{m}$	-0.0165	$\frac{1}{\text{year}}$
$\tilde{b}$	0.291	$\frac{1}{\text{year}}$
$\tilde{d}$	0.000978	$\frac{1}{\text{year}}$
$\tilde{e}$	0.00883	$\frac{1}{\text{year}}$
β_A	0.000312	$\frac{1}{\text{year}}$
β_P	0.0000286	$\frac{1}{\text{year}}$
θ_1	0.214	$\frac{1}{\text{year}}$
ε	2.507	$\frac{1}{\text{year}}$
γ	0.00502	$\frac{1}{\text{year}}$
θ_2	0.295	$\frac{1}{\text{year}}$
σ	0.101	$\frac{1}{\text{year}}$
ζ	0.199	$\frac{1}{\text{year}}$
θ_3	19.931	$\frac{1}{\text{year}}$
ν	0.000187	$\frac{1}{\text{year}}$
P_0	0.0827	dimensionless
A_0	0.00710	dimensionless
H_0	0.000464	dimensionless
R_0	0.00529	dimensionless
S_0	0.904446	dimensionless

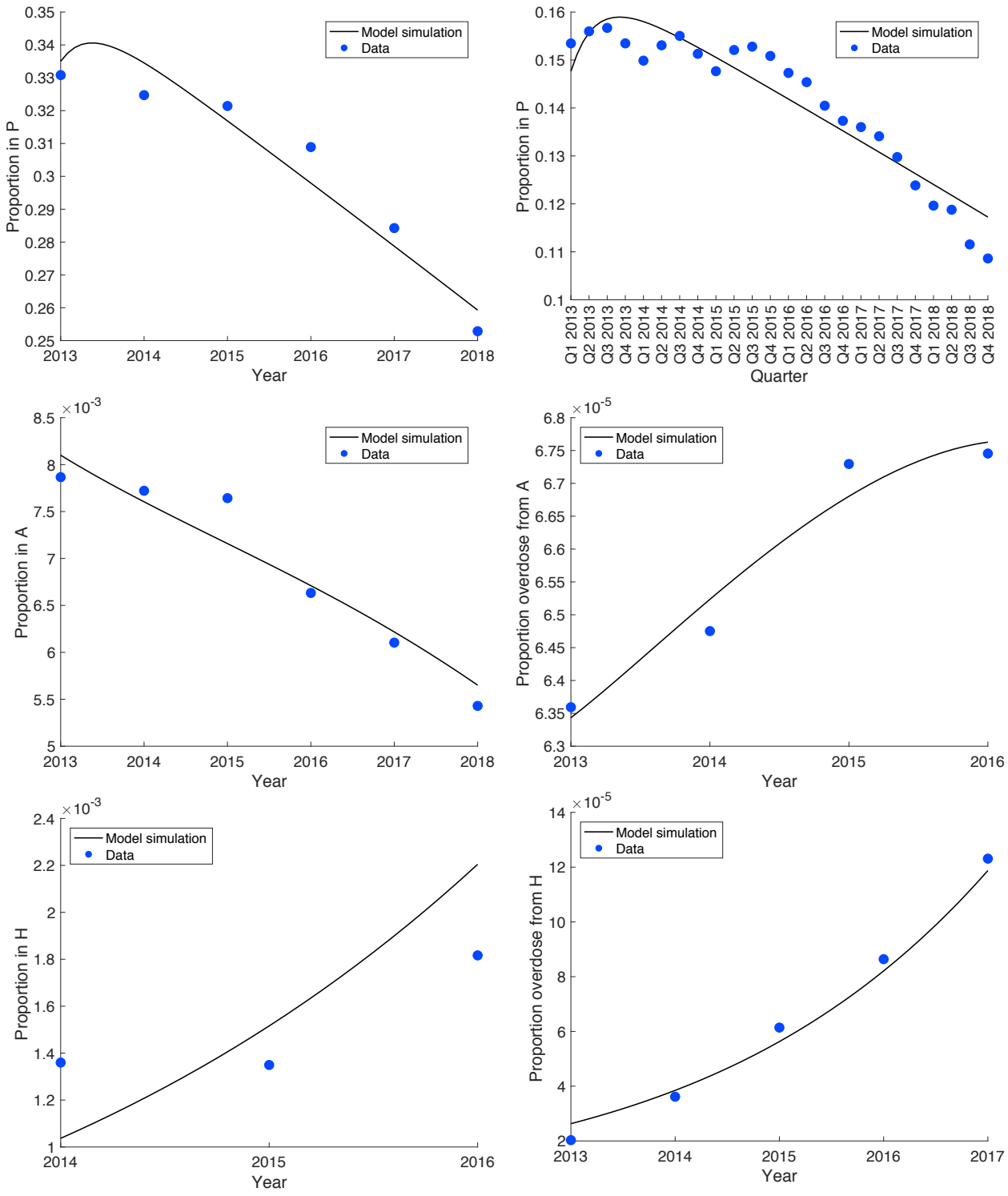


Figure 2.4: Model simulation fit to data for the α linear, μ_A linear model. This figure includes the fit to yearly prescription opioid user data, quarterly prescription opioid data, yearly prescription opioid addict data, yearly prescription opioid addict overdose death data, yearly heroin/fentanyl addict data, and yearly heroin/fentanyl overdose death data.

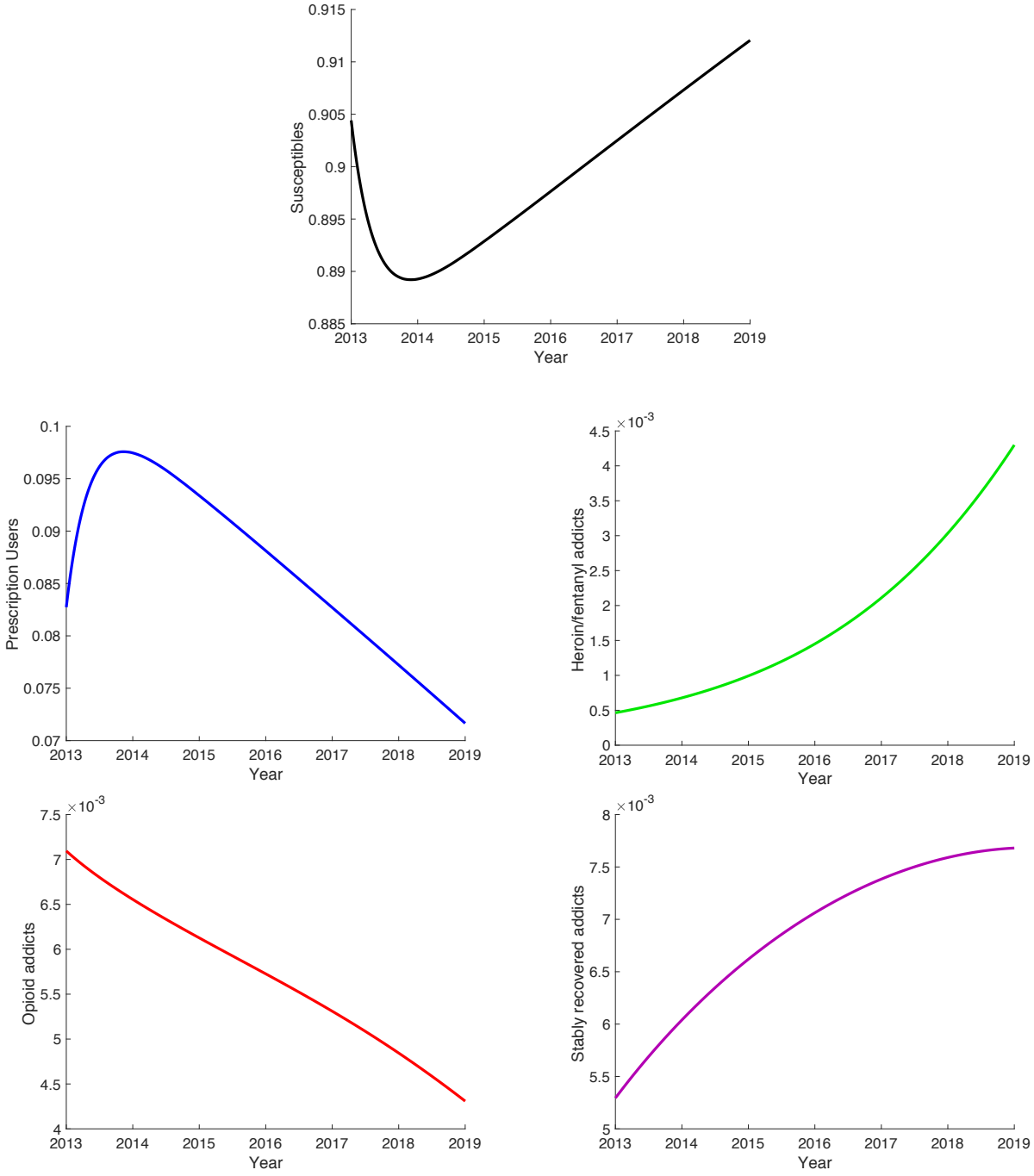


Figure 2.5: Numerical simulation for each of the population classes with parameters from Table 2.7 for the α linear, μ_A linear case.

as well as checking it annually if the patient continues to be in that opioid treatment plan, and for them to check the database if they believe the patient has illicit intentions with the controlled substance [35, 104]. Moreover, an updated requirement was put in place that the CSMD needed to be updated by the close of the next day (rather than within 7 days) and for patients with a new episode of treatment (i.e. not prescribed/obtaining opioids from that location), *dispensers* must also check the CSMD prior to dispensing certain substances [104].

Making alpha continuous adds one more parameter to be estimated, $\tilde{c}$, the slope of α after Quarter 2 of 2016. Specifically,

$$\alpha(t) = \begin{cases} \tilde{m} \cdot t + \tilde{b} \text{ before Quarter 2 2016 } (t \leq 3.25) \\ \tilde{m}(3.25) + \tilde{b} + \tilde{c}(t - 3.25) \text{ after Quarter 2 2016 } (t > 3.25) \end{cases}$$

Table 2.4 are the values of parameters assumed prior to the parameter estimation, including constant μ_A, and ranges on all parameters are the same as before as recorded in Table 2.5. With 1910 out of 2000 runs converging, Table 2.8 displays the 18 inputs that were estimated with this process, along with their resulting estimated values. The objective function value is equal to 0.4708.

Figure 2.6 show the fits of our model simulations to data. The parameters from Table 2.8 result in the solution curves found in Figure 2.7 of each class from the beginning of 2013 through the beginning of 2019.

Case 4: Piecewise Linear Function of Time Prescribing Rate (α) and Linear Function of Time Prescription Overdose Death Rate (μ_A)

For this case, we explore the prescribing rate and the prescription opioid addict overdose death rate both being both time-dependent. As before, we set

$$\alpha(t) = \begin{cases} \tilde{m} \cdot t + \tilde{b} \text{ before Quarter 2 2016 } (t \leq 3.25) \\ \tilde{m}(3.25) + \tilde{b} + \tilde{c}(t - 3.25) \text{ after Quarter 2 2016 } (t > 3.25) \end{cases}$$

and

$$\mu_A = \tilde{d} \cdot t + \tilde{e}.$$

Table 2.8: This table displays the values of the parameters that were estimated with our model from Case 3, in which the prescribing rate, α, is a piecewise linear function of time and the prescription opioid overdose death rate, μ_A, is constant. With the estimated values for $\tilde{m}, \tilde{b}$, and $\tilde{c}$, the time-dependent parameter α starts at 0.275 in 2013 and decreases to 0.178 by 2019.

Input	Estimated Value	Units
$\tilde{m}$	-0.00760	$\frac{1}{\text{year}}$
$\tilde{b}$	0.275	$\frac{1}{\text{year}}$
$\tilde{c}$	-0.0265	$\frac{1}{\text{year}}$
β_A	0.0000601	$\frac{1}{\text{year}}$
β_P	0.0000137	$\frac{1}{\text{year}}$
θ_1	0.284	$\frac{1}{\text{year}}$
ε	2.563	$\frac{1}{\text{year}}$
γ	0.00500	$\frac{1}{\text{year}}$
θ_2	0.356	$\frac{1}{\text{year}}$
σ	0.100	$\frac{1}{\text{year}}$
ζ	0.100	$\frac{1}{\text{year}}$
θ_3	18.064	$\frac{1}{\text{year}}$
ν	0.000181	$\frac{1}{\text{year}}$
P_0	0.0922	dimensionless
A_0	0.00764	dimensionless
H_0	0.000471	dimensionless
R_0	0.0000186	dimensionless
S_0	0.8996704	dimensionless

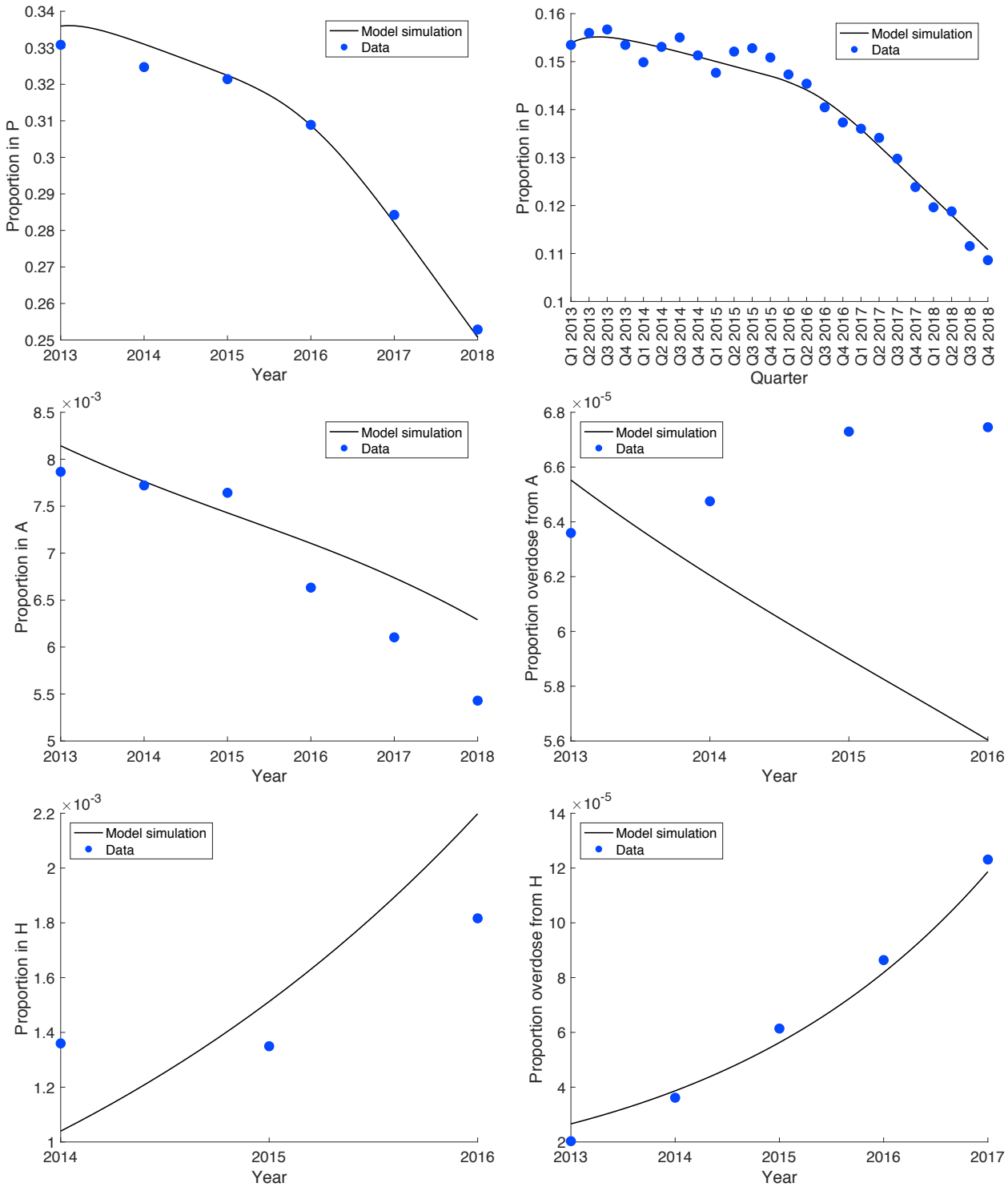


Figure 2.6: Model simulation fit to data for the α piecewise linear, μ_A constant model. This figure includes the fit to yearly prescription opioid user data, quarterly prescription opioid data, yearly prescription opioid addict data, yearly prescription opioid addict overdose death data, yearly heroin/fentanyl addict data, and yearly heroin/fentanyl overdose death data.

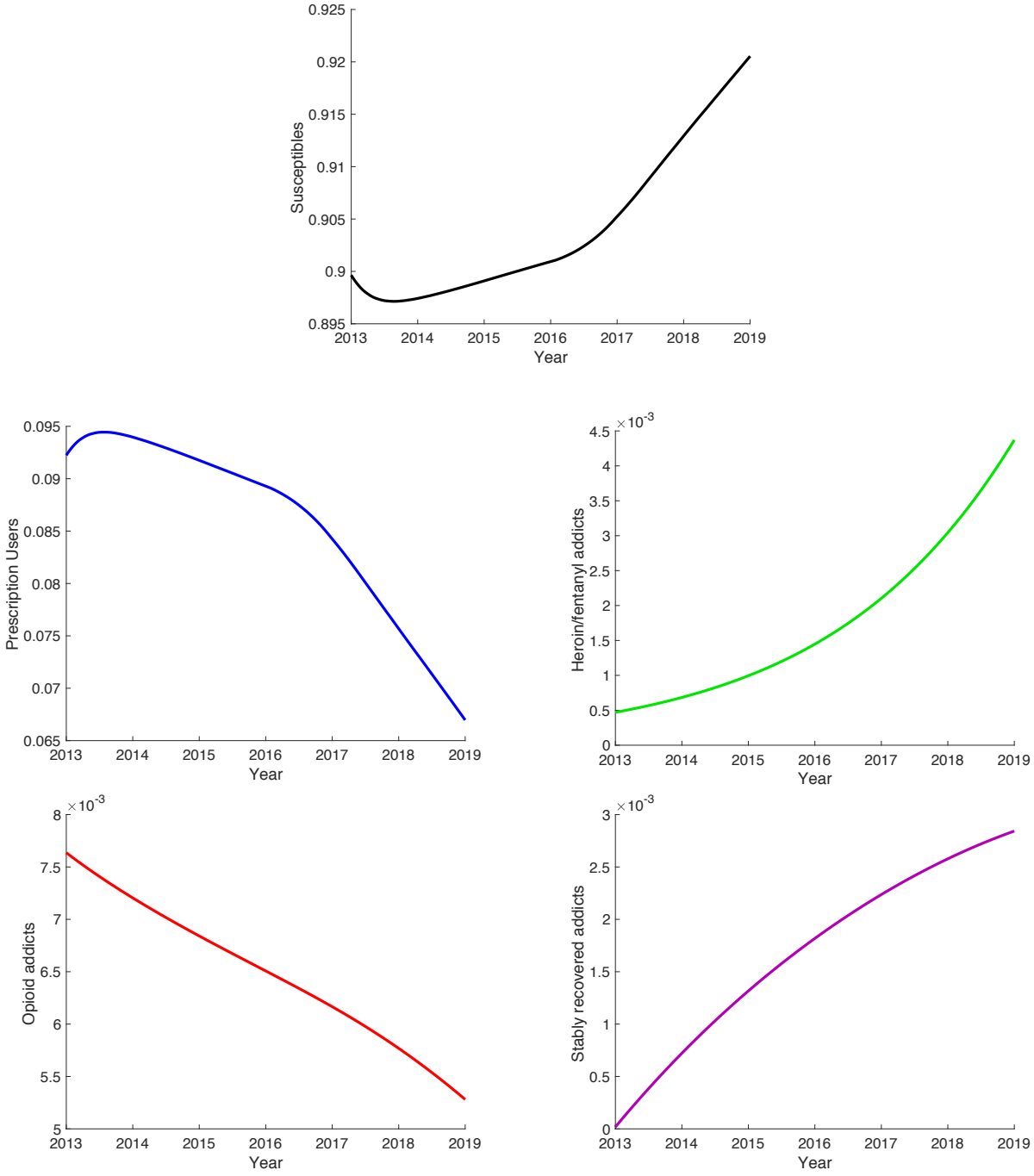


Figure 2.7: Numerical simulation for each of the population classes with parameters from Table 2.8 for the α piecewise linear, μ_A constant case.

The ranges on all parameters are the same as before as recorded in Table 2.5 and Table 2.4 gives the values assumed for μ, μ_H, and ω (excludes μ_A value). The results are shown in Table 2.9, which displays the 20 inputs that were estimated with this process along with their resulting estimated values, for the 1873 runs that converged out of the starting 2000. The objective function value is equal to 0.3273.

Figure 2.8 show the fits of our model simulations to data. The parameters from Table 2.9 result in the following solution curves found in Figure 2.9 of each class from the beginning of 2013 through the beginning of 2019.

We note that ordinary least squares is only accurate if the data we use is unbiased (i.e. if a survey does not take into consideration underreporting for heroin addict data). For the National Survey on Drug Use and Health, there are careful procedures used for the dwelling units and individuals selected to be surveyed [16]. Data collection procedures are designed "to increase respondents' cooperation and willingness to report honestly about sensitive topics, such as illicit drug use behavior" [15]. Therefore, the survey is more preventative of underreporting than corrective for truthfulness of responses. Thus, the accuracy in reporting is not clearcut and based more on the design of the survey. If we consider the data to be biased, we can use maximum likelihood estimation in order to estimate the parameters. However, several parameters hit lower and upper parameter bounds in the process, so there was no global optimization found that could give helpful information. Thus, we use the results of parameter estimation using ordinary least squares to continue analysis.

2.4.3 Comparison of Models with AIC

We use AIC (Akaike's Information Criterion) in order to compare the fit of each case of our model used for parameter estimation to the data [77]. The AIC score balances the change in the fit of the model to data with the change in the number of parameters being estimated. The idea is to determine whether the model fits the data better because of the addition of an additional parameter(s) or because it actually is a better fit, i.e. is it a better fit considering we add one extra (or more) parameter to estimate? The score is meaningless by itself and must be used in the context of comparing two scores. The AIC score is the sum of the lack of fit and the complexity of the model and is given by:

Table 2.9: This table displays the values of the parameters that were estimated with our model from Case 4, in which the prescribing rate, α, is a piecewise linear function of time and the prescription opioid overdose death rate, μ_A, is a linear function of time. With the estimated values for $\tilde{m}, \tilde{b}$, and $\tilde{c}$, the time-dependent parameter α starts at 0.270 in 2013 and decreases to 0.178 by 2019 and the time-dependent parameter, μ_A, starts at 0.00883 in 2013 and increases to 0.0147 by 2019 from estimated inputs $\tilde{d}$ and $\tilde{e}$.

Input	Estimated Value	Units
$\tilde{m}$	-0.00560	$\frac{1}{\text{year}}$
$\tilde{b}$	0.270	$\frac{1}{\text{year}}$
$\tilde{c}$	-0.0270	$\frac{1}{\text{year}}$
$\tilde{d}$	0.000977	$\frac{1}{\text{year}}$
$\tilde{e}$	0.00883	$\frac{1}{\text{year}}$
β_A	0.000878	$\frac{1}{\text{year}}$
β_P	0.0000654	$\frac{1}{\text{year}}$
θ_1	0.222	$\frac{1}{\text{year}}$
ε	2.528	$\frac{1}{\text{year}}$
γ	0.00505	$\frac{1}{\text{year}}$
θ_2	0.236	$\frac{1}{\text{year}}$
σ	0.102	$\frac{1}{\text{year}}$
ζ	0.198	$\frac{1}{\text{year}}$
θ_3	19.726	$\frac{1}{\text{year}}$
ν	0.000531	$\frac{1}{\text{year}}$
P_0	0.0950	dimensionless
A_0	0.00710	dimensionless
H_0	0.000465	dimensionless
R_0	0.00507	dimensionless
S_0	0.892365	dimensionless

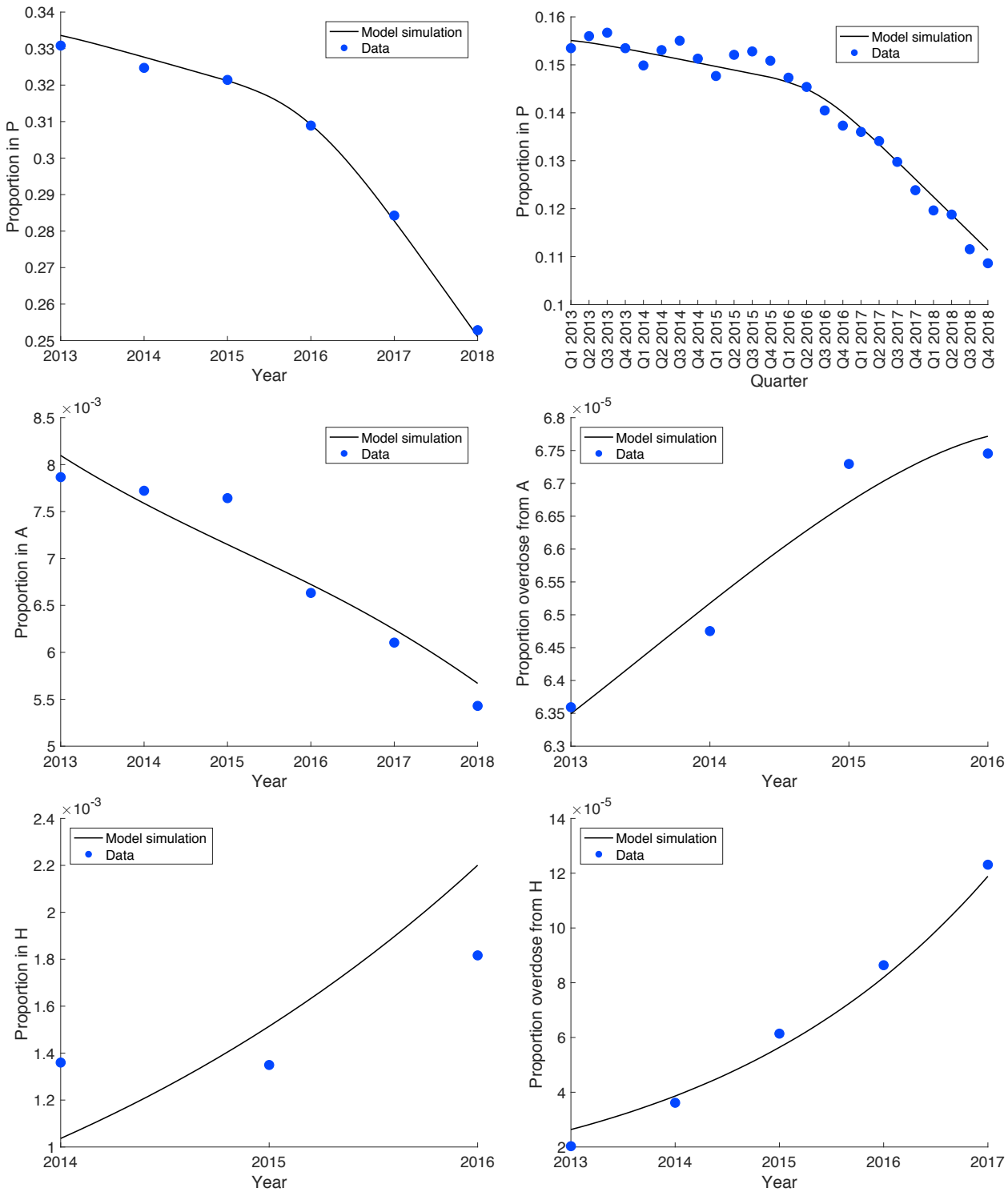


Figure 2.8: Model simulation fit to data for the α piecewise linear, μ_A linear model. This figure includes the fit to yearly prescription opioid user data, quarterly prescription opioid data, yearly prescription opioid addict data, yearly prescription opioid addict overdose death data, yearly heroin/fentanyl addict data, and yearly heroin/fentanyl overdose death data.

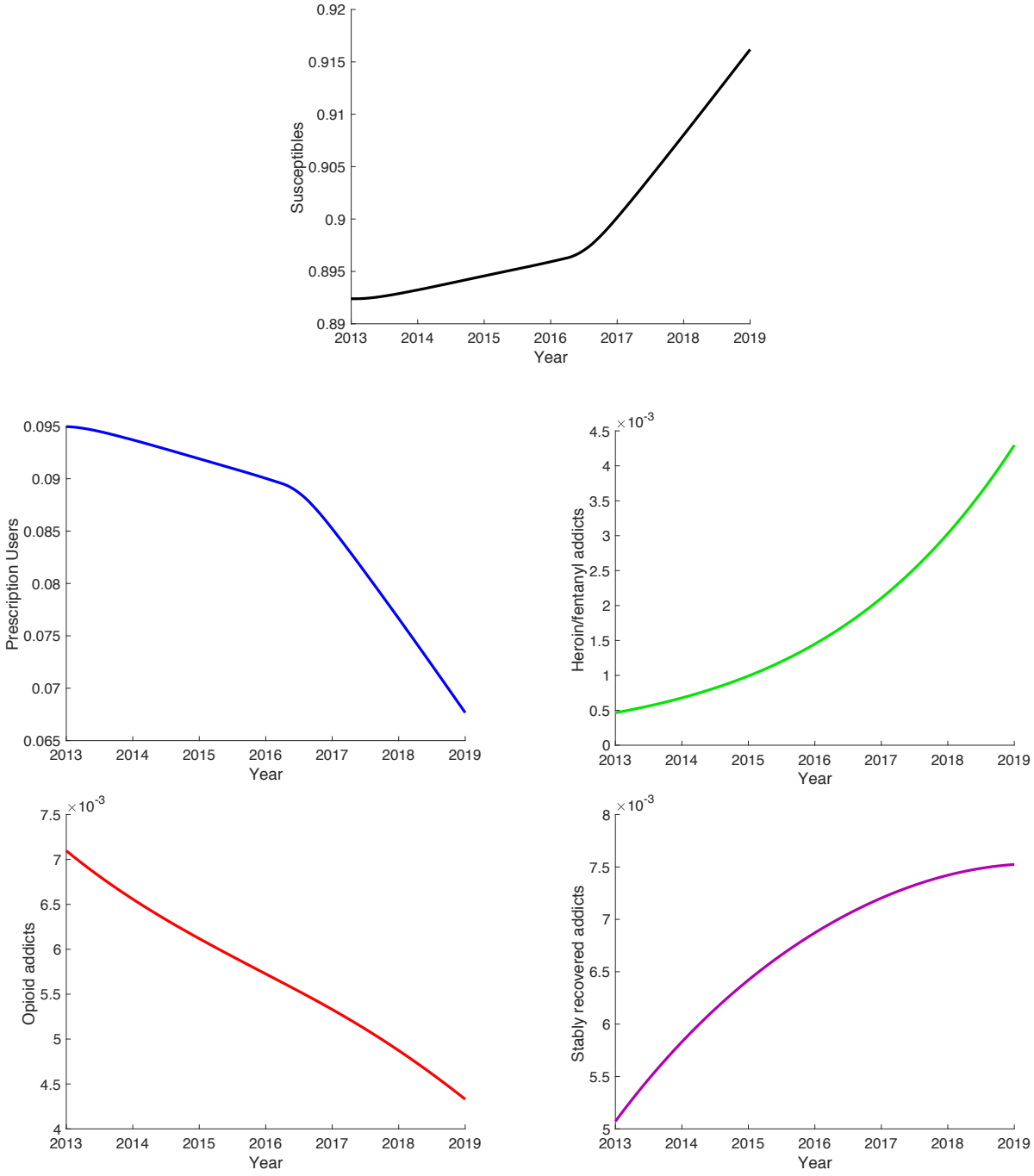


Figure 2.9: Numerical simulation for each of the population classes with parameters from Table 2.9 for the α piecewise linear, μ_A linear case.

$$\text{AIC} = N \ln\left(\frac{SS}{N}\right) + 2K$$

where N is the number of data points the model is fitting to, SS is the sum of squares of the differences between model simulated points and data points, and K is the number of parameters we estimate (with ordinary least squares in our case) plus one since the value of SS is also being estimated.

In our model, we have $N = 48$ data points. We will refer to the various model cases described before as Cases 1-4. For each case, we have the following number of inputs we estimate:

Case 1, α linear, μ_A constant: $17 \implies K_1 = 17 + 1 = 18$
Case 2, α linear, μ_A linear: $19 \implies K_2 = 19 + 1 = 20$
Case 3, α piecewise, μ_A constant: $18 \implies K_3 = 18 + 1 = 19$
Case 4, α piecewise linear, μ_A linear: $20 \implies K_4 = 20 + 1 = 21$.

Since our sample size $N = 48$ is not very large in general and in particular, since K is between 38% and 44% of this value (significantly smaller), it is recommended to use the corrected AIC scores for small sample sizes (denoted AIC_c). Here,

$$\text{AIC}_c = N \ln\left(\frac{SS}{N}\right) + 2K + \frac{2K(K+1)}{N-K-1}.$$

Note that if N were large, the denominator in this last fraction would be much larger than the numerator and therefore, the corrective term would be very small and therefore not necessary.

We make a slight modification to the AIC score to fit in the context of our model. Instead of using SS, the sum of squares of the differences between model simulated points and data points shown here,

$$SS = \sum_{i=1}^{5} \text{Diff1(i)}^2 + \sum_{i=1}^{5} \text{Diff2(i)}^2 + \sum_{i=1}^{3} \text{Diff3(i)}^2 + \sum_{i=1}^{24} \text{Diff4(i)}^2 + \sum_{i=1}^{4} \text{Diff5(i)}^2 + \sum_{i=1}^{5} \text{Diff6(i)}^2,$$

we use the value of our objective function which is a modification of the sum of squares. Our objective function takes the sum of squares for *each type of data* and weights each of these individually by the specific data set and *then* adds together these values to get a weighted sum of squares. This is due to the variation in the number of data points in the data sets, as well as the differing orders of magnitudes of the data. We will utilize this value, calling it OF in place of SS, since SS is not nearly as meaningful in the context of our model. Thus,

$$OF = \sum_{j=1}^{2} \frac{\sqrt{\sum_{i=1}^{6} \text{Diffj(i)}^2}}{\sqrt{\sum_{i=1}^{6} \text{Dataj(i)}^2}} + \frac{\sqrt{\sum_{i=1}^{3} \text{Diff3(i)}^2}}{\sqrt{\sum_{i=1}^{3} \text{Data3(i)}^2}} + \frac{\sqrt{\sum_{i=1}^{24} \text{Diff4(i)}^2}}{\sqrt{\sum_{i=1}^{24} \text{Data4(i)}^2}} + \frac{\sqrt{\sum_{i=1}^{4} \text{Diff5(i)}^2}}{\sqrt{\sum_{i=1}^{4} \text{Data5(i)}^2}} + \frac{\sqrt{\sum_{i=1}^{5} \text{Diff6(i)}^2}}{\sqrt{\sum_{i=1}^{5} \text{Data6(i)}^2}}.$$

Thus, we can calculate the corrected AIC score for each case.

In case 1,

$$\text{AIC}_{c1} = 48 \ln\left(\frac{0.4983}{48}\right) + 2(18) + \frac{2(18)(18+1)}{48-18-1} = -159.6648.$$

In case 2,

$$\text{AIC}_{c2} = 48 \ln\left(\frac{0.3609}{48}\right) + 2(20) + \frac{2(20)(20+1)}{48-20-1} = -163.6226.$$

In case 3,

$$\text{AIC}_{c3} = 48 \ln\left(\frac{0.4708}{48}\right) + 2(19) + \frac{2(19)(19+1)}{48-19-1} = -156.8311.$$

In case 4,

$$\text{AIC}_{c4} = 48 \ln\left(\frac{0.3273}{48}\right) + 2(21) + \frac{2(21)(21+1)}{48-21-1} = -161.8889.$$

The lower the AIC score, the better the model fits to the data. We see here that case 2 (α linear, μ_A linear) is the best fit since it is the lowest of the AIC numbers. Another way to see this is to subtract values using the equation

$$\Delta\text{AIC}_c = \text{AIC}_{c(\text{more complicated model})} - \text{AIC}_{c(\text{simpler model})},$$

where more complicated means more parameters.

Comparing cases 1 and 2,

$$\Delta\text{AIC}_c = \text{AIC}_{c2} - \text{AIC}_{c1}$$

$$= N(\ln(OF_2) - \ln(OF_1)) + 2(K_2 - K_1) + \frac{2K_2(K_2+1)}{N-K_2-1} - \frac{2K_1(K_1+1)}{N-K_1-1}$$

$$= 48(\ln(0.3609) - \ln(0.4983)) + 2(20-18) + \frac{2(20)(20+1)}{48-20-1} - \frac{2(18)(18+1)}{48-18-1}$$

$$\approx -3.960$$

We observe that $\ln(0.3609) - \ln(0.4983)$ is negative (since estimating 2 more parameters reduces the weighted sum of squares value from 0.4983 to 0.3609 and rewritten as $\ln\left(\frac{0.3609}{0.4983}\right)$, the argument is less than 1) and the remaining terms deal with the difference of adding 2 more parameters to be fit, which will always be positive. In this case, these positive terms added on are not enough to compensate for the first negative term, and the net result is negative; this means that the difference of the weighted sum of squares values is better than expected from the addition of 2 estimated parameters. Thus, case 2 is a better fit overall.

Next,

$$\Delta\text{AIC}_c = \text{AIC}_{c2} - \text{AIC}_{c3}$$

$$= N(\ln(OF_2) - \ln(OF_3)) + 2(K_2 - K_3) + \frac{2K_2(K_2+1)}{N-K_2-1} - \frac{2K_3(K_3+1)}{N-K_3-1}$$

$$= 48(\ln(0.3609) - \ln(0.4708)) + 2(20-19) + \frac{2(20)(20+1)}{48-20-1} - \frac{2(19)(19+1)}{48-19-1}$$

$$\approx -6.792$$

Here, $\ln(0.3609) - \ln(0.4708)$ is negative (estimating 1 additional parameter reduced the weighted sum of squares value from 0.4708 to 0.3609 and rewritten as $\ln\left(\frac{0.3609}{0.4708}\right)$, the argument will always be less than 1) and the remaining terms deal with the difference of adding 1 more parameter to be fit, which will always be positive. In this case, these positive terms added on do not compensate for the first negative term, and the net result is negative; this means that the difference of the weighted sum of squares values is better than expected from the addition of 1 estimated parameter. Thus, case 2 is a better fit overall.

Finally,

$$\Delta\text{AIC}_c = \text{AIC}_{c4} - \text{AIC}_{c2}$$

$$= N(\ln(OF_4) - \ln(OF_2)) + 2(K_4 - K_2) + \frac{2K_4(K_4+1)}{N-K_4-1} - \frac{2K_2(K_2+1)}{N-K_2-1}$$

$$= 48(\ln(0.3273) - \ln(0.3609)) + 2(21 - 20) + \frac{2(21)(21+1)}{48-21-1} - \frac{2(20)(20+1)}{48-20-1}$$

$$\approx 1.737$$

We observe that $\ln(0.3273) - \ln(0.3609)$ is negative (estimating 1 additional parameter reduced the weighted sum of squares value from 0.3609 to 0.3273 and rewritten as $\ln\left(\frac{0.3273}{0.3609}\right)$, the argument will always be less than 1) and the remaining terms deal with the difference of adding 1 more parameter to be fit, which will always be positive. In this case, these positive terms overcompensate for the negative term, and the net result is positive; this means that the difference of the weighted sum of squares values is worse than expected from the addition of 1 estimated parameter. Thus, case 2 is a better fit overall.

Overall, the α linear, μ_A linear model seems to be the best choice out of the 4 cases. We can calculate the probability that one model is better than another model by the following calculation:

$$\text{probability} = \frac{e^{-0.5(\Delta\text{AIC}_c)}}{1 + e^{-0.5(\Delta\text{AIC}_c)}},$$

where ΔAIC_c will now be the AIC score of the model with the lower AIC score we believe to be the better model − the AIC score of the model with the higher AIC score we believe to be the worse model. This comes from the idea that the likelihood of the model with the lower AIC score given the data is proportional to $e^{-0.5\Delta\text{AIC}_c}$ [11]. Thus, comparing the model with the lower AIC score to itself gives $\Delta\text{AIC}_c = 0$, which means $e^{-0.5\Delta\text{AIC}_c} = 1$ in the denominator and comparing the model with the lower AIC score to the model with the higher AIC score gives $e^{-0.5\Delta\text{AIC}_c}$ in the denominator. Therefore, the probability the model with the lower AIC score really is the best model is essentially the likelihood of that model out of the sum of the likelihoods of the two models being compared.

Therefore, the probability that the model in Case 2 is better than the other three models can be given by the following calculations:

$$\text{probability} = \frac{e^{-0.5(\text{AIC}_{c2} - \text{AIC}_{c1})}}{1 + e^{-0.5(\text{AIC}_{c2} - \text{AIC}_{c1})}}$$

$$= \frac{e^{-0.5(-3.960)}}{1 + e^{-0.5(-3.960)}}$$

$$\approx 0.879,$$

$$\text{probability} = \frac{e^{-0.5(\text{AIC}_{c2} - \text{AIC}_{c3})}}{1 + e^{-0.5(\text{AIC}_{c2} - \text{AIC}_{c3})}}$$

$$= \frac{e^{-0.5(-6.792)}}{1 + e^{-0.5(-6.792)}}$$

$$\approx 0.968,$$

and

$$\text{probability} = \frac{e^{-0.5(\text{AIC}_{c2} - \text{AIC}_{c4})}}{1 + e^{-0.5(\text{AIC}_{c2} - \text{AIC}_{c4})}}$$

$$= \frac{e^{-0.5(-1.737)}}{1 + e^{-0.5(-1.737)}}$$

$$\approx 0.704,$$

This means there is an 87.9% chance that the α linear, μ_A linear model is a better choice than the model in case 1 and a 96.8% chance it is a better choice than the model in case 3 regarding fit to the data with the additional parameter(s) being estimated. It also means there is a smaller (70.4%) chance that it is a better choice model than the α piecewise linear, μ_A linear case 4 model regarding the fit to data.

Furthermore, the evidence ratio tells us how many times more likely one model is correct over another and is defined as:

$$\text{evidence ratio} = \frac{\text{Probability a certain model is correct}}{\text{Probability that a different model is correct}}$$

$$= \frac{1}{e^{0.5(\Delta\text{AIC}_c)}},$$

where ΔAIC_c is going to be the AIC score of the model we believe is more correct $-$ the AIC score of the model we believe is not as correct. Note that some sources have a negative in the exponential if they define their ΔAIC in the opposite manner.

Thus, for our models, the evidence ratio gives information on how many times more likely the α linear, μ_A linear model is correct compared to any of the other models. First we have,

$$\begin{aligned}\text{evidence ratio} &= \frac{\text{probability } \alpha \text{ linear, } \mu_A \text{ linear model is correct}}{\text{probability } \alpha \text{ linear, } \mu_A \text{ constant model is correct}} \\ &= \frac{\frac{e^{-0.5(-3.960)}}{1+e^{-0.5(-3.960)}}}{\frac{e^{-0.5(3.960)}}{1+e^{-0.5(3.960)}}} \\ &= \frac{1}{e^{0.5(-3.960)}} \\ &= 7.243,\end{aligned}$$

which provides additional justification that the α linear, μ_A linear model is more accurate than the α linear, μ_A constant model.

Similarly,

$$\begin{aligned}\text{evidence ratio} &= \frac{\text{probability } \alpha \text{ linear, } \mu_A \text{ linear model is correct}}{\text{probability } \alpha \text{ piecewise linear, } \mu_A \text{ constant model is correct}} \\ &= \frac{\frac{e^{-0.5(-6.792)}}{1+e^{-0.5(-6.792)}}}{\frac{e^{-0.5(6.792)}}{1+e^{-0.5(6.792)}}} \\ &= \frac{1}{e^{0.5(-6.792)}} \\ &= 29.844,\end{aligned}$$

which provides additional justification that the α linear, μ_A linear model is more accurate than the α piecewise linear, μ_A constant model.

Finally,

$$\begin{aligned}\text{evidence ratio} &= \frac{\text{probability } \alpha \text{ linear, } \mu_A \text{ linear model is correct}}{\text{probability } \alpha \text{ piecewise linear, } \mu_A \text{ linear model is correct}} \\ &= \frac{\frac{e^{-0.5(-1.737)}}{1+e^{-0.5(-1.737)}}}{\frac{e^{-0.5(1.737)}}{1+e^{-0.5(1.737)}}}\end{aligned}$$

$$= \frac{1}{e^{0.5(-1.737)}}$$

$$= 2.383.$$

This suggests that the α linear, μ_A linear model is slightly more accurate than the α piecewise linear, μ_A linear model (although much more accurate than the prior two cases). However, given this very slight difference in the fit of the model to data, we believe there is a strong reason to make the prescribing rate (α) piecewise linear in time rather than simply linear, due to the stark contrast in the number of prescribed patients before and after Quarter 3 of 2016. In addition, work by Burnham and Anderson [11, 12] argues that if the difference between AIC scores for two models is less than or equal to 2, then there is substantial evidence that the model with the higher AIC score is actually the best approximating model. In our case, there is a 1.7227 difference in AIC scores between the α piecewise linear, μ_A linear model and the α linear, μ_A linear model. Therefore, since we have reason to, we choose Case 4, where α is piecewise linear in time and μ_A is linear in time as our model of choice.

2.4.4 Trajectory of the Epidemic

Using the parameters estimated in Table 2.9, we predict the trajectory of the epidemic from 2019-2022, beyond the point of available data. Figure 2.10 displays the extrapolation for each of the addicted class and predicts the total proportion of addicts (combined proportion from A and H classes) for the near future. These suggest that the epidemic is expected to worsen in those 3 years as far as the number of individuals affected. In addition, we see that heroin and fentanyl seem to be playing the largest role in sustaining the epidemic and that the prevalence of addiction is predicted to increase overall. This prediction agrees with the interpretation of the basic reproduction number, $\mathscr{R}_0$, in the sense that the size of θ_1 and θ_2, which are rates for heroin/fentanyl interaction terms, play a big role in the size of $\mathscr{R}_0$.

Moreover, Figure 2.11 displays the extrapolation of prescription opioid overdose deaths and heroin and fentanyl overdose deaths for 2019-2022, as well as the trajectory of the total number of overdose deaths. We see the number of prescription opioid overdose deaths decreasing. This seems reasonable as the one data point we did not use in parameter

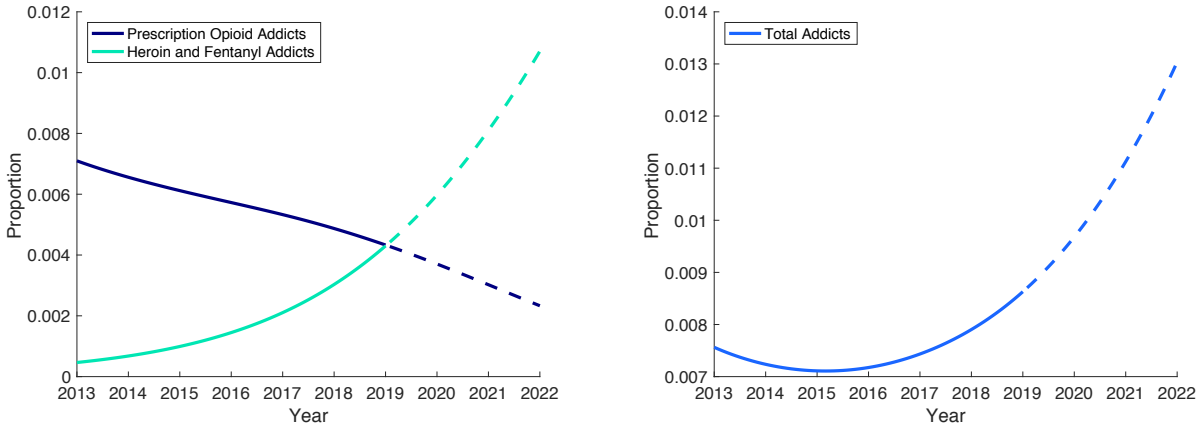


Figure 2.10: Numerical simulations for the addicted classes with parameters from Table 2.9 for the α piecewise linear, μ_A linear case with trajectories predicted for 2019-2022. The plot on the left shows the simulations of the prescription opioid addict class and the heroin/fentanyl addict class separately and the plot on the right shows the simulation for the proportion of total addicts.

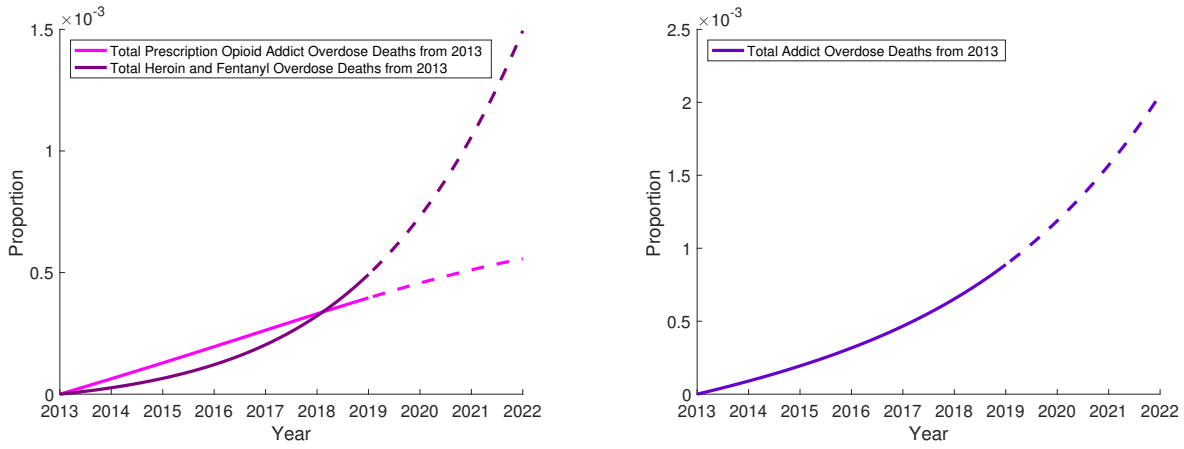


Figure 2.11: Numerical simulations for overdose deaths with parameters from Table 2.9 for the α piecewise linear, μ_A linear case with trajectories predicted for 2019-2022. The plot on the left shows the simulations for the prescription opioid addict overdose deaths and the heroin/fentanyl addict overdose deaths separately and the figure on the right shows the total proportion of overdose deaths.

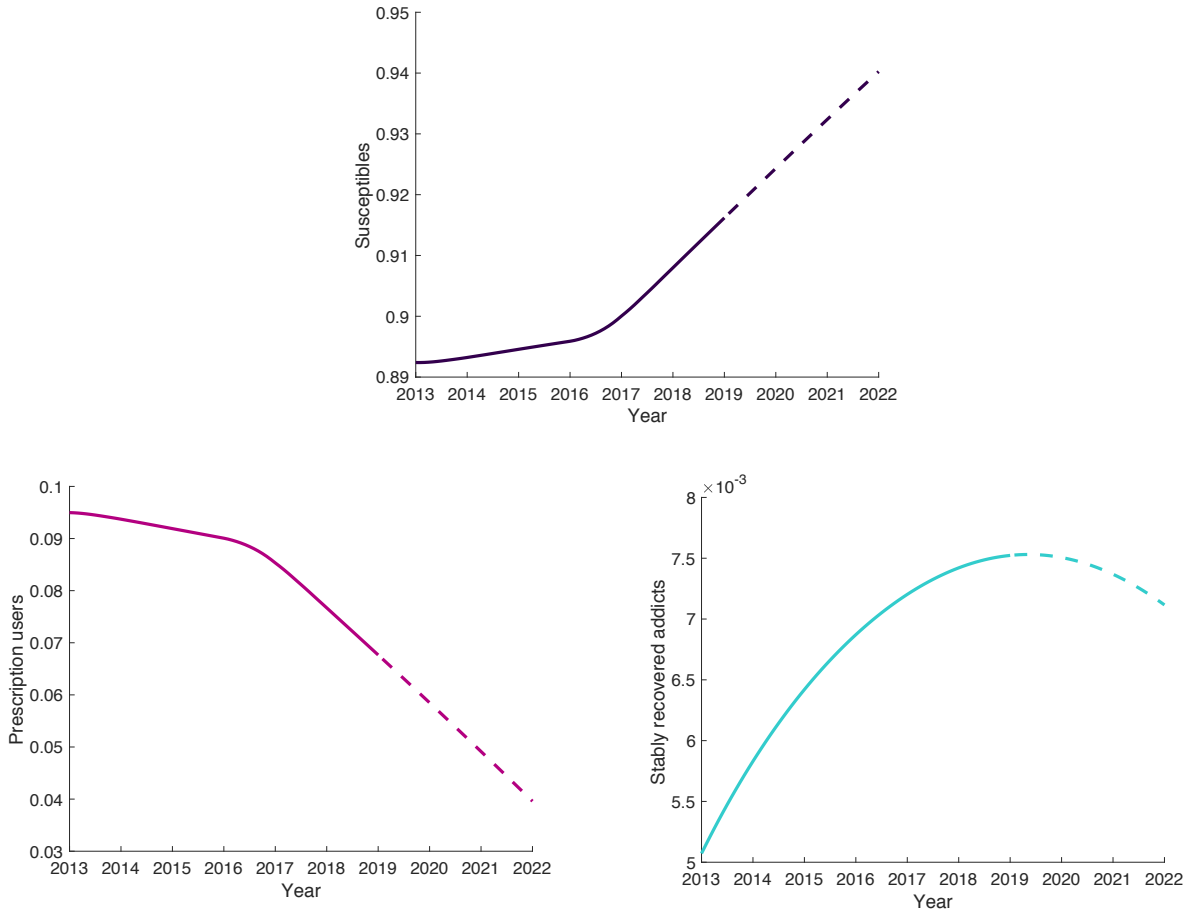


Figure 2.12: Numerical simulations for the susceptible, prescribed user, and stably recovered classes with parameters from Table 2.9 for the α piecewise linear, μ_A linear case with trajectories predicted for 2019-2022.

estimation (since it did not represent the major trend) was 309 prescription opioid overdose deaths in 2017, which is a decrease from 381 in 2016. On the other hand, there was a drastic increase in the number of heroin and fentanyl overdose deaths from 2013-2017 and our trajectory suggests that pattern will continue. Figure 2.12 displays the trajectories of the remaining classes, in which we expect a continued decrease in the number of prescribed users. Although stably recovered individuals were increasing from 2013-2019, a decrease in the number of individuals in this class is predicted after that, which may be from individuals relapsing back into the H class due to the predicted increase in the number of individuals in H.

We observe a drastic increase in the number of predicted heroin addicts and therefore, we wish to examine this a bit more. To do so, we consider a situation where the data on heroin addicts is assumed to be more accurate than the other data and we place a higher weight on the heroin addict data in order to estimate the parameters. First, we consider a case where the heroin addict data is weighted twice as much as the other sets of data. This results in a significant lowering in the heroin addict trajectory and total addict trajectory as shown in Figure 2.13 (compared to Figure 2.10), whereas the prescription opioid addict number is projected to be a bit higher. This had an objective function value of 0.4770 (compared to 0.3273). For a weight of 5 on the heroin addict data, the heroin addict and total addict trajectories are lowered even more, and the prescription opioid addict trajectory is even higher than both the non-weighted base case and the weighted 2 case, as shown in Figure 2.14, and similarly for a weight of 20 shown in Figure 2.15. These fits had objective value functions of 0.7035 and 1.7055, respectively. Despite these cases having a lowered total addict trajectory, all three cases suggested that the total addict trajectory would be increasing from 2019-2022.

Since the number of heroin overdose deaths relies on simulated heroin addicts, we investigate the case of putting a weight of 2 on both heroin addict data *and* heroin overdose death data, as well. Interestingly, the total addict trajectory is slightly larger in this case than the non-weighted case as shown in Figure 2.16 unlike the other weighted cases, with an objective function value of 0.5965. Thus, with this case and the ones before, our prediction holds that the total number of addicts is expected to increase from 2019 up to the beginning of 2022.

To better understand our system of ODEs as a whole, we wish to describe solutions based on a variety of feasible parameters for Tennessee. We focus on solutions for a 10-year period (2013-2023) since our analyses in this work are restricted to this timeframe and because α remains positive with its baseline estimated parameters for this period of time. We provide ranges of $\pm 50\%$ for *most* of the baseline estimated parameters/initial conditions for Tennessee so that we remain in reasonable ranges. However, bounds for inputs (m, b, c, d and e) of our time-dependent rates are carefully chosen to ensure α does not go negative and so that α and μ_A are also able to be constant (i.e. in the case that $m = 0$, $c = 0$, and

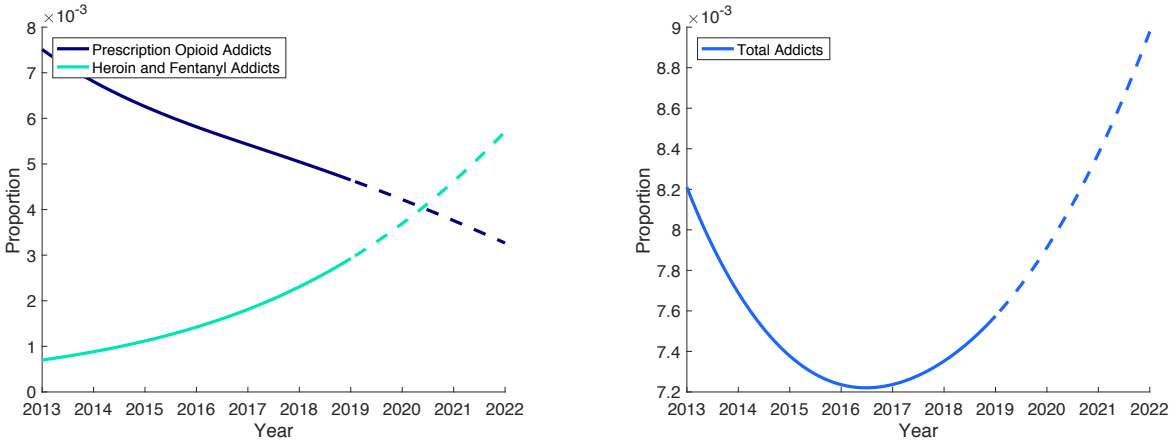


Figure 2.13: Numerical simulations for the addicted classes by putting a weight of 2 on the heroin data and letting α be piecewise linear and μ_A be linear. Trajectories are predicted for 2019-2022. The plot on the left shows the simulations of the prescription opioid addict class and the heroin/fentanyl addict class separately and the plot on the right shows the simulation for the proportion of total addicts.

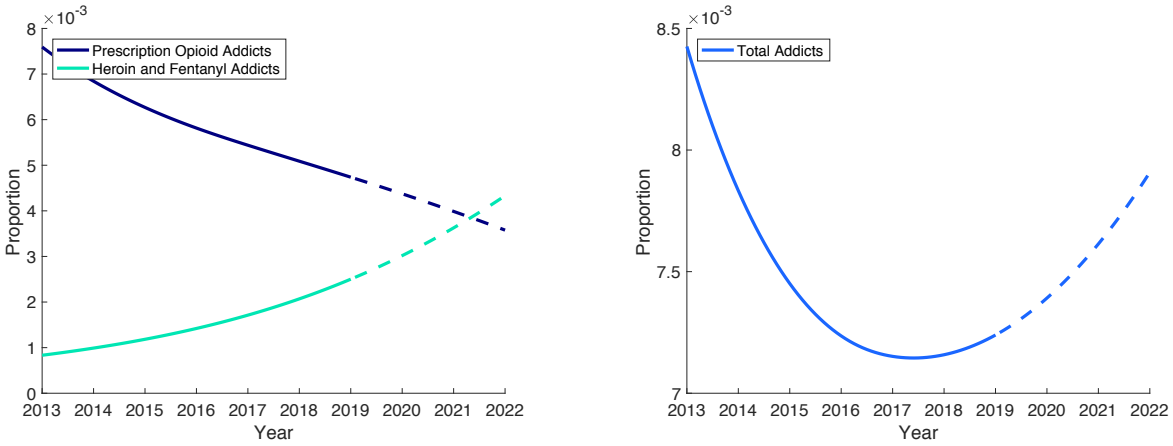


Figure 2.14: Numerical simulations for the addicted classes by putting a weight of 5 on the heroin data (with α piecewise linear and μ_A linear). Trajectories are predicted for 2019-2022. The plot on the left shows the simulations of the prescription opioid addict class and the heroin/fentanyl addict class separately and the plot on the right shows the simulation for the proportion of total addicts.

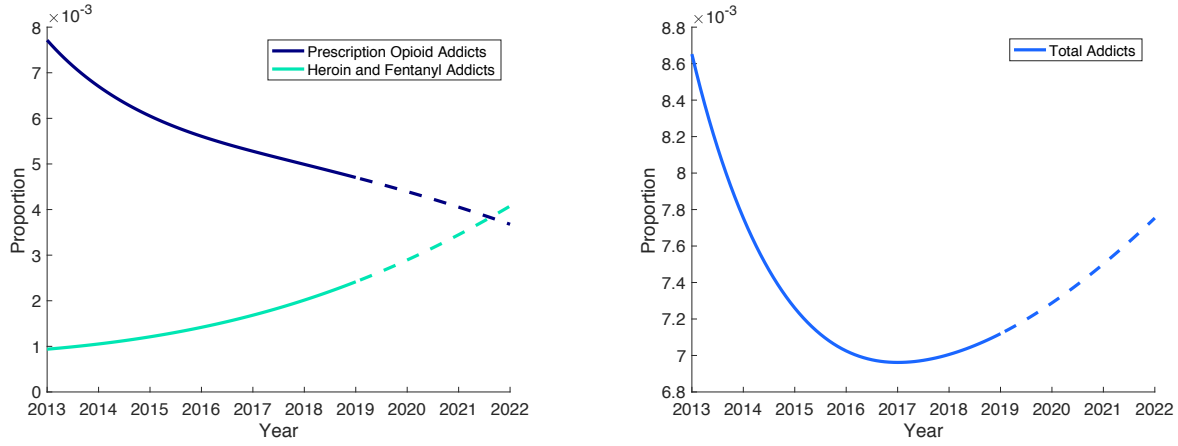


Figure 2.15: Numerical simulations for the addicted classes by putting a weight of 20 on the heroin data (with α piecewise linear and μ_A linear). Trajectories are predicted for 2019-2022. The plot on the left shows the simulations of the prescription opioid addict class and the heroin/fentanyl addict class separately and the plot on the right shows the simulation for the proportion of total addicts.

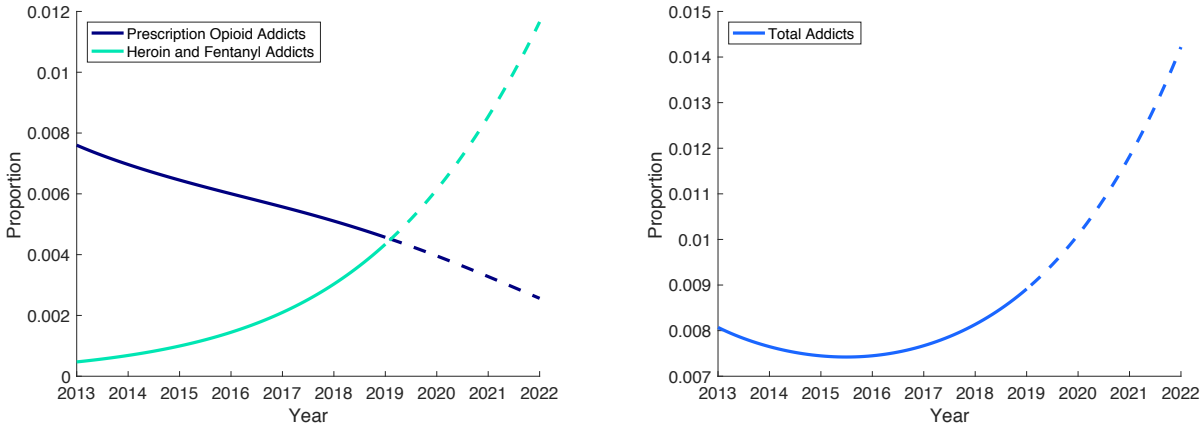


Figure 2.16: Numerical simulations for the addicted classes by putting a weight of 2 on the heroin data *and* the heroin overdose data (with α piecewise linear and μ_A linear). Trajectories are predicted for 2019-2022. The plot on the left shows the simulations of the prescription opioid addict class and the heroin/fentanyl addict class separately and the plot on the right shows the simulation for the proportion of total addicts.

$d = 0$). Then, we use Latin Hypercube Sampling (LHS) to choose 500 parameter sets and run the model for 10 years (2013-2023), in which details of this sampling method are found in Section 2.4.5.

Typical model solutions over this 10-year time period suggest that the P class ranges from approximately 0.02 to 0.2 in 2023 with solution curves having a combination of monotonically decreasing, monotonically increasing, or increasing and then decreasing to reach these values by 2023. This mixture of solution behavior is similar for the R class which ranges from 0.003 to 0.01 in 2023. The A class ranges from 0.0001 to 0.007 in 2023 and solution curves seem to either monotonically decrease, or increase and then decrease. The H class ranges from 0.002 to 0.07 and monotonically increases in this timeframe.

In 2023 for classes of most interest, the mean of the outputs for A is 0.00247 with a variance of 1.81e-6, the mean for the H class is 0.0162 with a variance of 8.36e-5, and the mean of the R class is 0.00727 with a variance of 4.09e-6. Moreover, inspecting the outputs of all 5 classes using a fine time mesh, we do not observe any oscillations for any of the classes in the 10 years.

2.4.5 Sensitivity Analysis

Here we use two global sensitivity analysis techniques to analyze how the uncertainty of our model inputs (parameters and initial conditions) affect the uncertainty in our model outputs from the α piecewise linear, μ_A linear model (Case 4). We identify which parameters are important to certain population class proportions at the final time and how the uncertainty in each output can be apportioned to the uncertainty in each of the inputs [72, 57].

Latin Hypercube Sampling/Partial Rank Correlation Coefficient Method

We implement Latin Hypercube Sampling, a type of uncertainty analysis, which examines the uncertainty in the output of a model based on the uncertainty in the inputs [72]. Each of our inputs is sampled from a uniform distribution; the parameter range is divided into N intervals of equal probability, and each interval is randomly sampled once for each parameter. Here, $N > p + 1$, where p is the number of inputs, is the minimum requirement. If input ranges do not span across several orders of magnitude, a linear scale is used for sampling; if

this is not the case, in order to prevent under-sampling in the outer ranges of the intervals, a log scale is used. This sampling technique ensures the entire range for the parameter is considered. This results in an $N \times p$ LHS matrix in which the model is evaluated from the set of inputs in each row of this matrix. One can study these outputs to gain information on how the variation in the parameter combinations affects differences in the outputs observed, in order to quantify the certainty one has with parameters.

Moreover, sensitivity analysis provides a way to quantify how much the uncertainty in specific model inputs affect specific model outputs. Inputs in biological models often have much uncertainty. Therefore, the information gained from local sensitivity analysis is limited since partial derivatives of the outputs are calculated multiple times based on a small variation in a single input; instead, global sensitivity analysis is advantageous in that inputs are varied simultaneously. Certain criteria are best for utilizing PRCC (a sampling-based method in which the effect of increasing/decreasing a particular input on a certain output is measured, after taking out the linear effects of all other inputs): nonlinear, monotonic relationships between inputs and outputs. Criteria most suitable for Sobol sensitivity analysis (a variance-based method in which the variability in the output can be apportioned to the uncertainty in an input or combination of inputs) is the following: nonlinear, non-monotonic relationships.

LHS/PRCC for α piecewise linear, μ_A linear model (case 4)

We are concerned with the sensitivity of A and H at the final time to 22 different model inputs and therefore need to check the monotonicity of A and H to these inputs in order to implement LHS and PRCC analysis. We set the ranges for the parameters to be $\pm$ 50% of the baseline parameter values with the exception of $\tilde{m}$, $\tilde{b}$, and $\tilde{c}$. These inputs are a part of the piecewise linear form of our prescribing rate, α, and must be handled carefully to ensure α stays positive, particularly when all three are varying. As a reminder of this time-dependent parameter, we have:

$$\alpha(x) = \begin{cases} \tilde{m} \cdot t + \tilde{b} \text{ before Quarter 2 2016 } (t \leq 3.25) \\ \tilde{m}(3.25) + \tilde{b} + \tilde{c}(t - 3.25) \text{ after Quarter 2 2016 } (t > 3.25). \end{cases}$$

For reference, the ±50% bounds for these inputs are:

$$\tilde{m} : [-0.0084, -0.0028]$$

$$\tilde{b} : [0.135, 0.405]$$

$$\tilde{c} : [-0.0405, -0.0135]$$

from the baseline value of $\tilde{m} = -0.0056$, $\tilde{b} = 0.27$, and $\tilde{c} = -0.027$ found in Table 2.9. We choose bounds for these inputs that allow the value of α in 2019 to vary ±50%. The value of α in 2019 using the baseline values is

$$\alpha(2019) = -0.0056(3.25) + 0.27 - 0.027(6 - 3.25) = 0.1778.$$

Thus, to attain a 50% reduction of α in 2019 of 0.089, we may use inputs of $\tilde{m} = -0.0075$, $\tilde{b} = 0.2$, and $\tilde{c} = -0.0315$. To increase α by 50% in 2019 to 0.2667, we may use $\tilde{m} = -0.0035$, $\tilde{b} = 0.3427$, and $\tilde{c} = -0.0235$. The values in these two cases were chosen to be reasonably balanced on either side of the baseline value and the resulting ranges,

$$\tilde{m} : [-0.0075, -0.0035]$$

$$\tilde{b} : [0.2, 0.3427]$$

$$\tilde{c} : [-0.0315, -0.0235],$$

stay within their individual ±50% ranges. The resulting parameter ranges to be used in sensitivity analyses are shown in Table 2.10.

The monotonicity plots are produced by varying a single parameter over its entire range while keeping all other parameters fixed at their baseline values for a total of $N = 800$ samples, the ODE being solved each time. The resulting plots are shown in Figure 2.17. We note that the plots that do not appear monotonic are essentially flat due to the scale on the values, and therefore considered monotonic. Specifically, the monotonicity plot of H with respect to $\tilde{m}$ is essentially flat due to the scale on the output values. This is because the output ranges from about 0.00430 to 0.004309 which is a maximum $0.004309 - 0.00430 =$

0.000009 change (a $\frac{0.000009}{0.00430} \approx 0.0021 = 0.21\%$ change) which is very negligible. Therefore, we deem the plot monotonic. Next, the monotonicity plot of H with respect to P_0 ranges between about 0.004308 and 0.004264 which implies the biggest change that occurs is $0.004308 - 0.004264 = 0.000044$ and therefore approximately a $\frac{0.000044}{0.004264} \approx 0.0103 = 1.03\%$ change, which is essentially flat and therefore monotonic.

Next, we construct our LHS matrix; although a minimum of $N = 22 + 1 = 23$ sample points is required for this case, we use a sample size big enough so that a similar set of parameters are deemed important for a certain output with consecutive runs of the PRCC analysis. To investigate the sensitivity of A and H with respect to the 22 inputs, two separate 800×22 LHS matrices are constructed where each column consists of 800 sampled points from the range of a certain parameter. Therefore, each row consists of a random sampling of parameter values in which the ODE system is solved. Solutions at the final time are stored for all 800 sets of parameters from these rows.

The mean of A at the final time is ≈ 0.00447 and the standard deviation ≈ 0.00146, which is approximately 33% of the mean and therefore, relatively large in size compared to the mean. This suggests that there is some uncertainty in the value of A at the final time. The mean of H at the final time is ≈ 0.00460 and the standard deviation is ≈ 0.00231 which is about 50% of the mean (and therefore significantly large compared to the mean), suggesting that uncertainty in the parameters is leading to variation in the outputs.

Therefore, we use PRCC analysis to identify which parameters are impacting the outputs the most. Results of the PRCC sensitivity analysis from the ODE solutions are given in Table 2.11 and Table 2.12. The p-values with an asterisk are those that are statistically significant. Out of these, the PRCC values closest to 1 or -1 for A are: ζ (rate prescription opioid addicts enter treatment), A_0 (initial condition for A class) , γ (rate prescribed individuals get addicted to their own prescriptions), and ε (rate prescribed individuals successfully finish their prescriptions). The PRCC values closest to 1 or -1 for H are: H_0 (initial condition of H class), θ_1 (rate susceptible individuals get addicted to heroin/fentanyl), θ_3 (rate prescription opioid addicts get addicted to heroin/fentanyl), and σ (relapse rate back to one of the addicted classes). A positive PRCC value signifies a positive correlation between that parameter and the class, i.e. increasing the parameter would increase the size of that class,

Table 2.10: Range of values for each parameter used for sensitivity analysis in the α piecewise linear, μ_A linear case, which are $\pm 50\%$ of the baseline values found in Table 2.4 (excluding the value of μ_A) and Table 2.9. The exception to the $\pm 50\%$ range is explained above for $\tilde{m}$, $\tilde{b}$, and $\tilde{c}$.

Parameter	Range of values
$\tilde{m}$	[-0.0075, -0.0035]
β_A	[0.000439,0.001317]
β_P	[0.0000327,0.0000981]
θ_1	[0.111,0.333]
ε	[1.265,3.795]
γ	[0.002525,0.007575]
σ	[0.051,0.153]
μ	[0.00355,0.01065]
μ_H	[0.0233,0.0699]
θ_2	[0.118,0.354]
ζ	[0.099,0.297]
θ_3	[9.85,29.55]
ν	[0.0002655,0.0007965]
ω	[0.00000000005,0.00000000015]
$\tilde{b}$	[0.2, 0.3427]
$\tilde{c}$	[-0.0315, -0.0235]
$\tilde{d}$	[0.0004885,0.0014655]
$\tilde{e}$	[0.004415,0.013245]
P_0	[0.0475,0.1425]
A_0	[0.00355,0.01065]
H_0	[0.0002325,0.0006975]
R_0	[0.002535,0.007605]

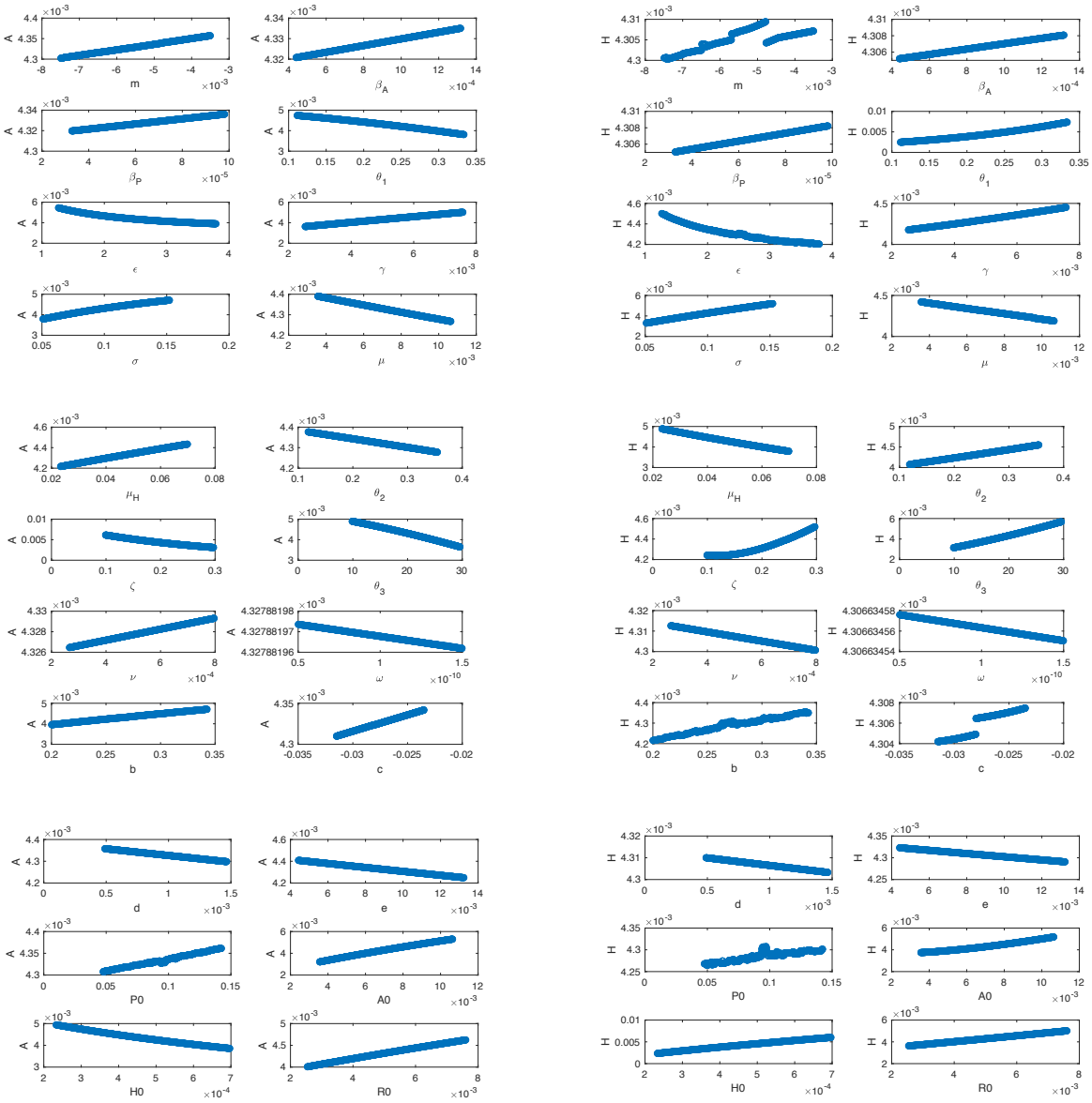


Figure 2.17: Monotonicity plots of A and H with respect to 22 parameters for the α piecewise linear, μ_A linear case. Each plot is formed by sampling one parameter across its range and holding all other parameters at their baseline values.

Table 2.11: Results from LHS/PRCC sensitivity analysis of the size of the prescription opioid addicted (A) class at the beginning of 2019 for the α piecewise linear, μ_A linear case run from 2013-2019 with 800 samples.

Input	PRCC for A class at beginning of 2019	p-value for A class at beginning of 2019
$\tilde{m}$	-0.029359	0.40695
β_A	-0.018476	0.6018
β_P	-0.023961	0.49856
θ_1	-0.46814	8.1499e-45*
ε	-0.75725	8.6473e-150*
γ	0.78049	5.8103e-165*
σ	0.66755	2.5246e-104*
μ	-0.0771	0.029217*
μ_H	0.11519	0.0010995*
θ_2	-0.070844	0.045162*
ζ	-0.93214	0*
θ_3	-0.63427	2.9293e-91*
ν	0.025334	0.47427
ω	-0.026267	0.45814
$\tilde{b}$	0.5368	6.6134e-61*
$\tilde{c}$	0.016847	0.63422
$\tilde{d}$	-0.018075	0.60971
$\tilde{e}$	-0.14234	5.3366e-05*
P_0	0.062519	0.077184
A_0	0.91835	1.9763e-323*
H_0	-0.6048	5.7877e-81*
R_0	0.49804	2.2582e-51*

Table 2.12: Results of LHS/PRCC sensitivity analysis of the size of the heroin/fentanyl addicted (H) class at the beginning of 2019 for the α piecewise linear, μ_A linear case run from 2013-2019 with 800 samples.

Input	PRCC for H class at beginning of 2019	p-value for H class at beginning of 2019
$\tilde{m}$	0.0074741	0.83283
β_A	0.02997	0.39724
β_P	0.055147	0.11911
θ_1	0.9379	0*
ε	-0.088819	0.011963*
γ	0.14415	4.2728e-05*
σ	0.73708	6.0214e-138*
μ	-0.11678	0.00093527*
μ_H	-0.51488	2.3083e-55*
θ_2	0.3477	3.789e-24*
ζ	0.16845	1.658e-06*
θ_3	0.84141	1.6932e-215*
ν	0.035945	0.3099
ω	-0.039433	0.26527
$\tilde{b}$	0.031239	0.37755
$\tilde{c}$	-0.025908	0.4643
$\tilde{d}$	0.016138	0.64855
$\tilde{e}$	-0.066608	0.059688
P_0	0.064268	0.069246
A_0	0.60493	5.2074e-81*
H_0	0.93879	0*
R_0	0.64435	4.8064e-95*

and decreasing the parameter results in a smaller class size. A negative PRCC value signifies a negative correlation between the parameter and class, i.e. increasing the parameter would decrease the size of that class, and decreasing the parameter would increase the class size.

It is beneficial to also implement Sobol sensitivity analysis in order to examine if there are any higher-order interactions among parameters that are occurring and also to be able to apportion the output variance to certain inputs.

Sobol Sensitivity Analysis Method

In order to explore the sensitivity of each of the population classes to the inputs (parameters and initial conditions), we implemented Sobol sensitivity analysis. The Saltelli sampler from the SALIB package in Python is utilized to generate N(2D+2) samples where N is the number of sample points and D is the number of inputs in the model [57]. The sampler selects points in the parameter space to test that are statistically likely and the outputs are the values of S, P, A, H and R at the final time (beginning of year 2019) for the different parameter and initial condition samples.

For first-order indices, only one parameter is varied and the rest are held constant, and measures how much the output variance would be reduced on average if that parameter was fixed [91]. For total-order indices, every combination of parameters is varied, from a single parameter varying alone to all higher-order interactions between parameters. The length of the colored bars in a plot from this analysis, with each color representing a specific class, measures the contribution of a certain parameter to the variance of each of the classes in the model. The longer the colored bar, the higher the effect the parameter has on that class of individuals. We are able to retrieve the confidence intervals on the sensitivity of each of the populations to a respective change in the parameter(s) for first order changes, second order changes, and total order changes; we report the first and total order indices for our analyses below.

Sobol sensitivity analysis for α piecewise linear, μ_A linear model (case 4)

The ranges we choose for each parameter for this analysis are the same as in Table 2.10, which are ±50% of the baseline values found from parameter estimation or calculations of the parameters, with the exception of $\tilde{m}$, $\tilde{b}$, and $\tilde{c}$.

In this case, N=100,000 and D=22 for a total of 4,600,000 samples, in which this value of N ensures that results do not change with a slightly higher N value (specifically for N=110,000). We ran this for 6 years and the sensitivities of the population classes to each of the parameters were calculated at the final time. Results are shown in Figure 2.18; we note the difference in the scales between the two graphs, resulting in some differences in the lengths of the colored bars on each graph. We see from the plot and from comparing first-order index values that the A class is most sensitive to ζ, the rate of individuals from A going into R; A_0, the initial condition of the A class; γ, the rate of prescribed users becoming addicted to their prescriptions; ε, the rate individuals finish prescriptions without becoming addicted; and finally, θ_3, the rate individuals in the A class get addicted to heroin/fentanyl. These results align with those from the PRCC sensitivity analysis. The H class is most sensitive to θ_1, the rate susceptible individuals become heroin/fentanyl addicts; H_0, the initial condition of the H class; θ_3, the rate of prescription opioid addicts transitioning to heroin addiction; and σ, the rate of relapse back to either the A or H class. These also agree with the results from the PRCC analysis. Overall, PRCC and Sobol sensitivity analyses suggested similar parameters were important to each of the classes.

We observe that the first-order index and total-order index results in Sobol sensitivity analysis are very similar to each other which suggests that there are not many higher-order interactions occurring, i.e. the dynamics that are occurring are first-order. First-order and total-order index values and their corresponding confidence intervals are shown in Appendix A. Overall, all of the first-order index results are within a 95% confidence interval of 0.00739 (the largest value) and all total-order index results are within a 95% confidence interval of 0.00590 (the largest value).

Due to our time-dependent parameters, we do not run sensitivity analysis longer than 6 years since the prescribing rate, α, needs to remain positive which requires more limited ranges on some of the inputs. Instead, we consider fixing the parameters for 2013-2020 and

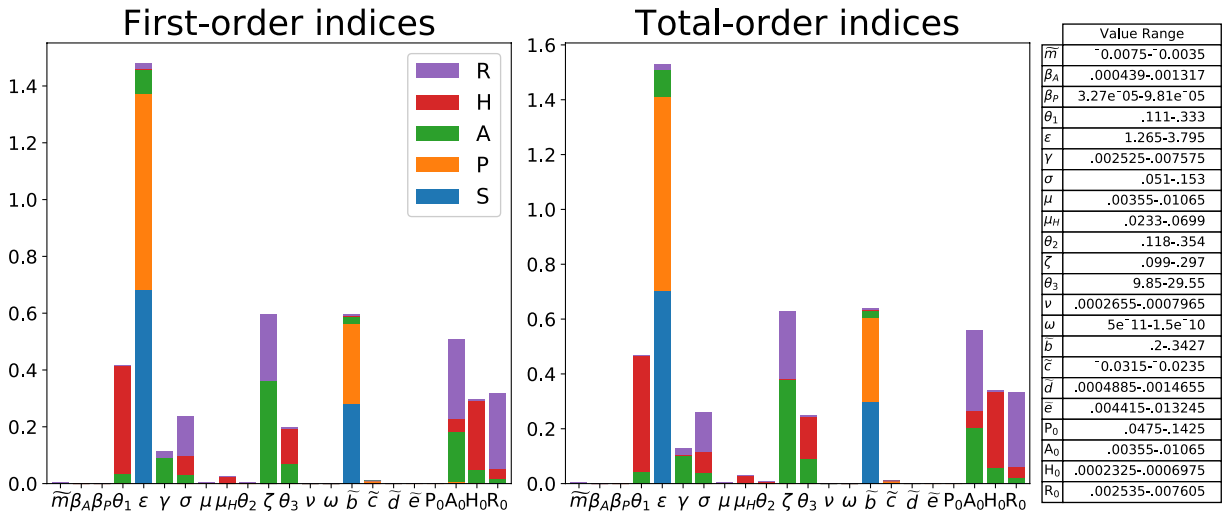


Figure 2.18: Sobol sensitivity results for the size each of the classes at the beginning of 2019 for the α piecewise linear, μ_A linear case run from 2013-2019 with 4,600,000 samples.

then allowing them to vary in a careful way from 2020-2023 for sensitivity analysis purposes in Section 2.5.

2.5 Management Strategies from 2020-2023

Results thus far have examined the epidemic once it was established. However, we are concerned with the epidemic in the near future, as well, and wish to explore practical mitigation strategies for managing the epidemic that is predicted in Figures 2.10 and 2.11 . First, we run the model from 2013-2020 to determine the proportions in each of the classes at the end of this time frame (beginning of 2020), which informs us on initial conditions for running the model starting in 2020. This results in $S_0 = 0.92432$, $P_0 = 0.0585$, $A_0 = 0.0037$, $H_0 = 0.00597$, $R_0 = 0.00751$. Therefore, running the model from the current time (beginning of 2020) to the beginning of 2023, we perform sensitivity analysis to examine the effect of parameters on the size of the classes at the beginning of 2023. We wish to utilize results from these sensitivity analyses in order to consider management strategies to decrease the number of addicted individuals and overdose deaths.

We pay special attention to the time-dependent parameters α and μ_A in this case. Instead of altering $\tilde{m}$, $\tilde{b}$, and $\tilde{c}$ as was done in the 2013-2019 and 2013-2023 sensitivity analysis, we impose a new parameter, $\tilde{g}$, for the slope of α from 2020-2023 to be able to clearly determine whether changing this slope affects the size of A and H in 2023. Thus, we take the value of α from 2020 using baseline parameter values from Table 2.9:

$$\tilde{m}(3.25) + \tilde{b} - 3.25\tilde{c} + \tilde{c} \cdot t$$

$$= -0.00560(3.25) + 0.270 - 3.25(-0.0270) - 0.0270(7)$$

$$\approx 0.151,$$

and make

$$\alpha = 0.151 + \tilde{g} \cdot t$$

for $t = 0$ to $t = 3$, where $\tilde{g}$ has the same baseline value as $\tilde{c}$ as before. Similarly, instead of allowing $\tilde{d}$ and $\tilde{e}$ to vary as a part of μ_A as was done in previous sensitivity analysis starting in 2013, we create a new parameter, $\tilde{h}$, to represent slope of μ_A from 2020-2023. We take the value of μ_A in 2020 using baseline parameter values from Table 2.9:

$$\tilde{d} \cdot t + \tilde{e}$$

$$= 0.000977(7) + 0.00883$$

$$\approx 0.0157,$$

and make

$$\mu_A = 0.0157 + \tilde{h} \cdot t$$

for $t = 0$ to $t = 3$ with $\tilde{h}$ taking on the same baseline value as $\tilde{d}$.

Instead of allowing these certain parameters to range $\pm 50\%$ as done with the other parameters, we want to consider ranges that allow α and μ_A to vary in a particular way. We first consider what the original values of each of these parameters would be in 2023 if baseline parameter values were used: $\alpha \approx 0.0699$ and $\mu_A \approx 0.0186$. We want to allow these

parameters to be ±50% of their 2023 values during sensitivity analysis. Therefore, in order to obtain a value 50% lower and higher than baseline α in 2023, we solve for the slope $\tilde{g}$:

$$\frac{0.0699}{2} = 0.151 + \tilde{g}(3) \implies \tilde{g} \approx -0.0386$$

and

$$1.5(0.0699) = 0.151 + \tilde{g}(3) \implies \tilde{g} \approx -0.0153.$$

Similarly, we solve for slope $\tilde{h}$ that enables μ_A to reach ±50% of its baseline value in 2023:

$$\frac{0.0186}{2} = 0.0157 + \tilde{h}(3) \implies \tilde{h} \approx -0.00212$$

and

$$1.5(0.0186) = 0.0157 + \tilde{h}(3) \implies \tilde{h} \approx 0.00408.$$

Thus, the ranges for the parameters during sensitivity analysis are shown in Table 2.13 and we note that we do not include the initial conditions as a part of the sensitivity analysis as these are not able to be altered.

For PRCC, the monotonicity plots are produced by varying a single parameter over its entire range while keeping all other parameters fixed at their baseline values for a total of $N = 700$ samples, the ODE being solved each time. The resulting plots are shown in Figure 2.19. The PRCC sensitivity results are shown in Tables 2.14 and 2.15 and the Sobol sensitivity results are shown in Figure 2.20. First-order and total-order index values and their corresponding confidence intervals are shown in Appendix A. Overall, all of the first-order index results are within a 95% confidence interval of 0.00842 and all total-order index results are within a 95% confidence interval of 0.00597.

We observe that the parameters that have any effect on the size of A or H at the beginning of 2023 in either set of sensitivity analysis are: θ_1, θ_3, ζ, γ, σ, ε, μ, μ_H, $\tilde{g}$ and $\tilde{h}$. We wish to use these results to inform potential management strategies for decreasing the number of addicted individuals and overdose deaths and note that in terms of management, we only explore the parameters that are realistically able to be controlled. Similar to before, the first-order indices and total-order indices results in the Sobol sensitivity analysis results are

Table 2.13: Range of values for each parameter used for management scenario sensitivity analysis in the α piecewise linear, μ_A linear case, which are $\pm 50\%$ of the baseline values found in Table 2.4 (except μ_A) and Table 2.9 with the exception of $\tilde{g}$ and $\tilde{h}$, which are chosen specifically due to their effect on time-dependent parameters α and μ_A.

Parameter	Range of values
β_A	[0.000439,0.001317]
β_P	[0.0000327,0.0000981]
θ_1	[0.111,0.333]
ε	[1.265,3.795]
γ	[0.002525,0.007575]
σ	[0.051,0.153]
μ	[0.00355,0.01065]
μ_H	[0.0233,0.0699]
θ_2	[0.118,0.354]
ζ	[0.099,0.297]
θ_3	[9.85,29.55]
ν	[0.0002655,0.0007965]
ω	[0.00000000005,0.00000000015]
$\tilde{g}$	[-0.0386,-0.0153]
$\tilde{h}$	[-0.00212,0.00408]

very similar to one another which suggests that there are not many higher-order interactions occurring, i.e. the dynamics that are occurring are first-order. Thus, we argue it is reasonable to target individual parameters when it comes to control strategies rather than pairs or sets of parameters.

Based on the results, we believe there is reason to explore the influence on the A and H classes that could be made based on changes in the rates of individuals accessing/entering treatment (ζ), recovering and maintaining that recovered state (σ), successfully completing prescriptions (ε), and the prescribing rate (α) coming from the sensitivity to $\tilde{g}$. The latter parameter is advantageous from a control perspective as controlling how much is prescribed is more manageable than preventing individuals from getting addicted to prescription opioids (i.e. controlling γ). We also remark on scenarios with changing θ_1, θ_2, and θ_3 values due to the availability of heroin, as well as overdose parameters, μ_A (which relies on $\tilde{h}$) and μ_H, as we wish to examine what would happen if the overdose death rates were decreased due to the availability and administration of Naloxone, an opioid-reversal drug that prevents death

Table 2.14: Results from LHS/PRCC sensitivity analysis of the size of the prescription opioid addicted class at the beginning of 2023 for the α piecewise linear, μ_A linear case run from 2020-2023 with 700 samples.

Input	PRCC for A class at beginning of 2023	p-value for A class at beginning of 2023
β_A	0.005806	0.87813
β_P	0.062877	0.096465
θ_1	-0.66908	4.7857e-92*
ε	-0.81359	1.5676e-166*
γ	0.83562	8.8477e-184*
σ	0.63866	1.7449e-81*
μ	-0.093183	0.01365*
μ_H	0.17632	2.6871e-06*
θ_2	-0.012939	0.73254
ζ	-0.9646	0*
θ_3	-0.95754	0*
ν	0.0355	0.34832
ω	-0.060632	0.10898
$\tilde{g}$	0.23732	2.0338e-10*
$\tilde{h}$	-0.12264	0.0011491*

from an overdose [80]. In [6], the most effective control efforts for the prescription-opioid only model included increasing the treatment entrance rate (which is related to our parameter ζ), reducing the time of completing prescriptions (which is our rate ε) and decreasing the prescribing rate (α), so the control efforts we explore align with these.

For each of the strategies discussed below, we calculate the effect of the strategies on the size of the A and H classes in comparison to the baseline value of the A class in the beginning of 2023 which is ≈ 0.001682 and the baseline value of the H class at the beginning of 2023 which is ≈ 0.01380 that result from running the model from 2020-2023 with the time-dependent parameters discussed above. (Note: these baseline values would be the same if the model were run from 2013-2023, as well).

2.5.1 Accessibility to Treatment: Management Strategy

One parameter that the sizes of A and H are sensitive to at the beginning of 2023 is ζ, which is the rate at which individuals enter the stably recovered class from the prescription opioid

Table 2.15: Results of LHS/PRCC sensitivity analysis of the size of the heroin/fentanyl addicted class at the beginning of 2023 for the alpha piecewise linear case run from 2020-2023 with 700 samples.

Input	PRCC for H class at beginning of 2023	p-value for H class at beginning of 2023
β_A	-0.0028471	0.94006
β_P	0.041193	0.27643
θ_1	0.99458	0*
ε	-0.18455	8.8163e-07*
γ	0.18813	5.3506e-07*
σ	0.94156	0*
μ	-0.36434	-0.36434
μ_H	-0.89095	1.6715e-241*
θ_2	0.4657	5.7134e-39*
ζ	-0.14592	0.00010686*
θ_3	0.91904	2.0263e-284*
ν	-0.069414	0.066437
ω	0.028154	0.45706
$\tilde{g}$	-0.049414	0.19161
$\tilde{h}$	0.062589	0.098006

addict class. Increasing this parameter, which could come from increased accessibility/entry into treatment, reduces the sizes of both the A and H classes. We have ζ range from it's original value from parameter estimation to 50% of that value (what we would assume would be the maximum value reasonable for a change in 3 years, as well as to align with the range used in Sobol sensitivity analysis). We also increase ν simultaneously, the rate heroin/fentanyl addicts enter the stably recovered class, since changes in treatment would be available for all opioid users and would not be separate based on the drug. The effects on the A and H classes are recorded in Table 2.16, as well as the percent change in the *total* number of overdoses from 2020-2023. Results suggest that there would be a substantial decrease in the number of prescription opioid addicts and a slight decrease in heroin/fentanyl addicts. This has a combined effect of considerably decreasing the number of overdose deaths over the 3-year period.

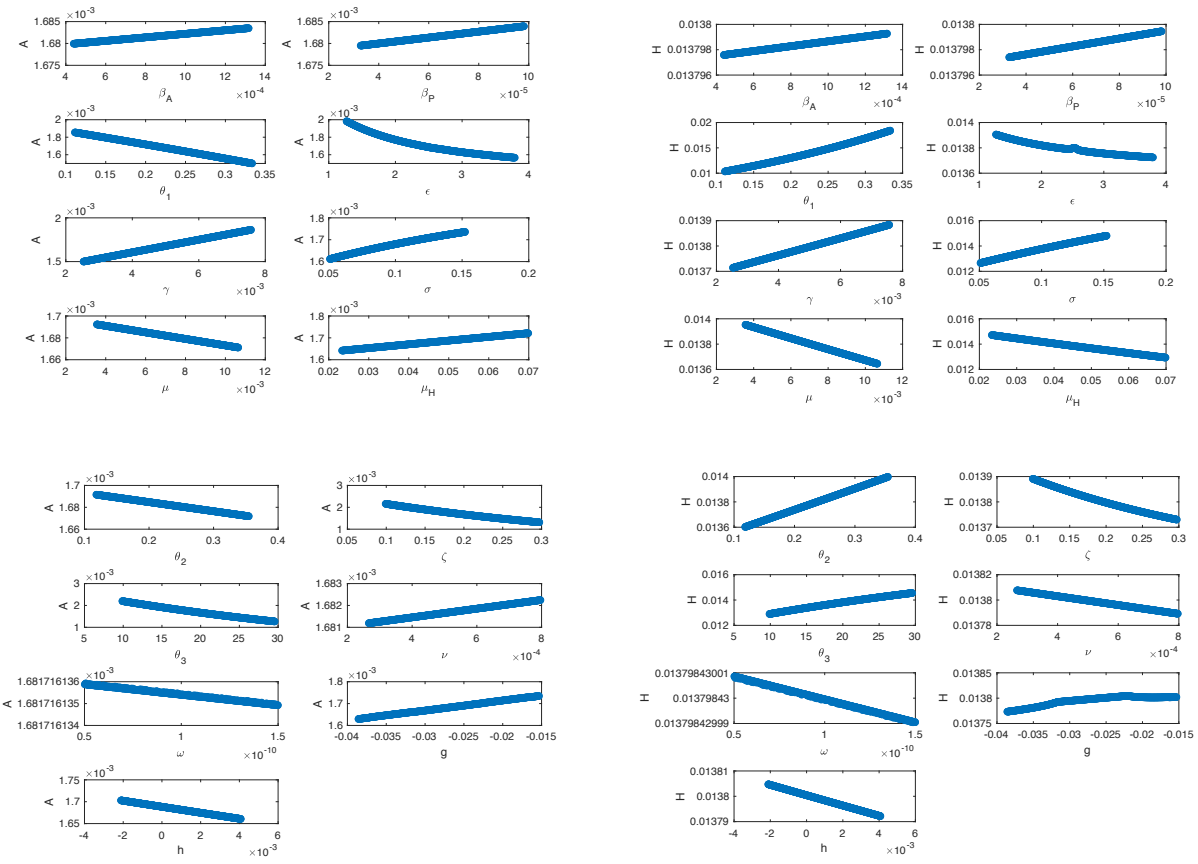


Figure 2.19: Monotonicity plots of A and H with respect to 15 parameters for the α piecewise linear, μ_A linear case. Each plot is formed by sampling one parameter across its range and holding all other parameters at their baseline values.

2.5.2 Case-holding in Stably Recovered Class: Management Strategy

The sensitivity results for PRCC suggest that σ is somewhat of is an important parameter in the size of the H class at the final time, and is a parameter that we are able to control in some way. Therefore, we want to consider how much of a reduction in this parameter would affect reduction in both A and H. Reduction of σ would require careful monitoring of those who are stably recovered from addiction and "holding" them in the R class. The effect on the size of the A and H classes at the beginning of 2023 are shown in Table 2.17 where we consider a maximum decrease of 50% for σ to align with the range for the parameter used

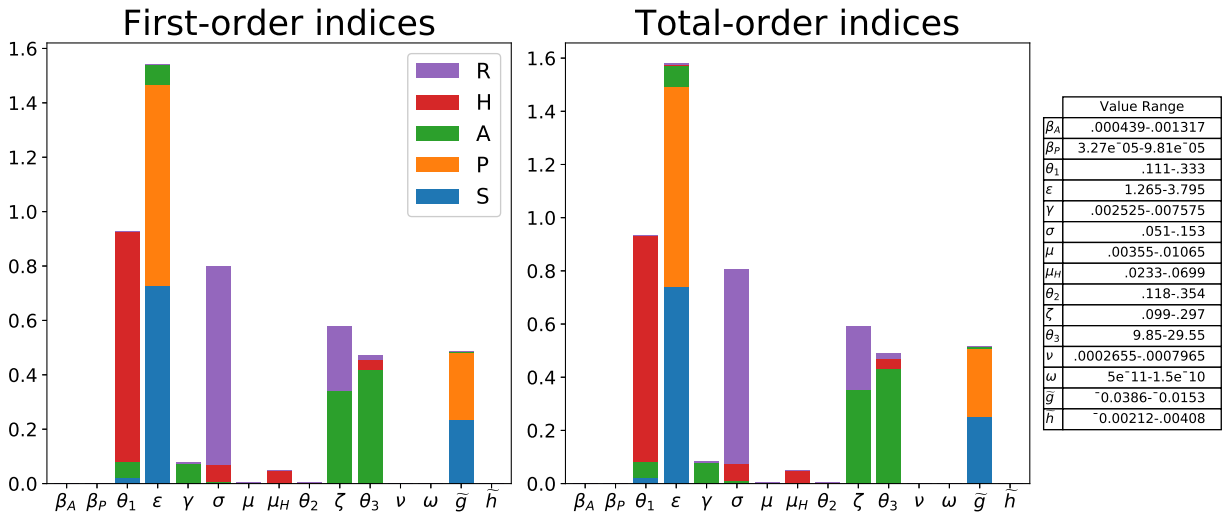


Figure 2.20: Sobol sensitivity results for the size of each of the classes at the beginning of 2023 for the α piecewise linear, μ_A linear case run from 2020-2023 with 3,800,000 samples.

in the sensitivity analyses. We also show results for the percent change of the total number of overdoses over the 3 year time period. There is a decrease in both the A and H classes, leading to an overall reduction in the number of opioids addicts and overdose deaths. It is important to point out that in the previous case with the ζ and ν management scenario, the percent decrease of overdose deaths was about 50% that of the percent decrease of opioid addicts. However, in this case, since a larger portion of the decrease of opioid addicts came from the heroin/fentanyl class which has a higher overdose death rate compared to the A

Table 2.16: Effect on size of A and H classes at the beginning of 2023 from increasing ζ and ν at the beginning of 2020 and the effect on the total number of overdoses in the time period from 2020-2023. The baseline values for the parameters are listed in the first row.

ζ	ν	% change in ζ, ν	% change in A	% change in H	% change in total addicts	% change in total overdoses
0.198	0.000531	–	–	–	–	–
0.218	0.000584	+10%	−4.8%	−0.1%	−4.9%	−2.4%
0.258	0.000691	+30%	−13.8%	−0.4%	−14.2%	−7.0%
0.297	0.000792	+50%	−21.8%	−0.6%	−22.4%	−11.2%

Table 2.17: Effect on size of A and H classes at the beginning of 2023 from decreasing σ at the beginning of 2020 and the effect on the total number of overdoses in the time period 2020-2023. The baseline value for σ is listed in the first row.

σ	% change in σ	% change in A	% change in H	% change in total addicts	% change in total overdoses
0.102	–	–	–	–	–
0.0914	−10%	−0.8%	−1.6%	−2.4%	−1.6%
0.0710	−30%	−2.4%	−4.9%	−7.3%	−5.0%
0.0507	−50%	−4.2%	−8.3%	−12.5%	−8.4%

class, this had a more significant impact on overdose deaths compared to the decrease in opioid addicts (i.e. better than a 50% ratio).

2.5.3 Heroin/Fentanyl Availability Scenarios

Sensitivity results suggest that θ_1 is the most important parameter in the size of the H class at the beginning of 2023, which is the rate individuals from the susceptible class transition to heroin use via interaction with heroin addicts, and θ_3 is very important to the size of the A class, which is the rate prescription opioid addicts enter the heroin/fentanyl class. We observe that θ_1 and θ_3 impact the size of the A and H classes at the beginning of 2023 in opposite ways (i.e. decreasing each of these parameters decreases the H class but increases the A class) from the sensitivity analysis results in Tables 2.14 and 2.15.

One management strategy relating to reducing these parameters would be to decrease the supply of heroin or make prescription opioids cheaper than heroin so that there are fewer addicts in H (and therefore fewer opportunities for those in S, P, and A to interact with a heroin/fentanyl addict and become addicted). Decreasing the availability could come from increased policing and the removal of street brokers and heroin deals, as [58] suggests that removing drug dealers directly may not be the most effective intervention, but instead targeting street brokers. However, the supply of heroin would be available to individuals in *all* three classes, S, P, and A, and we must consider all pathways to heroin/fentanyl use in this scenario. Thus, we consider the case of decreasing θ_1, θ_2, *and* θ_3. The results are shown in Table 2.18, which shows an overall *increase* in the total number of addicts at the

Table 2.18: Effect on size of A and H classes at the beginning of 2023 from decreasing $\theta_1, \theta_2, \theta_3$ at the beginning of 2020 and the effect on the total number of overdoses over the time period 2020-2023. The baseline values for the parameters are listed in the first row.

θ_1	θ_2	θ_3	% change of $\theta_1, \theta_2, \theta_3$	% change in A	% change in H	% change in total addicts	% change in total overdoses
0.222	0.236	19.726	–	–	–	–	–
0.200	0.213	17.752	-10%	$+7.8\%$	-7.0%	$+0.8\%$	-1.6%
0.156	0.166	13.803	-30%	$+23.5\%$	-19.9%	$+3.6\%$	-4.2%
0.111	0.118	9.853	-50%	$+39.0\%$	-31.2%	$+7.8\%$	-6.2%

beginning of 2023, but a decrease in the total number of overdose deaths in the 3-year time period. Since there are significantly fewer individuals in the H class (there is a substantial percent decrease for that class), the total overdoses decreases since the H class has a higher overdose rate than the A class, although the total number of addicts increases.

We also explore the case where there are places to buy prescription opioids safely (rather than from the black market and at a rate cheaper than prescriptions), to encourage prescription opioid addicted individuals not to turn to heroin/fentanyl use. Thus, we explore the effect of decreasing θ_3 on its own. Results are shown in Table 2.19 which actually shows an increase in the number of overall addicts and overdose deaths (since very few are leaving the heroin class as compared to results in Table 2.18). This result aligns with our basic reproduction number analysis, that decreasing θ_3 does not have an effect on the size of $\mathscr{R}_0$ at all, let alone decreasing it. Instead, $\mathscr{R}_0$ relies on the size of θ_1 and θ_2 (with the former being more important due to its multiplication with S which is big compared to P) which means that θ_1 is the driver for sustaining the epidemic and keeps H growing in the trajectory from Figure 2.10. Therefore, no matter how small θ_3 is, it will not bring down the number of opioid addicts and instead the other routes to heroin/fentanyl addiction will drive the size of the addicted classes. The analysis done above with decreasing all three parameters simultaneously is what we view as the most practical management strategy incorporating θ_1 and thus, we do not analyze it on its own.

Table 2.19: Effect on size of A and H classes at the beginning of 2023 from decreasing θ_3 only at the beginning of 2020 and the effect on the total number of overdoses over the time period 2020-2023. The baseline values for θ_3 is listed in the first row.

θ_3	% change of θ_3	% change in A	% change in H	% change in total addicts	% change in total overdoses
19.726	–	–	–	–	–
17.752	−10%	+5.7%	−1.2%	+4.5%	+1.3%
13.803	−30%	+17.7%	−3.8%	+13.9%	+9.3%
9.853	−50%	+30.6%	−6.5%	+24.1%	+7.0%

2.5.4 Prescription Rate Management Strategy

One parameter that the A class was sensitive to was $\tilde{g}$, which is the slope of the time-dependent parameter α from 2020-2023. Thus, we explore the effect on the sizes of the A and H classes from decreasing the prescribing rate in this 3-year time period, as well as the overdose deaths, in Table 2.20. This is important to investigate as a new law was passed in April 9, 2019 in Tennessee where prescribers must *electronically* submit prescriptions (called "e-prescribing") and have until January 2021 to implement this as it will be required at that time [103]. For $t = 0$ to $t = 3$ (i.e. starting in 2020), we consider the cases of keeping α the same function ($\alpha = 0.151 - 0.0270 \cdot t$), where 0.151 is the value of α in 2020, and thus having a value of 0.0699 in 2023; reducing α by 25% and having a resulting value of 0.0524 in 2023 from the function $\alpha = 0.151 - 0.0328 \cdot t$; and finally, cutting α by 50%, with the resulting value in 2023 being 0.0349 from $\alpha = 0.151 - 0.0386 \cdot t$. The entire function for α is shown graphically in Figure 2.21 from 2013-2023 with various cases. Results suggest there would be a minimal effect on reducing the number of addicted individuals and particularly overdose deaths.

2.5.5 Prescription Completion: Management Strategy

We have outlined the control strategy relating to our prescribing rate, α, but at some point that rate will be difficult to control, as it could get to a point of not being able to decrease any further (as we do not allow this parameter to go negative). With this in mind, controlling ε could be advantageous, which is the rate that individuals successfully

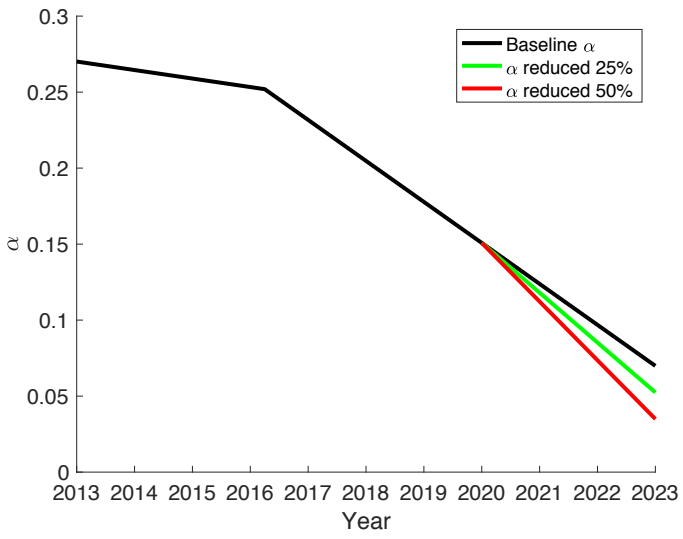


Figure 2.21: This plot shows three different cases of the piecewise linear function for the prescribing rate, α, in which α either maintains its baseline value in 2023 (black), reaches a 25% reduction in the baseline value in 2023 (green), or reaches a 50% reduction in the baseline value in 2023 (red). For management strategy analysis from 2020-2023, these cases are used to determine the effect that decreasing α has on the size of the A and H classes in 2023 and the total overdose deaths from 2020-2023. Results are shown in Table 2.20.

finish their prescription without becoming addicted. This could potentially be accomplished by increasing the information provided to opioid-prescribed patients on the risk of addiction or more carefully monitoring patients with prescriptions. Therefore, we consider the effect on the size of the A and H classes at the beginning of 2023 by increasing ε starting in 2020. Results are shown in Table 2.21 where we consider a maximum increase of 50% for ε to align with the sensitivity analysis range used for the parameter. We also provide results for the total percent change of overdoses over the 3 year time period. We see there are slight

Table 2.20: Effect on size of A and H classes at the beginning of 2023 from decreasing α at the beginning of 2020 to reach 25% or 50% of its baseline value in 2023. The baseline value for g is listed in the first row.

$\tilde{g}$	α in 2023	% change of α	% change of A	% change of H	% change total addicts	% change total overdoses
-0.0270	0.0699	–	–	–	–	–
-0.0327	0.0524	−25%	−1.5%	−0.1%	−1.6%	-0.3%
-0.0386	0.0349	−50%	−3.1%	−0.2%	−3.3%	-0.8%

reductions in the total number of addicts and overdose deaths but not nearly as effective as reducing ζ and ν or σ.

2.5.6 Overdose-Reversal Drug Management Strategy

Sensitivity results suggest that μ_H is important to the size of the H class at the final time, which is the rate individuals overdose from the heroin/fentanyl addict class, and $\tilde{h}$ slightly effects the A class, which is the slope of the time-dependent parameter μ_A from 2020-2023. We wish to examine the result of decreasing the overdose death rates μ_A and μ_H which could come from an increased availability and administration of Naloxone, an opioid-reversal drug that prevents death from an overdose (although we do not know what happens to individuals after being saved) [80]. Up to this point, we have focused on management scenarios with the goal of decreasing the number of addicts and total overdose deaths. With overdose deaths rates, we will solely focus on total overdose deaths from 2020-2023 (since decreasing overdose deaths will naturally increase opioid addicts so these two categories cannot be both managed simultaneously). The effect on overdose deaths in this 3-year time period from decreasing overdose death rates is shown in Table 2.22 which suggests that a management strategy involving Naloxone availability/usage could be very useful. The various cases that we implement for the time-dependent parameter μ_A are illustrated in Figure 2.22. Over the 3-year timeframe, we consider the cases of keeping μ_A the same function ($\mu_A = 0.000977 \cdot t + 0.0157$) where 0.0157 is the value of μ_A in 2020, and thus having a value of 0.0186 in 2023; reducing μ_A by 25% and having a resulting value of 0.0140

Table 2.21: Effect on size of A and H classes at the beginning of 2023 from decreasing ε at the beginning of 2020 and the effect on the total number of overdoses in the time period 2020-2023. The baseline value for ε is listed in the first row.

ε	% change in ε	% change in A	% change in H	% change in total addicts	% change in total overdoses
2.528	–	–	–	–	–
2.781	+10%	−1.7%	−0.2%	−1.9%	−0.9%
3.287	+30%	−4.7%	−0.4%	−5.1%	−2.2%
3.793	+50%	−6.9%	−0.5%	−7.4%	−3.2%

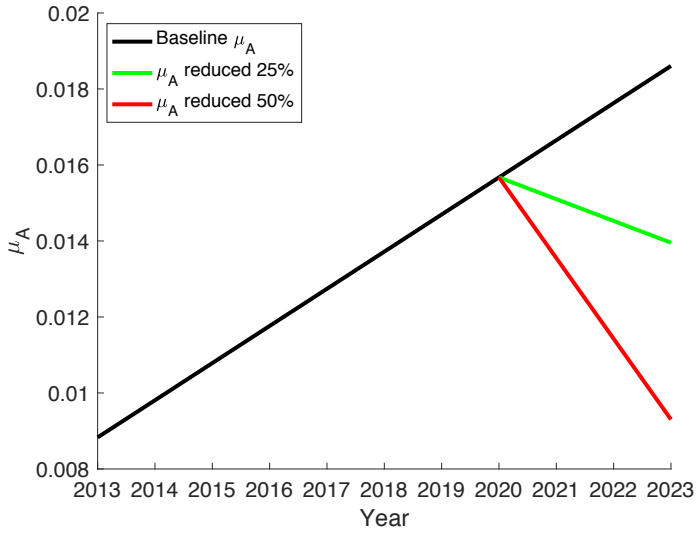


Figure 2.22: This plot shows three different cases of the function for the prescription opioid overdose death rate, μ_A, in which μ_A either maintains its baseline value in 2023 (black), reaches a 25% reduction in the baseline value in 2023 (green), or reaches a 50% reduction in the baseline value in 2023 (red). For management strategy analysis from 2020-2023, these cases are used to determine the combined effect that decreasing μ_A and μ_H have on the total overdose deaths from 2020-2023. Results are shown in Table 2.22.

in 2023 from the function $\mu_A = -0.000573 \cdot t + 0.0157$; and finally, cutting μ_A by 50%, with the resulting value in 2023 being 0.0093 from $\mu_A = -0.00212 \cdot t + 0.0157$.

2.6 Conclusions and Discussion

Upon formulating a compartmental model to describe the transition of individuals among classes of opioid use, we were able to describe the dynamics of the epidemic in Tennessee

Table 2.22: Effect on the total number of overdose deaths from 2020-2023 from decreasing μ_H and μ_A at the beginning of 2020 to reach 25% or 50% of their baseline values in 2023. The baseline values for the overdose rates are listed in the first row.

μ_H	$\tilde{h}$	μ_A	% change in μ_H, μ_A	% change in total overdose deaths
0.0466	0.00977	0.0186	–	–
0.0349	-0.00573	0.0140	-25%	-35.7%
0.0233	-0.00212	0.0093	-50%	-72.3%

from 2013 to 2023. Since the establishment of the opioid epidemic in 2012/2013, data regarding opioid use and overdoses have become publicly available. Using the data available for Tennessee, we were able to estimate parameters using ordinary least squares and used AIC to determine the best model to describe our data. Ultimately, the AIC scores were close to one another and we deemed the model with the time-dependent prescribing rate and prescription opioid addict overdose death rate to be the best choice. Using the estimated parameters from this case, the predicted trajectory of the epidemic is expected to increase in magnitude over the next few years and our results from the trajectory graphs and form of the basic reproduction number suggest that the epidemic is being driven by heroin and fentanyl users.

Sensitivity analysis was performed to determine which parameters and initial conditions played the biggest role in the size of the A and H classes at the beginning of 2019 when running the model from 2013, as well as which parameters were important at the final time running from 2020-2023. From management strategy analysis, we deem the most effective strategies for decreasing the number of opioid addicts and/or overdose deaths in the next 3 years to be increasing the availability of and accessibility to treatment with subsequent monitoring of individuals who become stably recovered, as well as increasing the implementation of opioid-overdose reversal drugs to help combat the overdose death crisis we have been facing and expect to continue seeing over the next few years.

For future work, there are several extensions to our model that can be made. In our current model we assume homogeneous mixing of the individuals in each of the compartments and therefore, each individual has the same probability of transitioning from one stage to another, interacting with individuals from other stages, or leaving the system via death. Although done for the purpose of simplification, this is not an accurate representation of reality since there are factors that affect these probabilities, such as race, gender, geographical location, and age. For example, there has been a shift in heroin use from urban areas to some suburban and rural areas and there is an increasing number of individuals ages 18-25 using the drug [80]. Using data from the 2008-2010 NSDUH studies, past year heroin use was twice as likely for men compared to women, and highest in the 18-25 year old age group [64]. West Virginia, New Hampshire, and Ohio had the highest rates of opioid-related overdose

deaths per 100,000 people in 2016 and Tennessee and Arkansas were among the states with the highest prescription rates per 100 people the same year [81]. In Tennessee specifically, the majority of individuals who overdosed either on heroin or fentanyl were white and male [84]. Men have a higher likelihood of overdosing on prescription pain relievers compared to women, but since 1999, there has been a steeper increase in the number of women overdoses than men [21]. In addition, women may form a quicker dependence on opioids compared to men, and have a higher probability of being prescribed higher doses and for longer periods of time [64]. Incorporating these ideas into the model would result in specific management actions for various subsets of the population.

Moreover, our model is focused on the timeframe from 2013-2023 for Tennessee, but shortly after (in 2025), our time-varying rate α goes negative when using its baseline parameters, which is no longer realistic. However, we do not currently have enough data to fit a non-linear, tapering function to α for this 10-15 year period and this could be a part of future work when more data is available. Although there is data on the misuse of opioids, we decided to focus specifically on addiction rather than misuse, due to the harmful consequences this behavior can have for an individual. However, the behavior and actions of individuals are not always very clearly defined, and there may be a benefit to expanding the spectrum of classes that individuals can fall into. A more detailed look could be given to the individual cases of hepatitis C for opioid users, as this is a rising public health concern, as well. Another choice for dealing with recovery could include having two recovered classes and more carefully tracking where individuals come from and where they go back to, or considering different terms between R and A or R and H with the classes we currently have. Moreover, a more detailed look into reducing stigma, harm reduction, and how trauma is connected to addiction are future avenues to explore, as well.

Chapter 3

Harvesting of Non-Timber Forest Products

3.1 Background

Khaya senegalensis (African Mahogany) is a large tree species in Benin, West Africa that is harvested lethally for its timber, in which the entire plant is removed, and non-lethally for both its leaves and bark [10, 44, 48]. The latter type of harvest of non-timber forest products (NTFP) holds economic and cultural significance; for instance, local cattle-herders, called Fulani, defoliate the trees in the dry season in order to feed their livestock. *K. senegalensis* is typically 30 meters high with a 3 meter diameter, and due to the risk of climbing for harvesting, Fulani maximize the amount of foliage they obtain per tree, with an estimated 80% of trees fully defoliated on average [44, 49].

Non-lethal harvesting does not directly kill the tree, but results in a reduction in reproduction and the population growth rate [48]. Lethal harvesting does directly kill the tree and also affects the growth rate of the population. Classical harvesting models incorporate only the direct removal of individuals from the population, but do not account for the indirect effects of non-lethal harvesting. Moreover, many stage-structured projection matrix models do not include *explicit* harvesting intensities, and therefore do not provide information on how harvest affects specific stage transitions.

A few models have incorporated non-lethal harvest in order to better explore the indirect effects it has on the population [48, 41, 44]. One of these models [48] aimed to understand the role of both types of harvesting on plant population dynamics and population growth rate. This was done for a general plant species experiencing timber and/or NTFP harvesting, a category in which *K. senegalensis* falls into. This model incorporated a pair of ordinary differential equations (ODEs) that represented the plant population density $x(t)$ and population intrinsic growth rate $r(t)$:

$$\frac{dx(t)}{dt} = r(t)x(t)(1 - \frac{x(t)}{K}) - h_L(t)x(t)$$
$$\tau\frac{dr(t)}{dt} = r_e - r(t) - (\alpha h_N(t) + \beta h_L(t)).$$

This work concentrated on stability analysis. Optimal control theory was then applied to determine optimal time-dependent non-lethal and lethal harvesting strategies for the population, with the goal of maximizing conservation and benefits of harvesters, while minimizing cost [41]. The optimal strategy consisted of performing nonlethal NTFP harvesting for a few years before beginning to incorporate lethal harvesting. Moreover, lethal or non-lethal harvesting rates needed to be less than 40% of the population density which was lower than most reported sustainable NTFP harvesting rates.

Another such model by Gaoue [44] was stage-structured and formulated in order to measure the impact of only non-lethal harvesting of adults. This model consisted of five population classes based on size:

1. Seedlings: 0 cm $<$ basal diameter $<$ 2 cm
2. Saplings: 2 cm $\leq$ basal diameter $<$ 5 cm
3. Juveniles: 5 cm $\leq$ diameter at breast height $<$ 20 cm
4. Small-reproductive adults (AD1): 20cm $\leq$ diameter at breast height $<$ 40 cm
5. Large-reproductive adults (AD2): diameter at breast height $\geq$ 40 cm.

Both reproductive adult classes were non-lethally harvested. Data was gathered from six populations in the Sudanian dry region of Benin, three of which were experiencing high

harvest and the remaining three experiencing low harvest, as well as six populations from the Sudano-Guinean moist region in Benin with the same split of high and low harvest. High harvest for a population was considered to have more than 50% of its trees defoliated with greater than 10% tree bark removed and low harvest for a population was considered to have less than 25% of its trees defoliated with less than 10% tree bark removed. Population matrices were built using average population structures and harvesting intensities over 4 years. Results from this work showed that the effect of NTFP harvest was greater in the short-term compared to the long-term by looking at differences in growth rates between low and high harvest intensities and that early stage survival was more important for transient dynamics than long-term dynamics from elasticity analysis. This work suggested that only using long-term growth rates to inform harvest management decisions can be misleading, and information from both short and long-term population dynamics should be used to guide management plans.

Although the model in [48] included different types of explicit, time-dependent harvest, it did not include size structure; on the other hand, the stage-structured model in [44] generalized harvest of adults as high or low to explore short and long term population growth rates, but was not explicit with the amount of harvest for each size class and harvest did not vary over time. In addition, this model did not include the non-lethal harvest of juveniles or the lethal harvest of adults, which is not realistic. These necessary features provide the motivation for the development of our model: a stage-structured, time-varying harvesting system of difference equations for *K. senegalensis*. Our model includes non-lethal harvesting of juveniles and both non-lethal and lethal harvesting of adults for the *K. senegalensis* population in order to investigate the effect of size-dependent harvesting strategies on tree population dynamics.

Our focus is on two areas of Benin where this tree species grows: the Sudanian northern dry region and the moist central Sudano-Guinean region with a longer growing season and lower temperatures than the former [44]. Benin experiences a cooler, dryer season from October to April, and a warmer, rainy season from May to September with rainfall ranging from 850-1900mm, with an average of 1100mm. Table 3.1 shows a monthly calendar for

Table 3.1: Events that occur each month for *K. Senegelensis* in Benin.

Month	Season	Events
October	dry	"early fire" to burn vegetation, lethal harvest, grass growth, flowering on trees begins
November	dry	lethal harvest, flowering continues on trees and fruit production begins at end of November
December	very dry	fruit production, non-lethal harvest, lethal harvest
January	very dry	fruit production, non-lethal harvest, fruits open and drop/disperse seeds, lethal harvest
February	dry	fruit production, non-lethal harvest, fruits open and drop/disperse seeds, lethal harvest, "late fire" begins
March	dry	non-lethal harvest, lethal harvest, "late fire" occurs
April	dry/start of wet season at end	germination of grass, "late fire" that kills trees, lethal harvest, absolutely no non-lethal
May	wet	grass growth
June	wet	seedlings emerge, grass growth
July	wet	seedlings emerge, grass growth
August	wet	flooding, some seedlings die because submerged, grass growth
September	wet/start of dry season at end	grass growth

events that occur [46]. Data collection on 12 *K. Senegelensis* tree populations happens on a yearly basis, usually in December [46].

Toward the end of the dry season in March, "late fire" is carried out in order to open up more land for crops and reduce shade for crops. In October, "early fire" is carried out before October 15^{th} to burn vegetation, as this is when grass is at its maximum height. This particular fire is carried out for two purposes: the primary purpose is to burn the vegetation before it is too dry, in order to prevent accidental burning later on that would also burn the trees, and the second is for ease of hunting, where all animals are pushed to one side. After the "early fire," non-lethal harvesting begins because the vegetation is gone, so trees offer the only fodder that is left for stock to eat. There is non-lethal harvesting of the trees only in the dry season since other vegetation is available for stock in the wet season. Lethal harvest only occurs in the dry season because it is easier for the logging companies than in the wet season and with the most difficult times in June, July, and August, the wettest months. For a first model, we are *not* going to include fire explicitly, but instead let it be

the implicit reasoning behind when harvest occurs: the "early" fire kills grass and since it's annual and not perennial, there is nothing else for stock to eat, so the local people *have* to harvest. Thus, harvesting occurs in the dry season and there is no harvest in the wet season. The growth of the trees, in terms of height and width, takes place mostly in the wet season; in the dry season, there is little to no growth.

Understanding how local people can sustainably use the environmental resources on which they depend for their livelihood is critical, and therefore, we explore different harvesting strategies and the corresponding impact on tree population dynamics. This work is in collaboration with Orou Gaoue, Suzanne Lenhart, and Christopher Strickland, and is part of advancing the overall understanding of the ecological processes that occur simultaneously when a tree population experiences harvest, which may influence management strategies in the short-term and/or long-term. We would like to thank Hal Caswell and Christina Edholm for their helpful comments and contributions, as well.

3.2 Model Formulation

Our discrete harvesting model is based on four size classes with units of number of trees [44]:

1. Seedlings (N): 0 cm $<$ basal diameter $<$ 2cm
2. Saplings (S): 2 cm $\leq$ basal diameter $<$ 5cm
3. Juveniles (J): 5cm $\leq$ diameter at breast height $<$ 20cm
3. Adults (A): diameter at breast height $\geq$ 20 cm.

Each of the size classes have initial positive values. We are operating under the assumption that seedlings do not reproduce nor are harvested, juveniles do not reproduce but are able to be non-lethally harvested, and finally, adults are able to reproduce and are both non-lethally and lethally harvested [45]. We define reproduction here as the new seedlings that emerge as a result of adult trees dispersing seeds from the fruits they produce. For simplicity, we grouped together what were previously referred to as the adult 1 (AD1) and adult 2 (AD2) classes in [44] and combined them into a single adult (A) class since they are both reproductive, and

both non-lethally and lethally harvested, and therefore not easily distinguished in the field [46]. The compression of these classes in the model from [44] is discussed in detail in Section 3.3.

For our discrete harvesting model, we denote different events for the trees as follows with $i = 1$ representing the seedling class, $i = 2$ the sapling class, $i = 3$ the juvenile class, and $i = 4$ the adult class. Here, k represents a year and $2k + 1$ represents the dry season, which is discussed in more detail below.

- σ_i is the survival probability for class i in the dry season; σ_{i+4} in the wet season
- γ_{ij} is the probability of transitioning from class i to class j
- ρ_{ij} is the shrinkage from class i to class j
- $\phi_A(h_N(2k+1), h_L(2k+1))$ is the fertility rate of the adult class which includes the survival of seedlings in their first wet season (i.e. probability of establishment)
- $h_J(2k+1)$ is the time-dependent non-lethal harvest rate of the juvenile class
- $h_N(2k+1)$ is the time-dependent non-lethal harvest rate of the adult class
- $h_L(2k+1)$ is the time-dependent lethal harvest rate of the adult class.

Harvesting can impose direct and indirect effects on the tree population. For example, the human trampling of seedlings and changes in adult canopy cover affect the survival rate of seedlings [10]. Saplings are too far from the adults to be affected by nonlethal harvesting and are only affected by the lethal harvest of adults due to the dragging of logs through the trees which damages the saplings [46]. In addition, the non-lethal harvesting of juveniles has no effect on saplings. The two types of non-lethal harvest do not affect juveniles because they are too strong at that size to be affected. The lethal harvest of adults directly impacts adult tree survival and both the non-lethal and lethal harvest of adults affects its reproduction.

We formulate a model that starts in the dry season that goes from October-April and then transitions to the wet season for May-September. The following section discusses assumptions made for each season and discusses each individual equation to clearly demonstrate the order of events.

Dry season: This season occurs from October-April. It begins with $2k$, which is the end of the wet season in year k, and results in $2k+1$, which is the end of the dry season in year k, as shown in equations (3.1). In the dry season, we have the following assumptions:

1. No diameter growth of the trees implies no transition to next size ($\gamma_{12} = \gamma_{23} = \gamma_{34} = 0$).
2. There is both non-lethal and lethal harvesting ($h_J(2k+1) > 0$, $h_N(2k+1) > 0$ and $h_L(2k+1) > 0$).
3. There is shrinkage of saplings to seedlings caused by fires or drought ($\rho_{21} > 0$).
4. There is no reproduction ($\phi_A(h_N(2k+1), h_L(2k+1)) = 0$).

Although seed dispersal occurs in some of the months, January and February, we let reproduction from the adult trees occur in the wet season after the adults from the dry season have been harvested.

For $k \geq 0$,

$$\begin{aligned}\boldsymbol{N(2k+1) = (1 - h_N(2k+1) - \alpha_1 h_L(2k+1) - h_J(2k+1))\sigma_1 N(2k)} \\ \boldsymbol{+\rho_{21}(1 - \alpha_2 h_L(2k+1))\sigma_2 S(2k)}\end{aligned}$$

First, a proportion of the seedlings from the previous wet season survive (σ_1), and then this is brought down by the indirect effects of all three types of harvest of juveniles and adults ($h_N(2k+1) + \alpha_1 h_L(2k+1) + h_J(2k+1)$), leaving $((1 - h_N(2k+1) - \alpha_1 h_L(2k+1) - h_J(2k+1))\sigma_1 N(2k))$ seedlings by the end of the dry season. Next, a proportion of the saplings from the previous dry season shrink and come into the seedling class by the end of the dry season ($\rho_{21}(1 - \alpha_2 h_L(2k+1))\sigma_2 S(2k)$).

$$\boldsymbol{S(2k+1) = (1 - \rho_{21})(1 - \alpha_2 h_L(2k+1))\sigma_2 S(2k)}$$

First, a proportion of the saplings from the previous wet season survive (σ_2), which is brought down by indirect effects of the lethal harvesting of adults ($\alpha_2 h_L(2k+1)$). Then, due to a proportion of the saplings that shrink and leave to go to the seedling class (ρ_{21}), the remaining saplings by the end of the dry season is represented by $((1-\rho_{21})(1-\alpha_2 h_L(2k+1))\sigma_2 S(2k))$.

$\boldsymbol{J(2k+1) = \sigma_3 J(2k)}$

A proportion of the juveniles from the previous wet season survive (σ_3) to the end of the dry season.

$\boldsymbol{A(2k+1) = (1 - h_L(2k+1))\sigma_4 A(2k)}$

First, a proportion of the adults from the previous wet season survive (σ_4), and then this is brought down by the lethal harvesting of adults ($h_L(2k+1)$), leaving ($(1-h_L(2k+1))\sigma_4 A(2k)$) adults by the end of the dry season.

Wet season: This season lasts from May-September. It begins with $2k+1$, which is the end of the dry season in year k, and results in $2k+2$, which is the end of the wet season in year k, as shown in equations (3.2). We have the following set of assumptions for the wet season:

1. There is transition to next size ($\gamma_{12} > 0$, $\gamma_{23} > 0$, $\gamma_{34} > 0$).
2. No non-lethal or lethal harvesting ($h_J(2k+1) = 0$, $h_N(2k+1) = 0$ and $h_J(2k+1) = 0$).
3. No shrinkage of sapling to seedlings caused by fires or drought ($\rho_{21} = 0$).
4. Reproduction of seedlings from adult trees occurs ($\phi_A(h_N(2k+1), h_L(2k+1)) > 0$).

We assume the reproduction of seedlings occurs in the beginning of the wet season (end of the dry season) after the adults from the dry season have been harvested, and then germinate by the end of the wet season. Growth is about 1 cm per year for first 5 years, then slower after that; since there is essentially no growth that happens in the dry season, then at the end of the second wet season, seedlings will transition to saplings (i.e. after 1.5 years instead of 2 full years) [46]. Also, at this point seedlings are at a size large enough to survive fire in the upcoming dry season, so we want them to be considered saplings [10, 42].

For $k \geq 0$**,**

$\boldsymbol{N(2k+2) = \phi_A(h_N(2k+1), h_L(2k+1))A(2k+1) + (1 - \gamma_{12})\sigma_5 N(2k+1)}$

First, a proportion of the seedlings from the previous dry season survive (σ_5), and due to

a proportion (γ_{12}) of those that transition out to the sapling class, the remaining seedlings by the end of the wet season are represented by $((1-\gamma_{12})\sigma_5 N(2k+1))$. Next, seeds are dropped based on the number of adults from the previous dry season, and a proportion of these germinate to become seedlings by the end of the wet season ($\phi_A(h_N(2k+1), h_L(2k+1))A(2k+1)$). (Note: $\phi_A(h_N(2k+1), h_L(2k+1))$ includes both the reproduction/fertility rate of the adults, which relies on the non-lethal and lethal harvesting rates of adults in the previous dry season due to pruning and cutting down of the trees, and the survival of these seedlings in the wet season).

$$\boldsymbol{S(2k+2) = \gamma_{12}\sigma_5 N(2k+1) + (1-\gamma_{23})\sigma_6 S(2k+1)}$$

First, a proportion of the saplings from the previous dry season survive (σ_6), and due to a proportion of those that transition out to the juvenile class (γ_{23}), the remaining saplings by the end of the wet season is represented by $((1-\gamma_{23})\sigma_6 S(2k+1))$. Next, a proportion of seedlings from the previous dry season transition into the sapling class by the end of the wet season ($\gamma_{12}\sigma_5 N(2k+1)$).

$$\boldsymbol{J(2k+2) = \gamma_{23}\sigma_6 S(2k+1) + (1-\gamma_{34})\sigma_7 J(2k+1)}$$

First, a proportion of the juveniles from the previous dry season survive (σ_7), and then a proportion of those transition out to the adult class (γ_{34}). Thus, the remaining juveniles by the end of the wet season is represented by $((1-\gamma_{34})\sigma_7 J(2k+1))$. Next, a proportion of the saplings from the previous dry season transition into the juvenile class by the end of the wet season ($\gamma_{23}\sigma_6 S(2k+1)$).

$$\boldsymbol{A(2k+2) = \gamma_{34}\sigma_7 J(2k+1) + \sigma_8 A(2k+1)}$$

First, a proportion of the adults from the previous dry season survive (σ_8) to the end of the wet season. Next, a proportion of the juveniles from the previous dry season transition into the adult class by the end of the wet season ($\gamma_{34}\sigma_7 J(2k+1)$).

Figure 3.1 gives an overview of the order of events that occur in each season. We note that our model does not incorporate density dependence since we assume that harvesting has a strong top-down effect and already keeps the population below carrying capacity. For

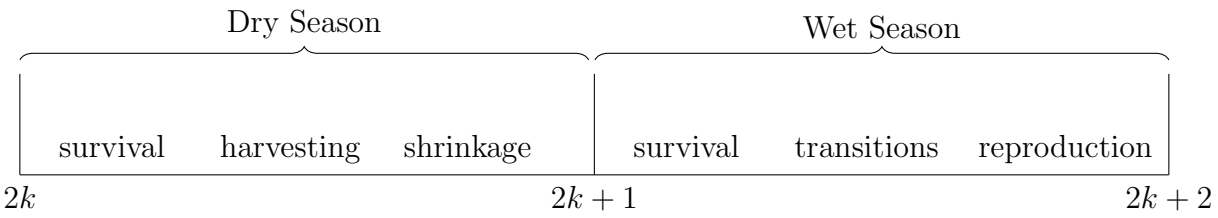


Figure 3.1: This provides a summary of the order of events in each season for *K. Senegelensis* in Benin where in year k, the dry season goes from $2k$ to $2k+1$ and the we season goes from $2k+1$ to $2k+2$.

populations that are not harvested but which we apply our model to, we will assume there is no density dependence for simplicity, as well.

Thus, our seasonal, discrete model consisting of four size classes is given by equations (3.1) for the dry season and (3.2) for the wet season with $k \geq 0$ as our time-step representing a year:

$$\begin{aligned}
N(2k+1) &= (1 - h_N(2k+1) - \alpha_1 h_L(2k+1) - h_J(2k+1))\sigma_1 N(2k) \\
&\quad + \rho_{21}(1 - \alpha_2 h_L(2k+1))\sigma_2 S(2k) \\
S(2k+1) &= (1-\rho_{21})(1 - \alpha_2 h_L(2k+1))\sigma_2 S(2k) \\
J(2k+1) &= \sigma_3 J(2k) \\
A(2k+1) &= (1 - h_L(2k+1))\sigma_4 A(2k)
\end{aligned} \tag{3.1}$$

$$\begin{aligned}
N(2k+2) &= \phi_A(h_N(2k+1), h_L(2k+1))A(2k+1) + (1-\gamma_{12})\sigma_5 N(2k+1) \\
S(2k+2) &= \gamma_{12}\sigma_5 N(2k+1) + (1-\gamma_{23})\sigma_6 S(2k+1) \\
J(2k+2) &= \gamma_{23}\sigma_6 S(2k+1) + (1-\gamma_{34})\sigma_7 J(2k+1) \\
A(2k+2) &= \gamma_{34}\sigma_7 J(2k+1) + \sigma_8 A(2k+1).
\end{aligned} \tag{3.2}$$

We start our model at the beginning of the dry season in October, and therefore set our initial conditions ($N(0) = N_0$, $S(0) = S_0$, $J(0) = J_0$, and $A_0 = A(0)$) as the number of trees at the end of the wet season.

In order to utilize data and rate information from [44, 43], we compose our seasonal model into a model with yearly time steps. First, we can represent our difference equations in the dry season with the following matrix population model (Leslie matrix model):

$$D = \begin{pmatrix} (1-h_N(2k+1)-\alpha_1 h_L(2k+1)-h_J(2k+1))\sigma_1 & \rho_{21}(1-\alpha_2 h_L(2k+1))\sigma_2 & 0 & 0 \\ 0 & (1-\rho_{21})(1-\alpha_2 h_L(2k+1))\sigma_2 & 0 & 0 \\ 0 & 0 & \sigma_3 & 0 \\ 0 & 0 & 0 & (1-h_L(2k+1))\sigma_4 \end{pmatrix}.$$

The difference equations for the wet season may be represented with the following Leslie matrix:

$$W = \begin{pmatrix} (1-\gamma_{12})\sigma_5 & 0 & 0 & \phi_A(h_N(2k+1), h_L(2k+1)) \\ \gamma_1 2\sigma_5 & (1-\gamma_{23})\sigma_6 & 0 & 0 \\ 0 & \gamma_{23}\sigma_6 & (1-\gamma_{34})\sigma_7 & 0 \\ 0 & 0 & \gamma_{34}\sigma_7 & \sigma_8 \end{pmatrix}.$$

Multiplying these two matrices together, first the dry season occurs and then the wet season (i.e. $Y = WD$), we arrive at a yearly model:

$$Y = \begin{pmatrix} y_{11} & (1-\gamma_{12})\sigma_5\rho_{21}(1-\alpha_2 h_L(2k+1))\sigma_2 & 0 & \phi_A(h_N(2k+1), h_L(2k+1))(1-h_L(2k+1))\sigma_4 \\ y_{21} & y_{22} & 0 & 0 \\ 0 & \gamma_{23}\sigma_6(1-\rho_{21})(1-\alpha_2 h_L(2k+1))\sigma_2 & (1-\gamma_{34})\sigma_7\sigma_3 & 0 \\ 0 & 0 & \gamma_{34}\sigma_7\sigma_3 & \sigma_8(1-h_L(2k+1))\sigma_4 \end{pmatrix}.$$

We will let y_{ij} represent entry i, j of matrix Y. The biological interpretations for entries of this matrix are outlined here:

- $y_{11} = (1-\gamma_{12})\sigma_5(1-h_N(2k+1)-\alpha_1 h_L(2k+1)-h_J(2k+1))\sigma_1$: seedlings survive in both the dry and wet seasons and do not transition to saplings (i.e. stay in the seedling class).
- y_{12}: saplings survive in the dry season and shrink back to the seedling class and survive as seedlings in the wet season but do not transition back to the sapling class.
- y_{13}: juveniles do not shrink back to seedlings or reproduce, so this entry is 0.
- y_{14}: adults survive in the dry season and reproduce seedlings in the wet season.

- $y_{21} = \gamma_{12}\sigma_5(1 - h_N(2k+1) - \alpha_1 h_L(2k+1) - h_J(2k+1))\sigma_1$: seedlings survive in both the dry and wet seasons and transition to saplings.

- $y_{22} = \gamma_{12}\sigma_5\rho_{21}(1-\alpha_2 h_L(2k+1))\sigma_2 + (1-\gamma_{23})\sigma_6(1-\rho_{21})(1-\alpha_2 h_L(2k+1))\sigma_2$: saplings survive in the dry season and shrink back to seedlings, survive as seedlings in the wet season and then transition back to the sapling stage + saplings survive in the dry season and do not shrink back to seedlings and then survive in the wet season but do not transition to juveniles (i.e. stay in the sapling class).

- y_{23}: juveniles do not shrink back to saplings, so this entry is 0.

- y_{24}: adults do not shrink back to saplings, so this entry is 0.

- y_{31}: seedlings do not skip the sapling stage and transition into juvenile stage directly, so this entry is 0.

- y_{32}: saplings survive in the dry season and do not shrink back to the seedling class and then survive in the wet season and transition to juveniles.

- y_{33}: juveniles survive in both the dry and wet seasons and do not transition to adults (i.e. stay in the juvenile class).

- y_{34}: adults do not shrink back to juveniles, so this entry is 0.

- y_{41}: seedlings do not skip the sapling/juveniles stages and transition to adults directly, so this entry is 0.

- y_{42}: saplings do not skip the juvenile stage and transition to adults directly, so this entry is 0.

- y_{43}: juveniles survive in both the dry and wet seasons and transition to adults.

- y_{44}: adults survive in both the dry and wet seasons (i.e. stay in the adult class and do not die).

3.3 Matrix Compression

In [44], there were 5 classes: seedling, sapling, juvenile, adult 1, and adult 2. Since both of the adult classes are reproductive and both non-lethally and lethally harvested, we wish to combine these into one large adult group. The matrix projection model in [44] is given by:

$$A = \begin{pmatrix} \sigma_1(1-\gamma_{12}) & \sigma_2\rho_{21} & 0 & \sigma_4\phi_4 & \sigma_5\phi_5 \\ \sigma_1\gamma_{12} & \sigma_2(1-\gamma_{23}-\rho_{21}) & \sigma_3\rho_{32} & 0 & 0 \\ 0 & \sigma_2\gamma_{23} & \sigma_3(1-\gamma_{34}-\rho_{32}) & \sigma_4\rho_{43} & 0 \\ 0 & 0 & \sigma_3\gamma_{34} & \sigma_4(1-\gamma_{45}-\rho_{43}) & \sigma_5\rho_{54} \\ 0 & 0 & 0 & \sigma_4\gamma_{45} & \sigma_5(1-\rho_{54}) \end{pmatrix}.$$

We consider $\rho_{32} = 0$, $\rho_{43} = 0$, and $\rho_{54} = 0$ since in our case, we do not consider the shrinkage of the juvenile, adult 1, or adult 2 classes. Thus, we consider the following matrix in which we would like to collapse classes 4 and 5:

$$U = \begin{pmatrix} \sigma_1(1-\gamma_{12}) & \sigma_2\rho_{21} & 0 & \sigma_4\phi_4 & \sigma_5\phi_5 \\ \sigma_1\gamma_{12} & \sigma_2(1-\gamma_{23}-\rho_{21}) & 0 & 0 & 0 \\ 0 & \sigma_2\gamma_{23} & \sigma_3(1-\gamma_{34}) & 0 & 0 \\ 0 & 0 & \sigma_3\gamma_{34} & \sigma_4(1-\gamma_{45}) & 0 \\ 0 & 0 & 0 & \sigma_4\gamma_{45} & \sigma_5 \end{pmatrix}.$$

We will compress matrices using two different algorithms, depending on if the goal is to maintain long-term or transient dynamics. A compression algorithm in [59] seeks to maintain the dominant eigenvalue λ from an original $n \times n$ Leslie matrix model U for the collapsed $(n-1) \times (n-1)$ matrix C, as well as the associated eigenvector in which that of U is $\mathbf{u}= (u_1, u_2, ..., u_i, u_{i+1}, ...u_n)^T$ and that of C is $\mathbf{c}= (u_1, u_2, ..., u_i + u_{i+1}, ...u_n)^T$.

The first step is to collapse the rows i and $i+1$ and place this in the i^{th} row; this is done by multiplying the original matrix U by an $(n-1) \times n$ matrix P of the form:

$$P = \begin{pmatrix} I_{i-1} & 0 & 0 & 0 \\ 0 & 1 & 1 & 0 \\ 0 & 0 & 0 & I_{n-i-1} \end{pmatrix}$$

where I_{i-1} and I_{n-i-1} are defined to be the $(i-1) \times (i-1)$ and $(n-i-1) \times (n-i-1)$ identity matrices, respectively. P has a form such that P**u**=**c**; thus, the effect of matrix P on U allows all entries in matrix PU to be the same as U except rows i and $i+1$ sum together to replace row i in U. In our case, $i = 4$ and $n = 5$, resulting in multiplying our original matrix U by a 4×5 matrix P:

$$PU = \begin{pmatrix} 1 & 0 & 0 & 0 & 0 \\ 0 & 1 & 0 & 0 & 0 \\ 0 & 0 & 1 & 0 & 0 \\ 0 & 0 & 0 & 1 & 1 \end{pmatrix} \begin{pmatrix} \sigma_1(1-\gamma_{12}) & \sigma_2\rho_{21} & 0 & \sigma_4\phi_4 & \sigma_5\phi_5 \\ \sigma_1\gamma_{12} & \sigma_2(1-\gamma_{23}-\rho_{21}) & 0 & 0 & 0 \\ 0 & \sigma_2\gamma_{23} & \sigma_3(1-\gamma_{34}) & 0 & 0 \\ 0 & 0 & \sigma_3\gamma_{34} & \sigma_4(1-\gamma_{45}) & 0 \\ 0 & 0 & 0 & \sigma_4\gamma_{45} & \sigma_5 \end{pmatrix}$$

$$= \begin{pmatrix} \sigma_1(1-\gamma_{12}) & \sigma_2\rho_{21} & 0 & \sigma_4\phi_4 & \sigma_5\phi_5 \\ \sigma_1\gamma_{12} & \sigma_2(1-\gamma_{23}-\rho_{21}) & 0 & 0 & 0 \\ 0 & \sigma_2\gamma_{23} & \sigma_3(1-\gamma_{34}) & 0 & 0 \\ 0 & 0 & \sigma_3\gamma_{34} & \sigma_4 & \sigma_5 \end{pmatrix}.$$

For our case, we demonstrate $P\mathbf{u} = \mathbf{c}$:

$$P\mathbf{u} = \begin{pmatrix} 1 & 0 & 0 & 0 & 0 \\ 0 & 1 & 0 & 0 & 0 \\ 0 & 0 & 1 & 0 & 0 \\ 0 & 0 & 0 & 1 & 1 \end{pmatrix} \begin{pmatrix} u_1 \\ u_2 \\ u_3 \\ u_4 \\ u_5 \end{pmatrix} = \begin{pmatrix} u_1 \\ u_2 \\ u_3 \\ u_4 + u_5 \end{pmatrix} = \mathbf{c}.$$

The next step is merging the columns, in which the algorithm assumes that the distribution of the stages in the merged group is the same as the proportions that are in **u**.

Consider the weights $\frac{u_i}{u_i+u_{i+1}}$ and $\frac{u_{i+1}}{u_i+u_{i+1}}$, the proportions from each stage from the stable stage distribution. Using these, we get weighted averages of columns i and $i+1$ that result in the new collapsed column i. This is done by multiplying (PU) on the right by Q of the form:

$$Q = \begin{pmatrix} 1 & 0 & 0 & 0 \\ 0 & 1 & 0 & 0 \\ 0 & 0 & 1 & 0 \\ 0 & 0 & 0 & \frac{u_i}{u_i+u_{i+1}} \\ 0 & 0 & 0 & \frac{u_{i+1}}{u_i+u_{i+1}} \end{pmatrix}$$

such that

$$A_c = (PU)Q = \begin{pmatrix} \sigma_1(1-\gamma_{12}) & \sigma_2\rho_{21} & 0 & \sigma_4\phi_4 & \sigma_5\phi_5 \\ \sigma_1\gamma_{12} & \sigma_2(1-\gamma_{23}-\rho_{21}) & 0 & 0 & 0 \\ 0 & \sigma_2\gamma_{23} & \sigma_3(1-\gamma_{34}) & 0 & 0 \\ 0 & 0 & \sigma_3\gamma_{34} & \sigma_4 & \sigma_5 \end{pmatrix} \begin{pmatrix} 1 & 0 & 0 & 0 \\ 0 & 1 & 0 & 0 \\ 0 & 0 & 1 & 0 \\ 0 & 0 & 0 & \frac{u_i}{u_i+u_{i+1}} \\ 0 & 0 & 0 & \frac{u_{i+1}}{u_i+u_{i+1}} \end{pmatrix}$$

$$= \begin{pmatrix} \sigma_1(1-\gamma_{12}) & \sigma_2\rho_{21} & 0 & \sigma_4\phi_4\frac{u_i}{u_i+u_{i+1}} + \sigma_5\phi_5\frac{u_{i+1}}{u_i+u_{i+1}} \\ \sigma_1\gamma_{12} & \sigma_2(1-\gamma_{23}-\rho_{21}) & 0 & \frac{u_i}{u_i+u_{i+1}}(0) + \frac{u_{i+1}}{u_i+u_{i+1}}(0) \\ 0 & \sigma_2\gamma_{23} & \sigma_3(1-\gamma_{34}) & \frac{u_i}{u_i+u_{i+1}}(0) + \frac{u_{i+1}}{u_i+u_{i+1}}(0) \\ 0 & 0 & \sigma_3\gamma_{34} & \sigma_4\frac{u_i}{u_i+u_{i+1}} + \sigma_5\frac{u_{i+1}}{u_i+u_{i+1}} \end{pmatrix}$$

$$= \begin{pmatrix} \sigma_1(1-\gamma_{12}) & \sigma_2\rho_{21} & 0 & \sigma_4\phi_4\frac{u_i}{u_i+u_{i+1}} + \sigma_5\phi_5\frac{u_{i+1}}{u_i+u_{i+1}} \\ \sigma_1\gamma_{12} & \sigma_2(1-\gamma_{23}-\rho_{21}) & 0 & 0 \\ 0 & \sigma_2\gamma_{23} & \sigma_3(1-\gamma_{34}) & 0 \\ 0 & 0 & \sigma_3\gamma_{34} & \sigma_4\frac{u_i}{u_i+u_{i+1}} + \sigma_5\frac{u_{i+1}}{u_i+u_{i+1}} \end{pmatrix}.$$

Note that Q has a form such that Q**c**=**u**:

$$Q\mathbf{c} = \begin{pmatrix} 1 & 0 & 0 & 0 \\ 0 & 1 & 0 & 0 \\ 0 & 0 & 1 & 0 \\ 0 & 0 & 0 & \frac{u_4}{u_4+u_5} \\ 0 & 0 & 0 & \frac{u_5}{u_4+u_5} \end{pmatrix} \begin{pmatrix} u_1 \\ u_2 \\ u_3 \\ u_4 + u_5 \end{pmatrix} = \begin{pmatrix} u_1 \\ u_2 \\ u_3 \\ u_4 \\ u_5 \end{pmatrix} = \mathbf{u}.$$

This form of Q, as well as the fact that $U\mathbf{u} = \lambda\mathbf{u}$ from our original matrix and $P\mathbf{u} = \mathbf{c}$, allows the following:

$$A_c\mathbf{c} = PUQ\mathbf{c} = PU\mathbf{u} = P\lambda\mathbf{u} = \lambda P\mathbf{u} = \lambda\mathbf{c},$$

resulting in the same dominant eigenvalue λ as U and stable stage distribution $\mathbf{c}$ for the collapsed matrix A_c. Any real eigenvector can be chosen to calculate the weights, and the corresponding eigenvalue will be maintained with this algorithm, but the other eigenvalues are not guaranteed to remain the same after the compression.

In [89], the previous algorithm explained in [59] is expanded for stage-based, rather than just age-based matrix models in which the matrix includes the survival of individuals in both classes that are being collapsed, probabilities of not transitioning out of the combined class, and transitions in from other classes. Stage-based models allow skipping stages or retrogressing; the same algorithm presented in [59] encompasses these types of models, as well.

The previous two papers have discussed compression for Leslie matrices, in which there are transitions and reproduction, and the goal is to maintain *long-term* behavior. However, for some populations, maintaining accurate *short-term*, or transient, dynamics is of interest, which we explore now. A compression algorithm by Spears [95] is for probability transition matrices (Markov chain models) Q in which $Q(j,k)$ represents the probability of transitioning from state j to state k in one step. (We note here that Q flips the rows and columns compared to our matrix models; i.e. in our matrices the rows represent stages and transitions happen up/down, whereas in Q the columns represent stages and transitions occur to the left/right).

The focus of this algorithm is on maintaining accurate transient behavior and minimizing the error in this.

In order to follow the algorithm presented in [95], here we only focus on the juvenile, adult 1, and adult 2 classes since those are the only *transitions* involved with the compression of the last two classes. Thus, we consider the following matrix:

$$M = \begin{pmatrix} \sigma_3(1-\gamma_{34}) & 0 & 0 \\ \sigma_3\gamma_{34} & \sigma_4(1-\gamma_{45}) & 0 \\ 0 & \sigma_4\gamma_{45} & \sigma_5 \end{pmatrix}.$$

We transpose matrix M to align with the algorithm and will denote it M_u for our uncompressed original matrix:

$$M_u = \begin{pmatrix} \sigma_3(1-\gamma_{34}) & \sigma_3\gamma_{34} & 0 \\ 0 & \sigma_4(1-\gamma_{45}) & \sigma_4\gamma_{45} \\ 0 & 0 & \sigma_5 \end{pmatrix}.$$

Once the two states are chosen to be compressed (which in our case is classes 4 and 5), the algorithm first consists of taking a weighted average of the two rows of these states based on what the proportion of each adult class is of the total adult population. To get these weights, we sum up the columns to be collapsed so that m_2 = column 2 sum (all trees in AD1 class) and m_3 = column 3 sum (all trees in AD2 class), which ultimately represent the time spent in each of these classes, and therefore get the weights to be $\frac{m_2}{m_2+m_3}$ for the AD1 class and $\frac{m_3}{m_2+m_3}$ for the AD2 class. This step results in:

$$M_r = \begin{pmatrix} \sigma_3(1-\gamma_{34}) & \sigma_3\gamma_{34} & 0 \\ \frac{m_2}{m_2+m_3}(0) & \frac{m_2}{m_2+m_3}\sigma_4(1-\gamma_{45}) & \frac{m_2}{m_2+m_3}\sigma_4\gamma_{45} \\ \frac{m_3}{m_2+m_3}(0) & \frac{m_3}{m_2+m_3}(0) & \frac{m_3}{m_2+m_3}\sigma_5 \end{pmatrix}.$$

$$= \begin{pmatrix} \sigma_3(1-\gamma_{34}) & \sigma_3\gamma_{34} & 0 \\ 0 & \frac{m_2}{m_2+m_3}\sigma_4(1-\gamma_{45}) & \frac{m_2}{m_2+m_3}\sigma_4\gamma_{45} \\ 0 & 0 & \frac{m_3}{m_2+m_3}\sigma_5 \end{pmatrix}.$$

The next step is to sum columns 2 and 3 and place in column 2 of M_c, and then add together rows 2 and 3 and place in row 2 of M_c; we obtain the compressed matrix:

$$M_c = \begin{pmatrix} \sigma_3(1-\gamma_{34}) & \sigma_3\gamma_{34} \\ \frac{m_2}{m_2+m_3}(0) + \frac{m_3}{m_2+m_3}(0) & \frac{m_2}{m_2+m_3}[\sigma_4(1-\gamma_{45}) + \sigma_4\gamma_{45}] + 0 + \frac{m_3}{m_2+m_3}\sigma_5 \end{pmatrix}$$

$$= \begin{pmatrix} \sigma_3(1-\gamma_{34}) & \sigma_3\gamma_{34} \\ 0 & \frac{m_2}{m_2+m_3}\sigma_4 + \frac{m_3}{m_2+m_3}\sigma_5 \end{pmatrix}$$

$$\implies M_c^T = \begin{pmatrix} \sigma_3(1-\gamma_{34}) & 0 \\ \sigma_3\gamma_{34} & \frac{m_2}{m_2+m_3}\sigma_4 + \frac{m_3}{m_2+m_3}\sigma_5 \end{pmatrix}.$$

This is comparable to the result for the juvenile and adult classes in matrix A_c from the algorithm in [59, 89] with an emphasis on maintaining different dynamics.

Perfect compression (i.e. no error) occurs when the two classes being collapsed are row or column equivalent (i.e. a multiple of one another), and therefore $(M_u^n)_c = M_c^n$ (i.e. compress the matrix at the n^{th} step versus compressing in the first step and then multiplying the compressed matrix n times). Although this is not always the case, such as with our matrix, we are choosing to collapse two classes based on their similar features, rather than based on their rate information.

We note that Spears' algorithm [95] only includes information on how to properly adapt transition probabilities, and not fertility rates, to obtain a compressed matrix. However, we observe that the result of the algorithm used for transition terms in [95] is comparable to the result of the algorithm in [59, 89] with the only difference being the weights, which depended on what dynamics it was trying to maintain. Thus, we apply a similar intuition for the fertility rates as the algorithm in [59, 89], where the fertility will now be weighted based on how long trees spend in each of the adult classes. This results in

$$\phi_A = \frac{m_2}{m_2+m_3}\sigma_4\phi_4 + \frac{m_3}{m_2+m_3}\sigma_5\phi_5.$$

Thus, from either algorithm, the probability of transitioning from J into the compressed state A is the sum of the probabilities of transitioning into either of the original states (J

to AD1 or AD2); however, in our case, juveniles only move into AD1, so that remains the same probability into A. The survival of the A class is the weighted average of the survival rates of each of the adult 1 and adult 2 classes based on how long individuals stay in each adult class in the short-term [95] or what their respective proportions are in the steady-state distribution out of all adults [59, 89], and the fertility rate is weighted similarly.

Thus, we have the following compressed matrix with 4 classes:

$$A_c = \begin{pmatrix} \sigma_1(1-\gamma_{12}) & \sigma_2\rho_{21} & 0 & \sigma_4\phi_4\frac{u_i}{u_i+u_{i+1}} + \sigma_5\phi_5\frac{u_{i+1}}{u_i+u_{i+1}} \\ \sigma_1\gamma_{12} & \sigma_2(1-\gamma_{23}-\rho_{21}) & 0 & 0 \\ 0 & \sigma_2\gamma_{23} & \sigma_3(1-\gamma_{34}) & 0 \\ 0 & 0 & \sigma_3\gamma_{34} & \sigma_4\frac{u_i}{u_i+u_{i+1}} + \sigma_5\frac{u_{i+1}}{u_i+u_{i+1}} \end{pmatrix}.$$

3.3.1 Compressing Matrices for Specific Populations

We wish to collapse the matrix population models with 5 classes found in [44, 43] to 4 classes. Two populations of *K. Senegalensis*, Barabon and Nipuni, are in the Sudanian northern dry region. They are gallery forests (forests along rivers or wetlands that project into dry landscapes) in a national park where they have never been logged or pruned, and therefore are considered unharvested or pristine. Two other populations, Nigoussourou and Soassararou, are found in the same region but not protected in a national park. Instead, they are populations in the wild that the Fulani people have been harvesting for several decades. Since Nipuni and Barabon are in the same ecological zone, we consider these populations to be unharvested baselines for the harvested populations Nigoussourou and Soassararou. In the short-term, the harvested populations fluctuate quite a bit due to fires and insects that remove biomass, and these disturbances affect growth and reproduction. However, we consider the transient phase of the trees to be 5 years because that is when management decisions need to re-evaluated and made due to human interference.

Nipuni population

Table 3.2: Rates for the Nipuni population.

Rate in [43]	Value of rate
σ_1	0.4354
γ_{12}	0.028
σ_2	0.7269
γ_{23}	0.2102
ρ_{21}	0
σ_3	1
γ_{34}	0.0304
σ_4	1
ϕ_4	0.0001
γ_{45}	0.0417
σ_5	0.9999
ϕ_5	0.1603
ρ_{54}	0

Since the Nipuni population is unharvested and protected in a national park, the population can be thought of as at equilibrium and therefore, we wish to maintain the long-term behavior of this population. The original matrix population model given in [43] is:

$$B = \begin{pmatrix} 0.4232 & 0 & 0 & 0.0001 & 0.1603 \\ 0.0122 & 0.5741 & 0 & 0 & 0 \\ 0 & 0.1528 & 0.9696 & 0 & 0 \\ 0 & 0 & 0.0304 & 0.9583 & 0 \\ 0 & 0 & 0 & 0.0417 & 0.9999 \end{pmatrix}.$$

The values of the individual rates that go into these entries are found in Table 3.2.

The dominant eigenvalue for this population matrix B is $\lambda = 1.001$ and the normalized stable stage distribution is

$$\mathbf{b} = \begin{pmatrix} 0.2053 \\ 0.0059 \\ 0.0285 \\ 0.0203 \\ 0.74 \end{pmatrix}.$$

Table 3.3: Nipuni compressed values with prop1 representing the proportion of adult 1's out of all adults in the stable-stage distribution and prop2 representing the proportion of the adults 2's out of all adults in the stable stage distribution.

Calculation for compression	Value of rate
prop1	0.0267
prop2	0.9733
$\sigma_A = \sigma_4(\text{prop1}) + \sigma_5(\text{prop2})$	0.9999
$\phi_A\sigma_4 = \phi_4\sigma_4(\text{prop1}) + \phi_5\sigma_5(\text{prop2})$	0.156

This means in the long-term that out of all of the adults, the proportion of adult 1's is: prop1= $\frac{0.0203}{0.0203+0.74} = 0.0267$ and the proportion of adult 2's is: prop2= $\frac{0.74}{0.0203+0.74} = 0.9733$. Following the algorithm in [59, 89] to maintain long-term behavior, we calculate

$$\sigma_A = \sigma_4(\text{prop1}) + \sigma_5(\text{prop2}) = 1(0.0267) + 0.9999(0.9733) = 0.9999$$

and

$$\phi_4\sigma_4(\text{prop1}) + \phi_5\sigma_5(\text{prop2}) = (0.0001)(1)(0.0267) + (0.1603)(0.9999)(0.9733) = 0.156,$$

the adult survival and reproduction rates, respectively. These are recorded in Table 3.3 and results in the following compressed matrix:

$$B_c = \begin{pmatrix} 0.4232 & 0 & 0 & 0.156 \\ 0.0122 & 0.5741 & 0 & 0 \\ 0 & 0.1528 & 0.9696 & 0 \\ 0 & 0 & 0.0304 & 0.9999 \end{pmatrix},$$

which has dominant eigenvalue $\lambda_c = 1.001$ and normalized stable stage distribution:

$$\mathbf{b}_c = \begin{pmatrix} 0.2053 \\ 0.0059 \\ 0.0285 \\ 0.7603 \end{pmatrix}.$$

Table 3.4: Rates for the Barabon population.

Rate in [43]	Value of rate
σ_1	0.5795
γ_{12}	0.0309
σ_2	0.8821
γ_{23}	0.2084
ρ_{21}	0.063
σ_3	1
γ_{34}	0.0001
σ_4	0.9744
ϕ_4	0.1252
γ_{45}	0.0508
σ_5	0.9999
ϕ_5	8.122
ρ_{54}	0

Adding together the proportion of adults in the original stable stage distribution $\mathbf{b}$, the total is 0.74+0.0203, which matches the total proportion of adults in $\mathbf{b}_c$. The other entries in the stable stage distributions $\mathbf{b}$ and $\mathbf{b}_c$ match exactly.

Barabon population

Similarly, the Barabon population is unharvested and protected in a national park, and we wish to maintain the long-term behavior of this population. The original matrix population model given in [43] is:

$$C = \begin{pmatrix} 0.5616 & 0.0556 & 0 & 0.122 & 8.121 \\ 0.0179 & 0.6427 & 0 & 0 & 0 \\ 0 & 0.1838 & 0.9999 & 0 & 0 \\ 0 & 0 & 0.0001 & 0.9249 & 0 \\ 0 & 0 & 0 & 0.0495 & 0.9999 \end{pmatrix}.$$

The values of the individual rates that go into these entries are found in Table 3.4.

Table 3.5: Barabon compressed values with prop1 representing the proportion of adult 1's out of all adults in the stable stage distribution and prop2 representing the proportion of adult 2's out of all adults in the stable stage distribution.

Calculation for compression	Value of rate
prop1	0.0608
prop2	0.9392
$\sigma_A = \sigma_4(\text{prop1}) + \sigma_5(\text{prop2})$	0.9983
$\phi_A\sigma_4 = \phi_4\sigma_4(\text{prop1}) + \phi_5\sigma_5(\text{prop2})$	7.635

The dominant eigenvalue for C is $\lambda = 1.0032$ and the normalized stable stage distribution is

$$\mathbf{c} = \begin{pmatrix} 0.2565 \\ 0.0127 \\ 0.7160 \\ 0.0009 \\ 0.0139 \end{pmatrix}.$$

This means in the long-term that out of all of the adults, the proportion of adult 1's is: prop1= $\frac{0.0009}{0.0009+0.0139} = 0.0608$ and the proportion of adult 2's is: prop2= $\frac{0.0139}{0.0009+0.0139} = 0.9392$. Following the algorithm in [59, 89] to maintain long-term behavior, we calculate the adult survival and reproduction rates, respectively:

$$\sigma_A = \sigma_4(\text{prop1}) + \sigma_5(\text{prop2}) = 0.9744(0.0608) + (0.9999)(0.9392) = 0.9983$$

and

$$\phi_A\sigma_4 = \phi_4\sigma_4(\text{prop1}) + \phi_5\sigma_5(\text{prop2}) = (0.1252)(0.9744)(0.0608) + (8.122)(0.9999)(0.9392)$$

$$= 7.635$$

and document the values of these rates in Table 3.5. This results in the following compressed matrix:

$$C_c = \begin{pmatrix} 0.5616 & 0.0556 & 0 & 7.635 \\ 0.0179 & 0.6427 & 0 & 0 \\ 0 & 0.1838 & 0.9999 & 0 \\ 0 & 0 & 0.0001 & 0.9983 \end{pmatrix}$$

which has dominant eigenvalue $\lambda_c = 1.0032$ and normalized stable stage distribution

$$\mathbf{c}_c = \begin{pmatrix} 0.2562 \\ 0.0127 \\ 0.7163 \\ 0.0148 \end{pmatrix}.$$

Adding together the proportion of adults in the original stable stage distribution $\mathbf{c}$, the total is $0.0009 + 0.0139 = 0.0148$, which matches the total proportion of adults in $\mathbf{c}_c$. The first and third entries of $\mathbf{c}$ and $\mathbf{c}_c$ differ by 0.03, but the stable stage distributions are very similar overall.

Soassararou population

On the other hand, Soassararou is a harvested population and we plan to best maintain the short-term or transient behavior of the population. The original matrix population model given in [43] with corresponding rates in Table 3.6 is:

$$F = \begin{pmatrix} 0.3968 & 0 & 0 & 0.0703 & 0.153 \\ 0.0001 & 0.7676 & 0 & 0 & 0 \\ 0 & 0.094 & 0.9512 & 0 & 0 \\ 0 & 0 & 0.0209 & 0.8767 & 0.0108 \\ 0 & 0 & 0 & 0.0837 & 0.9677 \end{pmatrix}.$$

We run this model for 5 years with initial conditions for dry, high harvest

$$[0.42, 0.05, 0.19, 0.18, 0.16]^T.$$

Table 3.6: Rates for the Soassararou population.

Rate in [43]	Value of rate
σ_1	0.3969
γ_{12}	0.0003
σ_2	0.8616
γ_{23}	0.1091
ρ_{21}	0
σ_3	0.9721
γ_{34}	0.0215
σ_4	0.9604
ϕ_4	0.0732
γ_{45}	0.0872
σ_5	0.9785
ϕ_5	0.1564
ρ_{54}	0.011

This results in the following normalized population vector:

$$\mathbf{f} = \begin{pmatrix} 0.1204 \\ 0.0243 \\ 0.2926 \\ 0.2094 \\ 0.3533 \end{pmatrix}.$$

We wish to compress matrix F into 4 classes and have it closely match this distribution of classes at the 5 year mark. Using Spears' algorithm found in [95], focusing on the juvenile, adult 1, and adult 2 classes gives:

$$M = \begin{pmatrix} 0.9512 & 0 & 0 \\ 0.0209 & 0.8767 & 0.0108 \\ 0 & 0.0837 & 0.9677 \end{pmatrix}.$$

Transposing M to match the algorithm and notation in [95],

$$M_u = \begin{pmatrix} 0.9512 & 0.0209 & 0 \\ 0 & 0.8767 & 0.0837 \\ 0 & 0.0108 & 0.9677 \end{pmatrix}.$$

Then, following the algorithm described in detail in Section 3.3, we obtain:

$$M_c = \begin{pmatrix} 0.9512 & 0.0209 \\ 0 & 0.9701 \end{pmatrix}$$

and

$$M_c^T = \begin{pmatrix} 0.9512 & 0 \\ 0.0209 & 0.9701 \end{pmatrix},$$

since $m_2 = 0.0209 + 0.8767 + 0.0108 = 0.9084$, $m_3 = 0 + 0.0837 + 0.9677 = 1.051$, and

$$\sigma_A = \sigma_4 \frac{m_2}{m_2 + m_3} + \sigma_5 \frac{m_3}{m_2 + m_3}$$

$$= (0.9604)\left(\frac{0.9084}{0.9084 + 1.051}\right) + (0.9785)\left(\frac{1.051}{0.9084 + 1.051}\right)$$

$$= 0.9701$$

which corresponds to the lower right entry in the matrix. Calculating the fertility rate, we have

$$\phi_A \sigma_4 = \sigma_4 \phi_4 \frac{m_2}{m_2 + m_3} + \sigma_5 \phi_5 \frac{m_3}{m_2 + m_3},$$

$$= (0.9604)(0.0732)\left(\frac{0.9084}{0.9084 + 1.051}\right) + (0.9785)(0.1564)\left(\frac{1.051}{0.9084 + 1.051}\right)$$

$$= 0.1147,$$

which gives the compressed matrix result of:

$$F_c = \begin{pmatrix} 0.3968 & 0 & 0 & 0.1147 \\ 0.0001 & 0.7676 & 0 & 0 \\ 0 & 0.094 & 0.9512 & 0 \\ 0 & 0 & 0.0209 & 0.9701 \end{pmatrix}.$$

Our compressed matrix has adult survival and adult reproduction rates as shown in Table 3.7 that correspond to the lower right hand entry and upper right hand entry, respectively.

Taking this 4 class matrix model and running it for 5 years with initial conditions $[0.42, 0.05, 0.19, 0.34]^T$ results in the following normalized population vector:

$$\mathbf{f}_c = \begin{pmatrix} 0.117 \\ 0.0244 \\ 0.2937 \\ 0.5649 \end{pmatrix}.$$

Comparing this to $\mathbf{f}$, we see there is a 2.8% error in the seedling stage ($\frac{0.1204-0.117}{0.1204} = 0.0282$), a 0.41% error in saplings ($\frac{0.0244-0.0243}{0.0243} = 0.0041$), a 0.38% error in juveniles ($\frac{0.2937-0.2926}{0.2926} = 0.0038$), and finally a 0.39% error in adults ($\frac{0.5649-0.5627}{0.5627} = 0.0039$).

We can check the accuracy of the compression according to [95] by comparing M_c^5 (i.e. compressing the original matrix and *then* performing matrix exponentiation for 5 time steps) and $(M_u)^5{}_c$ (i.e. performing matrix exponentiation of the original matrix for 5 times steps and *then* compressing the resulting matrix). Here,

$$M_c^5 = \begin{pmatrix} 0.7787 & 0.0890 \\ 0 & 0.8592 \end{pmatrix}$$

and

$$M_u^5 = \begin{pmatrix} 0.7787 & 0.0733 & 0.0142 \\ 0 & 0.5247 & 0.3048 \\ 0 & 0.0393 & 0.8561 \end{pmatrix}.$$

Table 3.7: Soassararou population compressed values where m_2 represents the sum of probabilities of staying in the AD1 class and m_3 represents the sum of probabilities of staying in the AD2 class.

Calculation for compression	Value of rate
$\frac{m_2}{m_2+m_3}$	0.4636
$\frac{m_3}{m_2+m_3}$	0.5364
$\sigma_A = \phi_4\sigma_4\frac{m_2}{m_2+m_3} + \phi_5\sigma_5\frac{m_3}{m_2+m_3}$	0.1147
$\phi_A\sigma_4 = \sigma_4\frac{m_2}{m_2+m_3} + \sigma_5\frac{m_3}{m_2+m_3}$	0.9701

Compressing this matrix using Spears' algorithm results in:

$$(M_u)^5{}_c = \begin{pmatrix} 0.7787 & 0.0875 \\ 0 & 0.8722 \end{pmatrix}.$$

The upper right hand entry of the matrix has a 1.7% error ($\frac{0.0890-0.0875}{0.0875} = 0.0171$) and the lower right hand entry of the matrix has a 1.5% error ($\frac{0.8722-0.8592}{0.8722} = 0.0149$).

Nigoussourou population

Nigoussourou is also a harvested population for which we want to maintain its short-term or transient behavior. The original matrix population model given in [43] is:

$$G_1 = \begin{pmatrix} 0.2295 & 0 & 0 & 0.043 & 0.85 \\ 0.0433 & 0.8238 & 0 & 0 & 0 \\ 0 & 0.1286 & 0.9215 & 0.0088 & 0 \\ 0 & 0 & 0.0001 & 0.9056 & 0 \\ 0 & 0 & 0 & 0.067 & 0.8871 \end{pmatrix}.$$

However, here we make the additional assumption that adult 1's cannot shrink back to juveniles. This is because [44] suggests that perturbation in the shrinkage of this long-living species has minimal influence on the elasticity of the population growth rate (the effect a proportional change in this vital rate has on λ [13]), and also shrinkage is rare enough that we can set $\rho_{43} = 0$. This results in an updated matrix that matches the form of our harvesting

model with corresponding rates in Table 3.8:

$$G = \begin{pmatrix} 0.2295 & 0 & 0 & 0.043 & 0.85 \\ 0.0433 & 0.8238 & 0 & 0 & 0 \\ 0 & 0.1286 & 0.9215 & 0 & 0 \\ 0 & 0 & 0.0001 & 0.9056 & 0 \\ 0 & 0 & 0 & 0.067 & 0.8871 \end{pmatrix}.$$

Running this model for 5 years with initial conditions for dry, high harvest as

$$[0.42, 0.05, 0.19, 0.18, 0.16]^T$$

results in the following normalized population vector:

$$\mathbf{g} = \begin{pmatrix} 0.2604 \\ 0.0867 \\ 0.2607 \\ 0.1819 \\ 0.2103 \end{pmatrix}.$$

We wish to compress matrix G into 4 classes and have it closely match this distribution of classes at the 5 year mark. Using Spears' algorithm found in [95], we target only the juvenile, adult 1, and adult 2 classes shown here:

$$M = \begin{pmatrix} 0.9215 & 0 & 0 \\ 0.0001 & 0.9056 & 0 \\ 0 & 0.067 & 0.8871 \end{pmatrix}.$$

Transposing M, again to align with the algorithm in [95], results in:

$$M_u = \begin{pmatrix} 0.9215 & 0.0001 & 0 \\ 0 & 0.9056 & 0.067 \\ 0 & 0 & 0.8871 \end{pmatrix}.$$

Table 3.8: Rates for the Nigoussourou population.

Rate in [43]	Value of rate
σ_1	0.2728
γ_{12}	0.1587
σ_2	0.9524
γ_{23}	0.1350
ρ_{21}	0
σ_3	0.9216
γ_{34}	0.0001
σ_4	0.9726
ϕ_4	0.0442
γ_{45}	0.0689
σ_5	0.8871
ϕ_5	0.9582
ρ_{54}	0

Then, following the algorithm described in detail in Section 3.3, we obtain:

$$M_c = \begin{pmatrix} 0.9215 & 0.0001 \\ 0 & 0.9287 \end{pmatrix}$$

and

$$M_c^T = \begin{pmatrix} 0.9215 & 0 \\ 0.0001 & 0.9287 \end{pmatrix},$$

since $m_2 = 0.0001 + .9056 = 0.9057$, $m_3 = 0 + 0.067 + 0.8871 = 0.9541$, and

$$\sigma_A = \sigma_4 \frac{m_2}{m_2 + m_3} + \sigma_5 \frac{m_3}{m_2 + m_3}$$

$$= (0.9726)\left(\frac{0.9057}{0.9057 + 0.9541}\right) + (0.8871)\left(\frac{0.9541}{0.9057 + 0.9541}\right)$$

$$= 0.9287$$

which corresponds to the lower right entry in the matrix. For the fertility rate, we calculate

$$\phi_A\sigma_4 = \sigma_4\phi_4\frac{m_2}{m_2+m_3} + \sigma_5\phi_5\frac{m_3}{m_2+m_3},$$
$$= (0.9726)(0.0442)\left(\frac{0.9057}{0.9057+0.9541}\right) + (0.8871)(0.9582)\left(\frac{0.9541}{0.9057+0.9541}\right)$$
$$= 0.457,$$

which gives the compressed matrix result of:

$$G_c = \begin{pmatrix} 0.2295 & 0 & 0 & 0.457 \\ 0.0443 & 0.8238 & 0 & 0 \\ 0 & 0.1286 & 0.9215 & 0 \\ 0 & 0 & 0.0001 & 0.9287 \end{pmatrix}.$$

We record the adult survival and reproduction rates for the compressed matrix for Nigoussourou in Table 3.9 which correspond to the lower right hand entry of G_c and upper right hand entry, respectively. Running G_c, the 4 class matrix model for Nigoussourou, for 5 years with initial conditions $[0.42, 0.05, 0.19, 0.34]^T$ results in the following normalized population vector:

$$\mathbf{g}_c = \begin{pmatrix} 0.2566 \\ 0.0885 \\ 0.2627 \\ 0.3922 \end{pmatrix}.$$

Table 3.9: Nigoussourou population compressed values where m_2 represents the sum of probabilities of staying in the AD1 class and m_3 represents the sum of probabilities of staying in the AD2 class.

Calculation for compression	Value of rate
$\frac{m_2}{m_2+m_3}$	0.487
$\frac{m_3}{m_2+m_3}$	0.513
$\sigma_A = \sigma_4\frac{m_2}{m_2+m_3} + \sigma_5\frac{m_3}{m_2+m_3}$	0.9287
$\phi_A\sigma_4 = \sigma_4\phi_4\frac{m_2}{m_2+m_3} + \sigma_5\phi_5\frac{m_3}{m_2+m_3}$	0.457

Comparing this to $\mathbf{g}$, we see there is a 1.5% error in the seedling stage ($\frac{0.2604-0.2566}{0.2604} = 0.0146$), a 2.1% error in saplings ($\frac{0.0885-0.0867}{0.0867} = 0.0208$), a 0.77% error in juveniles ($\frac{0.2627-0.2607}{0.2607} = 0.0077$), and finally no error in adults, as adult 1+adult 2 class in the 5 class normalized population vector equals 0.3922. We can check the accuracy of the compression according to [95] by comparing M_c^5 and $(M_u)^5{}_c$. Here,

$$M_c^5 = \begin{pmatrix} 0.6645 & 0.0004 \\ 0 & 0.6908 \end{pmatrix}$$

and

$$M_u^5 = \begin{pmatrix} 0.6645 & 0.0003 & 0.00005 \\ 0 & 0.6091 & 0.2163 \\ 0 & 0 & 0.5494 \end{pmatrix}.$$

Compressing this matrix, again following Spears' algorithm, results in:

$$(M_u)^5{}_c = \begin{pmatrix} 0.6645 & 0.0004 \\ 0 & 0.6717 \end{pmatrix}.$$

The lower right hand entry of the matrix has a 2.8% error ($\frac{0.6908-0.6717}{0.6717} = 0.0284$) with the other entries in both matrices the same.

3.4 Explicit Harvesting Models for Each Population

Here, we carefully demonstrate the matrix model that was developed in this work for each of these populations. Since Nipuni is an unharvested population and protected in a national park, all harvesting terms ($h_J(2k+1)$, $h_N(2k+1)$, and $h_L(2k+1)$) in Matrix Y in Section 3.3 are set to zero. This population does not shrink from sapling to seedling, so $\rho_{21} = 0$, as well. We note that yearly survival rates are equivalent to surviving both the dry season and wet season, which results in the multiplication of seasonal survival rates in our model. This results in the following matrix with rates in Table 3.10:

$$\text{Nipuni} = \begin{pmatrix} (1-\gamma_{12})\sigma_5\sigma_1 & 0 & 0 & \phi_A\sigma_4 \\ \gamma_{12}\sigma_5\sigma_1 & (1-\gamma_{23})\sigma_6\sigma_2 & 0 & 0 \\ 0 & \gamma_{23}\sigma_6\sigma_2 & (1-\gamma_{34})\sigma_7\sigma_3 & 0 \\ 0 & 0 & \gamma_{34}\sigma_7\sigma_3 & \sigma_8\sigma_4 \end{pmatrix}.$$

The Barabon population is also unharvested and therefore we set all harvesting terms equal to 0 from matrix Y in Section 3.3. For this population, we require the separate values of σ_2 and σ_5 to be able to apply our harvesting model to this population (note: this is because ρ_{21} is nonzero for this population in entry (1,2) and (2,2) of the matrix). We estimate these two rates using ordinary least squares and minimizing the objective function value which is the difference between data of the Barabon classes for 5 time steps from the compressed matrix and the simulated data of our harvesting model above (i.e. with all harvesting set to 0). We use MultiStart in the Global Optimization Toolbox of MATLAB together with fmincon as the local solver. We choose 0.001 as the lower bounds for each of the parameters and 1 as the upper bounds. The best objective function value for 200 runs is 0.02902 and the resulting parameters are: $\sigma_2 = 0.0043$ and $\sigma_5 = 0.004$. The form of the Barabon matrix with rates in Table 3.11 is given by the following matrix:

Table 3.10: Rates for Nipuni harvesting model using rate information from Tables 3.2 and 3.3.

Rate used in harvesting estimation	Value of rate	Rate in compressed [43] matrix
$\sigma_5\sigma_1 = \sigma_N$	0.4354	σ_1
γ_{12}	0.028	γ_{12}
$\sigma_6\sigma_2 = \sigma_S$	0.7269	σ_2
γ_{23}	0.2102	γ_{23}
$\sigma_7\sigma_3 = \sigma_J$	1	σ_3
γ_{34}	0.0304	γ_{34}
$\sigma_8\sigma_4 = \sigma_A$	0.9999	σ_A
$\phi_A\sigma_4 = \phi$	0.156	$\phi_A\sigma_4$

$$\text{Barabon} = \begin{pmatrix} (1-\gamma_{12})\sigma_5\sigma_1 & (1-\gamma_{12})\sigma_5\rho_{21}\sigma_2 & 0 & \phi_A\sigma_4 \\ \gamma_{12}\sigma_5\sigma_1 & \gamma_{12}\sigma_5\rho_{21}\sigma_2 + (1-\gamma_{23})\sigma_6(1-\rho_{21})\sigma_2 & 0 & 0 \\ 0 & \gamma_{23}\sigma_6(1-\rho 21)\sigma_2 & (1-\gamma_{34})\sigma_7\sigma_3 & 0 \\ 0 & 0 & \gamma_{34}\sigma_7\sigma_3 & \sigma_8\sigma_4 \end{pmatrix}.$$

Soassararou adults are non-lethally harvested but juveniles are not harvested, nor are adults lethally harvested. As a starting point, we will assume constant harvesting of this population and therefore, harvesting will occur at the same rate each dry season. From matrix Y in Section 3.3, we do not know the unharvested rates $\sigma_5\sigma_1 = \sigma_N$ and γ_{12} for Soassararou because harvesting is implicitly impacting these rates in the matrices in [44, 43]. Applying our model to the Soassararou population results in the rates given in Table 3.7 (in which the reproduction function is derived in Section 3.5 and the values of the unknown parameters are estimated in Section 3.6) and the following matrix:

$$\text{Soassararou} = \begin{pmatrix} (1-\gamma_{12})\sigma_5(1-h_N)\sigma_1 & 0 & 0 & \phi_A(h_N)\sigma_4 \\ \gamma_{12}\sigma_5(1-h_N)\sigma_1 & (1-\gamma_{23})\sigma_6\sigma_2 & 0 & 0 \\ 0 & \gamma_{23}\sigma_6\sigma_2 & (1-\gamma_{34})\sigma_7\sigma_3 & 0 \\ 0 & 0 & \gamma_{34}\sigma_7\sigma_3 & \sigma_8\sigma_4 \end{pmatrix}.$$

The specific form of the harvesting model for the Nigoussorou population and its reproduction function is left for future work.

3.5 Estimation of Soassararou Adult Reproduction Function Dependent on Non-lethal Harvesting

In order to determine the average level of non-lethal harvesting for adult individuals, we must first determine a form for the reproduction function for Soassararou that depends on the non-lethal harvesting of adults, $\phi_A(h_N)$. We do so by analyzing the individual tree data

Table 3.11: Rates for Barabon harvesting model using rate information from Tables 3.4 and 3.5.

Rate used in harvesting estimation	Value of rate	Rate in compressed [43] matrix
$\sigma_5\sigma_1 = \sigma_N$	0.5795	σ_1
γ_{12}	0.0309	γ_{12}
$\sigma_6\sigma_2 = \sigma_S$	0.8821	σ_2
γ_{23}	0.2084	γ_{23}
ρ_{21}	0.063	ρ_{21}
$\sigma_7\sigma_3 = \sigma_J$	1	σ_3
γ_{34}	0.0001	γ_{34}
$\sigma_8\sigma_4 = \sigma_A$	0.9983	σ_A
$\phi_A\sigma_4 = \phi$	7.635	$\phi_A\sigma_4$
σ_2	0.0043	–
σ_5	0.004	–

for the tree population [47]. Since harvesting (pruning) and seed dispersal from the fruits happen simultaneously throughout the dry season, we make the assumption that the number of fruits produced given in the data are *leftover* at the end of the dry season. Thus, they have the ability to disperse seeds, which have the potential of germinating/establishing to become seedlings. For any trees that had positive fruit leftover at the end of the season, we used an upper bound for the level of harvest to be 99.5% [47]. Moreover, we only used data from trees that had all three pieces of information for diameter breast height (DBH), pruning intensity (h_N), and fruit production.

Table 3.12: Rates for Soassararou harvesting model using rate information from Tables 3.6 and 3.7.

Rate used in harvesting estimation	Value of rate	Rate from compressed [43] matrix
$\sigma_5\sigma_1 = \sigma_N$	–	σ_1
γ_{12}	–	γ_{12}
$\sigma_6\sigma_2 = \sigma_S$	0.8616	σ_2
γ_{23}	0.1091	γ_{23}
$\sigma_7\sigma_3 = \sigma_J$	0.9721	σ_3
γ_{34}	0.0215	γ_{34}
$\sigma_8\sigma_4 = \sigma_A$	0.9701	σ_4
$\phi_A(h_N)$	–	ϕ_A
σ_4	–	–

We wish to investigate the relationship between the percent loss of foliage of adults (i.e. the percent harvested/pruned per adult individual) and the number of fruits produced (that disperse seeds for seedlings). To find the function that represents the effect of harvest on reproduction, we use generalized linear modeling [130]. This consists of three steps: choosing the response variable distribution, using predictor variables to define the systematic part (i.e. defining a linear combination of the predictor variables), and finally, choosing the link between the average of the response variable and the systematic part with predictor variables.

We first need to choose a distribution for our response variable such as Poisson or negative binomial, since our response variable consists of count data. A Poisson distribution is chosen if the mean and variance of the response variable are equivalent (i.e. ratio is close to 1), but in cases where the variance is much bigger than the mean, we call this overdispersed, and we need to use negative binomial instead. There is overdispersion in each of the cases we describe below, and therefore, results are from a negative binomial generalized linear model. We model our response variable, the number of fruits produced per adult individual per year, with a negative binomial distribution with a mean of μ. The systematic part is defined as

$$\nu = a + b(DBH) + c(h_N)$$

where DBH and h_N are the predictor variables and ν is related to the mean of the response variable, μ. This systematic part is linked together with μ by taking the logarithm of μ so that $log(\mu) = \nu$, or in other words,

$$\mu = e^{a+b(DBH)+c(h_N)}$$

which ensures non-negativity for the mean of our response variable. We wish to estimate the y-intercept (a) and the slopes (b, c) using maximum likelihood estimation. Thus, we want to find the values of a, b, and c such that the probability that these observations would occur is high. We implement negative binomial generalized linear models for various cases using R software, particularly implementing the bbmle package and mle2 function.

Soassararou Data

First, we used data for Soassararou in 2004 only, consisting of 58 adult trees ($DBH \geq 20$ cm) with an average DBH of 43.088. This resulted in the function

$$\mu(h_N) = e^{2.1188+0.0375(43.088)-1.3047h_N}$$

for the average number of fruits produced per adult individual in 2004 with the given average DBH. Note that since we do not have DBH explicitly in our model, we set $DBH = DBH_{\text{avg}}$ for the sample of trees in the data; thus, we have information on the average number of fruits produced given a certain DBH and harvesting level. In 2004, there were 1210 fruits produced overall for Soassararou with 27 seedlings that germinated. Thus, we make the assumption that each fruit produces $\frac{27}{1210} \approx 0.0223$ seedlings on average (i.e. we view each fruit as identical having the same number of seeds and potential for dispersing seeds/becoming seedlings). Therefore, to get the average number of seedlings per adult individual in 2004, we multiply the function μ by $\frac{\text{number of seedlings}}{\text{number of fruits produced}} = \frac{\text{27 seedlings in 2004}}{\text{1210 fruits produced in 2004}}$, which results in the average number of seedlings per adult individual per year represented by

$$\phi_A(h_N) = \frac{27}{1210} e^{2.1188+0.0375(43.088)-1.3047h_N}.$$

We are inherently making the assumption here that the percent reduction in fruit production from increased harvest is equivalent to percent reduction in seedlings by using the same exponential function (i.e. 80% reduction in fruit from harvesting will be an 80% reduction in seedlings). From Section 3.3.1, we know that the average number of seedlings produced per adult Soassararou individual per year is 0.1147. Although we can represent fruit production as a function of harvest, the converse is not an accurate process (i.e. given fruit/seedling production, we cannot accurately solve for harvesting levels). However, if we do set $\phi_A(h_N) = 0.1147$, we obtain $h_N = 1.6077$ which is unrealistic, as this value needs to be between 0 and 1 to represent the proportion harvested. Therefore, it provides information that the function is not an accurate representation of what we are looking for. We also note that this function has a value of 0.2534 at $h_N = 1$, whereas we would expect it to be close to 0.

We noticed that the data between 0 and 0.4 for the harvesting levels was sparse; therefore, we incorporated more tree data from different years to build this relationship of the number of fruits produced based on DBH and harvest levels. Using data from 2004-2007 for the Soassararou population, this led to a total of 171 adult individuals. We use the same germination rate of $\frac{27}{1210} \approx 0.0223$ for every tree. This resulted in

$$\mu = e^{-0.2674+0.0747(45.5117)-0.3709(h_N)}$$

and again, multiplying by $\frac{27}{1210}$, this resulted in the average number of seedlings per adult individual per year to be

$$\phi_A(h_N) = \frac{27}{1210} e^{-0.2674+0.0747(45.5117)-0.3709(h_N)}.$$

Setting this equal to 0.1147, we obtain a value of $h_N = 4.0313$, which is again unrealistic. Similarly, $\phi(1) = 0.3531$ is not close to 0 as expected.

In this process, we made two observations: even with the addition of more data points, there were still few data points in the initial region from 0 to 0.4 and in both of these cases, the function was not close to 0 at $h_N = 1$, as we would expect. The next attempt was to truncate Soassararou data at 0.4, so that only data points for harvesting levels of 0.4 to 1 were included, with the goal of getting closer to the x-axis at $h_N = 1$. Our reasoning behind this was that perhaps the data points near $h_N = 0$ were pulling up the entire function, so we would like to disregard those.

In the case of only using 2004 truncated data (average DBH of 45.7837), the resulting function was

$$\phi_A(h_N) = \frac{27}{1210} e^{4.3132+0.0445(45.7837)-4.1611h_N}$$

and setting this equal to 0.1147, we obtain $h_N = 1.1328$, which is also unrealistic. Again, $\phi(1) = 0.1993$ is not close to 0. Next, we tried using all of the 2004-2007 data truncated at 0.4 with the same assumptions as above, which had an average DBH of 47.6551. This resulted in

$$\phi_A(h_N) = \frac{27}{1210} e^{4.0758+0.0381(47.6551)-3.6284h_N}$$

and setting this equal to 0.1147, we obtain $h_N = 1.1725$ (which is above 1) and $\phi(1) = 0.2145$ (which is not close to 0), and therefore not what we would expect.

Soassararou, Nigoussourou, Gbeba Data

Thus, we decided to use all data from the Soassararou, Nigoussourou, and Gbeba populations from 2004-2007 (a total of 146 trees with an average DBH of 46.2089), since these populations are in similar ecological zones and all experience non-lethal harvesting of adults. We obtained a reproduction function that results in unrealistic harvesting values both in the case of using all of the data and truncating the data to only use trees with $h_N \geq 0.4$.

For these unrealistic cases thus far that have included different types of data/been truncated or not, the function was not near 0 at $h_N = 1$ as we would expect. Therefore, with the idea that perhaps data at lower harvesting levels is pulling up these functions and thus not allowing the functions to be near 0 at $h_N = 1$, we wish to consider a constrained scenario. We want to constrain our seedling function to be close to 0 when $h_N = 1$. First, we consider the constraint value to be 0.00001, so we would like

$$\phi_A(1) = \frac{279}{3076} e^{a+b(DBH_{avg})+c(1)} = 0.00001,$$

noting the total number of seedlings for these 3 populations is 279 out of 3076 fruits produced in 2004. Solving for a results in $a = -3.9576 - b(DBH_{avg}) - c$ and substituting a into our desired function, we obtain

$$\phi_A(h_N) = \frac{279}{3076} e^{-3.9576+b(DBH-DBH_{\text{average}})+c(h_N-1)}.$$

We specifically consider the case of DHB_{avg} (rather than an arbitrary DBH) since the function we ultimately want is the mean seedling production per adult individual. Then, using data from Soassaraou, Nigoussourou, and Gbeba, with data truncated at 0.4, we wish to solve for our values of b and c in the fruit reproduction function:

$$\mu(h_N) = e^{-3.9576+b(DBH-DBH_{\text{average}})+c(h_N-1)}.$$

We obtain $b = 0.1216$, $c = -15.0242$, and we can solve for $a = 5.4488$. Setting

$$\phi_A(h_N) = \frac{279}{3076} e^{5.4488+0.1216(46.2089)-15.0242h_N} = 0.1147,$$

we obtain $h_N = 0.72$, a realistic value.

With the same data, changing our constraint to be 0.001, we solve for $a = -1.9576 - b(DBH_{avg}) - c$. This results in $b = 0.1216$, $c = -15.0590$, and we can solve for $a = 7.4826$. Setting

$$\phi_A(h_N) = \frac{279}{3076} e^{7.4826+0.1216(46.2089)-15.0590h_N} = 0.1147$$

results in $h_N = 0.85$, also a realistic value. However, we observe that the value of the constraint does make a noticeable difference in the harvesting rate. Thus, we choose the function that gives us a seedling production value closest to 0 when harvesting is at 100% (i.e. $h_N = 1$), as we are ultimately going to vary levels of harvesting in future work. Therefore, the reproduction function for the Soassararou population is given by

$$\phi_A(h_N) = \frac{279}{3076} e^{5.4488+0.1216(46.2089)-15.0242h_N}$$

from the constraint case of 0.00001. The resulting seedling graph is shown in Figure 3.5.

3.6 Estimation of Soassararou and Nipuni Harvesting Rates with Constant Harvesting Intensity

From population level calculations in the field, Gaoue has observed 65% of Soassararou individuals are pruned, with an average pruning rate of 84% for adult individuals, and an average pruning rate of 54% for all individuals [47]. For individuals that were debarked, the average debarking intensity was 28.35%. However, we cannot necessarily use these observed percentages directly in our model and instead need to calculate h_N which is the effect harvesting has on certain vital rates, where we have assumed a linear effect on the survival rate of seedlings and a nonlinear effect on the reproduction rate. In addition, Soassararou has unknown rates that need to be estimated: σ_N, the survival rate of seedlings;

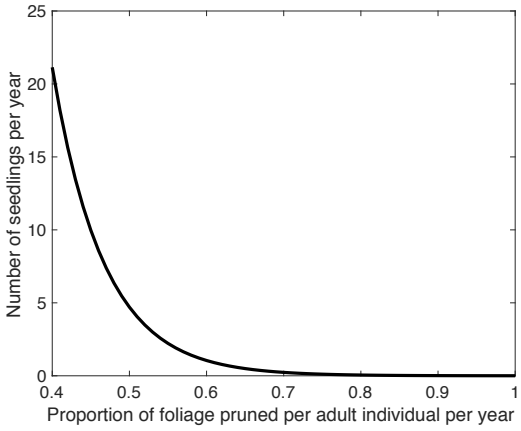


Figure 3.2: The reproduction function, $\phi_A(h_N)$, for the Soassararou population representing the average number of seedlings produced from an adult individual as a function of average proportion of foliage pruned per adult individual. When all of the foliage is removed at a harvesting level of 1, the seedling production is very close to 0 as would be expected.

γ_{12}, the rate of transition from the seedling to sapling class; and σ_4, the survival rate of adults in the dry season.

To estimate these rates, we would like to compare the observed data from the Soassararou population to simulations of our Soassararou harvesting model to determine what level of harvest gives the best fit and the optimal values of our unknown rates. In addition, we wish to take the unharvested, pristine Nipuni population, apply simulated harvesting to it, and match the output with observed data from the Soassararou naturally harvested population as best as possible. This allows us to to determine what harvesting level the Nipuni population would need to experience to best match observed data from a harvested population in a similar ecological zone. The matrices we will be using to simulate harvesting on these populations are the following:

$$\text{Soassararou} = \begin{pmatrix} (1-\gamma_{12})\sigma_5(1-h_N)\sigma_1 & 0 & 0 & \phi_A(h_N)\sigma_4 \\ \gamma_{12}\sigma_5(1-h_N)\sigma_1 & (1-\gamma_{23})\sigma_6\sigma_2 & 0 & 0 \\ 0 & \gamma_{23}\sigma_6\sigma_2 & (1-\gamma_{34})\sigma_7\sigma_3 & 0 \\ 0 & 0 & \gamma_{34}\sigma_7\sigma_3 & \sigma_8\sigma_4 \end{pmatrix}$$

and

$$\text{Nipuni}_{\text{harvested}} = \begin{pmatrix} (1-\gamma_{12})\sigma_5(1-h_N)\sigma_1 & 0 & 0 & \phi_A(h_N)\sigma_4 \\ \gamma_{12}\sigma_5(1-h_N)\sigma_1 & (1-\gamma_{23})\sigma_6\sigma_2 & 0 & 0 \\ 0 & \gamma_{23}\sigma_6\sigma_2 & (1-\gamma_{34})\sigma_7\sigma_3 & 0 \\ 0 & 0 & \gamma_{34}\sigma_7\sigma_3 & \sigma_8\sigma_4 \end{pmatrix}.$$

Our model is formulated to start in the dry season and since the data we have available is for December (a few months into the dry season), we will use that data for our initial conditions. From [43], we have data on the number of seedlings, juveniles, and adults from 2004-2007. The number of observed trees in December 2004 is 18 seedlings, 18 juveniles, and 54 adults; there is no information on the number of saplings so we will estimate that number. Therefore, the initial conditions for this process are given by:

$$\text{IC} = [18, S_0, 18, 54].$$

We are using these 2004 Soassararou observed data points as initial conditions for both the Nipuni and Soassararou harvesting models so we can observe the behaviors of the populations from the same starting point. Once the initial value of the sapling class is estimated from the Soassararou fitting process, we will use that value for the fitting process with Nipuni. The remaining data points from 2005-2007 are shown in Table 3.13.

We are assuming the form of the reproduction function is the same for Nipuni as Soassararou (i.e. $\phi_A(h_N) = \frac{279}{3076}e^{5.4488+0.1216(46.2089)-15.0242h_N}$) since a similar function cannot be built for Nipuni (as it is not a harvested population) and these populations are in a

Table 3.13: Soassararou 2005-2007 observed data used in parameter estimation process.

Class	Data	Notation
Seedling	$[12, 10, 8]$	Data_1
Juvenile	$[19, 19, 18]$	Data_2
Adult	$[53, 53, 54]$	Data_3

similar ecological zone. We need to know the value of σ_4 for both populations since it is multiplied by the reproduction function in entry (4,4) of either harvesting matrix. Since $\sigma_8\sigma_4 = 0.9701$ for the Soassararou population and each rate in this term is between 0 and 1, we know that each rate cannot be below 0.9701 (or the other would have to be above 1). Therefore, we set a lower bound of 0.9701 for σ_4 for estimation as shown in Table 3.14. For the Nipuni population, $\sigma_8\sigma_4 = 0.9999$ and therefore we make the simplifying assumption that $\sigma_4 = 0.9999$ and $\sigma_8 = 1$.

To have an idea of realistic bounds for σ_N and γ_{12} for the Soassararou fitting process, we use information from unharvested populations in a similar ecological zone. The Nipuni and Barabon populations have values of $\sigma_N = 0.4354$ and 0.5795, respectively, and therefore we set the bounds of σ_N to be 0.4 and 0.6. Moreover, these populations have rates of $\gamma_{12} = 0.028$ and 0.0309, respectively, and therefore, we set the range of γ_{12} to be 0.01 to 0.04. The bounds used for the estimation process are found in Tables 3.14 and 3.16.

In order to estimate the unknown parameters, we wish to minimize the difference between the Soassararou observed data and the simulated output from the Soassararou and Nipuni

Table 3.14: Bounds for Soassararou harvesting model rates in parameter estimation process.

Rate estimated	Bounds	Reasoning
$\sigma_5\sigma_1 = \sigma_N$	[0.4,0.6]	Based on rates from Nipuni and Barabon.
γ_{12}	[0.01,0.04]	Based on rates from Nipuni and Barabon.
σ_4	[0.9701,1]	Constraints of $\sigma_8 \leq 1$ and $\sigma_A = 0.9701$.
h_N	[0.001,1]	Wide range, effect less than 1 so entry (1,1) is non-negative.
S_0	[1,50]	Based on size of other classes in 2004.

harvesting models for each class, using the Ordinary Least Squares method. We do this by summing over the differences at each time step and for each class so we let Diff_1 be the vector that represents the differences between seedling data for Soassararou observed data and the simulated values from 2005-2007, Diff_2 the differences between juvenile data from 2005-2007, and finally Diff_3 the differences in the adult class data from 2005-2007. Then, our objective function takes the form of:

$$\text{objective function} = \sum_{i=1}^{3} \frac{\sqrt{\sum_{k=1}^{3} \text{Diff}_i(\text{k})^2}}{\sqrt{\sum_{k=1}^{3} \text{Data}_i(\text{k})^2}},$$

where the relative norm is taken due to differences in the sizes of the classes with k counting the years and i counting the classes. We again assume a constant harvest each dry season for the purposes of getting baseline harvesting values and use Multistart from the Global Optimization Toolbox in MATLAB to minimize our objective function. This means multiple points are used to find multiple local minima and ultimately the global minimum. Details for how this process works in general are outlined in Section 2.4.2. For the Soassararou harvesting model, we are estimating 5 parameters with 9 data points and for the Nipuni harvesting model, we are estimating 1 parameter with 9 data points.

In each case, we use 200 starting points, a sufficient number to obtain the same global minimum and resulting parameter values upon multiple runs. With bounds given in Table 3.14, the objective function value for fitting to the Soassararou harvesting matrix simulations is 0.1579 and the resulting rates for the Soassararou population are bolded in Table 3.15. The resulting value for S_0 was 14.4803, which we round down to 14. We observe that σ_N and γ_{12} achieve their upper and lower bounds, respectively. Although these parameters achieve any upper or lower bound that is provided, we note that with different upper bounds for σ_N and/or different lower bounds for γ_{12}, all of the resulting parameter estimates are very similar, with the objective function changing a little. For instance with an extreme case, when the upper bound is moved to 1 for σ_N and the lower bound for γ_{12} is made to be 0.0001, the objective function value is 0.1281, but the harvesting rate is essentially the same

Table 3.15: Rates for Soassararou harvesting model with **bold** rates determined from parameter estimation process.

Rate used in harvesting estimation	Value of rate
$\sigma_5\sigma_1 = \sigma_N$	**0.6**
γ_{12}	**0.01**
$\sigma_6\sigma_2 = \sigma_S$	0.8616
γ_{23}	0.1091
$\sigma_7\sigma_3 = \sigma_J$	0.9721
γ_{34}	0.0215
$\sigma_8\sigma_4 = \sigma_A$	0.9701
$\phi_A(h_N)$	$\frac{279}{3076}e^{5.4488+0.1216(46.2089)-15.0242\cdot 0.7031} = 0.150$
σ_4	**0.9701**
h_N	**0.7031**
S_0	**14**

(0.7166), along with the other rates. From the finalized parameters given in Table 3.15, the Soassararou matrix is given by:

$$\text{Soassararou} = \begin{pmatrix} 0.1764 & 0 & 0 & 0.1455 \\ 0.0018 & 0.7676 & 0 & 0 \\ 0 & 0.0940 & 0.9512 & 0 \\ 0 & 0 & 0.0209 & 0.9701 \end{pmatrix}.$$

We remark this matrix is different than the compressed matrix F_c found in Section 3.3.1 since that matrix was compressed from the 5×5 matrix from Gaoue [43], an average of matrices over four years (2004-2007). Our rates were estimated using yearly observed data instead, leading to a few terms that differ between the matrices. In Figure 3.3, the fits of the Soassararou harvesting model simulations to the seedling, juvenile, and adult Soassararou observed data points are shown.

Using the estimated initial condition of approximately 14 saplings in 2004 for the Soassararou population, the only rate needed to be estimated for the Nipuni harvesting model is h_N. With bounds on this rate given in Table 3.16, the objective function value for fitting to the Nipuni harvesting matrix simulations is 0.2453 and all of the rates for the Nipuni population are given in Table 3.17. We remark that if S_0 were estimated as well,

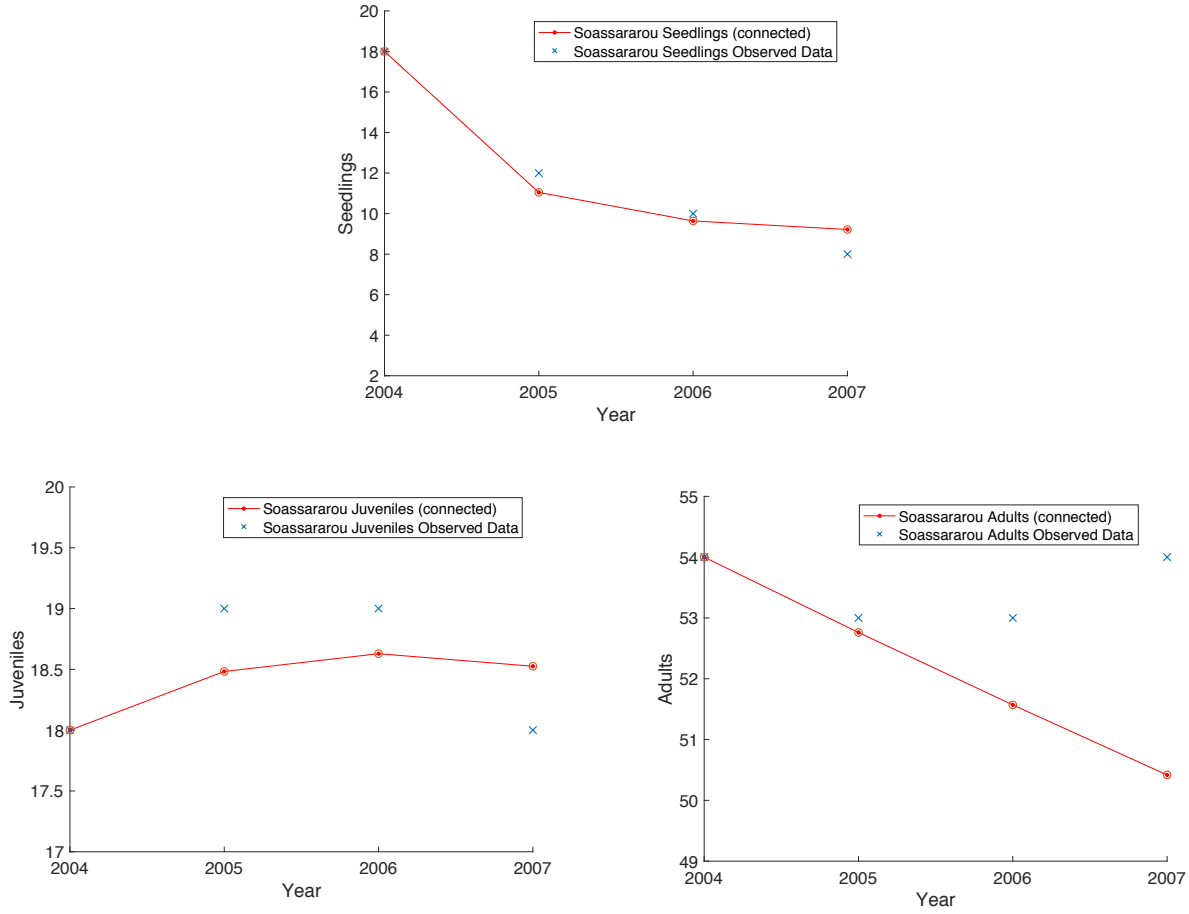


Figure 3.3: Comparison of Soassararou harvested model simulations to Soassararou observed data during fitting process for Soassararou rates.

Table 3.16: Bounds for Nipuni harvesting model rate in parameter estimation process.

Rate estimated	Bounds	Reasoning
h_N	[0.001,1]	Wide range, effect less than 1 so entry (1,1) is non-negative.

instead of using 14 from the Soassararou fitting process, then we obtain an objective function value of 0.183 with estimated $S_0 = 7$ and $h_N = 0.7019$, the latter being essentially equivalent to the case where S_0 is not estimated.

Using parameters from Table 3.17, the resulting Nipuni matrix is the following:

$$\text{Nipuni}_{\text{harvested}} = \begin{pmatrix} 0.1261 & 0 & 0 & 0.1527 \\ 0.0036 & 0.5741 & 0 & 0 \\ 0 & 0.1528 & 0.9696 & 0 \\ 0 & 0 & 0.0304 & 0.9999 \end{pmatrix}.$$

Note as explained before, this matrix is different than the compressed matrix B_c found in Section 3.3.1 since that matrix was compressed from the 5×5 matrix from Gaoue [43], an average of matrices over four years (2004-2007). Although we use many of those rates, we use yearly observed data from the Soassararou population to determine an effective harvesting rate, h_N, which make a few terms different in the matrices. In Figure 3.4, the fits of the Nipuni harvesting model simulations to the seedling, juvenile, and adult Soassararou observed data points are shown.

We use these estimated effective harvesting rates for Soassararou and Nipuni ($h_N = 0.7031$ and $h_N = 0.7020$, respectively) in order to compare population dynamics for these two populations. We compute the dominant eigenvalue, λ_1, and the damping ratio, $\frac{\lambda_1}{|\lambda_2|}$, for Soassararou to determine how a population that is regularly perturbed responds to even more perturbation. We also compute these values for the Nipuni population to provide insight on how a pristine, unharvested population responds to perturbation. The dominant eigenvalue gives the long-term growth rate of the population and the damping ratio suggests how quickly the population converges to the stable stage distribution [13].

Results are shown in Table 3.18. The long-term growth rate calculated for Nipuni is larger than that of Soassararou. These rates suggest the Nipuni population would be expected to

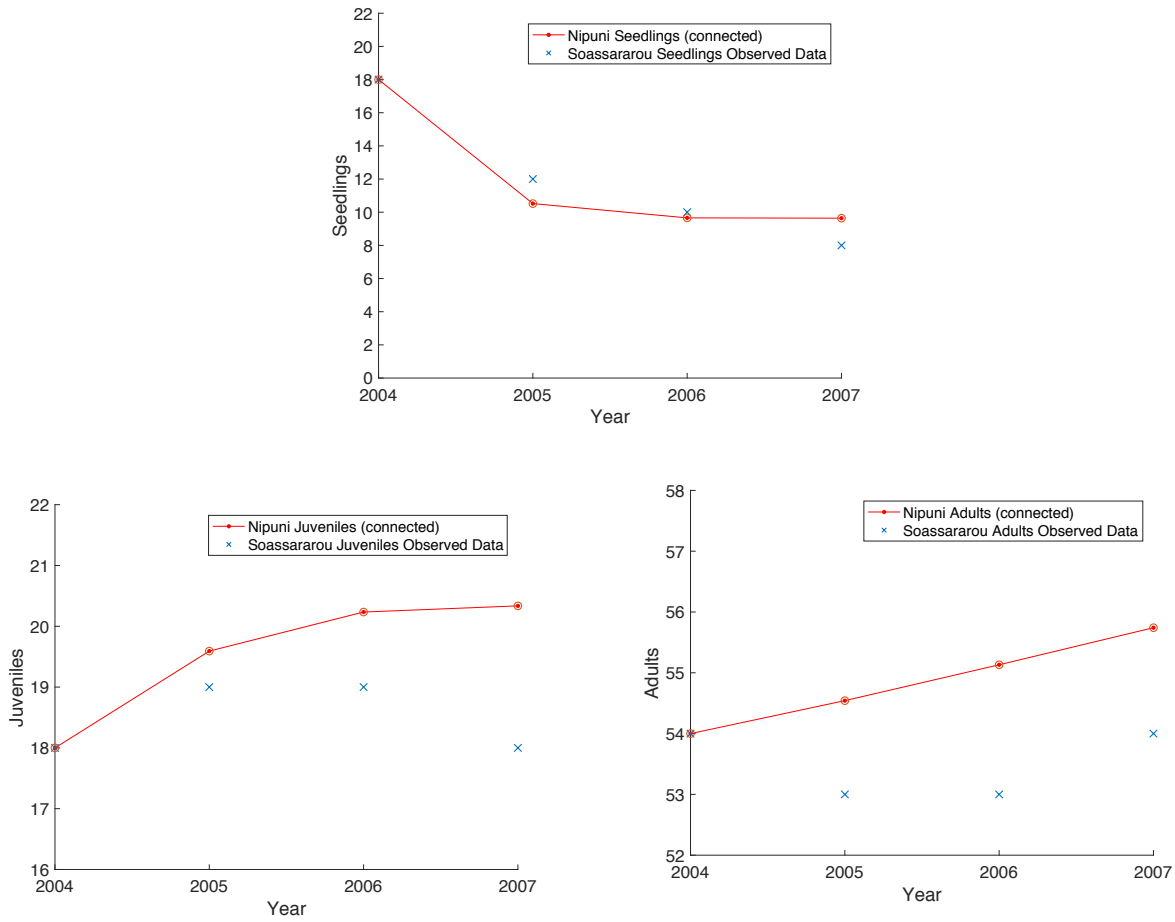


Figure 3.4: Comparison of Nipuni harvested model simulations to Soassararou observed data during fitting process for Nipuni harvesting rate.

Table 3.17: Rates for Nipuni harvesting model with the **bold** rate determined from parameter estimation process.

Rate used in harvesting estimation	Value of rate
$\sigma_5\sigma_1 = \sigma_N$	0.4354
γ_{12}	0.028
$\sigma_6\sigma_2 = \sigma_S$	0.7269
γ_{23}	0.2102
$\sigma_7\sigma_3 = \sigma_J$	1
γ_{34}	0.0304
$\sigma_8\sigma_4 = \sigma_A$	0.9999
$\phi_A(h_N)$	$\frac{279}{3076}e^{5.4488+0.1216(46.2089)-15.0242\cdot 0.7020} = 0.1527$
σ_4	0.9999
h_N	**0.7020**

grow in the long-term and the Soassararou population would be expected to decay. However, one limitation of this work is that we are fitting a deterministic model to noisy data, so these results are similar given that uncertainty. Moreover, the damping ratio for Nipuni is quite similar to that of Soassararou. We note that since our reproduction function is only defined for harvest levels 0.4 or above, we do not consider cases where harvest is set to 0 for baseline eigenvalues.

3.7 Conclusions and Discussion

Small and large adult trees are not easily distinguished in the field as they are both reproductive and experience both lethal and non-lethal harvesting. Therefore, our model combined these adults trees into the same size class. Doing so required matrices from previous work [43] to be compressed in order to inform corresponding rates in our model.

Table 3.18: Values of the dominant eigenvalue, λ_1, and the damping ratio, $\frac{\lambda_1}{|\lambda_2|}$ for the harvested Soassararou and Nipuni populations.

Population	Harvesting rate (h_N)	λ_1	$\frac{\lambda_1}{\lvert\lambda_2\rvert}$
Soassararou	0.7031	0.9703	1.0203
Nipuni	0.7020	1.0001	1.0318

Compression of these matrices used algorithms [59, 89, 95] that relied on weighting survival and fertility rates with proportions of small or large adults out of all adults in the stable stage distribution if long-term dynamics were of importance, or using information on how long individuals remain in a certain class if short-term dynamics were under consideration. We completed a novel application of these algorithms, in which the Nipuni and Barabon populations were compressed to maintain long-term dynamics, and the Soassararou and Nigoussorou populations were compressed with a focus on transient dynamics.

Prior to estimating the level of harvest the Soassararou and Nipuni populations experienced, we determined the relationship between the reproduction and pruning intensity of the Soassararou adult individuals. The resulting reproduction function was used for both populations, as Nipuni is viewed as an unharvested baseline for Soassararou. Using ordinary least squares and comparing model simulations to Soassararou observed data, we were able to estimate the level of effect harvesting has on the Soassararou population within our model, $h_N = 0.7031$ (corresponding to 84% actual observed harvest for adult individuals), and estimate how much harvest the Nipuni population would experience to best match the data, $h_N = 0.7020$. Further analysis with these respective harvesting rates suggested that both the long-term growth rate and damping ratio for the previously unharvested population Nipuni would be greater than those of Soassararou, suggesting that harvesting a pristine population does not capture the effects of harvest on a population that has undergone harvest in the past and instead underestimates those effects. In future work, the Nigoussorou population can be analyzed similarly to that of the Soassararou population using Nipuni and Barabon as baselines, as well. In addition, the effect on population dynamics from varying all three types of harvest simultaneously can be explored.

This work is part of advancing the overall understanding of the ecological processes occurring simultaneously with harvesting in order to influence managing strategies in the short- and/or long-term. We recognize that our model has some limitations. One such limitation is not including fire and drought explicitly in our model, which has effects on shrinkage of the trees, particularly from the sapling to seedling stage. Our model is currently deterministic, whereas fire and drought are stochastic processes. Other environmental factors

such as floods, rainfall, temperature, and insects on the trees could be incorporated in order to capture a more realistic environment, as well.

Bibliography

[1] Abdurahman, X., Shang, L., and Teng, Z. (2014). Global dynamics of a discretized heroin epidemic model with time delay. *Abstract and Applied Analysis*, 2014. 13

[2] Agar, M. H. (2001). Another complex step: A model of heroin experimentation. *Field Methods*, 13(4):353–369. 14

[3] American Pain Society Quality of Care Committee (1995). Quality improvement guidelines for the treatment of acute pain and cancer pain. *JAMA*, 274(23):1874–1880. 4

[4] American Psychiatric Association (2000). American psychiatric association: *Diagnostic and Statistical Manual of Mental Disorders Fourth Edition*. Available at https://dsm.psychiatryonline.org/doi/pdf/10.1176/appi.books.9780890420249.dsm-iv-tr (accessed 10/10/2018). 39

[5] Bailey, G. L., Herman, D. S., and Stein, M. D. (2013). Perceived relapse risk and desire for medication assisted treatment among persons seeking inpatient opiate detoxification. *Journal of Substance Abuse Treatment*, 45:302–305. 24, 64

[6] Battista, N. A., Pearcy, L. B., and Strickland, W. C. (2019). Modeling the prescription opioid epidemic. *Bulletin of Mathematical Biology*, 81:2258–2289. 15, 17, 23, 26, 31, 61, 108

[7] Baumblatt, J. A. G., Wiedeman, C., Dunn, J. R., Schaffner, W., Paulozzi, L., and Jones, T. F. (2014). High-risk use by patients prescribed opioids for pain and its role in overdose deaths. *JAMA Internal Medicine*, 175(5):796–801. 43, 46

[8] Bradley, B., Phillips, G., Green, L., and Gossop, M. (1989). Circumstances surrounding the initial lapse to opiate use following detoxification. *British Journal of Psychiatry*, 154:354–359. 24, 25, 26

[9] Broers, B., Giner, F., Dumont, P., and Mino, A. (2000). Inpatient opiate detoxification in geneva: follow-up at 1 and 6 months. *Drug and Alcohol Dependence*, 58:85–92. 24

[10] Bufford, J. L. and Gaoue, O. G. (2015). Defoliation by pastoralists affects savanna tree seedling dynamics by limiting the facilitative role of canopy cover. *Ecological Applications*, 25(5):1319–1329. 120, 125, 127

[11] Burnham, K. P. and Anderson, D. R. (2002). *Model Selection and Multimodel Inference: A Practical Information-Theoretic Approach*. Springer, second edition. 85, 88

[12] Burnham, K. P. and Anderson, D. R. (2004). Multimodel inference: Understanding aic and bic in model selection. *SAGE*, 33(2):261–304. 88

[13] Caswell, H. (2018). *Matrix Population Models: Construction, Analysis, and Interpretation*. Oxford University Press, 2nd edition. 147, 166

[14] CDC National Center for Injury Prevention and Control (2017). Prescription behavior surveillance system (pbss) issue brief. Available at https://www.cdc.gov/drugoverdose/pdf/pbss/PBSS-Report-072017.pdf (accessed 5/14/2019). 6, 7, 42

[15] Center for Behavioral Health Statistics and Quality (2016). *2015 National Survey on Drug Use and Health: Methodological Summary and Definitions*. Substance Abuse and Mental Health Services Administration, Rockville, Maryland. 78

[16] Center for Behavioral Health Statistics and Quality (2017). *2015 National Survey on Drug Use and Health Methodological Resource Book Section 11: Person-Level Sampling Weight Calibration*. Substance Abuse and Mental Health Services Administration, Rockville, Maryland. 78

[17] Center for Behavioral Health Statistics and Quality, Substance Abuse and Mental Health Services Administration (2015b). 2014 national survey on drug use and health methodological summary and definitions. Available at https://www.samhsa.gov/data/sites/default/files/NSDUH-MethodSummDefs2014/NSDUH-MethodSummDefs2014.pdf (accessed 8/8/2019). 37, 38

[18] Center for Behavioral Health Statistics and Quality, Substance Abuse and Mental Health Services Administration (2015a). 2016 national survey on drug use and health (NSDUH): Final approved CAI specifications for programming (english version). Available at https://www.samhsa.gov/data/sites/default/files/NSDUHmrbCAIquex2016v2.pdf (accessed 06/14/2018). 4

[19] Centers for Disease Control and Prevention (2016). Synthetic opioid overdose data. Available at https://www.cdc.gov/drugoverdose/data/fentanyl.html (accessed 05/01/2018). 7

[20] Centers for Disease Control and Prevention (2017a). Opioid data analysis. Available at https://www.cdc.gov/drugoverdose/data/analysis.html (accessed 05/01/2018). 3, 6, 7, 16, 17, 19, 40, 42

[21] Centers for Disease Control and Prevention (2017b). Prescription painkiller overdoses. Available at https://www.cdc.gov/vitalsigns/PrescriptionPainkillerOverdoses/index.html (accessed 7/19/2018). 4, 6, 119

[22] Centers for Disease Control and Prevention (2017c). U.s. state prescribing rates, 2017. Available at https://www.cdc.gov/drugoverdose/maps/rxstate2017.html (accessed 5/9/2019). 1, 7

[23] Centers for Disease Control and Prevention (2018a). Fentanyl. Available at https://www.cdc.gov/drugoverdose/opioids/fentanyl.html (accessed 5/14/2019). 6

[24] Centers for Disease Control and Prevention (2018b). U.s. opioid prescribing rate maps. Available at https://www.cdc.gov/drugoverdose/maps/rxrate-maps.html (accessed 5/9/2019). 7

[25] Centers for Disease Control and Prevention (2019). Prescribing practices. Available at https://www.cdc.gov/drugoverdose/data/prescribing/prescribing-practices.html (accessed 9/8/2019). 17

[26] Centers for Disease Control and Prevention: National Center for Health Statistics (2017). All injuries. Available at https://www.cdc.gov/nchs/fastats/injury.htm. 3

[27] Chen, Q., Larochelle, M. R., Weaver, D. T., Lietz, A. P., Mueller, P. P., and Sarah Mercaldo, e. a. (2019). Prevention of prescription opioid misuse and projected overdose deaths in the united states. *JAMA*, 2(2). 13

[28] Choo, J. (2018). Personal communication. University of Tennessee, Knoxville Science Forum: "Opioid Crisis: Dispelling Misconceptions and Spotlighting the Overlooked". 10

[29] Cicero, T. J., , Ellis, M. S., and Surratt, H. L. (2012). Effect of abuse-deterrent formulation of oxycontin. *New England Journal of Medicine*, 367(2):187–189. PMID: 22784140. 5

[30] Cicero, T. J. and Ellis, M. S. (2015). Abuse-deterrent formulations and the prescription opioid abuse epidemic in the United States: Lessons learned from oxycontin. *JAMA Psychiatry*, 72(5):424–430. 5

[31] Cicero, T. J., Ellis, M. S., Surratt, H. L., and Kurtz, S. P. (2014). The changing face of heroin use in the United States: A retrospective analysis of the past 50 years. *JAMA Psychiatry*, 71(7):821–826. 5

[32] Compton, W. M. (2017). Research on the use and misuse of fentanyl and other synthetic opioids. Available at https://www.drugabuse.gov/about-nida/legislative-activities/testimony-to-congress/2017/research-use-misuse-fentanyl-other-synthetic-opioids (accessed 07/18/2018). 3, 6, 7, 9

[33] Cooper, K. (2018). Personal Communication. 26

[34] Davis, S. (2019). University of tennessee, knoxville lecture: "the science of addiction". Personal Communication. 9

[35] Department of Health and Human Services (2019). Factsheet: Tennessee's oversight of opioid prescribing and monitoring of opioid use. Accessed at https://oig.hhs.gov/oas/reports/region4/41800124_Factsheet.pdf (8/17/19). 8, 74

[36] Department of Health and Human Services: Administration for Children and Families, Office of Child Care (2018). State/territory profile-tennessee. Available at https://childcareta.acf.hhs.gov/state-profiles/profiles/TN/pdf (accessed 11/5/18). 36

[37] Fang, B., Li, X.-Z., Martcheva, M., and Cai, L.-M. (2015a). Global asymptotic properties of a heroin epidemic model with treat-age. *Applied Mathematics and Computation*, 263:315–331. 12

[38] Fang, B., Li, X.-Z., Martcheva, M., and Cai, L.-M. (2015b). Global stability for a heroin model with age-dependent susceptibility. *Journal of Systems Science and Complexity*, 28(6):1243–1257. 13

[39] Felitti, V. J., Anda, R. F., Nordenberg, D., Williamson, D. F., Spitz, A. M., Edwards, V., Koss, M. P., and Marks, J. S. (1998). Relationship of childhood abuse and household dysfunction to many of the leading causes of death in adults. *American Journal of Preventive Medicine*, 14(4):245–258. 9

[40] Florence, C. S., Zhou, C., Luo, F., and Xu, L. (2016). The economic burden of prescription opioid overdose, abuse and dependence in the United States, 2013. *Medical Care*, 54(10):901–906. 3

[41] Gaoue, O., Agusto, F., Jiang, J., and Lenhart, S. (2016a). Optimal harvesting strategies for timber and non-timber forest products in tropical ecosystems. *Theoretical Ecology*, 9:287–297. 121

[42] Gaoue, O., Horvitz, C., Steiner, U. K., and Tuljapurkar, S. (2013). Defoliation and bark harvesting affect life history traits of a tropical tree. *Journal of Ecology*, 101:1563–1571. 127

[43] Gaoue, O. G. (2015a). Data from: Transient dynamics reveal the importance of early life survival to the response of a tropical tree to harvest. 130, 138, 139, 141, 143, 144, 147, 149, 152, 153, 154, 161, 164, 166, 168

[44] Gaoue, O. G. (2015b). Transient dynamics reveal the importance of early life survival to the response of a tropical tree to harvest. *Journal of Applied Ecology*, 53:112–119. 2, 120, 121, 122, 124, 125, 130, 132, 138, 147, 153

[45] Gaoue, O. G. (2017). Personal Communication. 2, 124

[46] Gaoue, O. G. (2018). Personal Communication. 123, 125, 127

[47] Gaoue, O. G. (2019). Personal Communication. 154, 159

[48] Gaoue, O. G., Ngonghala, C. N., Jiang, J., and Lélu, M. (2016b). Towards a mechanistic understanding of the synergistic effects of harvesting timber and non-timber forest products. *Methods in Ecology and Evolution*, 7:398–406. 120, 121, 122

[49] Gaoue, O. G. and Ticktin, T. (2007). Patterns of harvesting foliage and bark from the multipurpose tree khaya senegalensis in benin: Variation across ecological regions and its impacts on population structure. *Biological Conservation*, 137:424–236. 120

[50] Gladden, R. M., Martinez, P., and Seth, P. (2016). Fentanyl law enforcement submissions and increases in synthetic opioid–involved overdose deaths — 27 states, 2013–2014. *MMWR Morb Mortal Wkly Rep*. 6, 7, 42

[51] Gossop, M., Green, L., Phillips, G., and Bradley, B. (1989). Lapse, relapse and survival among opiate addicts after treatment: A prospective follow-up study. *British Journal of Psychiatry*, 154:348–353. 24, 25

[52] Gossop, M., Stewart, D., Browne, N., and Marsden, J. (2002). Factors associated with abstinence, lapse or relapse to heroin use after residential treatment: protective effect of coping responses. *Addiction*, 97:1259–1267. 24

[53] Han, B., Compton, W. M., Blanco, C., Crane, E., Lee, J., and Jones, C. M. (2017). Prescription opioid use, misuse, and use disorders in u.s. adults: 2015 national survery on drug use and health. *Annals of Internal Medicine*, 167(5):293–302. 41, 60, 62

[54] Harris, M. C., Kessler, L. M., Murray, M. N., and Glenn, M. E. (2019). Prescription opioids and labor market pains: The effect of schedule ii opioids on labor force participation and unemployment. *The Journal of Human Resources*. 15

[55] Heard, D., Bobashev, G. V., and Morris, R. J. (2014). Reducing the complexity of an agent-based local heroin market model. *PLOS ONE*, 9. 15

[56] Heather, N., Stallard, A., and Tebbutt, J. (1991). Importance of substance cues in relapse among heroin users: comparison of two methods of investigation. *Addictive Behaviors*, 16:41–49. 25

[57] Herman, J. and Usher, W. (2017). Salib-sensitivity analysis library in python. Available at https://salib.readthedocs.io/en/latest/ (accessed 05/01/2018). 1, 94, 102

[58] Hoffer, L. D., Bobashev, G., and Morris, R. J. (2009). Researching a local heroin market as a complex adaptive system. *Am J Community Psychol.*, 44(3-4):273–86. 14, 112

[59] Hooley, D. E. (2000). Collapsed matrices with (almost) the same eigenstuff. *The College Mathematics Journal*, 31(4):297–299. 132, 135, 137, 138, 140, 142, 169

[60] Hsieh, P.-F. and Sibuya, Y. (1993). *Basic Theory of Ordinary Differential Equations*. Springer. 33, 34

[61] Hughes, A., Williams, M. R., Lipari, R. N., Bose, J., Copello, E. A., and Kroutil, L. (2016). Prescription drug use and misuse in the united states: Results from the 2015 national survey on drug use and health. Available at https://www.samhsa.gov/data/sites/default/files/NSDUH-FFR2-2015/NSDUH-FFR2-2015.htm (accessed 3/14/19). 60

[62] Hunt, W. A., Barnett, L. W., and Branch, L. G. (1971). Relapse rates in addiction programs. *Journal of Clinical Psychology*, 27(4):455–456. 24

[63] Ihongbe, T. O. and Masho, S. W. (2016). Prevalence, correlates and patterns of heroin use among young adults in the United States. *Addictive Behaviors*, 63:74–81. 5

[64] Jones, C. M. (2013). Heroin use and heroin use risk behaviors among nonmedical users of prescription opioid pain relievers – united states, 2002–2004 and 2008–2010. *Drug and Alcohol Dependence*, 132(1):95 – 100. 5, 118, 119

[65] Jones, C. M., Einstein, E. B., and Compton, W. M. (2018). Changes in synthetic opioid involvement in drug overdose deaths in the united states, 2010-2016. *JAMA*, 319(17):1819–1821. 16

[66] Jr., G. P. G., Zhang, K., Bohm, M. K., Losby, J., Lewis, B., Young, R., Murphy, L. B., and Dowell, D. (2017). Vital signs: Changes in opioid prescribing in the united states 2006-2015. *MMWR Morb Mortal Wkly Rep*, 66:697–704. 40

[67] Knoxville Narcotics Anonymous Group (2018). Personal Communication. 11

[68] Kochanek, K. D., Murphy, S. L., Xu, J., and Arias, E. (2017). Mortality in the united states, 2016. NCHS Data Brief 293, National Center for Health Statistics, Hyattsville, MD. 46

[69] Liu, J. and Zhang, T. (2011). Global behaviour of a heroin epidemic model with distributed delays. *Applied Mathematics Letters*, 24:1685–1692. 12

[70] Ma, M., Liu, S., and Li, J. (2017). Bifurcation of a heroin model with nonlinear incidence rate. *Nonlinear Dynamics*, 88(1):555–565. 13

[71] Mandell, B. (June 2016). The fifth vital sign: A complex story of politics and patient care. *Cleveland Clinic Journal of Medicine*, 83(6). 4

[72] Marino, S., Hogue, I. B., Ray, C. J., and Kirschner, D. E. (2008). A methodology for performing global uncertainty and sensitivity analysis in systems biology. *Journal of Theoretical Biology*, 254(1):178–196. 1, 94

[73] MathWorks (2019a). Constrained nonlinear optimization algorithms. Available at https://www.mathworks.com/help/optim/ug/constrained-nonlinear-optimization-algorithms.html (accessed 9/20/19). 58

[74] MathWorks (2019b). How globalsearch and multistart work. Available at https://www.mathworks.com/help/gads/how-globalsearch-and-multistart-work.html (accessed 9/20/19). 57, 58

[75] MathWorks (2019c). What is global optimization? Available at https://www.mathworks.com/help/gads/what-is-global-optimization.html (accessed 9/20/19). 58

[76] MetroDrug Coalition: East Tennesee Opioid Conference (2019). Personal Communication. 11

[77] Motulsky, H. and Christopoulos, A. (2003). *Fitting Models to Biological Data Using Linear and Nonlinear Regression. A practical guide to curve fitting.* GraphPad Software Inc. 78

[78] Muhuri, P. K., Gfroerer, J. C., and Davies, M. C. (2013). Associations of nonmedical pain reliever use and initiation of heroin use in the United States. 4, 5, 64

[79] National Institute on Drug Abuse (2018a). Heroin. Available at https://www.drugabuse.gov/publications/drugfacts/heroin#ref (accessed 07/17/2018). 5, 6, 18

[80] National Institute on Drug Abuse (2018b). Heroin. Available at https://d14rmgtrwzf5a.cloudfront.net/sites/default/files/828-heroin.pdf (accessed 7/18/2018). 5, 6, 9, 22, 108, 116, 118

[81] National Institute on Drug Abuse (2018c). Opioid summaries by state. Available at https://www.drugabuse.gov/drugs-abuse/opioids/opioid-summaries-by-state (accessed 7/18/2018). 119

[82] National Institute on Drug Abuse (2018d). Prescription opioids and heroin. Available at https://d14rmgtrwzf5a.cloudfront.net/sites/default/files/19774-prescription-opioids-and-heroin.pdf (accessed 04/16/2018). 3, 5, 17, 41

[83] National Institute on Drug Abuse (2019). Abuse of prescription pain medications risks heroin use. Available at https://www.drugabuse.gov/sites/default/files/infographic_presc_heroin.pdf (accessed 3/27/19). 38, 40, 63

[84] Office of Information and Analytics Tennessee Department of Health (2018). Prescription drug overdose program 2018 report. Available at https://www.tn.gov/content/dam/tn/health/documents/pdo/PDO_2018_Report_02.06.18.pdf (accessed 5/9/2019). viii, 1, 6, 7, 8, 9, 37, 40, 41, 42, 43, 44, 45, 46, 61, 119

[85] Office of Information and Analytics Tennessee Department of Health (2019a). Data dashboard. Available at https://www.tn.gov/health/health-program-areas/pdo/pdo/data-dashboard.html (accessed 8/14/18 and 7/17/2019). viii, 1, 9, 22, 37, 38, 40, 43, 44

[86] Office of Information and Analytics Tennessee Department of Health (2019b). Tennessee's annual overdose report: Understanding and responding to the opioid epidemic in tennessee using mortality, morbitiy, and prescription data. Available at https://www.tn.gov/content/dam/tn/health/documents/pdo/2019_Report.pdf (accessed 5/8/2019). viii, 1, 8, 9, 37, 41, 44, 45, 61

[87] Pitt, A. L., Humphreys, K., and Brandeau, M. L. (2018). Modeling health benefits and harms of public policy responses to the us opioid epidemic. *AJPH*, 108(10):1394–1400. 14

[88] Rohatgi, A. (2018). Webplotdigitizer. Available at https://automeris.io/WebPlotDigitizer/ (accessed 4/29/2018). 44

[89] Salguero-Gómez, R. and Plotkin, J. B. (2010). Matrix dimensions bias demographic inferences: Implications for comparitive plant demography. *The American Naturalist*, 176(710-722). 135, 137, 138, 140, 142, 169

[90] Saltelli, A., Annoni, P., Azzini, I., Campolongo, F., Ratto, M., and Tarantola, S. (2010). Variance based sensitivity analysis of model output. design and estimator for the total sensitivity index. *Computer Physics Communications*, 181:259–270. 1

[91] Saltelli, A., Ratto, M., Andres, T., Campolongo, F., Cariboni, J., Gatelli, D., Saisana, M., and Tarantola, S. (2008). *Global Sensitivity Analysis: The Primer*. Wiley. 102

[92] Samanta, G. (2011). Dynamic behaviour for a nonautonomous heroin epidemic model with time delay. *Journal of Applied Mathematics and Computing*, 35(1-2):161–178. 13

[93] Smith, H. L. (1995). *Monotone dynamical systems: an introduction to the theory of competitive and cooperative systems*, volume 41. American Mathematical Society, Rhode Island. 32

[94] Smyth, B., Barry, J., and E. Keenan, K. D. (2010). Laspse and relapse following inpatient treatment of opiate dependence. *Irish Medical Journal*, 103(6):176–179. 23, 25, 64, 65

[95] Spears, W. M. (1998). A compression algorithm for probability transition matrices. *SIAM Journal on Matrix Analysis and Applications*, 20(1):60–77. 135, 136, 137, 138, 144, 146, 148, 151, 169

[96] Substance Abuse and Mental Health Services Administration (2015a). Medication and counseling treatment. Available at https://www.samhsa.gov/medication-assisted-treatment/treatment (accessed 07/16/2018). 4, 6

[97] Substance Abuse and Mental Health Services Administration (2015b). Substance use disorders. Available at https://www.samhsa.gov/disorders/substance-use (accessed 07/16/2018). 17

[98] Substance Abuse and Mental Health Services Administration (2017a). 2014-2015 NSDUH state-specific tables: Table 95 selected drug use, past year alcohol use disorder,and past year mental health measures in tennessee, by age group: Estimated numbers (in thousands), annual averages based on 2014-2015 nsduhs. Available at https://www.samhsa.gov/data/report/2014-2015-nsduh-state-specific-tables (accessed 2/7/19). viii, 1, 37

[99] Substance Abuse and Mental Health Services Administration (2017b). 2016 NSDUH report: America's behavioral health changes and challenges. Available at https://www.samhsa.gov/sites/default/files/topics/data_outcomes_quality/nsduh-ppt-09-2017.pdf (accessed 06/26/2018). 7

[100] Substance Abuse and Mental Health Services Administration (2017c). Key substance use and mental health indicators in the United States: Results from the 2016 national survey on drug use and health. Available at https://www.samhsa.gov/data/sites/default/files/NSDUH-FFR1-2016/NSDUH-FFR1-2016.pdf (accessed 06/14/2018). 4, 7

[101] Substance Abuse and Mental Health Services Administration (2018). 2015-2016 NSDUH state-specific tables: Table 95 selected drug use, perceptions of great risk, past year substance use disorder and treatment, and past year mental health measures in tennessee, by age group: Estimated numbers (in thousands), annual averages based on 2015-2016 nsduhs. Available at https://www.samhsa.gov/data/report/2015-2016-nsduh-state-specific-tables (accessed 11/27/17). viii, 1, 37, 38

[102] Substance Abuse and Mental Health Services Administration (2019). 2016-2017 NSDUH state-specific tables: Table 95 selected drug use, perceptions of great risk, past year substance use disorder and treatment, and past year mental health measures in tennessee, by age group: Estimated numbers (in thousands), annual averages based on 2016-2017 nsduhs. Available at https://www.samhsa.gov/data/report/2016-2017-nsduh-state-specific-tables (accessed 2/7/19). viii, 1, 37, 38

[103] Tennessee Department of Health (2019a). Board of pharmacy: Legislative update-2019. Available at https://www.tn.gov/health/health-program-areas/health-professional-boards/pharmacy-board/pharmacy-board/legislative.html. 114

[104] Tennessee Department of Health (2019b). Laws and policies. Available at https://www.tn.gov/health/health-program-areas/pdo/pdo/resources/r/laws-policies.html (accessed 6/13/2019). 8, 74

[105] Tennessee Department of Health, Tennessee Department of Mental Health and Substance Abuse Services, Tennessee Department of Safety & Homeland Security, and Tennessee Bureau of Investigation (2019). Public health & safety advisory on fentanyl. Available at https://www.tn.gov/content/dam/tn/health/healthprofboards/health-advisory/Fentanyl_Public_Health_Advisory.pdf (accessed 8/2019). 8

[106] Tennessee Department of Mental Health and Substance Abuse Services (2017). Trends in drug overdose deaths involving opioids: Tennessee and the united states 2014 and 2015. Available at https://www.tn.gov/content/dam/tn/mentalhealth/documents/Drug_Overdose_Deaths_CDC_2.14.2017_.pdf (accessed 9/25/18). 3

[107] Tennessee State Government, Office of the Governor (2018). Tn together. Available at https://www.tn.gov/former-governor-haslam/2018-legislative-priorities/tn-together.html (accessed 5/3/2020). 9

[108] The National Academies of Science, Engineering, Medicine (2019). Conference: Data, modeling, and policy making to address the opioid epidemic. Personal Communication. 11

[109] United Nations Office on Drugs and Crime (1953). History of heroin. Available at https://www.unodc.org/unodc/en/data-and-analysis/bulletin/bulletin_1953-01-01_2_page004.html (accessed 08/28/2018). 7

[110] United States Census Bureau (2019). 2010 census summary file 1, table pct12. Available at https://factfinder.census.gov/faces/tableservices/jsf/pages/productview.xhtml?pid=DEC_10_SF1_QTP2&prodType=table (accessed 7/1/2019). 36

[111] United States Census Bureau, Population Division (2018). Annual estimates of the resident population for the united states, regions, states, and puerto rico: April 1, 2010 to july 1, 2018 (nst-est2018-01). Available at https://www.census.gov/data/tables/time-series/demo/popest/2010s-national-total.html (accessed 5/5/19). 36

[112] United States Drug Enforcement Administration (2018). Drug scheduling. Available at https://www.dea.gov/druginfo/ds.shtml (accessed 07/17/2018). 5

[113] University of Tennessee, Knoxville Summit for Opioid Addiction and Response (2019). Personal Communication. 10

[114] U.S. Department of Health and Human Services (2016). Facing addiction in america: The surgeon general's report on alcohol, drugs, and health. Available at https://addiction.surgeongeneral.gov/key-findings/early-intervention (accessed 3/24/19). 64

[115] U.S. Department of Health and Human Services (2017). HHS acting secretary declares public health emergency to address national opioid

crisis. Available at https://www.hhs.gov/about/news/2017/10/26/hhs-acting-secretary-declares-public-health-emergency-address-national-opioid-crisis.html (accessed 4/16/2018). 3

[116] U.S. Department of Justic Drug Enforcement Administration Diversion Control Division (2018). Nflis-drug 2017 annual report. Available at https://www.nflis.deadiversion.usdoj.gov/DesktopModules/ReportDownloads/Reports/NFLIS-Drug-AR2017.pdf (accessed 5/9/2019). 3, 7, 42

[117] U.S. Department of Justice Drug Enforcement Administration (2015). Dea issues nationwide alert on fentanyl as threat to health and public safety. Available at https://www.dea.gov/press-releases/2015/03/18/dea-issues-nationwide-alert-fentanyl-threat-health-and-public-safety (accessed 5/14/2019). 6, 7, 19, 42

[118] U.S. Department of Justice Drug Enforcement Administration (2017). Drugs of abuse: A dea resource guide 2017 edition. Available at https://www.dea.gov/sites/default/files/sites/getsmartaboutdrugs.com/files/publications/DoA_2017Ed_Updated_6.16.17.pdf#page=40 (accessed 5/14/2019). 6

[119] U.S. Food and Drug Administration (2018). Timeline of selected FDA activities and significant events addressing opioid misuse and abuse. Available at https://www.fda.gov/downloads/Drugs/DrugSafety/InformationbyDrugClass/UCM566985.pdf (accessed 06/13/2018). 4

[120] van den Driessche, P. and Watmough, J. (2002). Reproduction numbers and sub-threshold endemicequilibria for compartmental models of disease transmission. *Mathematical Biosciences*, 180:29–48. 29

[121] van den Driessche, P. and Watmough, J. (2008). *Mathematical Epidemiology*, chapter 6: Further Notes on the Basic Reproduction Number, pages 159–178. Springer, Berlin, Heidelberg. 28, 29, 30

[122] Volkow, N. D. (2016). What science tells us about opioid abuse and addiction. Available at https://www.drugabuse.gov/about-nida/legislative-activities/testimony-to-congress/2018/what-science-tells-us-about-opioid-abuse-addiction (accessed 07/17/2018). 7

[123] Vowles, K. E., McEnteea, M. L., Julnesa, P. S., Frohea, T., Neyb, J. P., and van der Goes, D. N. (2015). Rates of opioid misuse, abuse, and addiction in chronic pain: a systematic review and data synthesis. *PAIN*, 156(4):569–576. 17, 64

[124] Wang, X., Yang, J., and Li, X. (2011). Dynamics of a heroin epidemic model with very population. *Applied Mathematics*, 2(6):732–738. 12

[125] Wangari, I. M. and Stone, L. (2017). Analysis of a heroin epidemic model with saturated treatment function. *Journal of Applied Mathematics*, 2017. 13

[126] Weiss, R. D. and Rao, V. (2017). The prescription opioid addiction treatment study: What have we learned. *Drug and Alcohol Dependence*, 173:48–54. 22, 24, 25

[127] White, E. and Comiskey, C. (2007). Heroin epidemics, treatment and ODE modelling. *Mathematical Biosciences*, 208:312–324. 12

[128] Wil Cantrell, P. (2018). Personal Communication. 10

[129] Zoorob, M. (2019). Fentanyl shock: The changing geography of overdose in the united states. *International Journal of Drug Policy*, 70:40–46. 15

[130] Zuur, A. F., Ieno, E. N., Walker, N., Saveliev, A. A., and Smith, G. M. (2009). *Mixed effects models and extensions in ecology with R*. Springer. 155

Appendices

A Index Values and Confidence Intervals for Sobol Sensitivity Analyses

The first-order index values and confidence intervals for each parameter corresponding to a certain population class for the α piecewise linear, μ_A linear case run from 2013-2019 (corresponding to Figure 2.18) are shown in Tables 19-23.

Table 19: Sensitivity of the susceptible class at the beginning of 2019 to each of the parameters with corresponding confidence intervals listed.

Parameter	S1	S1 confidence interval	ST	ST confidence interval
m	2.275752e-03	4.455366e-04	2.448994e-03	2.354794e-05
β_A	-3.250583e-09	1.928310e-06	6.777251e-08	6.874144e-10
β_P	1.859978e-07	2.932853e-06	9.229965e-08	9.657637e-10
θ_1	1.200695e-03	2.914291e-04	1.334379e-03	1.486694e-05
ε	6.843023e-01	7.213388e-03	7.035719e-01	5.898720e-03
γ	5.656852e-04	2.008849e-04	6.139787e-04	5.401807e-06
σ	2.983240e-05	6.101602e-05	4.513364e-05	7.420825e-07
μ	7.111057e-05	8.797075e-05	8.037528e-05	7.616318e-07
μ_H	7.278597e-05	8.548259e-05	8.287563e-05	1.096644e-06
θ_2	1.337771e-05	3.514066e-05	1.577315e-05	2.402411e-07
ζ	1.164882e-06	2.122396e-05	5.847119e-06	9.051769e-08
θ_3	8.436066e-05	1.007519e-04	1.169145e-04	2.034373e-06
ν	-3.253354e-09	3.889746e-07	2.015618e-09	3.439152e-11
ω	-5.240752e-13	8.911267e-13	1.285904e-20	7.425530e-21
b	2.799789e-01	4.351990e-03	2.988640e-01	3.166494e-03
c	4.539970e-03	6.211632e-04	4.807746e-03	4.661559e-05
d	8.018952e-07	8.403073e-06	8.341893e-07	8.741003e-09
e	7.509171e-06	2.865946e-05	8.638261e-06	9.561492e-08
P_0	2.648848e-06	1.931970e-05	3.383335e-06	4.110516e-08
A_0	4.334764e-03	5.574930e-04	4.371199e-03	4.657173e-05
H_0	4.798595e-04	2.228719e-04	5.673570e-04	7.326241e-06
R_0	2.457179e-03	4.615335e-04	2.461593e-03	2.784575e-05

Table 20: Sensitivity of the prescription opioid user class at the beginning of 2019 to each of the parameters with corresponding confidence intervals listed.

Parameter	S1	S1 confidence interval	ST	ST confidence interval
m	2.352452e-03	4.148165e-04	2.529831e-03	2.569653e-05
β_A	6.507629e-09	1.870669e-07	4.826227e-10	5.687253e-12
β_P	-4.086834e-08	2.263742e-07	9.164853e-10	1.309922e-11
θ_1	1.387622e-05	2.542211e-05	8.696538e-06	1.185245e-07
ε	6.881491e-01	7.393318e-03	7.078034e-01	5.304432e-03
γ	1.840744e-05	5.089188e-05	2.344919e-05	3.077110e-07
σ	-2.316173e-07	5.915152e-06	3.946890e-07	9.269238e-09
μ	4.603404e-06	2.085756e-05	6.191900e-06	8.825267e-08
μ_H	-1.709963e-08	5.968054e-06	5.564538e-07	8.377921e-09
θ_2	-9.064082e-07	6.861449e-06	7.553576e-07	1.502927e-08
ζ	1.891301e-07	1.802859e-06	4.148322e-08	6.923768e-10
θ_3	9.976413e-07	8.689813e-06	1.054205e-06	2.362184e-08
ν	1.936481e-09	3.588870e-08	1.742754e-11	2.926529e-13
ω	-2.835054e-13	5.910282e-13	4.627026e-21	8.154335e-21
b	2.848022e-01	4.664372e-03	3.041071e-01	2.965130e-03
c	4.815337e-03	6.175445e-04	5.095665e-03	5.109991e-05
d	3.679275e-08	6.414425e-07	5.474550e-09	7.195330e-11
e	2.289405e-07	2.106635e-06	6.477710e-08	8.001988e-10
P_0	3.822049e-08	1.744773e-06	3.376283e-08	5.223446e-10
A_0	3.192139e-05	4.783561e-05	3.577162e-05	3.803300e-07
H_0	2.546157e-06	2.217149e-05	4.805243e-06	7.982629e-08
R_0	1.706468e-05	3.590124e-05	2.001408e-05	2.240845e-07

Table 21: Sensitivity of the prescription opioid addicted class at the beginning of 2019 to each of the parameters with corresponding confidence intervals listed.

Parameter	S1	S1 confidence interval	ST	ST confidence interval
m	8.726254e-05	1.082865e-04	1.538523e-04	1.709570e-06
β_A	8.630865e-06	2.764438e-05	9.370305e-06	1.013679e-07
β_P	1.237382e-05	3.305933e-05	1.303751e-05	1.424828e-07
θ_1	3.415088e-02	1.815862e-03	4.023832e-02	4.846052e-04
ε	8.600719e-02	2.813640e-03	9.582307e-02	1.094406e-03
γ	9.001426e-02	3.044802e-03	1.007463e-01	1.245064e-03
σ	3.292027e-02	1.406633e-03	3.870554e-02	4.345481e-04
μ	6.599084e-04	2.289842e-04	7.405164e-04	8.105124e-06
μ_H	1.904058e-03	4.877465e-04	2.271357e-03	2.949009e-05
θ_2	4.759893e-04	2.123237e-04	6.264965e-04	9.832017e-06
ζ	3.617319e-01	4.566188e-03	3.782281e-01	3.921403e-03
θ_3	7.177609e-02	2.593488e-03	9.062526e-02	1.094594e-03
ν	4.981048e-07	5.642583e-06	3.733111e-07	4.701911e-09
ω	1.506115e-12	2.063475e-11	6.215260e-18	7.557254e-20
b	2.492505e-02	1.497258e-03	2.880101e-02	3.497033e-04
c	3.591174e-05	6.871586e-05	4.933551e-05	6.151423e-07
d	1.478004e-04	1.103857e-04	1.674800e-04	2.068552e-06
e	1.069274e-03	2.849759e-04	1.192399e-03	1.302711e-05
P_0	1.392623e-04	1.180072e-04	1.749339e-04	2.308147e-06
A_0	1.794479e-01	4.024977e-03	1.984807e-01	2.190500e-03
H_0	4.907559e-02	2.319694e-03	5.682071e-02	7.449135e-04
R_0	1.511152e-02	1.164060e-03	1.835870e-02	1.964375e-04

Table 22: Sensitivity of the heroin/fentanyl addicted class at the beginning of 2019 to each of the parameters with corresponding confidence intervals listed.

Parameter	S1	S1 confidence interval	ST	ST confidence interval
m	2.890126e-06	1.464512e-05	2.590110e-06	6.194853e-08
β_A	5.905765e-07	5.586149e-06	3.941648e-07	7.284808e-09
β_P	3.414707e-07	5.134618e-06	4.636363e-07	9.306012e-09
θ_1	3.797029e-01	6.236499e-03	4.251746e-01	5.420888e-03
ε	1.504414e-03	5.255985e-04	3.245309e-03	7.642745e-05
γ	1.762661e-03	5.790885e-04	3.634184e-03	7.617890e-05
σ	6.454197e-02	2.183596e-03	7.888547e-02	1.031210e-03
μ	1.021593e-03	2.781361e-04	1.240456e-03	1.573103e-05
μ_H	2.134145e-02	1.392714e-03	2.567778e-02	3.375555e-04
θ_2	4.817611e-03	6.522819e-04	6.339945e-03	9.010973e-05
ζ	7.361338e-04	5.674599e-04	4.527184e-03	7.768796e-05
θ_3	1.206387e-01	3.208296e-03	1.543571e-01	1.945423e-03
ν	1.113765e-06	1.680776e-05	3.018758e-06	3.575716e-08
ω	3.366398e-12	3.199406e-11	1.343249e-17	1.663923e-19
b	3.809202e-04	2.399216e-04	8.835397e-04	1.898373e-05
c	-1.269688e-07	4.182839e-06	2.452136e-07	5.098782e-09
d	2.192239e-06	1.579702e-05	2.419460e-06	5.328717e-08
e	4.440092e-05	5.784511e-05	5.109191e-05	1.114729e-06
P_0	9.973624e-06	6.316663e-05	4.859762e-05	1.156122e-06
A_0	4.276209e-02	2.171111e-03	6.291578e-02	9.460191e-04
H_0	2.428478e-01	4.103701e-03	2.774331e-01	3.144858e-03
R_0	3.332658e-02	1.767094e-03	4.227236e-02	5.026088e-04

Table 23: Sensitivity of the stably recovered class at the beginning of 2019 to each of the parameters with corresponding confidence intervals listed.

Parameter	S1	S1 confidence interval	ST	ST confidence interval
m	1.900440e-05	3.483479e-05	1.639926e-05	2.203641e-07
β_A	2.443082e-06	1.224853e-05	2.131714e-06	2.358282e-08
β_P	3.709661e-06	1.514696e-05	3.156364e-06	3.730927e-08
θ_1	1.727543e-03	4.038265e-04	2.063629e-03	2.521118e-05
ε	1.764063e-02	1.291175e-03	2.012841e-02	2.525678e-04
γ	2.157279e-02	1.448643e-03	2.455398e-02	3.019235e-04
σ	1.377646e-01	3.085558e-03	1.435786e-01	1.428222e-03
μ	2.243059e-03	4.381924e-04	2.411235e-03	2.283540e-05
μ_H	8.844906e-05	1.063622e-04	1.171245e-04	1.582557e-06
θ_2	3.296396e-05	5.721704e-05	3.251507e-05	5.534722e-07
ζ	2.344819e-01	4.269546e-03	2.470132e-01	2.517333e-03
θ_3	5.118562e-03	7.134459e-04	6.169470e-03	8.524333e-05
ν	6.808987e-07	8.648211e-06	9.289717e-07	1.232603e-08
ω	9.041248e-13	4.960787e-11	2.331493e-17	2.344334e-19
b	4.664355e-03	6.473720e-04	5.468251e-03	5.873537e-05
c	2.970811e-07	7.779852e-06	8.243027e-07	1.013906e-08
d	1.690581e-05	3.233393e-05	1.541800e-05	1.635504e-07
e	2.522610e-04	1.288575e-04	2.734907e-04	3.035197e-06
P_0	1.947581e-04	1.244439e-04	2.222367e-04	2.844203e-06
A_0	2.815084e-01	4.413462e-03	2.928327e-01	2.812336e-03
H_0	5.043824e-03	6.465155e-04	5.872927e-03	7.457656e-05
R_0	2.667836e-01	3.831808e-03	2.710416e-01	2.591399e-03

The first-order index values and confidence intervals for each parameter corresponding to a certain population class for the α piecewise linear, μ_A linear case run from 2020-2023 (corresponding to Figure 2.20) are shown in Tables 24-28.

Table 24: Sensitivity of the susceptible class at the beginning of 2023 to each of the parameters with corresponding confidence intervals listed.

Parameter	S1	S1 confidence interval	ST	ST confidence interval
β_A	1.065995e-08	1.269881e-06	1.837571e-08	1.740975e-10
β_P	2.968555e-09	1.561814e-06	3.230241e-08	3.441020e-10
θ_1	2.338709e-02	1.494347e-03	2.348219e-02	2.471934e-04
ε	7.258704e-01	7.977949e-03	7.391669e-01	5.970798e-03
γ	1.598246e-04	1.174784e-04	1.670281e-04	1.696112e-06
σ	9.983750e-05	1.045744e-04	1.201629e-04	1.360130e-06
μ	1.181616e-03	3.011764e-04	1.227048e-03	1.492741e-05
μ_H	4.063782e-05	6.755366e-05	4.603834e-05	5.719659e-07
θ_2	5.069971e-05	6.734414e-05	5.383644e-05	6.094446e-07
ζ	-8.995768e-07	6.276487e-06	5.026052e-07	9.252755e-09
θ_3	8.361526e-05	8.518545e-05	9.865983e-05	1.211301e-06
ν	1.241085e-08	8.296734e-07	8.242554e-09	1.007653e-10
ω	-3.084156e-14	9.422862e-13	9.382629e-21	1.408947e-22
g	2.355871e-01	3.856499e-03	2.488217e-01	2.275272e-03
h	2.180598e-06	1.135189e-05	1.837202e-06	1.991012e-08

Table 25: Sensitivity of the prescription opioid user class at the beginning of 2023 to each of the parameters with corresponding confidence intervals listed.

Parameter	S1	S1 confidence interval	ST	ST confidence interval
β_A	3.523232e-11	4.061116e-08	2.088257e-11	2.272421e-13
β_P	-1.511771e-10	5.946348e-08	4.753241e-11	7.040540e-13
θ_1	2.184097e-05	4.105771e-05	2.427651e-05	2.861673e-07
ε	7.408634e-01	8.419980e-03	7.546509e-01	5.606010e-03
γ	5.502705e-06	2.314964e-05	8.098918e-06	1.121585e-07
σ	1.002053e-07	3.944910e-06	2.083958e-07	3.041931e-09
μ	6.202876e-06	2.236267e-05	8.410396e-06	1.285329e-07
μ_H	1.250524e-06	1.058651e-05	1.286022e-06	1.589157e-08
θ_2	1.482845e-06	1.379123e-05	2.661592e-06	3.510000e-08
ζ	4.693056e-08	2.161490e-07	7.566989e-10	1.783496e-11
θ_3	3.809309e-07	3.100907e-06	1.672601e-07	2.372844e-09
ν	-1.811828e-10	3.681820e-08	1.406163e-11	1.946533e-13
ω	-3.282164e-17	3.626954e-14	1.635296e-23	2.300580e-25
g	2.452787e-01	4.376676e-03	2.590651e-01	2.740717e-03
h	-1.329747e-08	3.493456e-07	1.603736e-09	1.951678e-11

Table 26: Sensitivity of the prescription opioid addicted class at the beginning of 2023 to each of the parameters with corresponding confidence intervals listed.

Parameter	S1	S1 confidence interval	ST	ST confidence interval
β_A	6.046039e-06	2.277795e-05	6.545096e-06	5.897689e-08
β_P	1.141732e-05	3.068316e-05	1.148413e-05	1.304947e-07
θ_1	5.583807e-02	2.042939e-03	5.805521e-02	5.402914e-04
ε	7.269814e-02	2.614771e-03	7.980917e-02	9.401477e-04
γ	7.179804e-02	2.423607e-03	7.942893e-02	8.538415e-04
σ	8.220825e-03	9.136805e-04	1.006366e-02	1.258426e-04
μ	2.352673e-04	1.526106e-04	2.735420e-04	3.263211e-06
μ_H	2.871514e-03	4.592239e-04	2.962010e-03	3.358688e-05
θ_2	1.957970e-04	1.109274e-04	2.247748e-04	2.768543e-06
ζ	3.410548e-01	5.136337e-03	3.534021e-01	3.724071e-03
θ_3	4.178981e-01	5.599052e-03	4.315088e-01	4.073558e-03
ν	4.708946e-07	6.802877e-06	5.287215e-07	5.692517e-09
ω	-6.067844e-14	7.062135e-12	6.317875e-19	7.586013e-21
g	5.529401e-03	7.340045e-04	6.277775e-03	6.716458e-05
h	8.868537e-04	2.445085e-04	9.413243e-04	1.050310e-05

Table 27: Sensitivity of the heroin/fentanyl addicted class at the beginning of 2023 to each of the parameters with corresponding confidence intervals listed.

Parameter	S1	S1 confidence interval	ST	ST confidence interval
β_A	8.453102e-09	1.579937e-06	4.243669e-08	4.222730e-10
β_P	6.474010e-08	2.239466e-06	7.503162e-08	9.204551e-10
θ_1	8.477187e-01	7.662521e-03	8.506819e-01	6.494914e-03
ε	3.267336e-04	2.152168e-04	6.726112e-04	9.765215e-06
γ	4.147126e-04	1.780449e-04	5.234007e-04	6.691878e-06
σ	6.255201e-02	2.278980e-03	6.351833e-02	6.257382e-04
μ	1.273961e-03	3.343617e-04	1.325404e-03	1.206616e-05
μ_H	4.306741e-02	1.684827e-03	4.437849e-02	4.076448e-04
θ_2	2.403148e-03	4.091995e-04	2.696200e-03	2.724396e-05
ζ	3.145194e-04	2.271257e-04	6.113552e-04	9.475481e-06
θ_3	3.816221e-02	1.695415e-03	3.923746e-02	3.646752e-04
ν	6.016927e-06	1.862546e-05	4.789238e-06	4.084802e-08
ω	7.897547e-14	1.784379e-11	4.429133e-18	3.930180e-20
g	1.160360e-05	5.137588e-05	2.807733e-05	4.081844e-07
h	2.020570e-06	1.314319e-05	2.281573e-06	2.413001e-08

Table 28: Sensitivity of the stably recovered class at the beginning of 2023 to each of the parameters with corresponding confidence intervals listed.

Parameter	S1	S1 confidence interval	ST	ST confidence interval
β_A	4.045823e-07	6.320649e-06	4.282230e-07	4.020154e-09
β_P	8.056750e-07	7.358193e-06	7.510487e-07	7.200501e-09
θ_1	1.046680e-03	2.446682e-04	1.120588e-03	1.155795e-05
ε	3.292721e-03	5.782521e-04	3.785846e-03	4.798738e-05
γ	4.645128e-03	7.437446e-04	5.225248e-03	5.080196e-05
σ	7.301657e-01	7.077174e-03	7.305172e-01	5.295957e-03
μ	4.511768e-03	6.169977e-04	4.536602e-03	4.360129e-05
μ_H	4.654661e-05	6.231553e-05	5.736925e-05	6.123102e-07
θ_2	4.915206e-06	1.916071e-05	4.675904e-06	4.828101e-08
ζ	2.359034e-01	3.551756e-03	2.374176e-01	2.219779e-03
θ_3	1.833012e-02	1.162443e-03	1.907706e-02	1.849366e-04
ν	4.146100e-05	4.920192e-05	4.159025e-05	3.932549e-07
ω	-6.230308e-14	6.209968e-11	4.908577e-17	4.183862e-19
g	8.390129e-05	8.824425e-05	1.030037e-04	1.189480e-06
h	2.242909e-05	4.054123e-05	2.377392e-05	2.340548e-07

Vita

Tricia Marie Phillips was born in Williamson, New York to John and Janann Phillips and grew up with her older brother, Tyler. She attended Williamson Central High School and upon graduating in 2012, moved to Oneonta, New York to attend Hartwick College. In 2015, she graduated with her B.A. in Mathematics. With a dream job of being a professor at a small liberal arts institution, she moved to Knoxville, Tennessee in the summer of 2015 to pursue a PhD at the University of Tennessee, Knoxville. While there, she had ample opportunities to do what she loved most: teach. She worked closely with her mentors to improve as an educator and learned how to be a researcher in mathematical biology under the guidance of Suzanne Lenhart and Christopher Strickland in her last three years there.

Tricia finished her PhD in Mathematics in 2020. She will be moving to Birmingham, Alabama to begin the career she always dreamed of as an Assistant Professor of Mathematics at Birmingham-Southern College.